



The  
University  
Of  
Sheffield.

# **Development of a Low-Cost Automated In-Situ Consolidation Process for Self-Reinforced Polypropylene Composites**

THESIS BY

**Pablo Jaramillo Cevallos**

In partial fulfilment of the requirements for the degree of  
Doctor of Philosophy

The University of Sheffield  
Faculty of Engineering  
Department of Mechanical Engineering

October 2021

## Declaration

I confirm that the Thesis is my own work, except where work, which has formed part of jointly authored publications has been included. The contribution of the candidate and the other authors to this work has been explicitly indicated below. The candidate confirms that appropriate credit has been given within the thesis where reference has been made to the work of others. I am aware of the University's Guidance on the Use of Unfair Means ([www.sheffield.ac.uk/ssid/unfair-means](http://www.sheffield.ac.uk/ssid/unfair-means)). This work has not previously been presented for an award at this, or any other, university.

The testing rig and the open-loop force control system used in *chapter 3 Process and Machine development* of this thesis has appeared in publications as stated below.

- "Towards mould free composites manufacturing of thermoset prepregs. Incremental curing with localised pressure-heat (ICULPH)," *Procedia CIRP*, vol. 85, pp. 237-242, 2019, V. M. Cedeno-Campos, P. A. Jaramillo, C. M. Fernyhough, and J. P. A. Fairclough.
- "Towards mold-free composites. A novel control method to cure carbon fiber through punctual force," 2019 24th IEEE International Conference on Emerging Technologies and Factory Automation (ETFA), vol. 2019-September, pp. 1461-1465, 2019, V. M. Cedeno-Campos, P. A. Jaramillo, C. M. Fernyhough, and J. P. A. Fairclough.
- "Online non-intrusive curing identification of CFRP assisted by pattern recognition with a novel in-situ curing apparatus," 2019 IEEE International Conference on Systems, Man and Cybernetics (SMC), vol. 2019-October, pp. 391-396, 2019, V. M. Cedeno-Campos, P. A. Jaramillo, C. M. Fernyhough, and J. P. A. Fairclough.

In all three publications, I was responsible for designing and constructing the mechanical elements of the testing rig and provided technical support. The contribution of the other authors was V. M. Cedeno-Campos was responsible for writing the publication, the electronic design, the creation of the open-loop force control system. C. M. Fernyhough provided technical support for low surface coatings. P. A. Fairclough was in supervisory roles during these works.

# Acknowledgements

I first thanks God and Jesus for helping me to find the strength when I needed it the most.

I want to acknowledge and thank my supervisor, Professor Patrick Fairclough, for his ongoing support and guidance throughout the last 4 years and for the opportunities that he has provided. This work would not have been possible without his positive outlook and enthusiasm.

I would also like to thank the support of my colleagues in the research office, especially to Victor Cedeño, for introducing me to the wonderful world of making and controlling machines. Special thanks to all my PhD colleagues from different research groups for their ongoing moral and academic support and for sharing our experiences through this journey. Several technicians and support staff at the University of Sheffield have been instrumental throughout this work and have provided valuable guidance.

Finally, I would like to thank my family, girlfriend and future wife, and friends. To my mom and brothers for never losing hope in me that I will achieve this objective. To my girlfriend and future wife for countless days of support when I was not at my best. To my friends for helping me to enjoy the world outside the PhD journey.

# Abstract

Self-reinforced composites are a new trend of “composite” materials in which both the reinforcement and the matrix are the same polymer but present different morphologies. Other benefits of self-reinforced composites are recyclability and lightweight. There are several technologies to produce self-reinforced composites, but the most common procedure is based on Hot compaction of high modulus fibres/tapes or bicomponent tapes by selectively melting a thin surface of each fibre/tape, so when cooling, this region recrystallises as the matrix, making a self-reinforced composite.

This thesis presents a flexible approach to the hot compaction procedure by adopting a low-cost automated in-situ consolidation process for self-reinforced polypropylene composites. Here a closed mould is replaced by only one side mould, while the other side mould is replaced by a small tool. The tool can in-situ consolidate a stack of self-reinforced composite fabrics using automated forming paths while ensuring a precise temperature control that prevents the reinforcement phase from molecular relaxation and, therefore, a loss in mechanical properties. The physics behind the automated process is explained, including the bonding mechanism of two polymer interfaces and the heat transfer mechanism.

The machine consists of a gantry structure integrating open-source hardware, a piezoelectric force sensor, temperature sensors with PID temperature controllers, and control software. The control software provides several functions, including hardware communication, machine motion control with a g-code programming language, graphical user interface, monitoring, recording, online processing of force signals, and a software-PID force closed-loop actuation.

To prove the feasibility of the automated in-situ consolidation process, two-dimensional and three-dimensional laminates were formed under different processing parameters such as temperature and pressure. The laminates were characterised and compared against a benchmark manufacturing process: hot press. The results of this project demonstrate it is possible to achieve in-situ consolidation of self-reinforced polypropylene composites which also opens a window towards mould-less fabrication.



# TABLE OF CONTENTS

<b>1</b>	<b>Introduction .....</b>	<b>1</b>
1.1	Introduction to Polymers .....	1
1.2	Introduction to Fibre Reinforced Polymer Composites .....	3
1.3	Introduction to Manufacturing of Fibre Reinforced Polymer Composites .....	5
1.4	Introduction to Self-Reinforced Polymer Composites .....	7
1.5	Research Motivation & Statement of Novelty .....	10
1.6	Research objectives .....	13
1.6.1	Objectives .....	13
1.6.2	Thesis Outline .....	14
<b>2</b>	<b>Literature Review .....</b>	<b>15</b>
2.1	Composites Manufacturing .....	15
2.2	Additive Manufacturing of Fibre-Reinforced Composites .....	17
2.2.1	Material Extrusion .....	17
2.2.1.1	Fibre-Reinforced Filaments .....	18
2.2.1.2	Continuous Fibre Reinforcement – one deposition head .....	24
2.2.1.1	Continuous Fibre Reinforcement – Delivering the matrix and the fibres separately.....	26
2.2.1.2	Robotics .....	29
2.2.2	Sheet Lamination .....	30
2.2.3	Additive Manufacturing Summary .....	34
2.3	Incremental Sheet Forming of Fibre-Reinforced Composites .....	35
2.3.1	Polymer Composites .....	38
2.3.2	Polymer Nanocomposites.....	40
2.3.3	Fibre-Metal Laminates (FML) .....	40
2.3.4	Incremental Sheet Forming Summary .....	42
2.4	Alternative "Mould Free" Developments .....	43

2.5	Self-reinforced Composites .....	47
2.6	Literature Review Conclusions .....	51
<b>3</b>	<b>Process and Machine Development .....</b>	<b>53</b>
3.1	Structural Frame and Mechanical Actuators .....	55
3.2	Motion Controller.....	57
3.2.1	Speeds Limits .....	57
3.2.2	Motion Control: Hardware and Software Integration.....	58
3.3	Processing Parameters Control.....	60
3.3.1	Data acquisition .....	61
3.3.2	Temperature Control.....	62
3.3.2.1	Ultrasonic heating (UC).....	64
3.3.3	Force Control .....	65
3.3.3.1	Software capabilities .....	68
3.3.3.2	Forming stages and Open-Loop Control.....	68
3.3.3.3	Online Force Compensation .....	70
3.3.3.4	Target force approaching method and Datum Setting .....	71
3.3.3.5	Forming stage .....	72
3.3.3.6	Temperature influence .....	74
3.3.3.7	Closed-loop Control.....	76
3.3.4	Clamping .....	85
3.4	Energy Consumption .....	87
3.5	Automated In-situ Consolidation Workflow .....	89
3.6	Machine specifications.....	90
<b>4</b>	<b>Forming Mechanisms of Automated In-situ Consolidation.....</b>	<b>92</b>
4.1	Theory of bonding polymer interfaces: Autohesion .....	92
4.2	Heat Transfer.....	95
4.2.1	Experimental Set up .....	99
4.2.2	Results.....	100

4.2.3	Conclusions .....	102
<b>5</b>	<b>Two-dimensional laminates and Characterisation .....</b>	<b>103</b>
5.1	Introduction.....	103
5.2	Material .....	103
5.2.1	Temperature Processing Window .....	104
5.3	Specimen Manufacturing .....	106
5.3.1	Hot Press.....	107
5.3.1.1	Short processing Cycle.....	107
5.3.1.2	Long processing Cycle.....	109
5.3.2	Automated In-Situ Consolidation .....	110
5.3.2.1	Hot Mould Temperature Selection.....	110
5.3.2.2	Forming Speed Selection .....	112
5.3.2.3	Forming Path Separation Selection .....	116
5.3.2.4	Main Processing parameters: Pressure and Temperature.....	120
5.3.2.5	Force control vs No Control.....	124
5.3.2.6	Geometric Accuracy.....	129
5.3.2.7	Thickness .....	130
5.4	Material Characterisation .....	132
5.4.1	Interlaminar Properties .....	132
5.4.1.1	Results and Discussion.....	133
5.4.2	Tensile Properties .....	136
5.4.2.1	Methodology and Experimental Set up.....	139
5.4.2.2	Results and Discussions .....	141
5.4.3	Degree of Crystallinity .....	144
5.4.3.1	Methodology .....	144
5.4.3.2	Results and Discussion.....	145
5.5	Conclusions.....	149
<b>6</b>	<b>Three-dimensional laminates and characterisation .....</b>	<b>151</b>
6.1	Introduction.....	151
6.2	Dome Geometry Manufacturing.....	151

6.2.1	Hot Press Processing.....	151
6.2.2	Automated In-Situ Consolidation .....	153
6.3	Curved Geometries .....	155
6.4	Quality Control of Automated In-Situ Consolidated Parts.....	157
6.4.1	3D Scanning .....	158
6.4.2	Materials, Specimens and Experimental Set up.....	159
6.4.3	Results and Discussions .....	163
6.4.3.1	Dome Geometry .....	163
6.4.3.2	Curved Sample.....	169
6.4.4	Conclusions.....	172
6.5	Compressive Behaviour of Self-Reinforced Polypropylene Domes Between Two Platens.....	172
6.5.1	Introduction .....	173
6.5.2	Methodology .....	174
6.5.3	Results and Discussion.....	175
6.5.4	Conclusions.....	180
<b>7</b>	<b>Conclusions and future work .....</b>	<b>181</b>
7.1	Future Work .....	184
7.1.1	Mould Alignment.....	184
7.1.2	Force Sensor .....	184
7.1.3	Motion Controller .....	185
7.1.4	Ultrasonic Heating .....	185
7.1.5	Machine Learning .....	186
7.1.6	Mould-Free Composites .....	186
<b>8</b>	<b>References .....</b>	<b>188</b>
<b>9</b>	<b>Appendix A.....</b>	<b>204</b>
<b>10</b>	<b>Appendix B.....</b>	<b>206</b>

<b>11</b>	<b>Appendix C.....</b>	<b>216</b>
<b>12</b>	<b>Appendix D .....</b>	<b>221</b>

# LIST OF FIGURES

Figure 1-1 Types of fibre reinforced polymer (FRP) composites. They can be continuous, discontinuous (short), or continuous woven fabrics [9]. ..... 4

Figure 1-2. Number of publications per year of self-reinforced composites for the most common type of polymers (Source: Scopus search for self-reinforced, one polymer, all-polymer, or single polymer composites)..... 9

Figure 1-3 Tooling cost for different composite manufacturing techniques. In general, low-pressure systems are cheaper than high-pressure systems. Data obtained from [42] ..... 11

Figure 1-4. Schematic of the automated in-situ consolidation process. The temperature of the forming tool is higher than the temperature of the mould. The tool path copies the shape of the surface of the mould to produce a net shape component. .... 12

Figure 2-1 Representation of an FDM reinforced filament fabrication. In the first steps, the plastic and the reinforcement are blended before being extruded into a filament. The filament extrusion is repeated until a dense filament is achieved [60]. ..... 18

Figure 2-2 Microtomography of a freely extruded PLA filament reinforced with carbon fibres. The colours in the pictures show the orientation of the fibres. Blue is aligned with the Z-axis, green is aligned with the Y-axis, and red is aligned with the X-axis [67]. ..... 19

Figure 2-3 CT scans during extrusion of short-fibre thermoplastic composites on a 3D printing nozzle ..... 20

Figure 2-4 CT scans during extrusion of short-fibre thermoplastic composites after the filament exited a 3D printing nozzle..... 20

Figure 2-5 Microstructure of the cross-section of FDM dog bone samples without and with short-carbon fibre reinforcement. a) 0%  $V_f$ , b) 10%  $V_f$ , c) 20%  $V_f$  and d) 30%  $V_f$ . FDM printers produce a layered structure with triangular gaps in between each printing path. The addition of fibres modifies the microstructure reducing the size of these gaps. [59]..... 21

Figure 2-6. Schematic of Die-Swell in FDM. Reproduced with permission from the authors [72]. ..... 23

Figure 2-7 SEM micrographs comparison of fractured surfaces of ABS/CF composites. a)FDM printed cross-section with 10 wt.% carbon fibre, b) compression moulded cross-section with 10 wt.% CF loaded. [59]24

Figure 2-8 Process to reinforce a polymer filament with a continuous fibre in an extrusion material head for FDM Printers. Adapted from [77] ..... 24

Figure 2-9 Summary of continuous fibre-reinforcement for FDM processes developed by a) Nakawaga et al. [76], b) Yang et al. work [75], and c) Matsuzaki et al. work [74]. ..... 25

Figure 2-10 Schematic of a continuous fibre added to the matrix in an FDM process: (a) The matrix and fibre are extruded from the same nozzle, (b) the fibre is deposited with an additional nozzle [77]. ..... 27

Figure 2-11. Schematic of the MarkForge 3D printing process using a double print head [82] ..... 27

Figure 2-12 Schematic of the MarkForge 3D printing patterns: (a) Concentric Pattern following the exterior boundary, (b) Parallel or Isotropic Pattern, and (c) Lay-up configuration in which the black layer are the fibre reinforcements and the white layers are the nylon matrix [82]. ..... 28

Figure 2-13 Examples of 3D Printed samples produce with a MarkForge 3D printer showing the reinforcement patterns. Parallel patterns were achieved for glass and Kevlar fibres while concentric patterns were achieved with glass, Kevlar and carbon fibres [82].	28
Figure 2-14 SEM pictures of the morphology of 3D printed samples with different lay-up configurations: (a) Carbon Fibre (6 layers)/Nylon (4 layers), and (b) Carbon Fibre (2 layers)/Nylon (8 layers) [84].	29
Figure 2-15 FDM robotic Systems: a) 5-Axis Arevo Labs Robotic FDM 3D printer [87]; b) 8-Axis Stratasys Robotic 3D Composite Demonstrator [86].	29
Figure 2-16 Schematic of Laminated Object Manufacturing Process. Reproduced from [89].	30
Figure 2-17 a) Laminated object manufactured parts. The right and darkest part was cured in an autoclave while the left one was not cured, b) Micrograph of the morphology of the autoclave part showing good interfacial bond [89].	31
Figure 2-18 Laser-assisted tape placement process and final parts. There are a laser bonding and a laser cutting platform in which the part moves forward and backward[91].	31
Figure 2-19 SEM image of the cross-section of a LATP sample showing a good interlayer bonding achieved in the LATP process. [91].	32
Figure 2-20 Mechanical properties comparison between different additive manufacturing techniques. LATP composites have the best performance in comparison with other rapid prototyping techniques. [91].	33
Figure 2-21 Impossible Objects Composite 3D Printer process. Step 1: Feed fibre sheet into inkjet printer; Step 2: Load CAD slices into printer and print layer shape of object on fibre sheet; Step 3: deposit polymer powder onto printed sheet which stick to where the sheet is wet from print fluid; Step 4: Remove dry powder; only powder stack to the print fluid remains; Step 5: stack sheets in order, heat to melting Temperature of the polymer, and compress stack to final part height; Step 6: Remove unbonded portions of sheet fibres to net final part [94].	34
Figure 2-22 Schematic of Incremental Sheet forming process in which the forming tool incrementally deforms the metal sheet when it is moved down step by step [99].	36
Figure 2-23 Incremental forming Set-up and Variables involved in the process such as tool radius, angle wall, initial thickness, final thickness, and tool path [102].	37
Figure 2-24 Incremental forming assisted by hot air gun. The hot air will heat the workpiece to the melting point of the polymer so it can easily be shaped [115].	39
Figure 2-25 Vacuum-assisted SPIF of a thermoset composite. (a) experimental set up using a vacuum bag to hold the laminate, (b) resultant part showing a non-uniform distribution of resin at the bottom [118].	41
Figure 2-26 Fibre metal laminates under SPIF [118]. The laminate configuration is Aluminium/prepreg/aluminium. Both cases show a mechanical failure of the laminate during processing.	41
Figure 2-27 Net bending forming process [39].	43
Figure 2-28 Definition of "Net Bending" [39].	44
Figure 2-29 a) Strong's Incremental Forming Set Up. b) Top view of a part with a non-uniform cross-section [124, 125].	44

Figure 2-30 Reconfigurable multiple point tool [126] .....	45
Figure 2-31 Reconfigurable tool forming process and experimental set-up [126].....	45
Figure 2-32 Schematic of the hot compaction process. Fibres are first pressed and heated closed to the melting point to only melt the surface of the layers. The melting polymer then fill the gaps between the fibres, and when the temperature is reduced, the polymer recrystallizes as the matrix holding the fibres together. Reproduce with permission from the authors [28].....	48
Figure 2-33 schematic of the co-extrusion and solid-state drawing production line of self-reinforced polypropylene tapes. Repro. ....	49
Figure 2-34 Thermal and Pressure Processing Boundaries of self-reinforced composites: a) a high temperature may produce melting or molecular relaxation of the reinforcement phase, b) too much pressure can cause flow and molecular dealignment, c) and d) are the minimum levels of pressure and temperature to ensure proper consolidation [16, 28, 133].....	50
Figure 3-1. Schematic of the automated in-situ consolidation process. The temperature of the forming tool is higher than the temperature of the mould. The tool path copies the shape of the surface of the mould.53	
Figure 3-2. Main components of the automated in-situ consolidation machine. ....	55
Figure 3-3 V-slot aluminium profile holding a movable carriage through wheels that stand over the slots. ....	56
Figure 3-4. Automated in-situ consolidation machine based on a single forming tool.....	56
Figure 3-5. xPro V1 CNC motion Controller based on GRBL software. It is capable of driving 4 stepper motors and has a USB port for Serial communication. ....	57
Figure 3-6. Time to travel and Error in a motion profile for the open-loop motion controller. ....	58
Figure 3-7. g-code generation and execution in LabVIEW®. The code creates a communication channel with the motion controller (Visa Configure Serial Port). The user input as displacement is transformed into a string sent to the motion controller (Visa abc W).....	59
Figure 3-8. Software Graphical Interface: Motion control with force closed-loop system. ....	60
Figure 3-9. Temperature Control System. Reproduce with permission from the authors [153]. ....	61
Figure 3-10 Schematic of a Data Acquisition system composed of sensors, a data acquisition measurement hardware, and application software in a computer. Reproduce with permission from the authors [154]. .....	61
Figure 3-11. a) Schematic of the principle of a thermocouple [155]; b) CAL 3300 PID temperature Controller [156]; c) Picolog Temperature Datalogger [157].....	62
Figure 3-12. Voltage leaking through thermocouples to Data Acquisition Hardware.....	63
Figure 3-13. Typical forming tool installation. The forming tool is heated with a cartridge heater connected to the output of a temperature controller. A tool holder keeps the forming tool attached to the Z axis. The thermocouple is located a close as possible to the tip of the forming tool. ....	64
Figure 3-14. Ultrasonic welding of self-reinforced polypropylene promotes melting of both the matrix and reinforcement phases. ....	65
Figure 3-15. a) principle of a piezoelectric material in which a force exerted produces a voltages [163] ; b) 3-axes piezoelectric dynamometer based (cable not included in figure) [162]; c) signal amplifier of the	



dynamometer signal (cables not included in figure) [164]; d) USB data acquisition device that perform signal conditioning and transfers data to the computer [165].	66
Figure 3-16. Automated in-situ consolidation set-up with its subsystems.	66
Figure 3-17 LabVIEW® Graphical Interface showing the graphical approach to programming	67
Figure 3-18 Parallel Tasks in LabVIEW®	67
Figure 3-19 Force vs time profile representing the forming cycle stages of the automated process. Several stages are needed for signal conditioning before proceeding with the actual forming of the part	70
Figure 3-20 Online Drift Compensation. As the force data acquisition starts, the values of the force increase over time. These values are then used to perform an online drift compensation to the current values. It can be seen that a 1 kg load applied in the vertical direction (Z) does not increase over time due to the online compensation. The online compensation is equally performed in the X and Y axes, but as no load is applied in this directions, there is no change of force values for Fx and Fy.	71
Figure 3-21 Stages of the force approaching procedure. First the tool moves down slowly to start compressing the material. Once the compression force achieves an arbitrary value of 1N, then the tool is move down faster to speed up the procedure before the target force. Then it again moves down slowly to not overshoot the target force. A K=40 was used for polypropylene.	72
Figure 3-22. Path planning (left) and force measurements (right) during open-loop forming for a flat laminate.	74
Figure 3-23. Left: measuring the alignment of the mould. Right: surface mapping of the mould.	74
Figure 3-24. Force signals without (a) and with (b) temperature influence.	75
Figure 3-25. Measures to reduce heat transfer from the mould to the force sensor	75
Figure 3-26 Force Target Approach with a proportional Control to target force of 10N	77
Figure 3-27. Force control approaches: a) Proportional Control, b) Proportional + Integral Control (PI), c) Proportional + Integral + Derivative (PID), d) fixed small steps. The color lines are set point target forces to demonstrate the performance of the control algorithms.	78
Figure 3-28. Force signals without (a) and with (b) loads under the temperature cycles of automated in-situ consolidation processing	78
Figure 3-29. Temperature effect compensation using short forming cycles and an online-drift compensation. The forming process in this figure does not perform any force control system.	80
Figure 3-30. Proportional Control on	81
Figure 3-31. Tool Path transformation: a) original tool path and b) new tool path with additional coordinates	82
Figure 3-32. a) Forming forces with and without a Force closed-loop system (Proportional Control). b) zoom of the forming forces with a Force closed-loop system. FC=Force controlled	82
Figure 3-33. Forming forces with force closed-loop system with coordinates separated by a distance of 2 mm, 5 mm, and 10 mm.	83
Figure 3-34. Forming forces with force PID closed-loop system with coordinates separated by a distance of 2 mm, 1 mm, and 0.5 mm.	85
Figure 3-35. in-situ consolidated laminate without (a) and with (b) clamping.	86

Figure 3-36 Clamping mechanism of the laminate over the hot mould. The layers are cut and stacked .....	86
Figure 3-37. Energy consumption comparison between Hot Press and Automated in-situ consolidation of Self-reinforced polypropylene composites. HM=Hot mould, FS= Force Sensor. Error bars are small (~0.01) and have been omitted for clarity .....	87
Figure 3-38. Automated In-situ Consolidation Workflow.....	89
Figure 4-1. Schematic of autohesion or self-diffusion between two contact surfaces of the same polymer. Public use permitted [175].....	92
Figure 4-2. Reptation Model of polymer chains. Public use permitted [175]. .....	93
Figure 4-3. Reptation at an interface between two polymer surfaces. Public use permitted [175] .....	94
Figure 4-4 Interfacial bonding strength as a function of the fourth root of contact time for a given polymer at different temperatures (T). The higher the temperature, the faster the contact time required to achieve maximum strength. Public use permitted [175] .....	95
Figure 4-5. Schematic of single-point in-situ consolidation.....	96
Figure 4-6. Through-thickness temperature distribution is caused by a transient heat transfer when the forming tool and the mould are at the same temperature at different forming tool speeds. The slower the speed, the smaller the gradient, and the highest the average temperature. ....	98
Figure 4-7. Through-thickness temperature distribution is caused by a transient heat transfer when forming tool has a higher temperature than the mould at different forming tool speeds. The slower the speed, the smaller the gradient.....	98
Figure 4-8. Thermocouples (represented by a colour dot) located in each interface through the thickness of a 6-ply laminate. The dark blue thermocouple represents the room temperature reading. ....	99
Figure 4-9. Typical Temperature readings a 6-ply laminate manufactured via automated in-situ consolidation at a forming speed of 90 mm/min, a forming temperature of 140°C and a compression force of 7 bars. ..	101
Figure 4-10 Temperature Distributions at different Speeds. Fix parameters for simulation are: $\alpha = 0.16Wm^{\circ}K, Cp = 70Jkg^{\circ}K, \rho = 904kgm^3$ . Experimental values correspond to the maximum temperature reading recorded in each experiment. ....	102
Figure 5-1. (a) Torodon™ Fabric Structure: Plain; (b) Torodon™ Fabric as received. [17] .....	104
Figure 5-2 DSC trace of a co-extruded self-reinforced polypropylene tape showing a temperature processing window. Both copolymer and homopolymer show a double melting behaviour .....	105
Figure 5-3 Crystalline structure of self-reinforced polypropylene measured by WAXD. Three strong equatorial $\alpha$ -form peaks of (110), (040), (130) at $2\theta = 14.09, 16.90, \text{ and } 18.66^{\circ}C$ , are present .....	106
Figure 5-4. Time-Temperature and Time-Pressure fast-cycle manufacturing profile .....	107
Figure 5-5 Hot Compaction manufacturing via Hot press and a Fast cycle like the Automated in-situ consolidation.....	109
Figure 5-6 Time-Temperature and Time-Pressure profile of Hot-Pressing manufacturing.....	109
Figure 5-7 Hot Compaction manufacturing via Hot pressing for a 5-layer composite produced at a) 130°C and 10 bars of pressure b) 150°C and 10 bars of pressure .....	110

Figure 5-8 Three-dimensional surface finish of the layer in contact with the hot mould at different mould temperatures .....	112
Figure 5-9. a) schematic of a peel test, b) schematic of forming paths without overlapping each other. The red arrow indicates the direction of the peel test c) forming a laminate via automated in-situ consolidation. ....	113
Figure 5-10 Through-thickness interlaminar strength as a function of the forming speed in automated in-situ consolidation with a flat tool. Forming speeds: a) 90 mm/s b) 180 mm/s c) 360mm/s, d) 720 mm/s.....	114
Figure 5-11. Average force through the thickness as a function of the speed .....	116
Figure 5-12 Forming tools for automated in-situ consolidation: a) 8, 10, 12-mm hemi-spherical tools, b) “Flat tool”. Though the term “flat” tool is used, it has a high diameter at the end to avoid deformation due to shearing forces.....	117
Figure 5-13 Interlaminar strength comparison for different forming path separations (legends) with different tool geometries: a) 8 mm hemi-spherical, b) 10 mm hemi-spherical, c) 12 mm hemi-spherical, d) 17 mm Flat. The interlaminar strength of a specimen manufactured via Hot Press at 135°C and 10 bar of pressure is also shown to have a quality reference. ....	118
Figure 5-14. Force vs crack propagation for different layers in an automated in-situ consolidated laminate using a forming path separation of a) 2 mm and b) 8 mm when the interfaces are pulled apart. Because there is no overlap in the 8 mm path separation, the force presents peaks and valleys related to bonded and unbonded areas. *Tool=12 mm. ....	120
Figure 5-15. Load vs crack propagation of specimens with non-overlapping forming paths. The Full width at half maximum is calculated for each interface. ....	121
Figure 5-16 Influence of the compression force on the contact diameter of a forming tool with a processing temperature of 150°C, a forming force of 30N, and a forming speed of 1.5 mm/s.....	122
Figure 5-17. Path planning for automated in-situ consolidation of flat laminates.....	124
Figure 5-18 Automatic Grinder and polisher .....	125
Figure 5-19 Microscope images of three different mounted samples in which material removal was not achieved successfully. ....	126
Figure 5-20 Microscope images of (a) grinded and (b) polished specimens. The grinding marks have been greatly removed due to polishing. *Red epoxy resin was used to mount the samples, and therefore, the red colour. ....	126
Figure 5-21 Microscope images of specimens manufactured via Hot compaction with a benchmark Hydraulic Hot Press with a 5X magnification at processing temperatures of 130°C, 150°, and 170°C. *Clear epoxy resin was used to mount the samples. ....	127
Figure 5-22 Microscope images of specimens manufactured via Hot compaction with a benchmark Hydraulic Hot Press with a 20X magnification at processing temperatures of 130°C, 150°, and 170°C.....	128
Figure 5-23 Microscope images of specimens manufactured via Automated in-situ consolidation under the influence of pressure with a 5X magnification. High Pressure for a spherical tool is 10 bar. Low Pressure	

for a spherical tool is 7 bar. High Pressure for a flat tool is 7 bar. Low Pressure for a spherical tool is 2.7 bar. ....	128
Figure 5-24 Microscope images of specimens manufactured via Automated in-situ consolidation using a flat tool at 140°C, a forming speed of 90 mm/min, and a consolidation pressure of 7 bar. ....	129
Figure 5-25 Cross-section from both manufacturing processes showing warpage: a) Automated in-situ consolidation, b) Hot Press Forming .....	130
Figure 5-26 Laminate thickness as a function of the compaction temperature and pressure for both automated in-situ consolidation and Hot press specimens. a) Automated in-situ consolidation with a spherical 12 mm tool, b) Automated in-situ consolidation with a flat 17 mm tool. ....	132
Figure 5-27 Interlaminar Strength vs Temperature for all tested configurations .....	134
Figure 5-28. Summary of Interlaminar strengths reported in literature [32, 133, 189, 206, 207]. ....	134
Figure 5-29 Peel test traces (Interlaminar strength vs crack propagation) at different temperatures and pressure for both manufacturing processes: Hot press and automated in-situ consolidation. ....	135
Figure 5-30 Root mean squared error of the interlaminar strength traces for both Hot press and automated in-situ consolidated specimens under different processing parameters. ....	136
Figure 5-31 Stress vs Strain Curve Types for plastics. a) Brittle Materials, b) and c) tough materials with yield point, d) tough materials without yield point. Reproduced with permission from the authors [208]. ....	137
Figure 5-32 Tensile Profiles of Automated in-situ consolidated specimens with different strain measurement methods. Samples 1 and 5 use a video extensometer. Samples 2 to 4 use the grip-to-grip distance. ....	138
Figure 5-33 Video Extensometer Camera. The yellow lines help users to align the samples with the testing direction properly. The red lines narrow the target window of the video extensometer to avoid the surroundings and only focus on the specimens. The algorithm detects the marks and creates two blue lines at the centre of the marks. As the material is elongated, the marks, and therefore the blue lines move with it which allows the measurement of the deformation or strain of the material. ....	138
Figure 5-34. Direction of the force and forming paths (red arrows) in Tensile specimens. The blue and white squares represent tapes of the fabric .....	139
Figure 5-35 ProtoMax WaterJet Cutter used for cutting composite panels. Reproduced with permission from the authors [212]. ....	139
Figure 5-36 Water Jet Cutter of Self-Reinforced Polypropylene Composite Panels. Left images show rough edges after the process. The right image shows a better edge quality after using an aluminium plate as support. ....	140
Figure 5-37 Universal Testing machine adapted for tensile testing with a Computer showing the video Extensometer software. ....	140
Figure 5-38. Tensile Modulus vs Temperature. Specimens main axis are a) perpendicular and b) parallel to the forming path in an automated in-situ consolidation process. Hot press specimens are also presented for comparison purposes. ....	142

Figure 5-39 Tensile Strength vs Temperature. Specimens main axis are a) perpendicular and b) parallel to the forming path in an automated in-situ consolidation process. Hot press specimens are also presented for comparison purposes.....	142
Figure 5-40. Strain to failure vs Temperature. Specimens main axis are a) perpendicular and b) parallel to the forming path in an automated in-situ consolidation process. Hot press specimens are also presented for comparison purposes.....	143
Figure 5-41 DSC aluminium pans and lids with self-reinforced polypropylene composite samples. (a) Pan without bent edges over the lid (b) Pan with bent edges over the lid to ensure a good thermal transfer between the material and the pan. ....	145
Figure 5-42 Degree of Crystallinity as a function of the temperature for the copolymer and homopolymer, respectively. ....	146
Figure 5-43 Material Properties as a function of the temperature for Hot Press specimens .....	146
Figure 5-44 Material Properties as a function of the temperature for Automated in-situ consolidation specimens with a 12 mm to with processing pressures of a) 7 bar and b) 10 bar .....	148
Figure 5-45 Material Properties as a function of the temperature for Automated in-situ consolidation specimens with a 17 mm to with processing pressures of a) 2.7 bar and b) 7 bar .....	149
Figure 6-1 Time-Temperature and Time-Pressure profile of Hot-Pressing manufacturing.....	152
Figure 6-2 Hot Compaction manufacturing via Hot pressing for a 5-layer laminate .....	152
Figure 6-3. Left: CAD part of the mould. Right: Toolpath simulation using a CAM milling operation. The start position of the toolpath is in the centre of the dome following concentric paths, and the finish position is in the outer boundaries .....	153
Figure 6-4. New Toolpath plan from Matlab Post-processing in which the separation between coordinates is reduced to 0.5 mm. The start of the path is at the apex of the dome and the end is the outer point in the mould plane. ....	153
Figure 6-5. The preform is manually pressed against the mould to aid the forming process .....	154
Figure 6-6. Dome laminates manufactured via automated in-situ consolidation at different temperatures....	155
Figure 6-7. Path Planning for Curved laminates. a) Parallel to the curvature, b) Perpendicular to the curvature .....	156
Figure 6-8. Forming Forces for curved laminates. a) Forming forces when the tool path is parallel to the curvature of the path. b) Forming Forces when the tool path is parallel to the curvature of the part ....	156
Figure 6-9. Automated in-situ consolidation of curvature laminates. a) experimental set-up in process*, b) consolidated laminate*, c) post-processed laminate. *The blue boundary in the laminates is blue tape that was used to improve the cutting process of the preform and it is not related to any processing parameter. ....	157
Figure 6-10 Triangulation base system using structured light. Reproduce with permission from the authors [220]. ....	158
Figure 6-11 Automated in-situ consolidated domes after post processing .....	159

Figure 6-12 Triangulation-based scanner with turntable (Left). Scan of a curved shape self-reinforced polypropylene manufactured via automated in-situ consolidation (right).....	160
Figure 6-13. 3D scans: (a) repairable scan model. (b) Non-repairable scan model.....	160
Figure 6-14 True CAD model of the dome: (Left) Isometric View; (Right) dimensional drawing showing the radius of the dome, radius of the fillet, and major diameter for both top and bottom surfaces. ....	161
Figure 6-15 True CAD model of a curved shape laminate .....	161
Figure 6-16 Geometrical features to be measured and compared in the true part. A sphere is the geometry that is used to measure either the diameter of the top and bottom surfaces (concentric diameters), while the toroid is the geometry that can be used to measure the radius of the fillet in the edge tangent to the dome. ....	162
Figure 6-17 Tolerance colour-difference maps for hot pressed consolidated scanned parts against the true part. Yellow or red points regions are out of tolerance with a positive discrepancy, while turquoise or blue regions are out of tolerance with a negative discrepancy. Due to reflections, only the bottom surface of the sample processed at 125°C could be scanned. *Tolerance units: mm. ....	163
Figure 6-18. Manufactured parts via hot press consolidation at 125°C (Left) and 170°C (Right).....	164
Figure 6-19 Tolerance colour-difference maps for Non-Force Controlled Automated in-situ consolidation scanned parts against the true part. Yellow or red points regions are out of tolerance with a positive discrepancy, while turquoise or blue regions are out of tolerance with a negative discrepancy. Purple regions indicate a discrepancy higher or lower than 0.6 or -0.6 mm respectively. Units: mm .....	164
Figure 6-20 Tolerance colour-difference maps for Force Controlled Automated in-situ consolidation scanned parts against the true part. Yellow or red points regions are out of tolerance with a positive discrepancy, while turquoise or blue regions are out of tolerance with a negative discrepancy. Purple regions indicate a discrepancy higher or lower than 0.6 or -0.6 mm respectively. Scanned models at 140°C intersect the true model, and therefore, the whole colour-difference map cannot be observed. The last column indicates only the projected scanned model without superimposing the true CAD part. *Tolerance units: mm .....	166
Figure 6-21 Tolerance performance of Scanned Models compared with the True Part for Dome Geometries.	168
Figure 6-22 Mean and Standard deviation of Scanned Models compared with the True Part for Dome Geometries.....	168
Figure 6-23 Tolerance inspection colour difference maps for Force Controlled Automated in-situ consolidation scanned parts. Yellow or red points regions are out of tolerance with a positive discrepancy, while turquoise or blue regions are out of tolerance with a negative discrepancy. Purple regions indicate a discrepancy higher or lower than 0.6 or -0.6 mm respectively. Scanned models at 140°C intersect the true model, and therefore, the whole colour-difference map cannot be observed. The last picture indicates only the projected scanned model without the true CAD part. ....	171
Figure 6-24 Right: Side view picture of the curved shape laminate with a printed profile as a reference for qualitative evaluation. Left: Visible void in between layers in the laminate. ....	171

Figure 6-25 Typical load-displacement curve for a quasi-static compression test. Reproduce with permission from the authors [237].	174
Figure 6-26. Experimental Set up for compression tests.	174
Figure 6-27 Load-Displacement compression profile of domes like structures. Legends: "C" stands for force controlled, "NC" stands for no-force controlled, "HP" stands for hot press.	176
Figure 6-28 Dome deformation while being compressed.	176
Figure 6-29 Energy Absorbed by the samples during a quasi-static crash test	177
Figure 6-30 Deformed shapes for different dome structures made with different manufacturing techniques and/or processing parameters. Blue and black lines represent the direction of the buckling while the red lines represent the direction of the fabric structure.	178
Figure 6-31. Microscope photographs of the cross section of the apex of a dome for both hot press and automated in-situ consolidation specimens at different processing temperatures and pressure.	179
Figure 7-1. Automated Double-Point forming of Fibre reinforced composites.	187
Figure 9-1 Force Control programming in LabVIEW®	205
Figure 10-1. Schematic of a circle in contact with a plane	206
Figure 10-2. Geometry of a rolling sphere over a surface	209

# LIST OF TABLES

Table 1-1 Processing properties and requirements for selected polymers (adapted from [7, 9]) .....	2
Table 1-2 Light weighting potential of different materials in comparison with mild steel. On average, the most significant savings could be achieved with carbon fibre composites (Reproduced and Adapted from [15]). .....	5
Table 2-1 Advantages and disadvantages of heating methods .....	16
Table 2-2 Material properties of Short-Fibre Reinforced Filaments. The highest values have been achieved using engineering thermoplastic polymers and high fibre volume fractions. Reproduce with permission from the authors [23]......	21
Table 2-3. Mechanical Properties comparison of MarkForge 3D printed samples with other manufacturing processes and high-performance aluminium alloys. Adapted with permission from the authors [82, 83]. .....	28
Table 2-4 Classification of Reconfigurable tools [131]. .....	46
Table 3-1. Estimated manufacturing times for automated in-situ consolidation according to the length of the forming path .....	84
Table 3-2. PID Control Parameters found empirically .....	84
Table 3-3 Automated in-situ consolidation machine specifications.....	91
Table 5-1 Properties of Torodon™ as described by its manufacturer [187].....	104
Table 5-2 Estimated consolidation pressure with different tools and different compression forces. *S=Hemispherical, *F=Flat .....	123
Table 5-3 Estimated consolidation pressure for the forming tools selected for the rest of this thesis. *S=Hemispherical, *F=Flat .....	123
Table 5-4 Processing Parameters .....	124
Table 5-5 Grinding and Polishing Procedure. ....	125
Table 6-1 Specimens and Process Parameters. ....	159
Table 6-2. Discrepancy of deviations between Scanned models from the True Part for Dome Geometries. (-) data could not be obtained due to parts being out of tolerance or difficult to scan.....	169
Table 6-3. The discrepancy of Scanned models with the True Part for a Curved Geometries .....	170
Table 6-4 Manufacturing Processing Parameters.....	175
Table 12-1 Discrepancy of deviations between Scanned models from the True Part for Dome Geometries. (-) data could not be obtained.....	221
Table 12-2 Deviation measure for geometric features for a Dome Geometry with different manufacturing processes such as Hot Pressing and Automated in-situ Consolidation. (-) data could not be obtained..	223



# 1 Introduction

Since their appearance, composite materials, especially those based on fibres and polymers, have attracted the attention of scientist and industries due to their high strength, high stiffness, and light weight when compared to most metal allows. Furthermore, their anisotropy allows to tailor the behaviour of a part according to the loading condition, which make them useful for load bearing applications while keeping low weights. For this reason, composite materials have been adopted in countless applications where weight reductions represent significant contributions in performance. They are extensively used in industries such as aerospace, sports, construction, prothesis, and many others.

## 1.1 Introduction to Polymers

Polymers, also known as plastics, accompany us in our everyday life. Polymer applications range from standard household products (e.g. packaging, toys, fabrics, diapers, cookware, adhesives, etc.) to high-end applications and emerging technologies (e.g. bulletproof vests, aerospace structures, artificial hip joints, resorbable sutures, plastic electronics, electric cars, fuel cells, etc.) [1]. The term polymer comes from the Greek words: *poly* and *meros*, meaning many parts. In other words, polymers are built up of many molecules (or macromolecules) that contain similar repeating units called monomers, and the process of joining or linking monomers to form polymers is called polymerisation.

There are two categories of polymers: Thermoplastics and Thermosets. Thermoplastics form long-chain molecules (Linear Polymers) which interact together via intermolecular forces and physical chain entanglements. On the other hand, thermosets chains are linked in a network fashion (cross-linked polymers), forming complex 3D networks connected with strong covalent bonds. That difference in molecular chain formation means that thermosets can only soften or burn upon heating while thermoplastics will additionally melt and flow [2].

Molecule chains in thermoplastics can be randomly oriented or highly ordered structures. The first is known as an amorphous polymer, meaning it has 0% crystallinity. The most common analogy of an amorphous polymer is to think of it as a piece of cooked spaghetti because it is randomly folded and intertwined with the other spaghetti [3]. On the

other hand, polymers with ordered structures are called semicrystalline polymers. In this case, the chains form ordered stacks known as lamellae which resemble the arrangement of atoms in crystals. The term *semicrystalline* refers to the fact that polymers are never fully crystalline. Most polymers present amorphous and crystalline regions, and therefore, polymers are categorised by their degree of crystallinity (DOC), while thermosets can be characterised by the cross-linking density [4]. It is known that molecular structure and the degree of crystallinity influences different material properties in semicrystalline polymers [5].

In terms of processing, thermoplastics are first synthesised (polymerised) as raw material and then melted, moulded, and cooled to solidify [6]. The solidification mechanism is called crystallisation. This process can be fast (a matter of seconds) if high cooling rates can be achieved. The ability to be melted and cooled repeatedly allows thermoplastics to be reused since they can be moulded into a different shape [7]. On the other hand, for thermosets, their monomers are first mixed in a liquid state and poured into the mould before being stimulated (e.g., heat or light) to accelerate polymerisation. The polymerisation process of thermoset polymers is commonly termed the *curing reaction* or *curing stage*. During the curing stage, the polymer chains form a cross-linked network that cannot be modified as described before [8].

Table 1-1 Processing properties and requirements for selected polymers (adapted from [7, 9])

Polymer Type	Viscosity*	Temperature **	Pressure **	Processing Time ***	Health and Safety
	Pa · second	°C	MPa		
Thermoplastics					
Polypropylene (PP)	100 at 230 °C	185-230	1	Minutes	None
Polyetheretherketone (PEEK)	380 at 380 °C	360-400	1	Minutes	None
Thermosets					
Unsaturated Polyester (UP)	0.1-1 at RT (up to 100****)	20	0.1	Minutes or hours	Inhalation, Contact, Risk of fire
Epoxy (EP)	0.1-1 at RT (up to 100****)	20-120	0.1	Hours	Inhalation, Contact, Risk of fire

\* Matrix material before and during processing.

\*\* Requirements during consolidation before achieving dimension stability

\*\*\* Relates to the entire processing cycle.

\*\*\*\* Partly cross-link thermoset polymers

The processability of thermoplastics and thermosets depends on many factors such as viscosity, pressure, temperature, time, and health and safety. A summary of processing properties and requirements is presented in Table 1-1. As can be seen, thermoplastics are at

least two orders of magnitude more viscous than thermosets. Higher temperatures and levels of pressure are required to achieve the required conditions for thermoplastics to flow. On the other hand, thermosets have lower viscosities, and therefore, they flow easily to impregnate fibres very well at low temperatures. The values of viscosity shown in Table 1-1 corresponds to a specific temperature; however, viscosity decreases with temperature because of the increased molecular mobility [8]. The processing time for thermoplastics (melting, shaping, and cooling) may take seconds or minutes, while thermosets could take days at the other extreme. During processing, polymerisation of thermosets may release volatiles, potentially toxic substances, and exothermic reactions leading to high temperatures. On the other hand, thermoplastics are almost chemically inert, which avoids hazardous substances [7].

The properties of polymer parts are determined by their internal structure and the manufacturing process. However, polymers would not be used to the extent they are currently used if not for additives that improve the engineering properties (e.g., antioxidants, fillers and fibres for reinforcement, plasticisers, or halogens for fire retardant purposes) [6]. The combination of two or more constituents is usually known as a *composite material*. Several sources can help the reader with a broader introduction and history of these materials [10-13].

## **1.2 Introduction to Fibre Reinforced Polymer Composites**

Fibre Reinforced Polymer (FRP) composites are a combination of fibres and a polymer. Fibres are stiffer and stronger than polymers, and the mixture of the two is expected to show intermediate properties of the constituents. The fibres act as the reinforcement, while the polymer is the matrix. The term *reinforcement* refers to the increment in rigidity and strength achieved by the combination [14]. The term *matrix* refers to the polymer holding the fibres together in the shape of the product. This transfers most of the mechanical loads to the fibres, and protects them from external damage (e.g. environment and/or handling) [6].

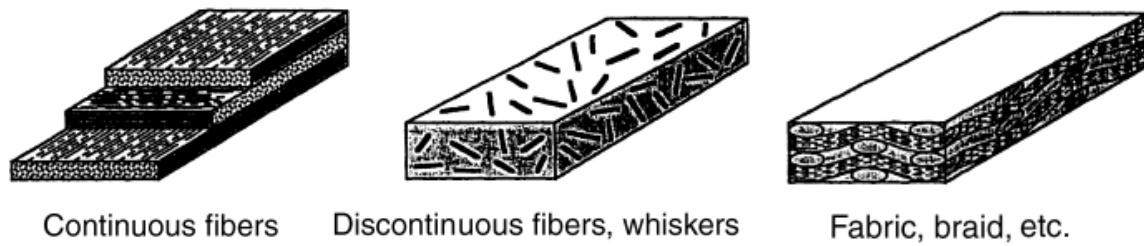


Figure 1-1 Types of fibre reinforced polymer (FRP) composites. They can be continuous, discontinuous (short), or continuous woven fabrics [9].

Fibre reinforcements can be *continuous, short-fibre or discontinuous*, or continuous woven fabrics, as illustrated in Figure 1-1. The figure also shows that fibre reinforced composites are made up via stacking layers with specific orientations. The orientation in each ply enables to tailor the final properties of the composite part by aligning them to the high load direction(s). In this way, less material is used on nonessential reinforcement. Discontinuous fibres are an exception since they are dispersed in random orientations.

FRP composites excel compared with other composite materials due to their high strength, stiffness, tailorable properties, lightweight, and ability to form complex shapes. They are used in weight-sensitive structural component applications mainly due to their high specific strength and modulus compared to metals. The term *structural* refers to the ability to support substantial mechanical loads [7]. Table 1-2 shows the light-weighting potential of different materials in comparison with mild steel. For instance, Carbon Fibre composites offer the highest weight savings and specific mechanical properties. Therefore, FRPs compete with advanced metal alloys and other materials as one of the main light-weighting tools for load-bearing applications in different industries such as aerospace, automotive, sports, and many others. For these industries, a reduction in weight can represent an improvement in fuel efficiency and a reduction in greenhouse emissions [15].

Table 1-2 Light weighting potential of different materials in comparison with mild steel. On average, the most significant savings could be achieved with carbon fibre composites (Reproduced and Adapted from [15]).

Material	Density (g/cm <sup>3</sup> )	Comparison to Steel			
		Strength/Density	Modulus/Density	Cost £	Mass reduction Potential
Mild Steel	7.87	1	1	1	0%
High-strength steel	7.87	1.86	1	0.9-1.2	10%
Adv high-strength steel	7.87	3	1	0.8-1.5	10%-28%
Gen 3 high-strength steel	7.87	7	1	1.0-2.0	15%-30%
Ceramics	3.9	0.7	3.05	1.5-3.0	10%-30%
Sheet moulding Compound	1.1-1.9	4.39	1.16	0.5-1.5	20%-30%
Glass Fibre composites	1.4-2.4	4.74	5.75	0.9-1.5	25%-35%
Plastics	0.9-1.5	0.82	0.08	0.7-3.0	20%-50%
Aluminium	2.7	3.95	1.02	1.3-2.0	30%-60%
Titanium	4.51	4.73	0.98	1.5-10	40%-55%
Metal Matrix composites	1.9-2.7	5.41	35.28	1.5-3.0	50%-65%
Magnesium	1.74	3.66	1.02	1.5-2.5	30%-70%
Carbon Fibre Composites	1.0-1.6	20.9	5.41	1.5-5.5	50%-70%
Self-Reinforced polypropylene composites[16, 17]	<b>0.7-0.9</b>	3.935	0.2	<b>0.80-1.5</b>	-

### 1.3 Introduction to Manufacturing of Fibre Reinforced Polymer Composites

One drawback of fibre reinforced composites is that the final properties rely on the processing characteristics of the matrix because both the final material and the product are manufactured simultaneously [9, 10, 18]. Because of this, a good understanding from both designer and manufacturer of how processing parameters influence the resulting mechanical properties is required. The selection of a processing route to produce structural components depends on several factors, but the most common are described below:

- **What is utilised as a mould to give the composite its shape?**

A mould is “a hollow container with a particular shape into which soft or liquid substances are poured so that when the substance becomes hard, it takes the shape of the container [19].” Another definition of mould more applicable to composites is: “any object that somehow helps maintain the liquid reinforcement-matrix mass in an exact predetermined shape until a dimensionally stable composite is obtained [8].” Moulds can be manufactured from different materials such as metals, wood, and other types of composites.

- **How will the mix of fibres and polymer conform to the mould, and how is the impregnation process achieved?**

*Conforming* refers to the process of manipulating the raw material (fibres and matrix) to copy the shape of the mould, which depends on the manufacturing method. For example, the fibres and matrix can be handled as two separate raw materials as in transfer moulding processes or as a single raw material, in which the fibres are already pre-impregnated of the matrix (also known as prepregs). Conforming is performed by laying up layers of the raw material in different orientations onto the mould to form a stack or laminate. *Impregnation* refers to the mixing or impregnation of the fibres with the polymer matrix, which requires a pressure gradient to ensure the flow of the polymer. Thermosets have a lower viscosity than thermoplastics and therefore are easier to flow even at room temperature. On the other hand, thermoplastics need heat to melt and flow, which require higher temperatures and pressures

- **How is the consolidation pressure applied, and how is the temperature controlled?**

*Consolidation* refers to the compaction process of the mix of fibres and polymer. Both pressure and temperature should be closely controlled during the moulding process, and if possible, in the component. An adequate pressure level is vital to keep the liquid polymer in place and constrained until the matrix solidifies and becomes dimensionally stable. A good level of consolidation ensures a successful solidification process. As described before, the solidification process differs if the polymer is a thermoplastic (crystallisation during cooling) or a thermoset (Curing process while heating or reacting).

- **What type of post-processing is required?**

As with every manufacturing process, composite parts are not exempt from further processing and finishing after the primary processing steps. Different post-processing techniques are usually required after consolidation and demoulding, such as edge trimming, drilling, fastening, painting, joining and others [20].

Most of the previous steps are labour intensive and require skilled technicians and expensive equipment to achieve industry standards. Furthermore, they commonly lack repeatability and can create final defects such as fibre misalignment, buckling, wrinkles, voids content, or others. As a result, due to the difficulty of obtaining defect-free parts, fibre reinforced composites are mainly used in applications in which a high structural performance accompanied by low weight is more critical than its manufacturing price, such in aerospace

and Formula 1. Nevertheless, their application has extended to almost every industry, such as military, sports, medical equipment, prosthetics, construction, etc.

There is a wide range of automated and semi-automated manufacturing processes for fibre reinforced composites as it is claimed they can improve process and cost efficiency for large composite parts. The most known automated processes are Automated Tape lay-up (ATP) or Automated Fibre Placement (AFP), in which tapes or fibres are selectively deposited over a mould or mandrel with the aid of heating and pressing devices. However, high capital investments are required for their adoption, limiting their widespread use for small-to-medium manufactures [21].

Digitally-driven strategies such as additive manufacturing offer a new possibility for low-cost automation in composite materials. The main advantage of additive manufacturing is producing fibre-reinforced composites without the need for a template or a mould [22, 23], which can reduce the price of composite components for low volumes. However, as explained in the following chapter (see Literature Review), there are several challenges to achieve composite parts with similar performance with benchmark manufacturing processes for composite materials.

## 1.4 Introduction to Self-Reinforced Polymer Composites

In most fibre reinforced composites, the reinforcement and the matrix are chemically inert with different surface energies, which hampers direct bonding between them. Ensuring proper adhesion in the interface is essential for composites materials. It has been shown that the interfacial bond strength between reinforcement and matrix controls different mechanical properties in the short and long-term performance, such as tensile and compression strength, work-to-fracture, creep and fatigue resistance [24]. The most common solution to improve bonding between the fibre/matrix interfaces is using coupling agents on the surface of the fibres (also known as *sizing* or *fibre size*) [25]. However, this increases the cost of fibres and, therefore, the final part.

The concept of *Self-reinforced composites* (also called *one polymer composites*, *single-polymer composites*, or *all-polymer composites*) was first introduced in 1975 [26] by creating a material in which both the reinforcement and the matrix are the same polymer but present

different morphologies. Because of the better chemical compatibility, a strong and stable interface between reinforcement and matrix can be achieved. Self-reinforced composites rely on high-performance thermoplastic fibres with high strength and tensile modulus. This increase in mechanical properties is usually achieved by orienting the molecules when the fibres are produced [16]. However, the main challenge of self-reinforced composites is their processing, as high processing temperatures may promote molecular relaxation, decreasing the mechanical properties or losing their reinforcement role [27, 28]. Other benefits of self-reinforced composites are recyclability and lightweight. Ease of recycling is an advantage as in this case, only one material can be recovered and re-processed to create a new part compared to composites reinforced with other fibres such as glass or carbon fibres. At the same time, they can achieve lightweight components due to their lower density (see Table 1-2) compared with other composites like Glass-Fibre or Carbon-Fibre composites.

There are several technologies to produce self-reinforced composites, but the most common procedure is based on Hot compaction [29] of high modulus fibres/tapes or bicomponent tapes [16, 28, 30-35]. When high-modulus fibres/tapes are used, the process is based on selectively melting a thin surface of each fibre, so when cooling, this region recrystallises as the matrix, making a self-reinforced composite. This process requires precise control of the processing temperature only to melt the surface of the fibres, which is generally achieved at a processing temperature of 5°C to 10°C lower than the melting point of the high modulus fibre. Bicomponent tapes have a high modulus tape surrounded by a lower melting point polymer that acts as the matrix, allowing a wider processing temperature window. The most common polymer for bicomponent tapes is polypropylene, in which the oriented tape is a homopolymer with a high modulus and highly aligned molecules. In contrast, the surrounding polymer is a copolymer with random molecular orientation. For example, homopolymer and copolymer polypropylene have melting points of 168°C and 130°C, respectively.



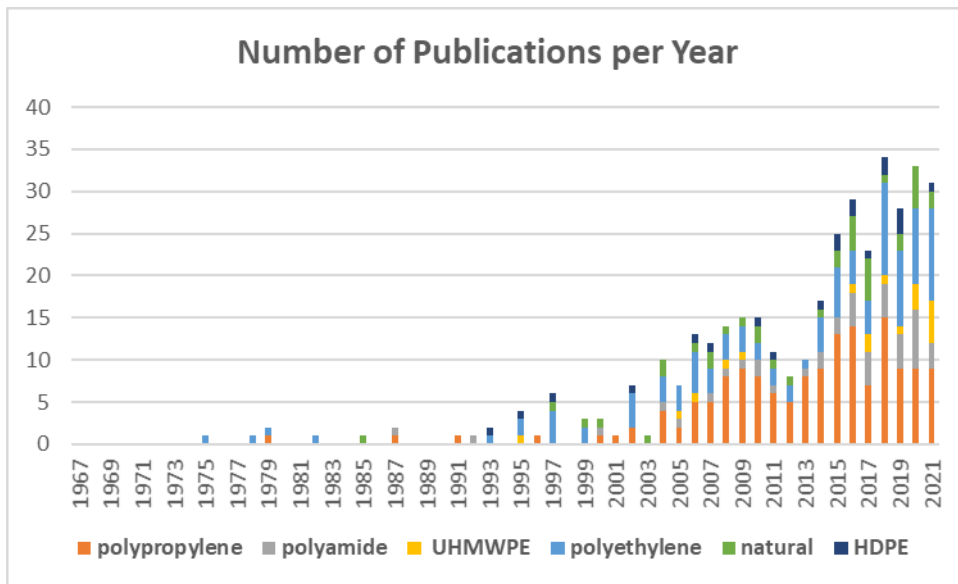


Figure 1-2. Number of publications per year of self-reinforced composites for the most common type of polymers (Source: Scopus search for self-reinforced, one polymer, all-polymer, or single polymer composites).

There has been a growing interest in self-reinforced composites from both commercial and scientist since the first development of self-reinforced composites. The number of publications relating to self-reinforced polymer composites has increased consistently, as shown in Figure 1-2. Most of the work in the literature towards studying manufacturing methods of self-reinforced composites focuses on polypropylene due to several factors such as high toughness, good impact and creep resistance, chemically inert, and low cost. Bulk polypropylene has been used in many applications such as food packaging industry, automotive components, ropes, toys, and household goods.

One of the advantages of self-reinforced polymer composites made with polypropylene is that it achieves high volume fractions (~90%). This compensates the low mechanical properties of polypropylene in comparison with other stiffer fibres such as UHMWPE. Because of its low prices and thermal stability, it has successfully being introduced into commercial production for raw materials branded as Curv [36], Pure [37], and Torodon [17]. Therefore, its application from a commodity plastics have been extended to load bearing and high impact resistance applications such as protective sports equipment, automotive panels, luggage, body armour, etc [28].

## 1.5 Research Motivation & Statement of Novelty

The rapidly evolving technological and manufacturing environment is pushing the implementation of low-cost, flexible, low-energy consumption, and responsive manufacturing strategies capable of processing various materials including composite materials [38]. Apart from additive manufacturing, which price has reduced considerably during the last years, small-to-middle-size manufacturers of composite materials have no automated processes to produce relatively small and complex components for low volumes because of the high capital investment required in automation equipment. Digital fabrication approaches enable fast development from design to manufacturing with the aid of computer-aided-design (CAD), computer-aided-manufacturing (CAM) software, and motion control hardware and software.

As mentioned, hot compaction is the preferred route to manufacture self-reinforced composites because of its relative simplicity, and therefore, commercial developments have scaled up and automated the hot compaction process for high volumes (e.g.: suitcases, or body armour). However, scientific and commercial developments of self-reinforced composites rely on the use of closed moulding processes, which implies the construction of expensive and time-consuming matching moulds, especially for low volume applications in which the cost per part of making the mould could be one of the largest capital expenses as shown in Figure 1-3. While there are moulding options from \$6K for a composite mould for Prepreg manufacturing up (Low volume and labour intensive), it can go above \$50K for a metal Mould for Sheet Moulding Compound (High volume and CNC machined). In addition, though the relative cost of tooling is low in comparison with the price of equipment, it introduces other manufacturing limitations that penalise the production of customised products [39], such as:

1. Large moulds are limited to the size of the equipment available such as CNC machines, autoclaves, and presses, leading to increased costs due to outsourcing. However, this is debatable since investment in bigger facilities might be even more expensive.
2. The difference in the coefficient of thermal expansion (CTE) between the FRPs and the mould material may promote geometric distortions in the finished product. It is desired to have a mould with the same or expected CTE of the final part if possible.

3. High-quality moulds consume long leading times, which affects the overall manufacturing productivity. Usually, the time of making a mould is longer than making the product itself.
4. Moulds made of composite materials have less durability because they tend to lose their ability to sustain vacuum and/or pressure integrity [40].
5. Moulds offer limited flexibility in case of damage. If the mould suffers some type of damage, it must be repaired (if possible) or re manufactured, leading to a delay in production. The last scenario directly affects the supply chain of composites manufacturing [41].

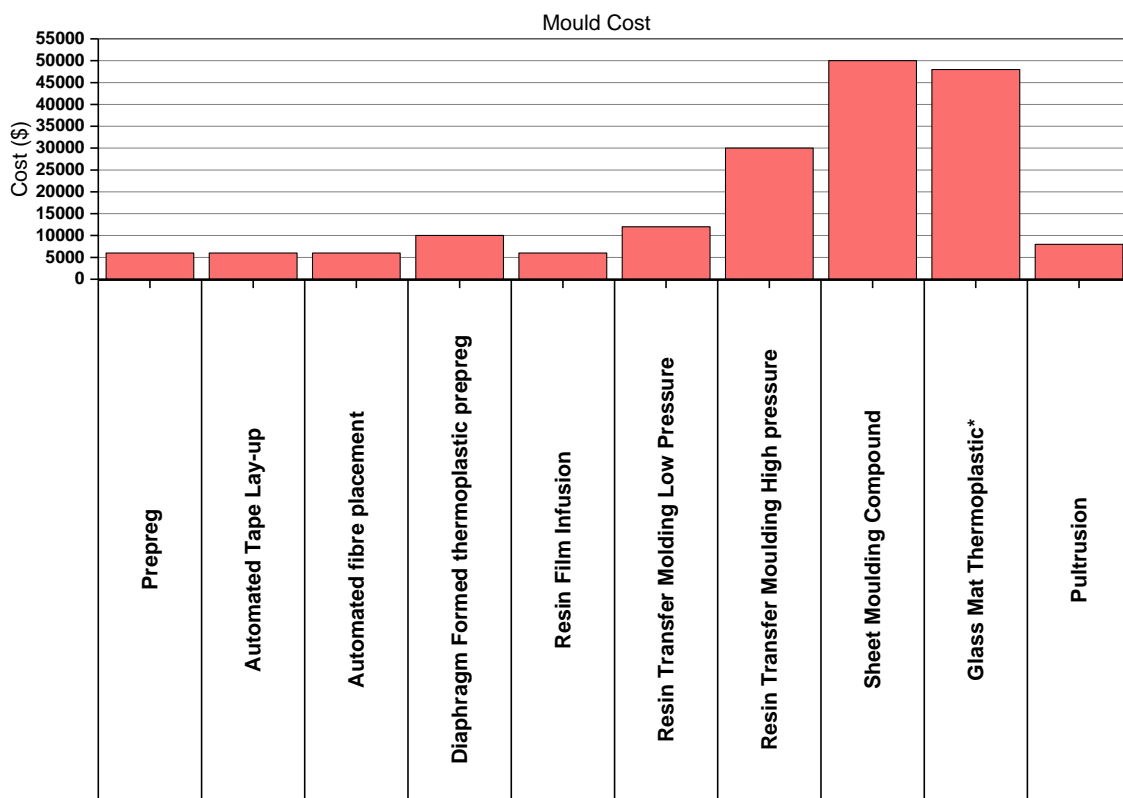


Figure 1-3 Tooling cost for different composite manufacturing techniques. In general, low-pressure systems are cheaper than high-pressure systems. Data obtained from [42]

In the past few years, rapid prototyping techniques such as additive manufacturing or incremental sheet forming have attracted special attention due to the possibility to eliminate the production of moulds for different materials such as polymers and metals. However, their research field is still in early stages, thus resulting in products with defects and poor properties

such as high void content and poor interfacial strength between fibres and polymers (See Chapter 2 Literature Review).

To the author's knowledge, there has been no attempt to replace a close mould in a flexible approach in which only a one side mould is used with the addition of a small tool that in-situ consolidates self-reinforced composites. This is the first attempt to partially eliminate the use of closed moulding in self-reinforced composites. This new concept might to reduce time and costs, especially for low volume productions. Manufacturing time will be reduced because only the bottom mould is manufactured. The top mould is then replaced by the thermoforming action of one small and easy-to-manufacture tool that in-situ consolidates the raw material by conforming it to the mould as illustrated in Figure 1-4.

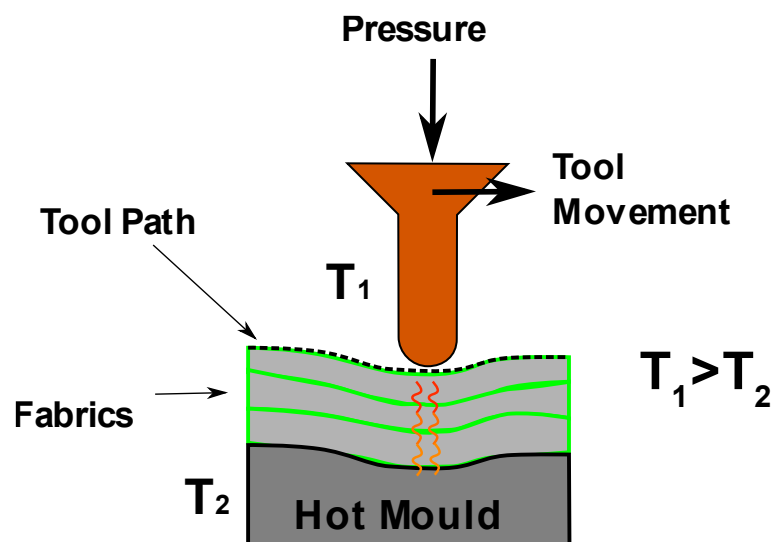


Figure 1-4. Schematic of the automated in-situ consolidation process. The temperature of the forming tool is higher than the temperature of the mould. The tool path copies the shape of the surface of the mould to produce a net shape component.

Furthermore, this research is part of the first steps towards mould-less fabrication of fibre-reinforced composites at the University of Sheffield in which both moulds can be replaced by small thermoforming tools that in-situ consolidate and give shape to the material. It is envisioned that this system can reduce time and costs, especially for low volume productions. Manufacturing time will be reduced as the time to cool down the matrix does not depend on the cooling down the mould. Costs will be reduced as there is no need to manufacture two pieces of moulds, and there is no energy required to heat a mould. Similarly, it could lead to the exploration of new flexible routes for outside-factory production, and it can be built with low-cost materials and low-cost automation products. However, mould-less

fabrication of fibre-reinforced composites was out of scope of this project due to time constraints.

## 1.6 Research objectives

This PhD thesis documents the development of a low-cost automated in-situ consolidation manufacturing process for the production of self-reinforced polymer composites. The preform selected is based on polypropylene in the form of bicomponent tape due to their commercial availability. Flat and double curvature laminates have been investigated under different processing parameters such as pressure and temperature to understand their influence on final material properties. This required a number of objectives:

### 1.6.1 Objectives

- To design and built a low-cost automated system for in-situ consolidation of self-reinforced polypropylene composites. Furthermore, sensors are installed to control processing parameters such as temperature and force.
- To create a thermal transfer model and validate it through experimentation
- To fully characterise fabricated components to assess the influence of processing parameters on the resultant material properties and compare them against a benchmark process such as Hot Compaction. The characterisation techniques and their primary objective of study that were used in this thesis are listed below:
  - Mechanical Properties
    - T-peel tests: Interlaminar strength
    - Tensile tests: Young's modulus and maximum strength
  - Morphological properties
    - Microscopy: Qualitative information about the microstructure.
    - DSC: Changes in Crystallinity
- To study the formability of the material using a simple case study including material characterisation: Dome

## 1.6.2 Thesis Outline

Chapter 2 *Literature Review* provides a comprehensive literature review of the new automated manufacturing techniques for fibre reinforced composites and discusses their advantages, disadvantages, and challenges.

Chapter 3 *Process and Machine Development* describes the manufacturing process and documents the development of the automated platform. It details the selection of suitable manufacturing hardware for motion control and the software strategies to achieve a control system of processing parameters. It also describes the manufacturing workflow of the automated process. Finally, its energy consumption is studied to determine its efficiency compared with a benchmark manufacturing process.

Chapter 4 *Forming mechanisms* explain the physics behind the automated process, including the bonding mechanism of two polymer interfaces and the heat transfer mechanism.

Chapter 5 *Two-dimensional laminates and characterisation* documents the manufacturing process of flat laminates under the proposed automated process. It also characterises the properties of the laminate to understand the influence of processing parameters. The results are compared with flat laminates developed with a benchmark manufacturing process.

Chapter 6 *Three-dimensional laminates and characterisation* documents the manufacturing process of laminates with three-dimensional curvatures under the proposed automated process. The resultant parts were characterised and compared with a benchmark manufacturing process for their energy absorption and geometric accuracy.

Chapter 7 *Conclusions and Future work* summarises the key findings from this project and proposes future work that can improve the reliability of the process or expand its use for further developments.

## 2 Literature Review

This literature review describes in general terms how a composite material can be produced before exploring current automated techniques for manufacturing fibre-reinforced composites to reduce manufacturing costs, especially for low volumes. The main techniques discussed are additive manufacturing and incremental sheet forming. They attempt to eliminate the use of moulds/tooling, which is one of the most expensive processes in composites manufacturing. This chapter intends to summarise the scientific efforts, highlight their advantages, and critically review the disadvantages.

### 2.1 Composites Manufacturing

A composite component can be produced by maintaining the fibres and the polymer (in liquid or a malleable state) in the required shape until it becomes solid. Nevertheless, choosing a manufacturing technique mostly depends on the material feedstock, type of polymer, geometry, and available facilities[43]. Most composite feedstocks are a combination of dry fabrics that will be subsequently impregnated with a liquid matrix, or in some cases, pre-impregnated fabrics. Because of this, most parts are created in a layer-by-layer approach since individual plies are laid up or stacked over each other to form a composite laminate. These individual plies can be cut to size by hand or by an automated process. The size and complexity of the geometry of the component limit the type of mould and consolidation process. For example, simple geometries can be formed with almost all techniques, but hollow structures require different approaches like closed moulds or pultrusion.

The degree of consolidation is often determined by the processing parameters (e.g., pressure and temperature), which are determined by the facilities available [10, 43]. For example, autoclaves are used for good degrees of consolidation due to the uniform pressure distribution over the whole surface. Hot presses also achieve good consolidation and faster cycle times. However, they cannot apply a uniform pressure distribution on vertical surfaces limiting geometric flexibility. Automated tape placement or automated fibre placement can achieve in-situ consolidation while laying up prepreg tapes or yarns. However, post-consolidation is often required to improve the quality of the part because of the compaction pressure variability while laying up [44, 45].

In general, to achieve a good consolidation quality, each technique must ensure conformability of the material to the mould, pressure to keep the material together, and heat transfer to promote phase transformations in the matrix. Conformability generally depends on the raw materials being used and the complexity of the shape. Dry fabrics have better drapability than pre-impregnated fabrics since fibres are less restricted to conform to the mould. The Heat transfer mechanism is critical in thermoplastic composites manufacturing because material transitions phases depend on it (e.g., melting, solidification, and crystallisation). Higher temperatures are required for the polymer to achieve a low viscosity. Second, the heating method should quickly raise and decrease the temperature of the component for rapid manufacturing cycles. However, this is a complex engineering challenge mainly because of the low thermal conductivity of polymers and the big thermal masses of the moulds.

Table 2-1 Advantages and disadvantages of heating methods

Heat Transfer Method	Advantages	Disadvantages
Radiation IR & lasers, microwave	Rapid-Heat transfer High local heat capacities Low cost for Infrared lamps	Dependent on the absorption spectrum of the material Difficult control on dynamic applications Easy to overheat the material Difficult to heat non-flat materials Large temperature gradients through-the-thickness High cost for Lasers
Convection Hot gas	Low risk of overheating No risk of oxidation or ignition if an inert gas is used Uniform through-the-thickness in materials with high surface-to-volume-ratios (powder, commingled, prepregs)	Low heat transfer rate
Conduction Hot moulds	Good heat transfer control	Adhesion to moulds
Mixed Open flame (radiation + convection)	Low cost Local heat area capacity Reduces oxidation	Difficult to control Risk of ignition and overheating

Any reasonable heating method has attempted to improve heat transfer in manufacturing cycles [46]. The most common heat transfer methods are conduction, convection, and radiation. Radiation is usually generated through Infrared lamps (IR), lasers or microwaves; convection heat transfer is caused by flowing a hot gas next to a surface, and conduction is generated through direct contact with hot material. A summary of the advantages and disadvantages of heating methods is presented in Table 2-1.



## **2.2 Additive Manufacturing of Fibre-Reinforced Composites**

Additive manufacturing (AM) or 3D printing creates a three-dimensional structure by the successive addition of layers [47]. It has several advantages since tooling is no longer required, material waste is reduced, and repeatability can be achieved. Many industries adopt additive manufacturing since it allows building complex near-net-shape three-dimensional structures that are impossible or difficult to produce via traditional techniques in different materials (i.e. polymers, metals, ceramics, etc.) from a CAD model. Currently, it is mostly used for rapid prototyping purposes and low volume applications such as jewellery and prosthesis. In the composites field, additive manufacturing has been used in direct or indirect approaches. In the direct approach, a composite part is created without using a conventional mould, while in the indirect approach, AM is used to manufacture a mould rapidly. The next sections show how some of those processes have been adapted to produce fibre reinforced composites. In addition, it also presents a critical evaluation of significant processing parameters and the resultant mechanical and morphological properties of composite specimens.

### **2.2.1 Material Extrusion**

Fused Deposition Modelling (FDM) is the most known material extrusion technique. Generally, a filament of low-melting-point thermoplastic material is introduced, heated and melted on a nozzle, and further extruded into a bed (X-Y plane) in a controllable manner to create layers. Each layer is fused, cooled and solidified to the previous one to create a three-dimensional part. The first FDM patent process was granted to Stratasys in 1992 [48], and since it expired, this process has been widely spread due to the reduction of the 3D printer prices. However, 3D printing thermoplastics present structural limitations. Because molten layers are deposited over cool layers, the interfacial bond strength is weak, resulting in parts with low stiffness and strength, especially in the Z-axis direction, which has limited its application to structural components. In addition, three different approaches have been recognised to overcome this limitation by using fibre reinforcements: 1) to use a reinforced filament as feedstock, 2) to adapt the deposition head, so the fibres are impregnated by matrix inside it, or 3) to deliver both fibre and matrix separately to create composites like a sandwich structure.

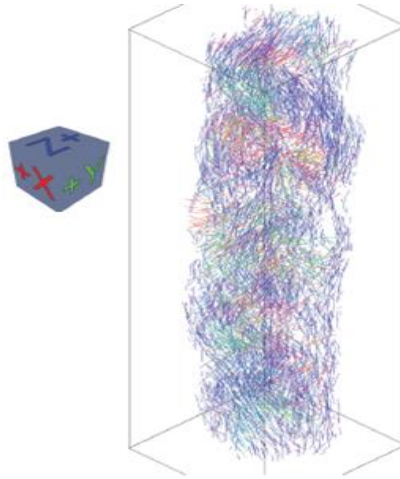
### 2.2.1.1 Fibre-Reinforced Filaments

Most of the scientific effort has been concentrated on using fillers such as particles [49-52], nanoparticles [53-57] and short-fibres to reinforce the polymer filament. For the latter, short-glass and carbon fibres [58-67] were mainly used because they are commercially available and provide a better improvement in mechanical properties. In the same way, the use of other fibre reinforcements such as recycled wood fibres has also been reported [68]. As shown in Figure 2-1, a short-fibre-reinforced filament is created via several processes. First, the fibres and the polymers are blended before being extruded as a filament. The filament is further extruded to obtain a dense reinforced filament. However, long fibres break during the mixing process, which reduces the mechanical properties since the length of fibres is shorter than the critical length for an optimal reinforcement [69]. On the other hand, long and continuous fibre-reinforced filaments have been developed using pultrusion based processes that impregnate a thermoplastic matrix in a readily available commingle yarn, leading to fibre volume ratios up to 60%. [70].



Figure 2-1 Representation of an FDM reinforced filament fabrication. In the first steps, the plastic and the reinforcement are blended before being extruded into a filament. The filament extrusion is repeated until a dense filament is achieved [60].

One important aspect of FRP composites that adds to optimal mechanical properties is the orientation of the fibres aligned with the load path. Hofstatter *et al.* [67] investigated the position and orientation of fibres in a freely extruded filament of PLA/Carbon in a vertical position, as shown in Figure 2-2. The different colours indicate the orientation of the fibres in the X, Y, and Z-axis, respectively, after being extruded. It can be observed that most of the fibres are aligned with the direction of the polymer flow. The extrusion nozzle is usually aligned with the Z-axis, but the deposition process is in the X-Y [22-32]. It is believed that this alignment results in increased stiffness and strength in comparison with the base material.



*Figure 2-2 Microtomography of a freely extruded PLA filament reinforced with carbon fibres. The colours in the pictures show the orientation of the fibres. Blue is aligned with the Z-axis, green is aligned with the Y-axis, and red is aligned with the X-axis [67].*

Yang et al [71] have studied the flow fibre flow and void formation during 3D printing of short fibre reinforced thermoplastic composites using CT scanning which helped to understand the void formation and alignment process during filament deposition. Basically, during the extrusion process inside the nozzle, fibres are kept aligned according to the flow direction or the extrusion boundaries (nozzle walls), and voids are kept to a minimum or are barely noticed as shown in Figure 2-3. However, while the filament reaches the exterior of the nozzle, the die swell effect promotes voids, and therefore, fibre misalignment around them as shown in Figure 2-4. The main reason for void formation and fibre misalignment is a combined effect between the die swell effect of the polymer a weak fibre-matrix bonding. After being extruded the internal pressure of the polymer is released and compensated with the atmospheric pressure promoting die swell which is partially constrained by the short fibres. During the die swell, the lateral expansion forces the fibres to lose the alignment, and this misalignment then promotes void formation.

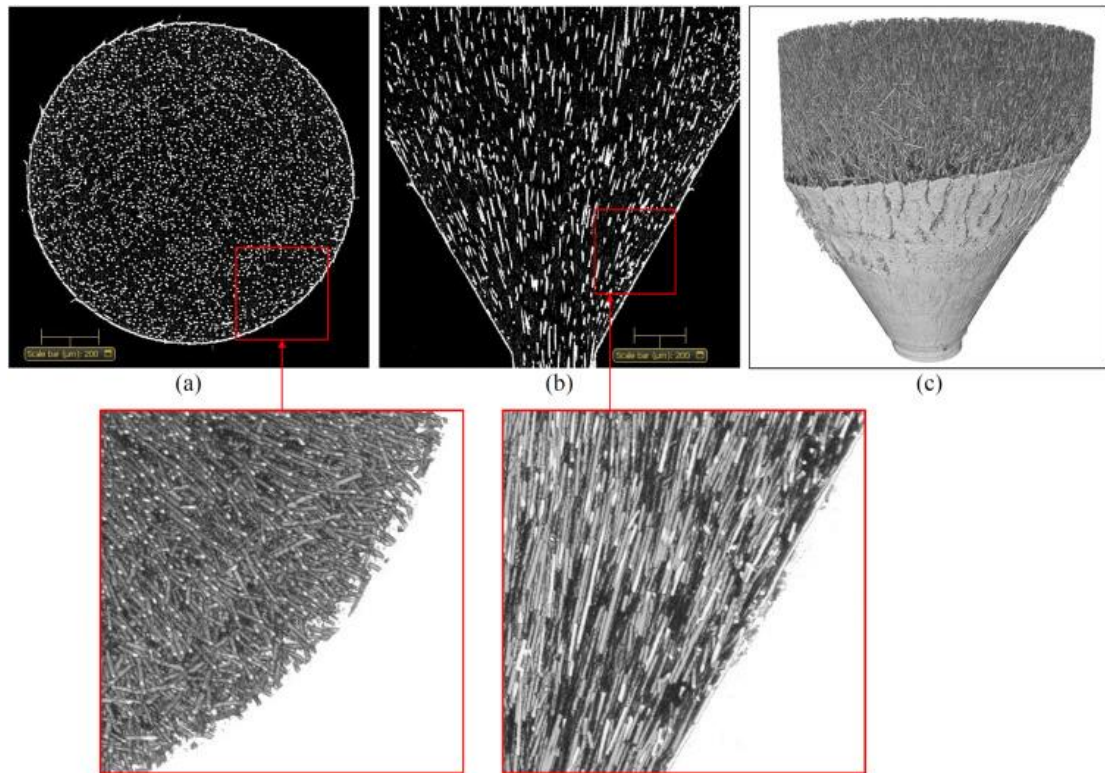


Figure 2-3 CT scans during extrusion of short-fibre thermoplastic composites on a 3D printing nozzle

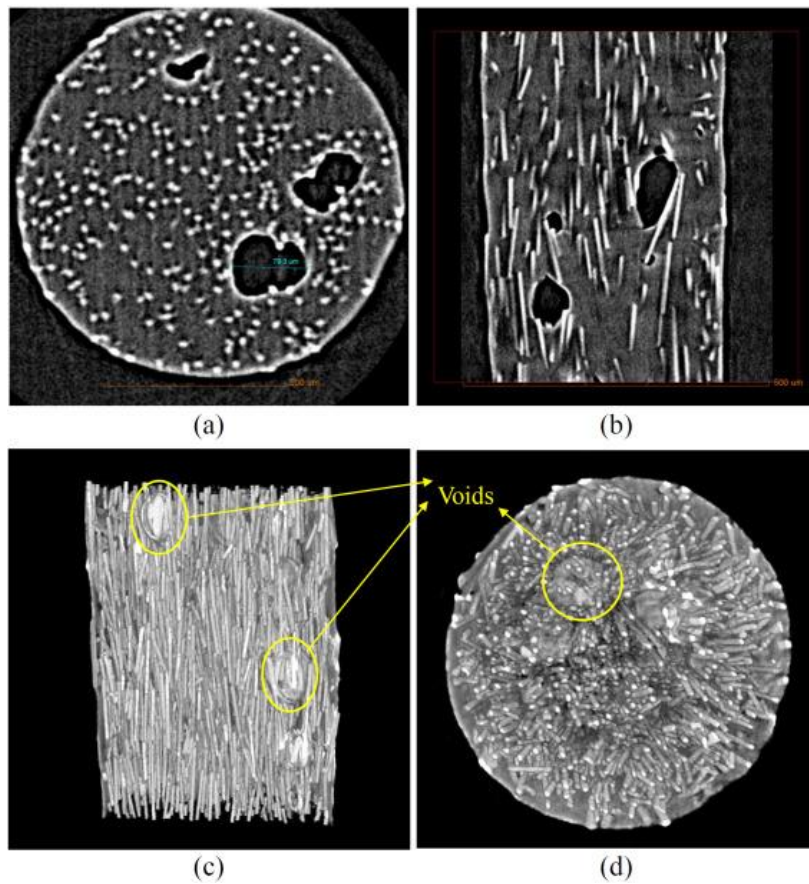
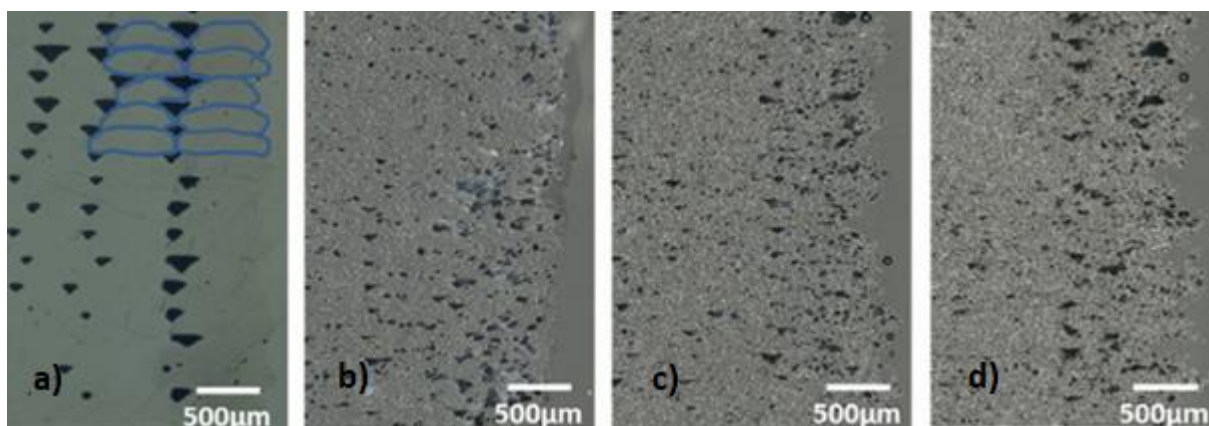


Figure 2-4 CT scans during extrusion of short-fibre thermoplastic composites after the filament exited a 3D printing nozzle

Most of the literature focused on the resultant mechanical properties and microstructure of different matrices and reinforcement. Table 2-2 shows the fibre orientation and the fibre volume fraction achieved. The highest strength (257 MPa) has been obtained from all the materials tested with a PEEK/Carbon composite, while the highest modulus (24.54 GPa) with an Epoxy/carbon fibre/silicon carbide composite [23].

*Table 2-2 Material properties of Short-Fibre Reinforced Filaments. The highest values have been achieved using engineering thermoplastic polymers and high fibre volume fractions. Reproduce with permission from the authors [23].*

Material	Fibre Content	Orientation to print direction (degrees)	Young's Modulus (GPa)	Strength (MPa)
Carbon Fibre-ABS	10	0	~8	~52
	20	0	~11	~60
	30	0	~14	~65
	40	0	~14	~68
SWNT-ABS	5	NA	~0.3	~22
			~1.75	~33
VGCF-ABS	5	NA	~0.25	~20
			~1.3	~27
VGCF-ABS	10	0	0.79	37.4
	10	10/0	NA	24.4
Glass fibre-ABS-LLDPE-PE	10.2-13	0	NA	38.93-58.60
		90	NA	0.72-11.15
Silicon Carbide Whiskers-Epoxy	32	0	16.10	96.6
	32	90	10.61	69.8
Carbon fibre/Silicon Carbide Epoxy	34.8	0	24.54	66.2
	34.8	90	8.06	43.9
Carbon Fibre Peek	30	0	9.4	257
	30	90	3.6	124
Glass Fibre-Polycarbonate	30	0	7	130
	30	90	7	130
Carbon Fibre Reinforced PLA	1	0	5.8	90.0



*Figure 2-5 Microstructure of the cross-section of FDM dog bone samples without and with short-carbon fibre reinforcement. a) 0%  $V_f$ , b) 10%  $V_f$ , c) 20%  $V_f$  and d) 30%  $V_f$ . FDM printers produce a layered structure with triangular gaps in between each printing path. The addition of fibres modifies the microstructure reducing the size of these gaps. [59]*

Figure 2-5 shows typical morphologies taken from the cross-section of tensile coupons at different fibre volume fractions ( $V_f$ ). The microstructure without reinforcement ( $V_f=0\%$ ) shows tube-like extrusions which are highlighted as “blue ellipses” in Figure 2-5(a). The triangular black spaces correspond to the resultant voids promoted by the shape of the extruded filaments that are deposited one next to each other. This phenomenon is explained by Tekinalp *et al.* [59] as the interaction between external and internal forces in the material, such as normal substrate force and polymer chain relaxation (Die-swell). After extrusion, the material is deposited and pressed against the previous layers, which flattens the bottom of the extruded filament. The top of the extrusion is then left to cool without any pressure, which allows chain relaxation, forming round edges. As the fibre volume fraction increases (Figure 2-5(b), Figure 2-5(c), and Figure 2-5(d)), it can be seen that the size of the voids is greatly reduced because carbon fibres restricts the die-swell of the polymer [59].

Die-swell, also known as the "barus effect", is defined as an increment in the diameter of an extruded polymer filament compared to the diameter of the extrusion nozzle [72], as illustrated in Figure 2-6. It is governed by the interaction of three factors: molecular weight, molecular distribution, and flow conditions such as shear rate and share stress. The dimension and shape of fillers added to the polymer strongly affect the flow behaviour of the resultant material. Fibres resist the flow as they enter the nozzle increasing the shear stress of the polymer. This shear stress then forces the fibres to align according to the flow direction. Once the polymer mixed with fibres exits the nozzle, the polymer will naturally die-swell, which is now restricted by fibres[73].



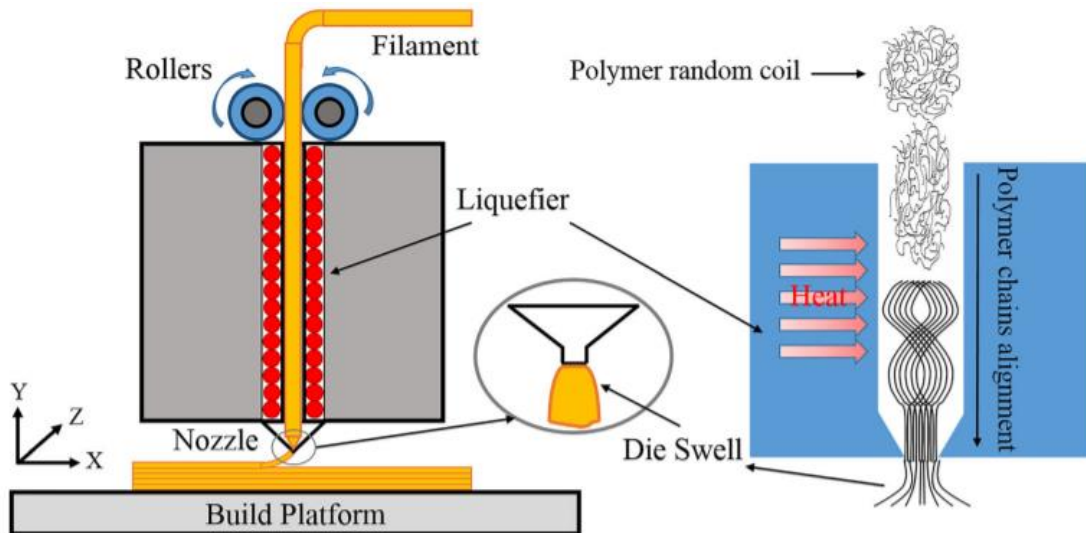


Figure 2-6. Schematic of Die-Swell in FDM. Reproduced with permission from the authors [72].

Figure 2-7 shows the morphology of a FDM component and a compression moulded component. The FDM component presents triangular gaps created by the deposition process compared with a relatively smoother surface from the compression moulded component. Furthermore, the FDM morphology shows a superior lack of material around the fibres compared with compression moulded component. This is associated with the difficulty to impregnate the fibres with the FDM process leading to a poor fibre/matrix interface, and therefore, reduced mechanical properties [26]. A weak interface increases the critical fibre length for optimum reinforcement since the matrix needs more time to build the stress required to break the fibres. More effort is needed to address the chemistry of the system to improve the fibre/matrix interface.

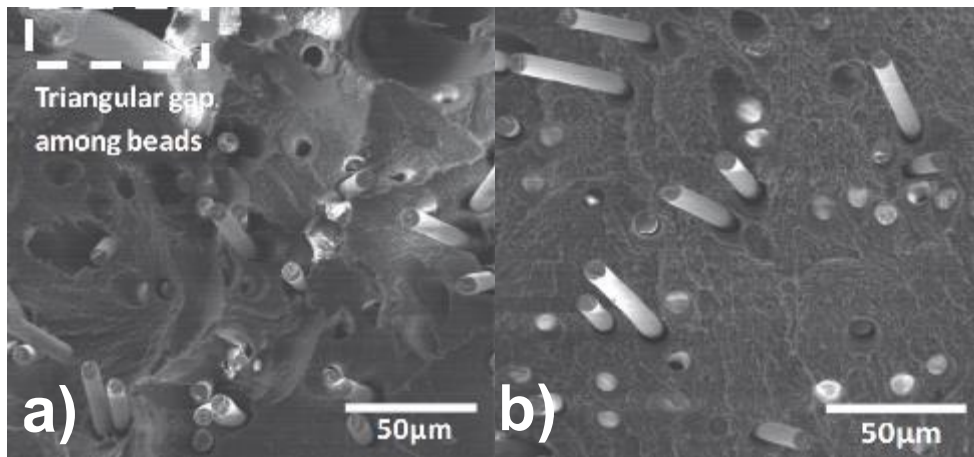


Figure 2-7 SEM micrographs comparison of fractured surfaces of ABS/CF composites. a) FDM printed cross-section with 10 wt.% carbon fibre, b) compression moulded cross-section with 10 wt.% CF loaded. [59]

### 2.2.1.2 Continuous Fibre Reinforcement – one deposition head

Attempts have been made to create an extrusion system that combines the reinforcement and the matrix in the deposition head [74-78] to produce a composite with continuous fibre reinforcement. Generally, both reinforcement and matrix are delivered separately into a heated nozzle, and then, by the action of heat, the matrix melts, wetting the reinforcement as illustrated in Figure 2-8. The extruded material then pulls the fibres in the printing process.

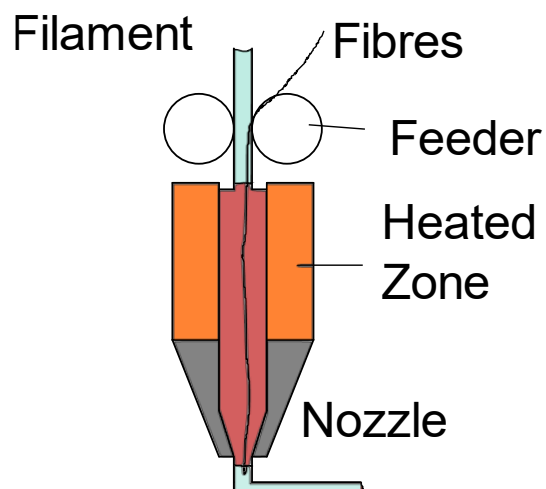


Figure 2-8 Process to reinforce a polymer filament with a continuous fibre in an extrusion material head for FDM Printers. Adapted from [77]



The first published attempt developed by Nakawaga *et al.* [76] was a failure because the polymer could not bond with the fibres, causing fibre breaking, poor fibre distribution and poor fibre volume fraction, as shown in Figure 2-9-a. However, real continuous reinforcement and improvements in fibre distribution and fibre volume fraction were later reported by Yang *et al.* [75]. Figure 2-9-b shows the cross-section of the printed part in which a carbon fibre bundle was directly inserted into the polymer in a molten state. The addition of carbon fibres resulted in an increment in the flexural and tensile mechanical properties. For example, flexural modulus and flexural strength increased 390% and 60%, respectively, while tensile modulus and tensile strength increased 200% and 300%, respectively, compared with the base material. Even though these results are a promising start for further development, these 3D printed parts do not match the properties of a composite produced via injection moulding. Another drawback is that the interlaminar strength was 8.5 times lower than the base material made via injection moulding. Finally, they have claimed to achieve 10% of fibre volume fraction, but in reality, it was a rough estimation not based on data.

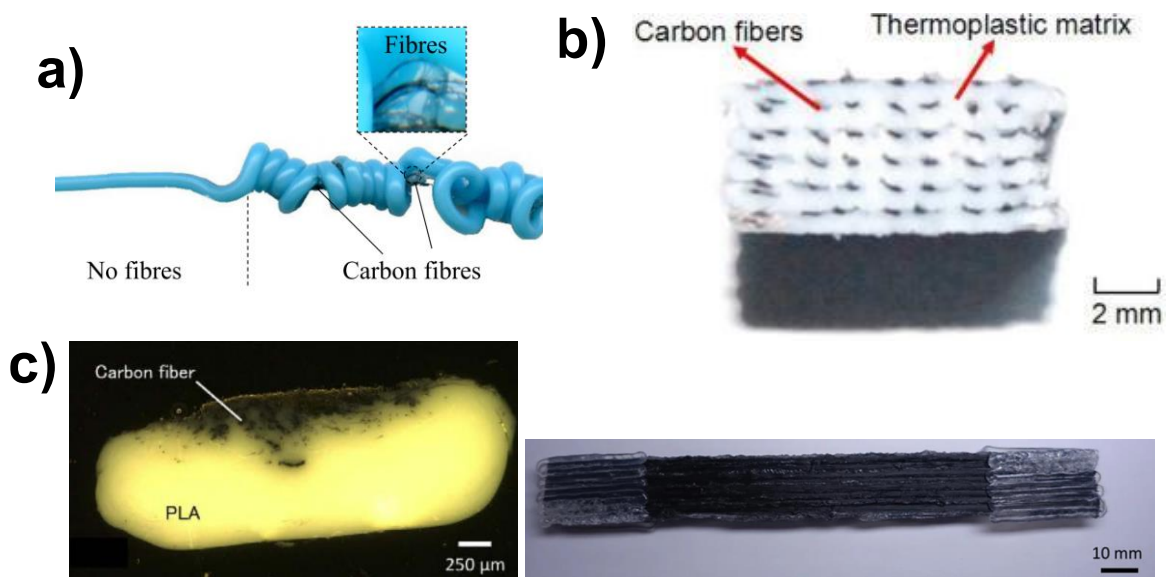


Figure 2-9 Summary of continuous fibre-reinforcement for FDM processes developed by a) Nakawaga *et al.* [76], b) Yang *et al.* work [75], and c) Matsuzaki *et al.* work [74].

Figure 2-9-c shows the results of work conducted by Matsuzaki *et al.* [74] to reinforce PLA with carbon and natural fibres using the same methodology but heating the fibres just

before delivering them into the nozzle. This improved the impregnation of fibres to the matrix, allowing extrusion of a continuous reinforced filament. However, low fibre volume fractions were achieved (e.g., 6.6% and 6.1% for carbon and natural fibres, respectively). The resultant Cf/PLA composite achieved an impressive increment of 499% and 335% in their tensile modulus and strength, respectively, compared to the base material. On the other hand, the reinforced improvement due to the addition of jute fibres is 57% and 34% in the tensile modulus and strength, respectively. Shortly after Matsuzaki's report, Yang *et al.* [79] also reported the printing process of a continuous reinforced 3d printed composite with carbon fibres and PLA. The improvement in mechanical properties found in this study also suggests possible structural applications.

Though advances are promising due to the reinforcement effects, they still do not represent a match for other composite manufacturing techniques [80]. For example, the process achieves low fibre volume fractions (~6%), poor interfacial bonding between fibres and matrix, high content of voids, and still cannot orient fibre in the three axes. These factors limit the mechanical properties and, therefore, their use in real-life applications. Similarly, to short-fibre, most of the focus of the literature was on mixing different polymers and reinforcement rather than addressing the chemistry of the system to improve the interface strength.

#### **2.2.1.1 Continuous Fibre Reinforcement – Delivering the matrix and the fibres separately**

Contrary to the previous technique, another approach that has been applied is to deliver the fibres and the matrix separately using one or two deposition heads (or nozzles) as illustrated in Figure 2-10 (a) and Figure 2-10 (b). In this case, the fibres can be deposited above a previous layer of matrix material using rollers inside or outside the nozzle. These rollers could also be used to press the fibres against the matrix to improve fibre impregnation. Finally, a mechanism is required to cut the filament according to the printing path.

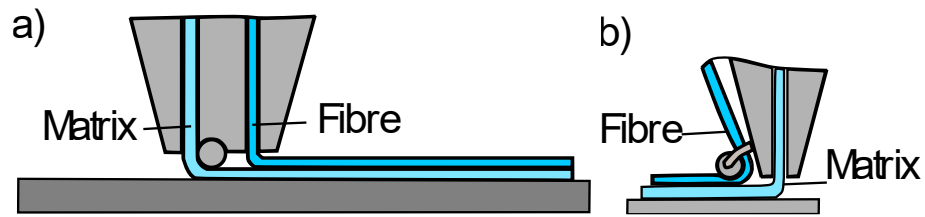


Figure 2-10 Schematic of a continuous fibre added to the matrix in an FDM process: (a) The matrix and fibre are extruded from the same nozzle, (b) the fibre is deposited with an additional nozzle [77].

Another approach developed, patented, and commercialised by MarkForge [81] uses two deposition heads to create composites like sandwich structures. One head prints a layer of nylon, and afterwards, the second deposits the continuous reinforcement (Carbon, glass or Kevlar) as illustrated in Figure 2-11. According to the patent, the yarn is pre-impregnated when passing through the reinforcement head in resin in an attempt to reduce the presence of voids.

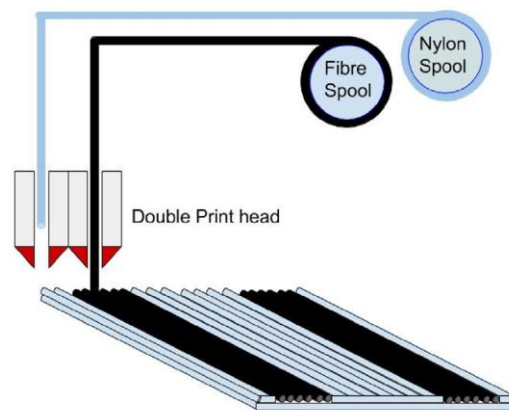


Figure 2-11. Schematic of the MarkForge 3D printing process using a double print head [82]

Two printing patterns were developed to offer fibre continuity, as illustrated in Figure 2-12(a) and Figure 2-12(b). A concentric pattern starts on the outside and moves inwards, and a parallel pattern (also called "isotropic") starts at one edge to finish in the other end. Figure 2-12(c) shows a schematic of the layered structure that is created in which the black layer are the fibre reinforcements, and the white layers are the nylon matrix. It was found that Kevlar and Glass fibres can be deposited with concentric and parallel patterns, while carbon was only suitable for the concentric pattern as shown in Figure 2-13. The authors suggest that a deposition pattern with two right angles too close to each other promote a break in the fibre due to the high stiffness of the carbon fibre [82].



Figure 2-12 Schematic of the MarkForge 3D printing patterns: (a) Concentric Pattern following the exterior boundary, (b) Parallel or Isotropic Pattern, and (c) Lay-up configuration in which the black layer are the fibre reinforcements and the white layers are the nylon matrix [82].

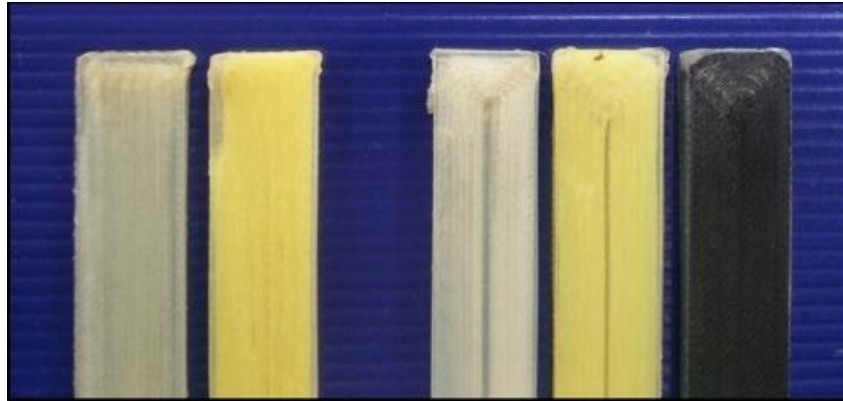


Figure 2-13 Examples of 3D Printed samples produce with a MarkForge 3D printer showing the reinforcement patterns. Parallel patterns were achieved for glass and Kevlar fibres while concentric patterns were achieved with glass, Kevlar and carbon fibres [82].

Due to its low price (~\$5000), it has attracted the attention of companies and researchers who have studied the mechanical properties, as shown in Table 2-3. The resultant material is several times improved in comparison to the base material. Though the modulus has relatively low values in comparison with metals, the tensile strength achieves promising values when the  $V_f$  increases. In fact, a maximum strength of 41 MPa for a 30-layer-glass specimen was obtained with a calculated 33% of  $V_f$  using an isotropic pattern [82]. This strength almost matches some aluminium alloys used in the aerospace industry, such as AL2024-T3 and AL6061-T6 [83].

Table 2-3. Mechanical Properties comparison of MarkForge 3D printed samples with other manufacturing processes and high-performance aluminium alloys. Adapted with permission from the authors [82, 83].

Reinforcement and Pattern	$V_f$	Elongation at break %	Elastic Modulus (GPa)	Tensile Strength (MPa)	Flexural Modulus (GPa)	Flexural Strength (MPa)	Flexural toughness (J/m <sup>2</sup> )
CF-Concentric [82]	11	4.51	8.46	198	13.02	250.23	356.51
KF-Concentric [82]	8	4.75	4.26	110	4.61	106.6	367.12
GF-Concentric [82]	8	7.21	3.29	156	3.87	165.79	650.90
KF-Parallel [82]	10	5.45	4.76	161	6.65	125.8	390.62
GF-Parallel [82]	10	8.6	4.91	212	4.21	196.75	693.88
Nylon [82]	0	439	0.53	61	1.06	41.98	262.32
Nylon [84]	0	-	0.9	-	-	-	-
CF_Parallel_2 layers [84]	34.5	1.05	1.25	149.5	-	-	--
Cf_Parallel_6 Layers [84]	34.5	1.65	35.7	464.4	-	-	-
Aluminium alloy 2024-T3			70	485			
Aluminium alloy 6061-T6			70	310			

However, its microstructure has revealed a high voids content, as shown in Figure 2-14 for Carbon/Nylon Specimens. In addition, analysis of the fracture zone revealed fibre pull out, which indicates a poor interfacial strength. In addition, the process is still inadequate to create out-of-plane fibre orientations, placing the process behind common manufacturing techniques.

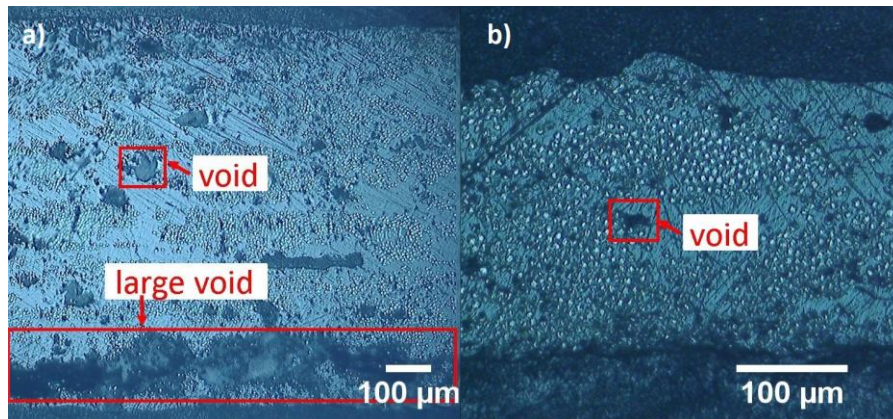


Figure 2-14 SEM pictures of the morphology of 3D printed samples with different lay-up configurations: (a) Carbon Fibre (6 layers)/Nylon (4 layers), and (b) Carbon Fibre (2 layers)/Nylon (8 layers) [84].

### 2.2.1.2 Robotics

Currently, few companies have showcased using robotics arms with FDM deposition heads to create three-dimensional reinforced structures, as shown in Figure 2-15. Arevo Labs, a U.S. company, presented in 2016 the first type of robotic FDM printer with a 6-axis-motion [85]. It has a high-performance thermoplastic-deposition head that can print continuous fibre reinforced 3D printed parts. Similarly, Stratasys released a Robotic 3D Composite Demonstrator [86] with an 8-axis robotic arm. It is claimed that there is a true possibility to create a true 3-axis alignment of fibres to optimise the mechanical properties, which could be an advantage over traditional methods. However, there are no reports of the final quality of the composites created.

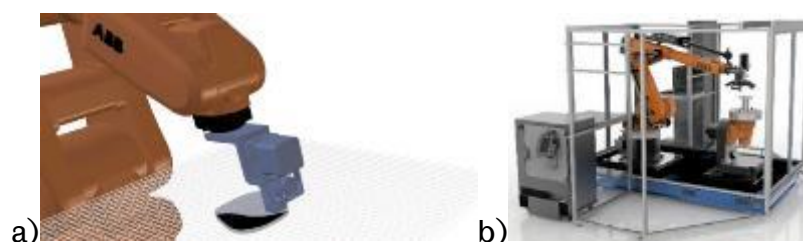


Figure 2-15 FDM robotic Systems: a) 5-Axis Arevo Labs Robotic FDM 3D printer [87]; b) 8-Axis Stratasys Robotic 3D Composite Demonstrator [86].

## 2.2.2 Sheet Lamination

Sheet lamination or laminated Object Manufacturing (LOM) is a process in which sheets or layers of materials (paper, plastic, ceramics, etc.) are cut according to a CAD model and stacked, compressed and glued together to form a three-dimensional object in an automated approach [47, 88]. LOM machines usually have a mobile platform with a feed system that moves the sheet through it, a cold or hot lamination roller that improves consolidation between layers, a laser cutting system, and a reservoir for the waste material, as shown in Figure 2-16.

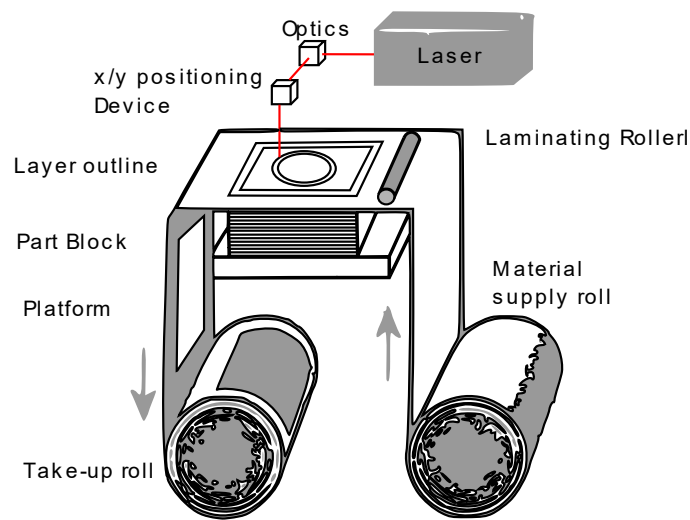


Figure 2-16 Schematic of Laminated Object Manufacturing Process. Reproduced from [89].

The first adoption of this technique to fibre reinforced composites was in 1996 by Chartoff *et al.* [89, 90]. They created composite panels from non-woven and unidirectional (aerospace grade) glass-epoxy prepregs rolls using a LOM machine. Though a roller was adequate to bond layers between each other, it was not enough for achieving full consolidation and curing. For this reason, the final part had to be moved to an autoclave, adding extra steps to the process, and therefore, eliminating automation. Figure 2-17(a) shows the resultant parts without (left part) and with autoclave curing (right and darkest part), while Figure 2-17(b) shows the morphology of the cross-section of the autoclave-cured part showing good matrix impregnation and no presence of voids. Though the consolidation levels are acceptable, the material waste might have stopped a broader adoption of the technique as new advances were not seen for several years. In fact, current advanced automated



manufacturing techniques of composites moved forward the deposition of fibres or tapes of fibres to decrease material waste.

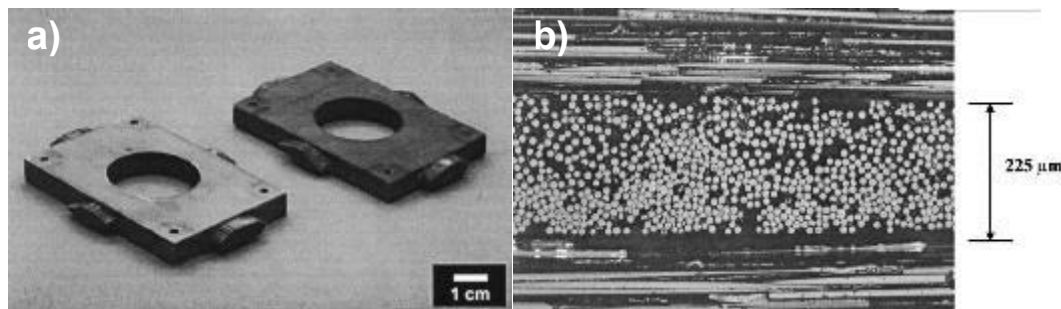


Figure 2-17 a) Laminated object manufactured parts. The right and darkest part was cured in an autoclave while the left one was not cured, b) Micrograph of the morphology of the autoclave part showing good interfacial bond [89].

In 2017, Parandoush *et al.* [91] proposed a similar approach called Laser-Assisted Tape Placement (LATP) technique. It uses unidirectional or bi-directional thermoplastic prepreg tapes and a laser to improve the compaction levels. The use of tapes instead of wider fabrics reduces waste material. The set-up has two platforms with CO<sub>2</sub> lasers. The first one heats the layers before compaction, while the second cut the tapes to their final dimension, as illustrated in Figure 2-18. Each layer is made of several tapes; therefore, all layers are first laid-up in the roller stage, and later, the final shape is trimmed in the cutting stage. This combination created composites with no visible voids or gaps between layers, as shown in Figure 2-19. However, excessive energy of the lasers can cause distortion and shrinkage of the material.

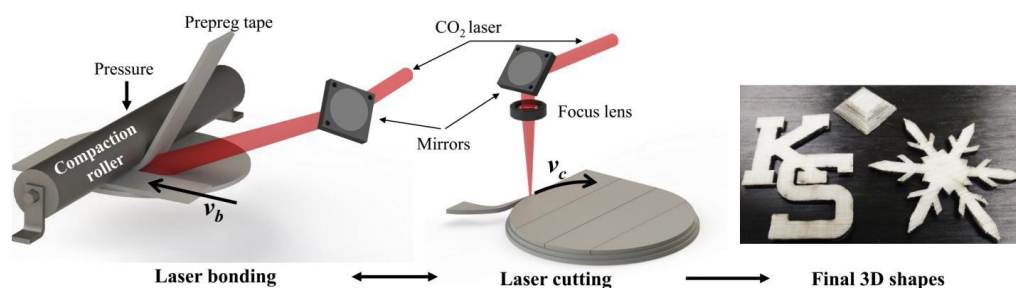
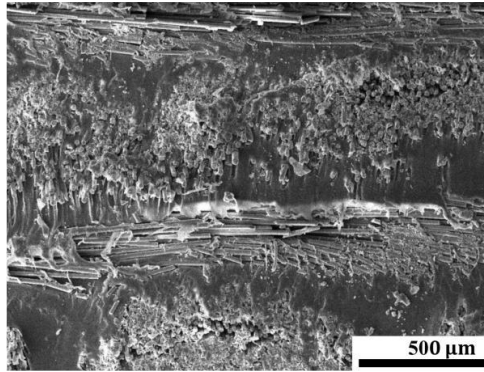


Figure 2-18 Laser-assisted tape placement process and final parts. There are a laser bonding and a laser cutting platform in which the part moves forward and backward[91]



*Figure 2-19 SEM image of the cross-section of a LAMP sample showing a good interlayer bonding achieved in the LAMP process. [91]*

Figure 2-20 shows the results of the mechanical properties investigated from the resultant composites. The parts have shown superior tensile strength and stiffness in comparison to the base material. Moreover, the tensile strength almost matched composites produced via compression moulding, and the flexural modulus achieved a 100% improvement. However, the Young's tensile modulus is about half the value of compression moulding composites. While using a heated roller might improve the compaction and bonding of the tapes, it has also been shown that it is not enough to achieve a sufficient interlayer bond strength in LOM parts [89, 90].



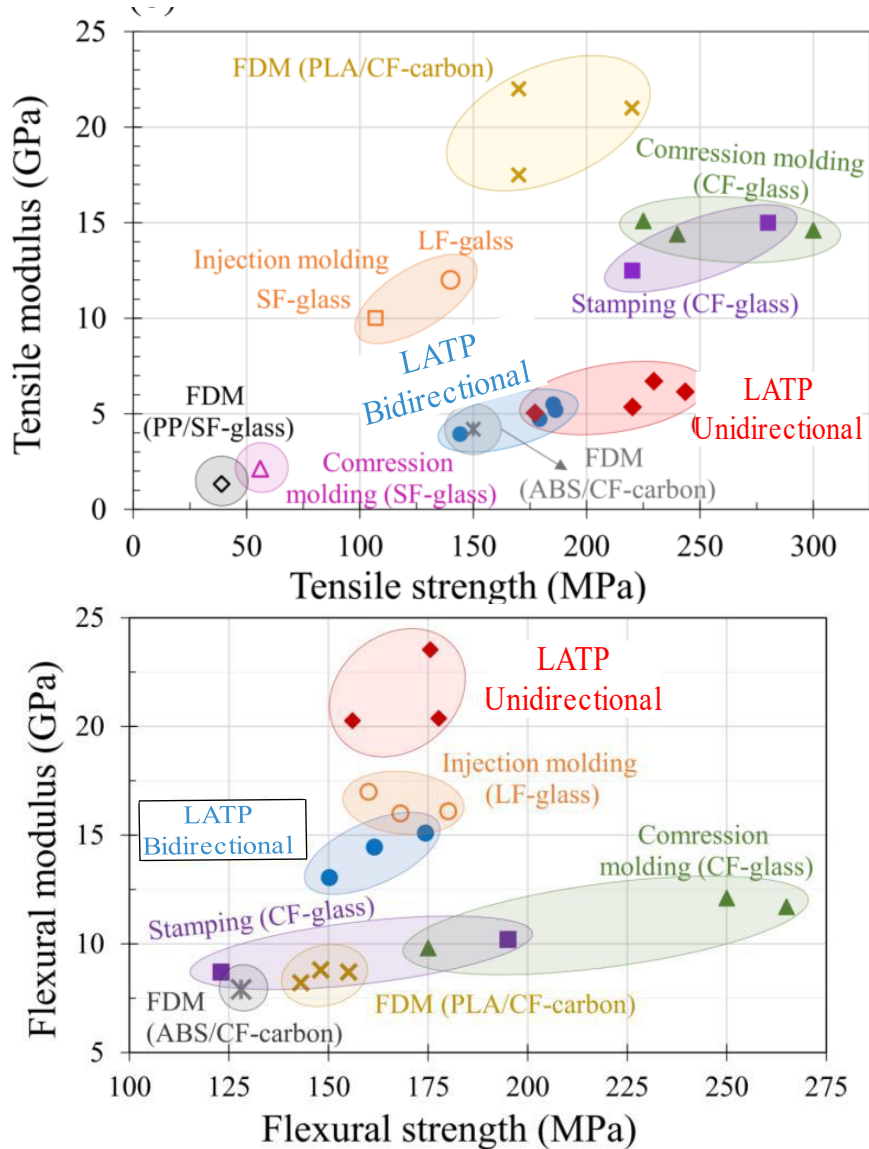


Figure 2-20 Mechanical properties comparison between different additive manufacturing techniques. LATP composites have the best performance in comparison with other rapid prototyping techniques. [91].

In the case of commercial systems, two companies showcased similar sheet lamination methods in 2016. Impossible objects [92] developed a patented technology that uses inkjet printing. They emphasise that its process is like printing a book in which each page is different from the other [93] and is illustrated in Figure 2-21.

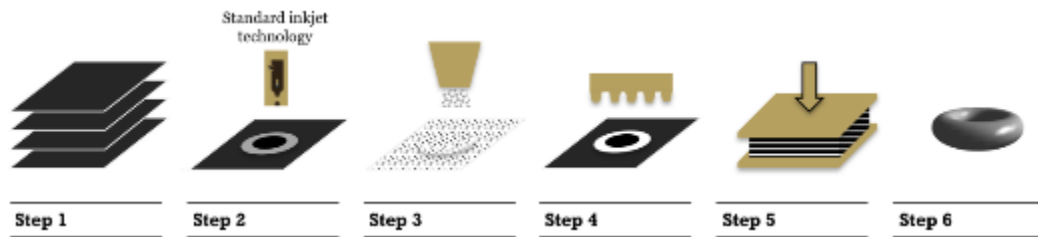


Figure 2-21 Impossible Objects Composite 3D Printer process. Step 1: Feed fibre sheet into inkjet printer; Step 2: Load CAD slices into printer and print layer shape of object on fibre sheet; Step 3: deposit polymer powder onto printed sheet which stick to where the sheet is wet from print fluid; Step 4: Remove dry powder; only powder stack to the print fluid remains; Step 5: stack sheets in order, heat to melting Temperature of the polymer, and compress stack to final part height; Step 6: Remove unbonded portions of sheet fibres to net final part [94].

The system uses a thermal inkjet head that selectively deposits a layer of an unknown liquid in separate sheets of woven or non-woven fabrics. The deposition pattern depends on a two-dimensional slice that resulted from a three-dimensional part from a CAD model. Then, the thermoplastic or thermosettable plastic powder is spread over the sheet, but it will only stick to the printed liquid areas. The excess powder that is not in contact with the liquid is then mechanically removed. Heat is then added to the system to evaporate the liquid and melt the polymer to impregnate the fibres. The resultant layer is then stacked and pressed (sometimes heated) one on top of the other to improve interlaminar consolidation. This process is repeated until a stack-up is formed, baked in an oven, or autoclave to be fused. Finally, excess material is removed using sandblasting or other techniques to obtain the final part. It can be understood that the system requires a lot of processing steps, and the advertised tensile strength is not better than other manufacturing processes.

Similarly, EnvisionTEC, a company with many years in the AM market, released the first industrial thermoplastic reinforced woven composite printer in 2016 [95]. It is advertised as a layer-by-layer approach called Selective Lamination Composite Object Manufacturing (SLCOM) to bond carbon, Kevlar, or glass thermoplastic prepreg sheets. However, the patent is pending, so it is difficult to evaluate how exactly it works.

### 2.2.3 Additive Manufacturing Summary

Though additive manufacturing might be considered one of the new industrial revolution technologies, the current techniques are not yet able to compete with other composite structures. All approaches gathered from the literature present significant

disadvantages such as 1) significant presence of voids and porosity, 2) poor matrix impregnation, 3) poor interfacial adhesion strength, 4) fibres smaller than the critical length for short-fibre reinforcement, and most important, 5) no out-of-plane fibre orientation. The first four factors are important to create good quality composites, while the last one could represent a significant advantage and a ground-breaking development. Generally, there is a lack of discussion of the polymer physics involved in the processes. Thus, literature related to the quality of the product has not been reported. Additionally, universities and businesses' use of these technologies is limited due to their high price (e.g. \$200000 - Impossible Objects, €1,000,000 - EnvisionTec machine.)

At present, there is only one system, the MarkForge 3D printer, which matches the strength of an aluminium alloy using nylon and continuous carbon fibre with the limitations described [82]. Moreover, the use of robotics seems to offer great innovative potential in developing true three-dimensional reinforcement, which can lead to optimal reinforcement in the direction of the force. Though there has been a great deal of effort and investment to implement this technology in every industry from aerospace to fashion, this review should inspire reflections on whether this technology will build high performance, lightweight, and strong parts made of fibre reinforced composites. Possible future research areas include overcoming actual limitations such as poor interfacial adhesion between fibres and matrix, voids and porosity, fibre alignment, fibre length, fibre continuity, and strength or stiffness tailored structures. It could also involve the use of high-performance fibre reinforced thermoplastics suitable for the aerospace or automotive industries such as PEEK or Polyamide; the suitability for fibre reinforced thermoset prepregs and its processing parameters; the characterisation of defects; and the investigation of case studies for load-bearing applications.

### **2.3 Incremental Sheet Forming of Fibre-Reinforced Composites**

A new sheet metal manufacturing technology has evolved during the last few years due to its ground-breaking concept. The need for an expensive and complex mould is eliminated. It is called Incremental Sheet Forming (ISF) because a spherical-end tool incrementally forms by deforming/stretching a metal sheet until a specific geometry is formed, as illustrated in Figure 2-22. It is also considered a cost-effective technique due to the reductions of costs associated with mould making. This technology has attracted the attention of the automotive

industry due to the flexibility it offers to create customised parts in low volume productions and short forming cycles, and short development [96].

Incremental sheet forming has further been divided into two main categories. When a single tool is used, it is named Single-Point Incremental Forming (SPIF), and similarly, when using two opposing tools, it is known as Two-Point Incremental forming (TPIF). The advantage of TPIF is that it allows the formation of more complex geometries. Apart from this main divisions, other types of sheet-metal incremental approaches have been found in the literature such as spinning, flow-forming or water jet incremental sheet [97, 98].

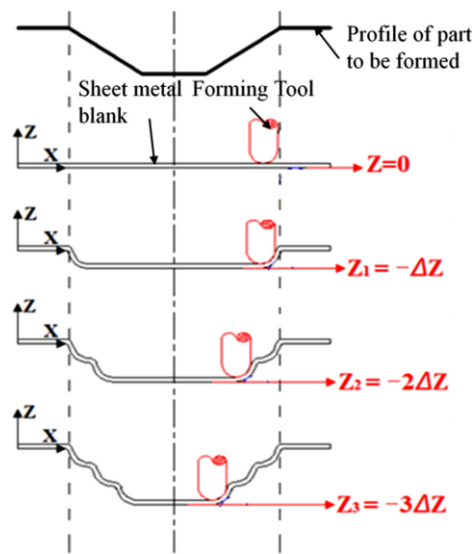


Figure 2-22 Schematic of Incremental Sheet forming process in which the forming tool incrementally deforms the metal sheet when it is moved down step by step [99].

Due to the advantages mentioned above, this technique was also adopted to form polymers sheets. The first report was published by Franzen *et al.* [100] in 2008. The formability of a commercial polyvinylchloride (PVC) sheet was evaluated under SPIF. From this study, other polymers were studied in the subsequent years: Polypropylene (PP) by Le *et al.* [101]; polyoxymethylene (POM), polyethylene (PE), polyamide (PA), polyvinylchloride (PVC) and polycarbonate (PC) by Martins *et al.* and [102]; polyethylene terephthalate (PET) by Marques *et al.* [103]; and Polycaprolactone (PCL) and UHMWPE by Bagudanch *et al.* [104]

Most of the studies focused on the formability limits of the material and the processing parameters involved. Figure 2-23 illustrates a typical set-up and its variables for clarification purposes. The analysis of the available literature reveals that tool diameter, step size, feed rate, and spindle speed are common parameters that influence the final formability of

thermoplastic materials. In contrast, a cone-shape generated by a spiral path of the forming tool is the usual test geometry. The formability of the sheet is related to the maximum wall angle or depth of the cone before tearing and/or failure. Failure modes involve 1) tearing in the circumferential direction at the boundary between the wall and the corner radius; 2) wrinkling in the circumferential direction, 3) tearing in the radial direction at the formed wall, and 4) flying shards of melted material due to the friction generated by the tool. Furthermore, whitening of the samples is commonly seen due to the induction of crazes associated with the disentanglement or change of orientation of the polymer chains [105].

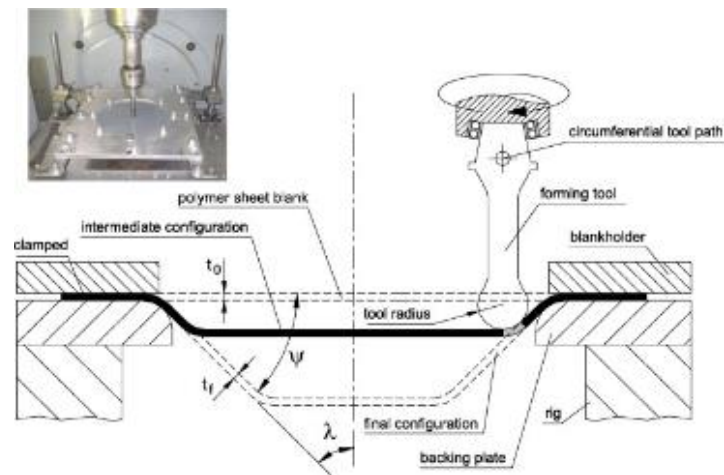


Figure 2-23 Incremental forming Set-up and Variables involved in the process such as tool radius, angle wall, initial thickness, final thickness, and tool path [102].

Since 2010, knowledge of SPIF of Polymers has started to expand. Silva *et al.* [106] provided the first theoretical forming model of SPIF of polymers based on a membrane approach developed for SPIF of metals by the same team in 2008 [107]. However, it could only explain the increased formability with thicker polymer sheets. Their model requires further development to explain the relationship between all processing parameters and experimental results. Silva *et al.* [108] also investigated the applicability of SPIF in polymers to produce Hole-Flange sheets with PET and PC. Results suggest that PC shows better formability than PET under single point incremental forming. In 2014, Yonan *et al.* [109] studied the applicability of a sheet metal forming theory to plastic flow and failure in SPIF of PVC sheets. The results showed that the model could not be applied to polymers due to the different failure modes between metals and polymers.

Later, Bagudanch *et al.* [104, 110-112] executed several experiments to find: 1) the effects of processing parameters over the required forming force and temperature on SPIF of PVC, 2) the energy consumption and cost associated with SPIF of PC and PVC, and 3) the influence of spindle speed on the formability of different thermoplastic polymers. The results revealed that spindle speed is one of the parameters that contribute the most to formability, maximum forming force, and energy consumption of the process.

### **2.3.1 Polymer Composites**

To the author's knowledge, there is few attempts to adapt single point incremental forming in fibre-reinforced composites. For carbon fibre epoxy composites, one dummy sheet on top of a prepreg preform was used to indirectly incrementally form the composite prepreg. Then, because the resin is not cured but glued (prepreg is sticky) to the dummy sheet, the prepreg was later cured in an oven [113]. The dummy sheet is used to protect the prepreg from the breaking the fibres and promoting unnecessary misalignment in the fabric. For thermoplastic composites, not only a dummy sheet was used but a heating device was also added to soften the material while it is formed [114]. Parts with a maximum angle of 40° were formed before cracks appear. Following one dummy sheet a glass-fibre reinforced composite (PA6GF47) was incrementally formed using an already consolidated laminate between two Teflon sheets and two sacrificial metal sheets to form a sandwich workpiece [115]. Then, the sandwich structure is heated by a hot air gun only on the bottom surface before and during the forming process, as illustrated in Figure 2-24. The metal sheets protect the composite against the friction of the forming tool and confer the final shape to the composite. The Teflon layers stop the polymer from adhesion to the metal sheets. The samples achieved maximum angles of 55° degrees before cracks started to appear in formability tests. Though it is not pointed out in the study, it is clear the heating approach adopted (only heating the bottom surface) generated a temperature gradient in the workpiece (140°C on the Bottom metal layer) that might not enough to melt the polymer through-thickness. If the polymer doesn't melt, the fibres cannot move relative to each other in the matrix. Instead, the heating approach adopted suggests that the polymer is still solid when it is stretched by the forming process, and therefore, cracks appear. A similar approach was also followed by Conte *et al* [116] with similar results about the feasibility of incremental sheet forming on thermoplastic composites.

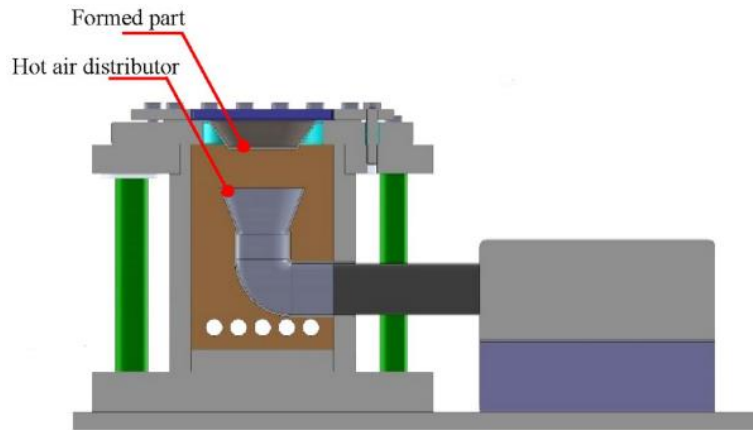


Figure 2-24 Incremental forming assisted by hot air gun. The hot air will heat the workpiece to the melting point of the polymer so it can easily be shaped [115]

The complexity of using incremental sheet forming approaches in composite materials relies in the fact that it is based on using pre-consolidated laminates with a complex internal structure and a different deformation mechanism than metals due to several factors such as raw constituents, fabric structure, fibre/matrix interface, anisotropy, among others. Thermoplastic composites are more ductile than thermoset composites, and can be reshaped; however, the deforming forces must overcome the fibre/matrix interface strength. A simple scenario would be using unidirectional laminates, but composites are characterised by its complex lay-up configuration, and therefore, there are fibre to fibre interactions that adds complexity to the forming mechanism. If the laminate is being deformed below its glass transition, the material will be rigid and strong due to the reinforcement effect of the fibres, therefore, a local deformation can lead to local fibre and/or matrix failure. If the material is being deformed above its glass transition, the matrix softens, but the crystals have not melted which complicates the relative movement of fibres in the matrix. Ideally, the matrix should be above its melting temperature for allowing the fibres to move, but without a mould, the melted matrix will fall due to gravity. Therefore, a sacrificial sheet is needed.

Global heating and single point forming of thermoplastic composites have been attempted by [116, 117]; and as mentioned, the reinforcement structure greatly influences its formability. In both cases, short fibres were used only to influence local deformation. If long fibres were used, higher forming forces would be required. The effect of a local deformation will also influence further deformation in the rest of the laminate because of the fibre matrix interactions.

### 2.3.2 Polymer Nanocomposites

Composites made of polypropylene and functional multiwall carbon nanotubes (f-MWCNT) have also been investigated to study the formability of the resultant material under SPIF [105]. Composite sheets with different weight concentrations of MWCNT (0.01% to 1%) were prepared via melt mixing and a hot compression moulding. The nanoparticles had a reinforcement effect on the material that reduced the formability as all specimens failed by cracking. Moreover, a variation in the colour was observed in the surface that was not in contact with the forming tool, which is associated with the appearance of crazes. It appears that due to the stretching of the polymer, tension forces appear in the outer surface leading to the disentanglement of the polymer chains. In addition, two-dimensional SAXS patterns revealed that both polymer chains and carbon nanotubes are mechanically oriented by the action of the forming tool in the z-axis. It was found that this behaviour had a bigger effect when the forming tool spins since it generates heat due to friction softening the material and allowing higher chain mobility. A major limitation was the agglomeration of f-MWCNT due to a poor dispersion in the matrix. Further research should improve this limitation and start to study the formability of the material as the next step.

### 2.3.3 Fibre-Metal Laminates (FML)

Fibre-metal laminates (FML) are composites made of thin metal layers and fibre reinforced composites (FRC). This combination of materials offers better damage tolerance to crack growth and impacts, particularly useful in aerospace applications. Fiorotto *et al.* [118] briefly investigated the application of SPIF to FML in two configurations: Metal/FRC and Metal/FRC/Metal. For both cases, Kevlar and glass-fibre thermoset prepregs were the raw material. In the first case (Metal/FRC), an aluminium sheet acted as a medium to avoid resin removal by the forming tool as shown in Figure 2-25(a). If the tool were in direct contact with the composite laminate, the polymer would stick to the forming tool. Vacuum bagging was used to improve the prepreg conformation to the aluminium sheet and to improve consolidation. As a result, as shown in Figure 2-25 (b), wrinkle-free parts were obtained after room temperature curing. Still, a minimal non-uniform distribution of resin was detected in the deepest zone of the cone.





Figure 2-25 Vacuum-assisted SPIF of a thermoset composite. (a) experimental set up using a vacuum bag to hold the laminate, (b) resultant part showing a non-uniform distribution of resin at the bottom [118].

For the second case (metal/FRC/Metal), the part started to show wrinkles and failed before reaching the final geometry, as shown in Figure 2-26. According to the authors, the incompressible nature of the prepregs might have prevented the transfer of stress between the aluminium sheets. Nevertheless, this statement is incorrect since an incompressible material only transfers stress. On the other hand, a compressible material deforms, and therefore, only part of the load is transferred. Additionally, this difficulty creating a defect-free part in a single operation led them to develop two separated aluminium sheets which were further used to make an FML composite (Al/composite/Al). This approach could be used to rapidly produce composite sheet tooling with savings in costs and time[119].



Figure 2-26 Fibre metal laminates under SPIF [118]. The laminate configuration is Aluminium/prepreg/aluminium. Both cases show a mechanical failure of the laminate during processing.

### 2.3.4 Incremental Sheet Forming Summary

The field of Incremental sheet forming in polymers is not mature. Similarly, as for metals, most early studies and current work have almost exclusively focused on formability of thermoplastic polymers since they are more malleable than thermosets, mainly brittle (except rubber). It was found that polymers present different additional modes of failure, such as crazing and tearing in the radial and circumferential directions. Most of the research found in the literature tends to focus on formability limits, with a lack of discussion of how polymers or their composites are processed. For example, no discussion about consolidation or bonding mechanism was found.

Though it is not mentioned in the literature, there are several limitations that SPIF presents for both thermoset and thermoplastic polymers and composites. In the case of thermosets, they cannot be reprocessed, and therefore reshaped once they have been already cured because they achieve a like “glass” brittle behaviour (except for rubber) which will make them crack and break under the presence of loads that exceeds their mechanical limits. Recently, a special type of re-shapable thermoset resins have appeared called vitrimers. [120]. Under the effect of temperature, the bonds of the crosslink network move from chains allowing them to be deformable and therefore being able to acquire a new shape when cool down. Nevertheless, trying to deform a common thermoset laminate will probably lead to local and brittle failure like performing a destructive flexural test

In the case of thermoplastics, they have the advantage of being *recyclable*. In other words, they can be reshaped if the material is heated, deformed, and cooled. Because the forming tool spins, it heats and softens the material due to friction, and that is why some success forming cone-like structures was obtained. If it is not heated, it will elastically or plastically deform until failure. Nevertheless, optimal processing of thermoplastic polymer and composites involves melting, flowing to shape a mould and/or impregnating the fibres, and cooling. This means that it needs to be contained in some boundaries. Otherwise, the melted polymer will drop and/or separate from the reinforcements due to gravity. That is why sacrificial metal sheets were used to protect the material and constrain it in a close boundary while under hot temperatures. Case studies, material characterisation, and life cycle analysis are required to make a proper comparison to suggest their use in industry. Finally, no study

has been found in which incremental forming can locally heat, form, bond, consolidate, and cool the material.

## 2.4 Alternative "Mould Free" Developments

As mentioned, Fibre-reinforced thermoplastic composites might take advantage of their material properties since they can be heated, softened, melted, and reshaped as many times as desired. However, fewer examples in the literature were found to exploit this ability. A technique developed and patented as a prototyping alternative was presented by Miller *et al.* [39, 121-123] in 1990. It can be claimed as the first attempt to create a die-less forming process of thermoplastic composites. The process propagates bends from the perimeter of the sheet into the interior by locally heating the material as it is moved through a forming zone, as illustrated in Figure 2-27. The composite is heated to the softening state and then bent as it passes through a cluster of automated rollers. The roller spacing is reconfigurable to control the type and degree of bending. Finally, the composite sheet is cooled by an "air knife" to leave the forming zone.

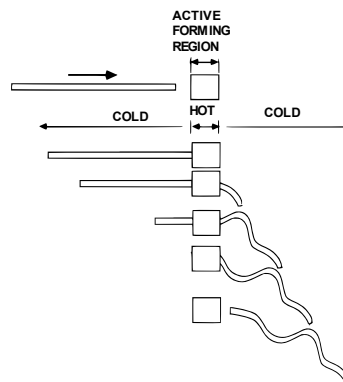


Figure 2-27 Net bending forming process [39]

This continuous curvature propagation assumes intraply sliding in the hot region and no change in the length of the fibres in the whole process. This assumption solves the problem in simple bending of composite laminates with continuous fibres, promoting fibre misalignment in the inside or fibre fracture on the outside, as illustrated in Figure 2-28. The team claimed the process was able to form constant and variable curvature parts. However, no evidence of the parts or their quality has been found.

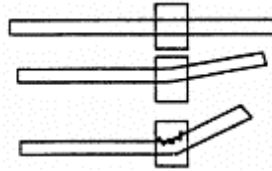


Figure 2-28 Definition of "Net Bending" [39]

Another attempt to incrementally form fibre reinforced composites (Glass fibre and Polypropylene matrix) was introduced and patented by Strong *et al.* [124, 125] in 1989. In this process, as illustrated in Figure 27a, a continuous transfer system holds a laminate and allows its movement from a small oven to a press with modular or interchangeable moulds. In this way, a non-linear and integrated part with non-uniform cross-sections is fabricated incrementally (or step-by-step), as shown in Figure 2-29b.

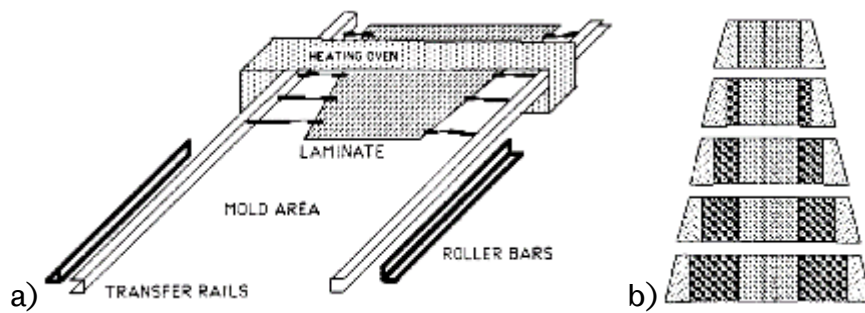


Figure 2-29 a) Strong's Incremental Forming Set Up. b) Top view of a part with a non-uniform cross-section [124, 125]

The oven allows the local heating of selected laminate regions until the thermoplastic matrix reaches a flowable condition. As the material is pre-impregnated, the polymer can flow to shape the new geometry. Another advantage of modular moulds is that they work as heat sinks, improving material cooling until solidified into its final shape. Then the next section is heated, and the protocol is repeated. It was found that using consolidated laminates led to better properties than un-consolidated laminates with a 55% higher tensile strength (541 MPa) and 252% higher impact strength (209 N/cm). Furthermore, good surface and defect-free parts could be formed since the movement between the pre-consolidated layers is constrained.



Figure 2-30 Reconfigurable multiple point tool [126]

Another approach was developed and patented by Northrop Grumman Corporation in 1997 and investigated by Walczyk *et al.* [126]. An automated reconfigurable tool was developed to analyse the potential formability of complex geometries via the diaphragm forming process. This type of tooling can modify its geometry during the forming process by increasing or decreasing the heights of their pins, as shown in Figure 2-30. Each pin has internal threads, so they are moved by a combination of drive motors, lead screws and sub-controllers. These are commanded by the main controller [127].

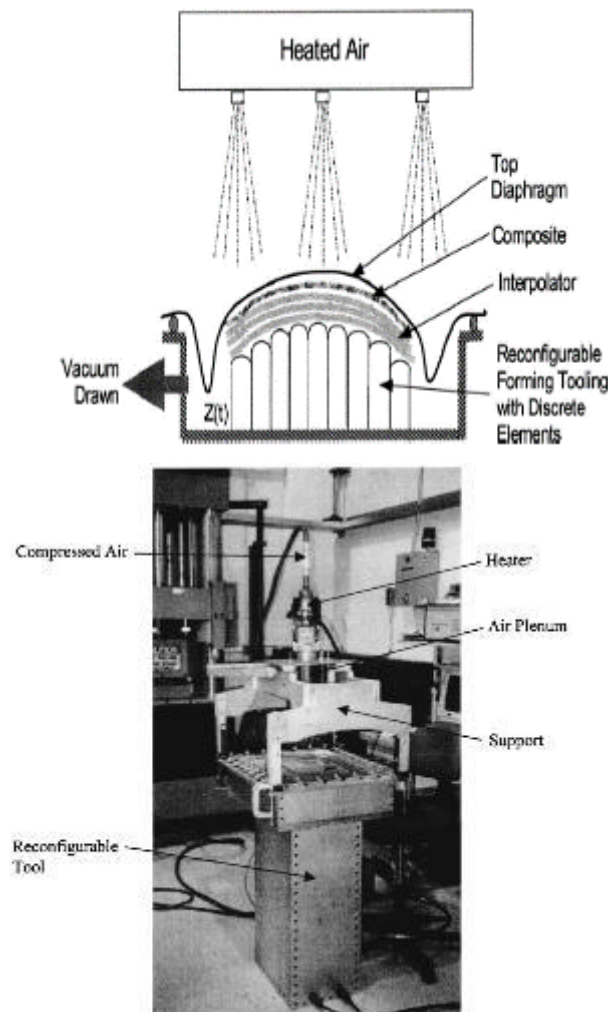


Figure 2-31 Reconfigurable tool forming process and experimental set-up [126]

As illustrated in Figure 2-31, a composite laminate is placed between a top diaphragm and an interpolator in this development. The diaphragm is pulled to the tool by the negative pressure caused by a vacuum pump, while the pins in the tool increase their height up to a position that forms the required geometry. The end of the pins could promote dimpling (local deformation); therefore, an interpolator was used to minimise this effect. The main advantage of this process is the availability to have thousands of mould designs stored in CAD models, thus saving time and economic resources in production and physical storage. Further studies led to the addition of a diaphragm between the interpolator and the laminate since the interpolator expands when the vacuum pressure is deactivated, changing the final shape of the resultant composite [128]. This new diaphragm allows the system to maintain the vacuum after the part is safely released. After the patent expired, some companies have commercialised the process [129, 130].

Munro *et al.* [131] presented a literature review focused on reconfigurable tools, which are defined as "a machine that can be repeatedly configured by a user for shaping mechanical parts in a manufacturing setting". It can be applied to form, mould or cast complex parts in different materials from metals to composites without dedicated tooling.

*Table 2-4 Classification of Reconfigurable tools [131].*

<b>Classification</b>	<b>Description</b>
Pin Density	Closed-packed or uniformly spaced
Pin Actuation Method	Mechanical, pneumatic, hydraulic, robotic
Pin Position Control Method	Manually or automatically (single or multiple pins)
Tool Surface smoothing method	Deformable interpolating layer, deformable tip pins, or hardenable surface
Degrees of Freedom	2D or 3D
Tool Use	Direct or Indirect

Table 2-4 shows a classification of reconfigurable tools. Since the first appearance of this type of tool, the basics of the design have been translated to further research and patents such as secure packing of pin matrix, leadscrew positioning of pins, square pin shape, and hemispherical pin tips. The future challenge of the reconfigurable pin-type tool is to develop an economical tool design with an acceptable resolution and size suitable for different applications[132].

Another development employing a reconfigurable tool for making composites was presented by Kaufman *et al.* [87] in the 90s, consisting of two components: a reconfigurable surface that heats, forms, and compresses prepreg tapes, and a six-degree robot arm that

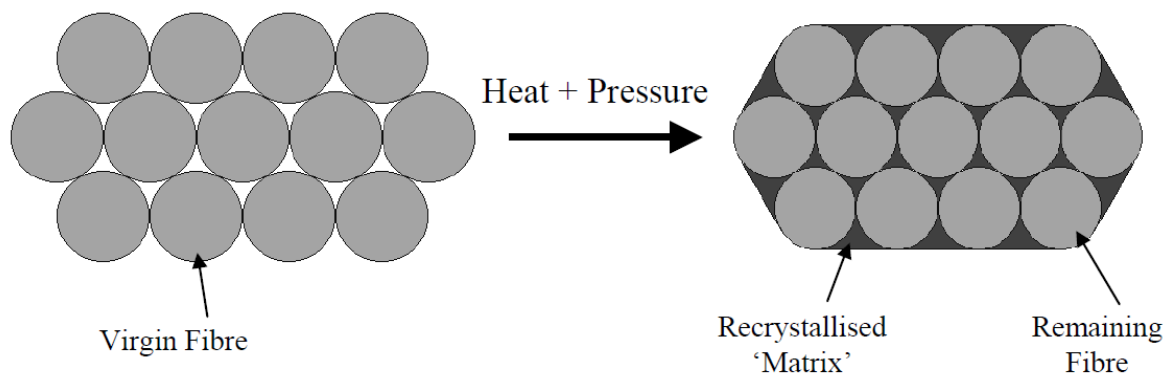
positions the part created in the reconfigurable tool. The reconfigurable forming surface comprises a number of identical 'leaves' whose position is adjusted by a cam. The cam is driven by an x-y table and moves in a slot at the leaves' bottom. When the 'leaves' are in the desired position, a locking clamp secures them. Then the material is moulded and cured by the addition of heat and pressure. However, no evidence was found related to the resultant parts and their quality, which might have led to the abandonment of the topic.

## 2.5 Self-reinforced Composites

As mentioned in the introduction chapter, fibres are polymers are the main constituent for fibre reinforced polymer composites being the fibre the reinforcement phase and the polymer the matrix phase. There has been extensive research for chemically inert constituents between inorganic fibres (Carbon, glass, etc) and polymers. However, high performance fibres from different thermoplastic polymers have also been created (e.g. ultrahigh molecular weight polyethylene, polyamide, polyethylene Terephthalate and Polypropylene), which present better mechanical properties than bulk polymers [28]. The mechanical properties have been improved by reorienting the polymer molecules in the loading direction [133]. Thermoplastic fibres can also be combined with a polymer to create a fibre reinforced composite material but are usually mixed with an isotropic thermoplastic matrix of the same, or similar material, and thus, they are called, self-reinforced composites. Furthermore, giving the opportunity to commodity, and sometimes cheap, thermoplastics to be used for load bearing applications can reduce the manufacturing costs. For example, in 2022, the cost of a carbon fibre prepreg is around £50 per square meter while the cost of a self-reinforced polypropylene preform is around £2 per square meter [17].

*Self-reinforced composites* (also called *one polymer composites*, *single-polymer composites*, or *all-polymer composites*) are an emerging field that resembles fibre reinforced composites [28]. The concept of *one polymer composite* was first introduced in 1975 [26], by creating a material in which both the reinforcement and the matrix are the same polymer (polyethylene) but present different morphologies. These composites were developed as an effort to create a strong and stable interface between reinforcement and matrix. There are both advantages and disadvantages of self-reinforced polymer composites when compared with conventional composites. Since they are mainly based on thermoplastics, few of them

can stand higher or close temperatures as thermosets. Furthermore, they are more processing-property dependent on temperature which requires a precise control on the temperature, which also increases the manufacturing costs. As their advantages, most polymers being able to be self-reinforced have very low densities resulting in lighter structures. Moreover, since only one type of polymer is used with no external elements, no further separation may be needed at the end of the product life facilitating recyclability and reuse.



*Figure 2-32 Schematic of the hot compaction process. Fibres are first pressed and heated closed to the melting point to only melt the surface of the layers. The melting polymer then fill the gaps between the fibres, and when the temperature is reduced, the polymer recrystallizes as the matrix holding the fibres together. Reproduce with permission from the authors [28].*

Hot compaction has been the main manufacturing approach for producing self-reinforced composites and is illustrated in Figure 2-32. It is based on selectively melting the exterior surface of the fibres while applying pressure so the melted material can fill the voids. When the temperature is reduced, the polymer recrystallizes as the matrix holding the fibres together, and therefore resembling a fibre-reinforced composite. Different type of polymers have been reported to be used to create self-reinforced composites such as Polypropylene, Polyamide, polyethylene Terephthalate, poly(methyl methacrylate), poly(lactic acid), natural polymers (e.g. cellulose) and others [27, 28].

The most studied self-reinforced composite has been polypropylene due to its commercial availability under several brands and processes. Polypropylene has several advantages such as thermal stability, high toughness, low cost, and wider industrial spread in many applications. One of the advantages of self-reinforced polymer composites made with polypropylene its high-volume fraction (~90%). This compensates the low mechanical properties of PP in comparison with other stiffer fibres such as UHMWPE. Self-reinforced



polypropylene composites have been produced using hot compaction techniques by using fibres or bicomponent tapes. These ones are later used to form a fabric structure being able to conform the mould.

Bicomponent tapes are constructed in a sandwich structure in which the outer layers (matrix) correspond to a thin copolymer layer, and the middle layer (reinforcement) corresponds to a homopolymer layer [133, 134]. However, they have different molecular structures with different melting points. The homopolymer due to its high molecular orientation presents a higher melting temperature than the copolymer. The copolymer is mainly amorphous with a random orientation, and therefore, it presents a lower melting temperature. This difference in the melting temperatures give a temperature processing window to produce composite structures without changing the properties of the homopolymer layer. The construction of bicomponent tapes is illustrated in Figure 2-33, in which both the copolymer and homopolymer are co-extruded at the same time from a molten state. Then, the system is quenched to crystallise and drawn in a first oven (at low temperature) to create a first molecular orientation of the homopolymer. A subsequent high temperature drawing is followed that further orientates the molecules of the system. Since the copolymer is amorphous, most of the molecular orientation is performed on the homopolymer

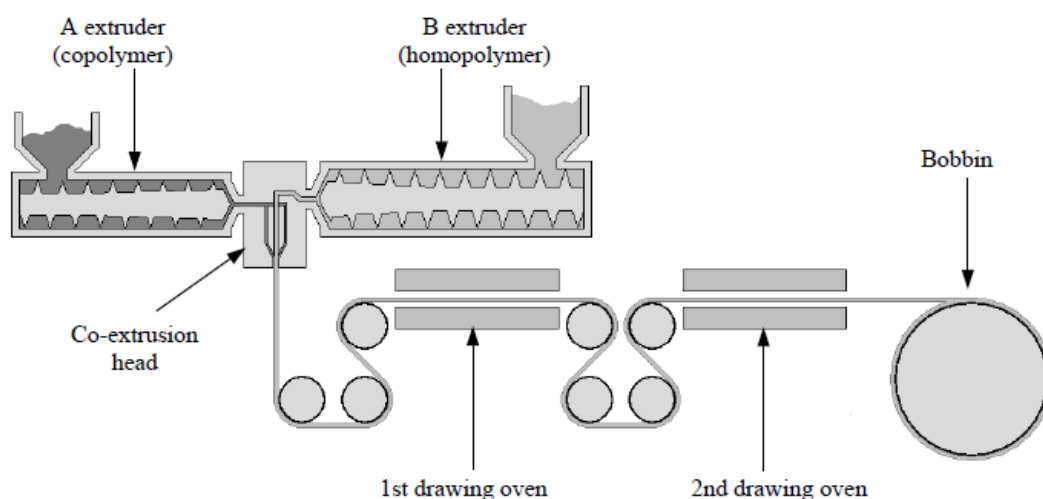
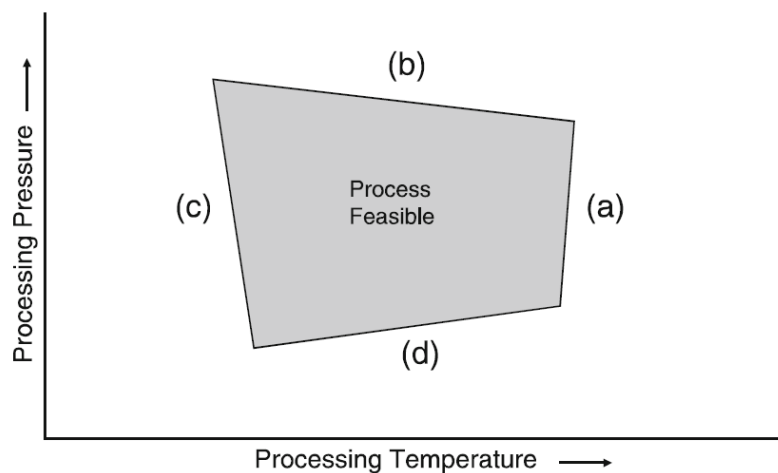


Figure 2-33 schematic of the co-extrusion and solid-state drawing production line of self-reinforced polypropylene tapes. *Repro.*

Though hot compaction looks simple in theory, it involves engineering challenges which can increased their manufacturing cost. This is because it is key to keep the reinforcement

properties of the fibre while processing, which is difficult when both matrix and reinforcement have similar melting points [135]. Figure 2-34 shows a schematic of the processing window of self-reinforced composites via hot compaction methods. The size and shape of the processing window depends on the type of polymer being chosen. Higher temperatures promote temperature relaxation and/or melting of the reinforcement constituent. High pressures promote excessive flow or molecular misalignment which reduces mechanical properties. Both low temperature and/or low pressure are critical since a minimum level is required to achieve proper consolidation. A proper consolidation or to avoid the loss of mechanical properties determine the corners of the boundaries. If the fibres are constrained, shrinkage is prevented. This leads to a higher artificial melting temperature and therefore, a higher temperature can be used. This corresponds to the corner between boundaries (a) and (b). Similarly, a minimum temperature to promote bonding combined with higher pressure determine the corner between borders (c) and (d), or a lower pressure combined with a higher temperature can also promote enough consolidation. Time is a parameter that was not considered in the schematic shown. Quicker consolidation is beneficial since long times at lower temperatures promotes molecular relaxation in polymers and therefore a loss of mechanical properties. This is the opposite to short times at higher temperatures. Other processing routes of self-reinforced composites are not related to the focus of this project and can be found in the literature [133].



*Figure 2-34 Thermal and Pressure Processing Boundaries of self-reinforced composites: a) a high temperature may produce melting or molecular relaxation of the reinforcement phase, b) too much pressure can cause flow and molecular dealignment, c) and d) are the minimum levels of pressure and temperature to ensure proper consolidation [16, 28, 133].*

From the literature it can be determined that forming of pre-consolidated laminates [32] or impregnated fabrics with the matrix phase in a fluid state may be possible by selecting fibre and matrix phases with as large a difference as possible between matrix and fibre melting temperatures. Furthermore, since their appearance, the use of the hot compaction technique has not changed for either scientific or commercial developments.

## **2.6 Literature Review Conclusions**

There is a need to create low-cost innovative, and sustainable processes that are also friendly to the environment. The present literature review has summarised a wide range of automated and semi-automated manufacturing processes for fibre reinforced composites. It is claimed they can improve process and cost-efficiency. The most known automated processes are Automated Tape lay-up (ATP) or Automated Fibre Placement (AFP), in which tapes or fibres are selectively deposited over a mould or mandrel with the aid of heating and pressing devices. However, high capital investments are required for their adoption, limiting their widespread use for small-to-medium manufactures [21].

Digitally-driven strategies such as additive manufacturing or incremental sheet forming offer a new possibility for low-cost automation in composite materials. The main advantage of these processes is the ability to produce fibre-reinforced composites without the need for an expensive template or a mould [22, 23], which can reduce the price of composite components for low volumes. However, these techniques present several limitations to achieve composite parts with similar performance with benchmark manufacturing processes for composite materials.

The recent commercialisation of various self-reinforced composite technologies suggest that self-reinforced polymer composites will continue to warrant investigation in the coming years. Ease of forming with low tooling costs is advantageous for low volume applications which can be suitable for early applications to show the potential of new materials or manufacturing routes. The easiest way to process self-reinforced composites is to form the part directly from fibre or tape. In the case of using tapes, give a bigger temperature processing window which can be used to facilitate automation processes without risking damaging the reinforcement effect of the material.



### 3 Process and Machine Development

The proposed low-cost automated in-situ consolidation machine controls the motion and temperature of a forming tool to compress and transfer heat to a stack of fabrics that rests over a mould, as illustrated in Figure 3-1. In theory, it could work on both thermosets and thermoplastic composites. For thermoset composites, the forming tool will cure the polymer, in-situ, as it moves. Because of the heat transfer, as it moves, the forming tool will in-situ cure or in melt the polymer matrix, for thermosets or thermoplastics composites, respectively. Furthermore, the forming tool moves according to a tool path that copies the mould shape. In this way, it compresses and brings the fabrics close to each other and against the mould to ensure proper bonding between their interfaces. When the forming tool moves past the area, the material is already solid for a thermoset polymer or cools down and crystallises to achieve complete solidification for a thermoplastic matrix.

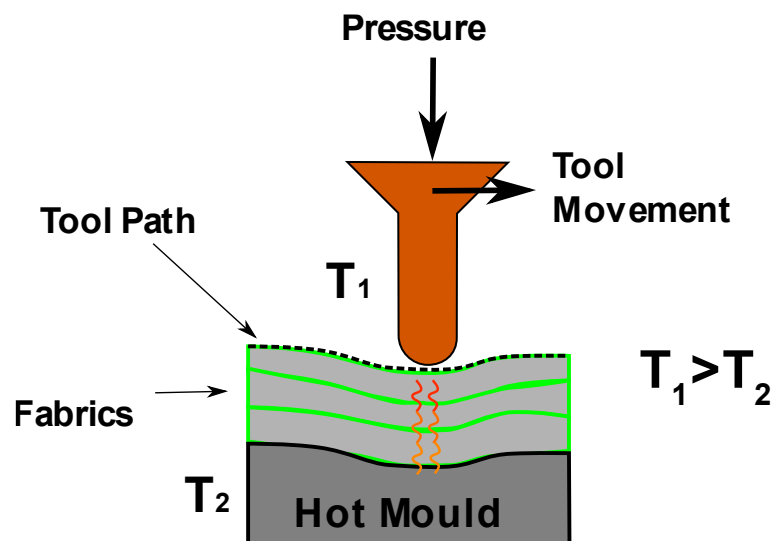


Figure 3-1. Schematic of the automated in-situ consolidation process. The temperature of the forming tool is higher than the temperature of the mould. The tool path copies the shape of the surface of the mould.

This concept was implemented in carbon/epoxy composites by the author's research group in the following publications [136-138]; however, it was never used to produce self-reinforced composites (both reinforcement and matrix are the same material). This process also differentiates from automated lay-up methods because the whole stack of material is clamped on the mould, and therefore, all the layers are formed simultaneously. Throughout this work, the term material, laminate, or stack refers to layers of self-reinforced polypropylene fabrics. The fabrics are made of bicomponent tapes in which the reinforcement

phase is surrounded by a lower melting point polymer that acts as the matrix. The reinforcement phase is a homopolymer with a high modulus and highly aligned molecules which results in a high melting temperature. In contrast, the surrounding polymer is a copolymer with random molecular orientation, resulting in low degrees of crystallinity and, therefore, a low melting temperature [28]. To create a laminate, the copolymer layers of each tape in a fabric must melt to promote bonding between the interfaces of the other tapes, while preventing the melting or molecular relaxation of the reinforcement phase in order to maintain their enhanced mechanical properties [133]. For this reason, the temperature of the mould is lower than the temperature of the forming tool. The temperature of the mould is set just below the melting temperature of the copolymer to create a lower temperature gradient when the forming tool passes over the material.

The automated system was composed of a structural frame with driven mechanisms, a copper forming tool, a hot mould, an open-loop motion controller, different control systems (e.g., Temperature and Force), and software that communicates with the motion controller, as shown in Figure 3-2. A detailed explanation of the hardware and software that achieves this task will be introduced in this chapter. After understanding how the automated process works, a manufacturing workflow is described to help the user in future developments. Finally, the energy consumption is compared with a benchmark process to understand if the process is energy efficient.

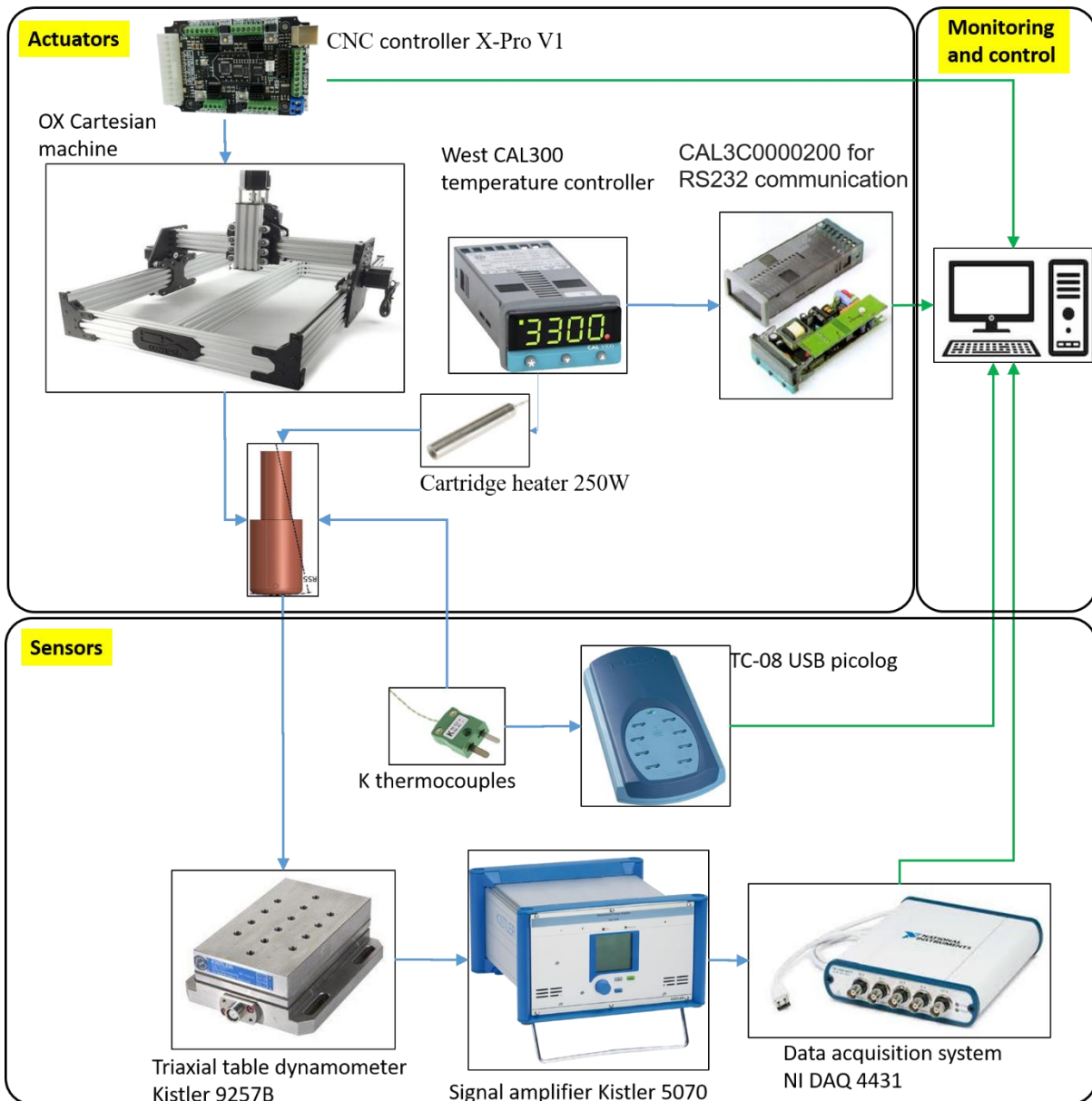


Figure 3-2. Main components of the automated in-situ consolidation machine.

### 3.1 Structural Frame and Mechanical Actuators

A gantry structure can move a load in three degrees of freedom and was selected due to the ease of set-up, relative stiffness and low cost. Gantry systems are widely used for different applications (Machining, 3D printing, adhesive dispensing, etc.). The structure (Workbee CNC machine, Ooznest, UK [139]) is made of aluminium extrusion with V slots, which allows the wheel to stand on the slots, as shown in Figure 3-3. In this way, the structure frame becomes the rails for the mechanical actuators saving weight (and cost) as rail guides are not required [140]. Each frame/mechanical actuator is connected through connector

plates, and the linear motion is driven by timing belt pulleys and belts using open-loop stepper motors. The Z-axis is held by the Y-axis, which is held by the X-axis. The end effector carriages the forming tool, which travels up and down in the Z-axis. Figure 3-4 shows the final structure with the forming tool included. The design of the forming tool will be explained later in this chapter.

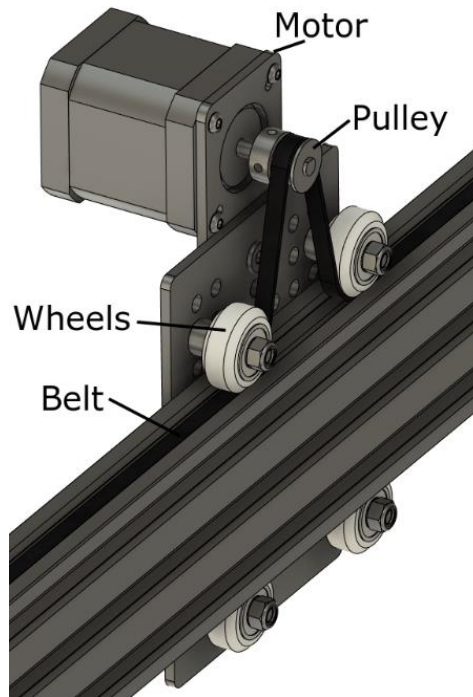


Figure 3-3 V-slot aluminium profile holding a movable carriage through wheels that stand over the slots.



Figure 3-4. Automated in-situ consolidation machine based on a single forming tool



## 3.2 Motion Controller

A motion controller is the brain of any automated machine as it controls the motors which move a specific component in a machine [141]. Motion controllers can be open-loop or closed-loop feedback devices, which oversees developing trajectories of motion profiles for the motor and monitors different input and output devices [142]. In an open-loop system, there is no feedback on the position of the load, but it is the preferred choice for low-cost systems. For this project, an open-loop, open hardware motion controller hardware (xPro V1, Spark Concepts [143]) based on open-source software, GRBL [144-148], was selected. GRBL is a CNC g-code ([149]) interpreter and motion controller that creates the pulse sequences for the stepper motors. The advantages of the xPro V1 motion controller are that the motor drivers are embedded into the hardware, which saves space and wiring time (Figure 3-5). The communication between software and controller is performed through a USB port, available for any computer.



*Figure 3-5. xPro V1 CNC motion Controller based on GRBL software. It is capable of driving 4 stepper motors and has a USB port for Serial communication.*

### 3.2.1 Speeds Limits

Displacements of the linear stages were used to validate the motion profile of the machine using a dial gauge mounted to end effector. The commands to perform the displacements were sent through Universal Gcode Sender [147, 150], a java-based windows application that acts as a graphical interface (GUI). The time it took the stage to move a

distance of 60 mm was recorded at different motion speeds between 15 mm/min to 90 mm/min. Figure 3-6 shows both the expected time and the measured time to complete a 60 mm displacement at a specific X and Y axis speed. Figure 3-6 also shows the measured time error of the displacements for both axes. It can be observed that the timer error to complete a 60 mm displacement is higher at lower speeds. This error decreases as the speed increases between 15 mm/min to 75/min. Finally, the error is negligible from 75 mm/min. For example, at a 15 mm/min speed, the machine should move the load a displacement of 60 mm in 240 seconds; however, it took 53 seconds (78% error). It appears the motion controller has a default limitation for motion profiles at speeds lower than 75 mm/min. Therefore, for this project's scope, the minimum speed that will be evaluated is 90 mm/min to prevent any errors in the motion.

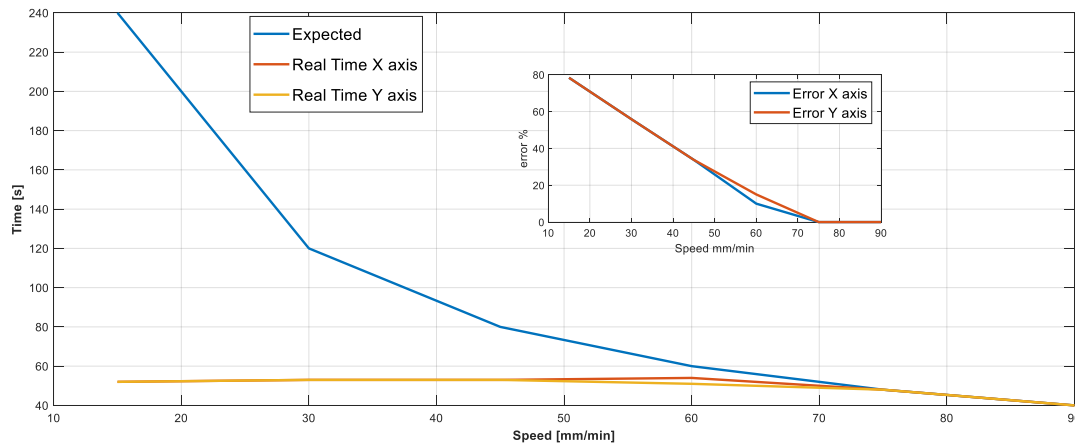


Figure 3-6. Time to travel and Error in a motion profile for the open-loop motion controller.

### 3.2.2 Motion Control: Hardware and Software Integration

Using Universal Gcode sender as a graphical interface and communication with the motion controller has several limitations. First, the graphical interface cannot be modified for other purposes. Second, users can only send g-code lines one at a time or a list of commands from a file. Finally, it does not have any feedback interface, which prevents the implementation of a closed-loop system.

To overcome this limitation, LabVIEW®[12] software was used to communicate with the controller by sending the g-code lines via serial communication. "User interaction with Grbl is performed by sending it a string of characters, followed by an enter. Grbl will then process the

string and execute it accordingly [151]”. Therefore, using LabVIEW® serial communications functions (e.g., Visa Configure Serial port[152]), a g-code line can be sent to the motion controller to be executed. For example, when the g=code: “G21 G91 G0 X50” is sent to the controller, the tool will move 50 mm on the X-axis. Figure 3-7 shows how the command is created. The graphical interface of LabVIEW® (Figure 3-8) has a numeric indicator and a button to send the signal. The numeric indicator in the programming language shown in orange with the label “X mm” is then compared with the limits of the machine and then transformed into a string with a value of “50”. This new string is then concatenated to a previous string, “G21G91G0X”, to create the g-code line. Once the button in the front panel is activated, the case structure (box) is activated, sending the g-code line to the microcontroller. In this way, the machine can be controlled to execute displacements and to set up different parameters such as speeds or the origin of the working coordinate system. Though several open-source graphical interfaces have been created to use Gbrl-based motion controllers [151], there is no record of an application that uses LabVIEW® for a motion control system with feedback from a force sensor. Being able to control the pressure in an automated process is essential in composites manufacturing. Therefore, this system has the potential to allow low-cost automation capabilities with feedback control from different sensors.

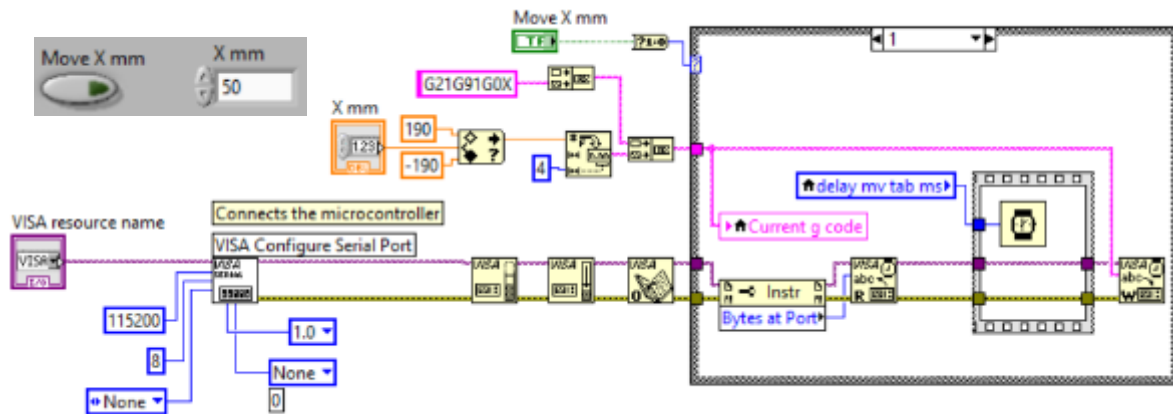


Figure 3-7. g-code generation and execution in LabVIEW®. The code creates a communication channel with the motion controller (Visa Configure Serial Port). The user input as displacement is transformed into a string sent to the motion controller (Visa abc W).

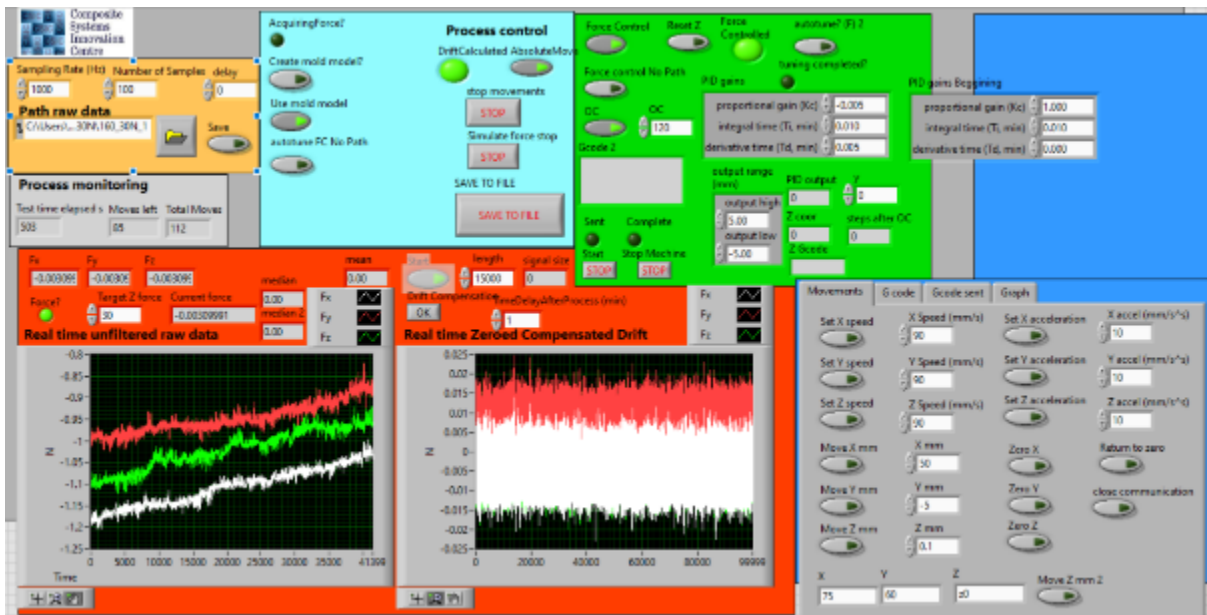


Figure 3-8. Software Graphical Interface: Motion control with force closed-loop system.

### 3.3 Processing Parameters Control

The forming tool needs to simultaneously compress the material and raise its temperature to specific targets selected by the user. Force and temperature are two different phenomena, and they need to be measured before being controlled. Throughout this thesis, force and temperature will be called process variables or processing parameters. Measuring these variables can be performed through data acquisition, which is the process of measuring an electrical or physical signal with a computer. A closed-loop system can be created if the data acquired is used as feedback to create a control signal to manipulate a phenomenon (Force or Temperature) by comparing the programmed inputs with the measured values[153]. Figure 3-9 shows a schematic diagram of temperature control of an electric furnace. The furnace temperature is the process variable, which is measured and converted into a digital signal that can be read by a controller using an interface. This digital temperature is the feedback which is then used to calculate the error from the desired setpoint temperature. If there is an error, the controller activates a heater to bring the temperature to the desired value[153]. In general, a closed-loop system is composed of a data acquisition system, a controller, and an actuation process to manipulate the process variable.

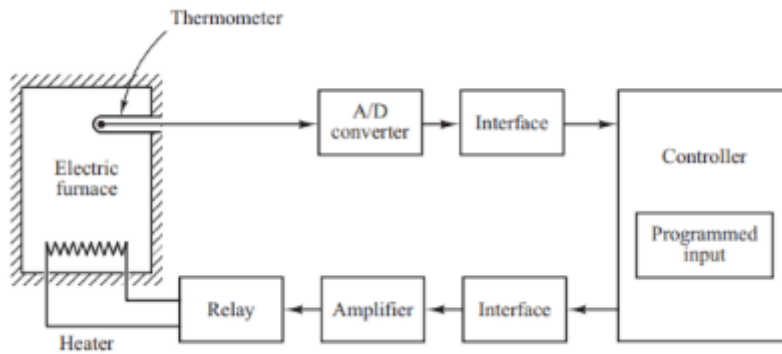


Figure 3-9. Temperature Control System. Reproduce with permission from the authors [153].

### 3.3.1 Data acquisition

A data acquisition system is composed of sensors, data acquisition measurement hardware, and a computer with application software [154], as shown in Figure 3-10. Sensors are devices or mechanisms that convert a physical phenomenon like temperature or force into a measurable electrical signal like voltage or resistance. A data acquisition device (DAQ) acts as the interface between a computer and the sensor signals by digitising them to be computer-readable (Analog to Digital converters[153]). Finally, data acquisition software is required to process, visualise, and store the measured data. Because there are two process variables: Force and Temperature, the automated development requires two separate control systems described later in this chapter.

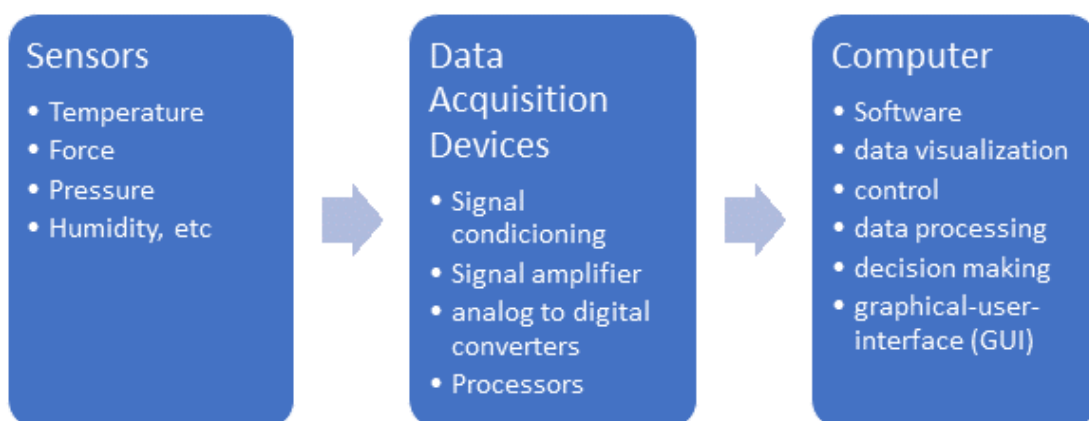


Figure 3-10 Schematic of a Data Acquisition system composed of sensors, a data acquisition measurement hardware, and application software in a computer. Reproduce with permission from the authors [154].

### 3.3.2 Temperature Control

The temperature data acquisition system will be described first and then later how it is controlled. The temperature sensor used in this project is a thermocouple type K. In a thermocouple, two dissimilar electric conductors (wires) are joined (Figure 3-11. a). This joint will generate a voltage, characteristic of a given temperature. In a type K thermocouple, the conductors are nickel (Ni) and Chromium (Cr) and can be used to measure temperatures in a range between 0 and 1100°C. For this project, two temperature data acquisition systems were used. One for controlling the temperature of the forming tool (Figure 3-11. b), and another that measures and records temperature values from several thermocouples (Figure 3-11. c). In the first case, the data acquisition system is embedded in a PID temperature controller (CAL3300, West Control Solutions, USA), which communicates the temperature signal to computer software (CALGRAFIX, West Control Solutions, USA). The second system is a laboratory temperature data logger (Picolog TC-08 Datalogger, Pico Technology).

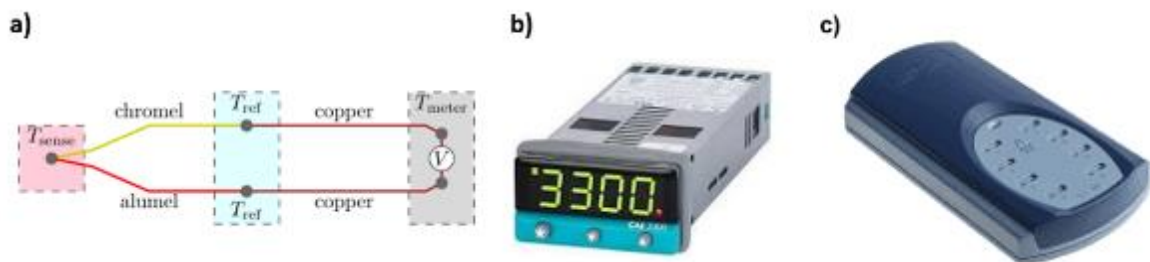


Figure 3-11. a) Schematic of the principle of a thermocouple [155]; b) CAL 3300 PID temperature Controller [156]; c) Picolog Temperature Datalogger [157]

Temperature control is required for two different components in the automated system. The first one is to control the temperature of the forming tool, and the second one is to control the temperature of the mould. The forming tool and the mould are made of copper and aluminium, respectively. Copper was selected due to its high heat conductivity, allowing a fast heat transfer to the stack of material. On the other hand, aluminium was selected for its mould because of its higher strength and lower price than copper.

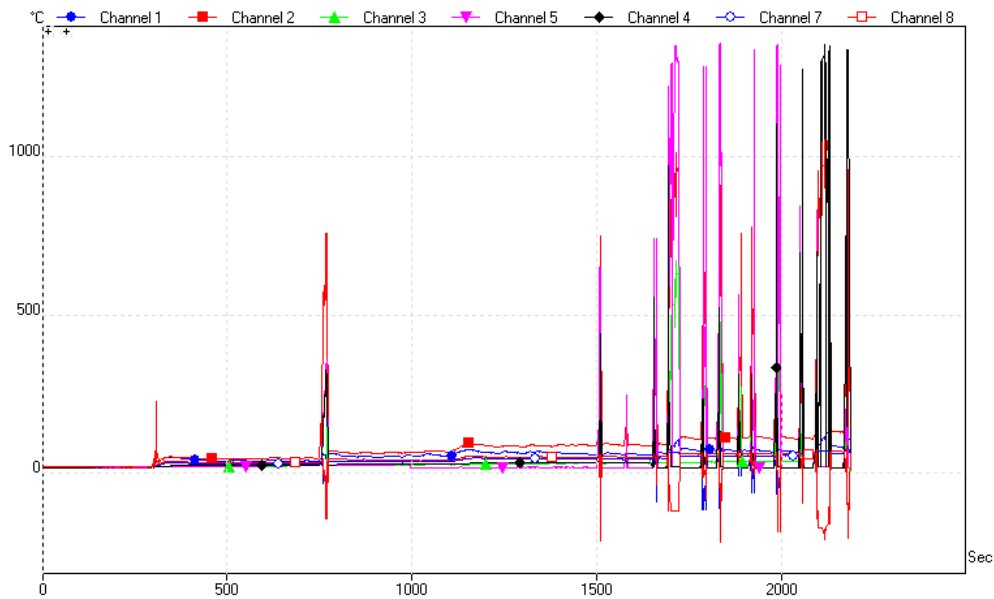


Figure 3-12. Voltage leaking through thermocouples to Data Acquisition Hardware

Both the forming tool and the mould are heated using electrical cartridge heaters controlled through PID Controllers. Cartridge heaters were selected as a heating element due to their reliability, ease of installation and use [158]. However, cartridge heaters generally work with alternating current and high voltages, which can potentially damage the hardware of the data acquisition systems. Figure 3-12 shows an example of temperature records when the contact with the copper tool with the thermocouple induces high voltages, causing unexpected temperature peaks in both positive and negative directions in the readings. This was solved by coating the thermocouple with thermal paste, then covered by an electrically insulating tape, recoated with thermal paste, and then fixed to the forming tool. Thermal paste improves heat transfer, reducing the delays caused by the insulating tape with low thermal conductivity. The thermocouple was attached using a jubilee clip or a bolt that holds both thermocouple and earth connection for the cartridge heater, as shown in Figure 3-13. The earth connection is a safety measure to prevent an electric shock if there is a failure of insulation in the cartridge heaters. Moreover, the forming tool is held by a PTFE mounting bracket, reducing the heat transfer to the gantry structure.

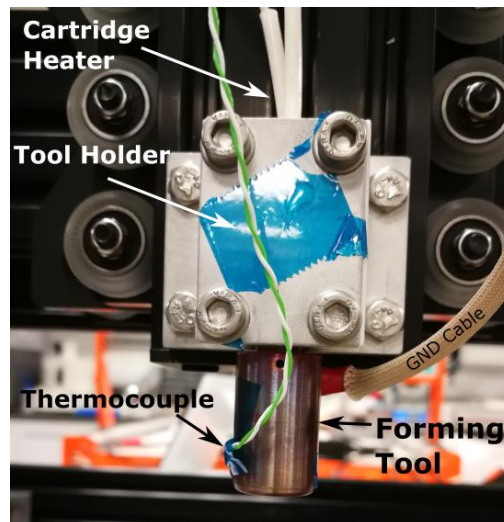
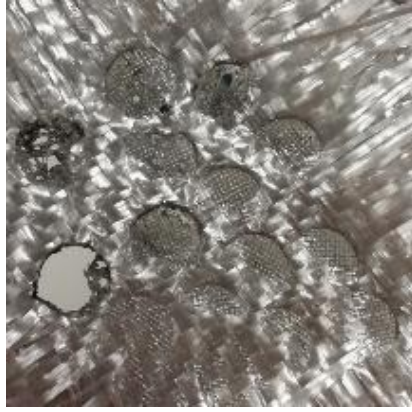


Figure 3-13. Typical forming tool installation. The forming tool is heated with a cartridge heater connected to the output of a temperature controller. A tool holder keeps the forming tool attached to the Z axis. The thermocouple is located as close as possible to the tip of the forming tool.

### 3.3.2.1 Ultrasonic heating (UC)

Ultrasonic heating is mostly used for welding processes in thermoplastic applications [46]. Heat is generated by the internal friction created by the vibration of a horn at high frequencies (10s of thousands of hertz), which can reduce the amount of energy used to in-situ consolidate a thermoplastic composite laminate [38]. However, preliminary tests with a low power handheld ultrasonic welder (Branson LPe 500W, Emerson) immediately melted the material (both matrix and reinforcement) even with the lowest power setting (10%), as shown in Figure 3-14. Because the objective is to melt only the matrix but not the reinforcement, this technique was discarded as it represents a disadvantage for self-reinforced composites forming. Moreover, ultrasonic consolidation presents an engineering challenge to implement a closed-loop system as it is difficult to monitor the temperature of the material while it is consolidated because the probe heats the material but not the instrument. Although in many heat transfer mechanisms it is also difficult to monitor the temperature of the material, but for example in a heat conduction mechanism, the processing temperature can easily be constrained to the temperature of the heating elements that transfer heat to the material. It may be possible to use ultrasonic welding to consolidate the system by using a lower power system than that available to us on our limited budget. This could be a potential direction for further research.





*Figure 3-14. Ultrasonic welding of self-reinforced polypropylene promotes melting of both the matrix and reinforcement phases.*

### **3.3.3 Force Control**

Currently, built-in systems automate force data acquisition with a combination of hardware and software that includes a load cell (Force sensor), signal conditioning to amplify the signal, and a data acquisition device to measure and digitalise the signal. Commonly, data acquisition devices already combine signal conditioning and data acquisition in an individual piece of hardware. National Instruments, the owners of LabVIEW®, have readily available and easy-to-use DAQs for force sensing applications [159-161].

The force sensor used in this project is a 5 kN 3-axis dynamometer (Model Type 9257B, Kistler [162], Figure 3-15(b)). This is based on piezoelectric sensors that produce a proportional electric voltage when they are deformed under the action of a force, as shown in Figure 3-15(a). Among the advantages of piezoelectric force sensors are the ability to cover large measuring ranges from small to large forces and high rigidity with negligible deformation [163]. The electric charge generated is small, which makes it difficult to be measured. For this reason, the signal produced by the dynamometer is sent to an amplifier which transforms into a proportional voltage (Kistler Type 5070A [164], Figure 3-15(c)). Then, the amplifier transmits an easier to read voltage to the data acquisition measurement device using the signal cables. The data acquisition device is a NI USB-4431 (National Instruments [165], Figure 3-15(d)) and the data acquisition software is LabVIEW®, both from National Instruments. The dynamometer is connected to the amplifiers, connected to the DAQ, which then sends the signal to a laptop with the software. Furthermore, piezoelectric force sensors are very sensitive to temperature and temperature changes leading to errors and long-term

fluctuations. To prevent this temperature influence, a 25-mm piece of epoxy block with a low thermal conductivity was attached between the force sensor and the mould, as shown in Figure 3-16.

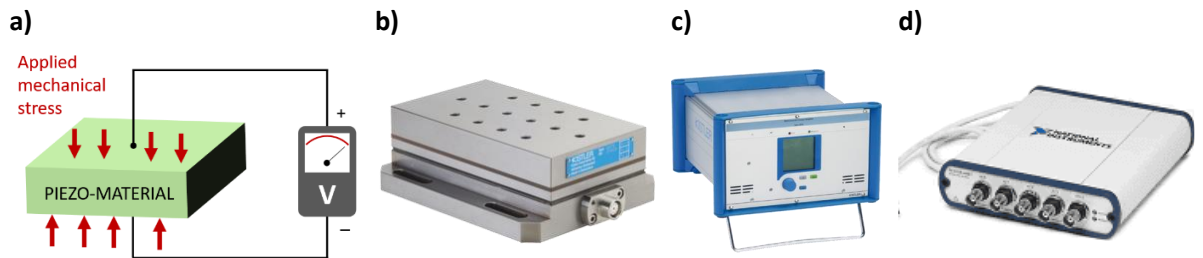


Figure 3-15. a) principle of a piezoelectric material in which a force exerted produces a voltages [163] ; b) 3-axes piezoelectric dynamometer based (cable not included in figure) [162]; c) signal amplifier of the dynamometer signal (cables not included in figure) [164]; d) USB data acquisition device that perform signal conditioning and transfers data to the computer [165].

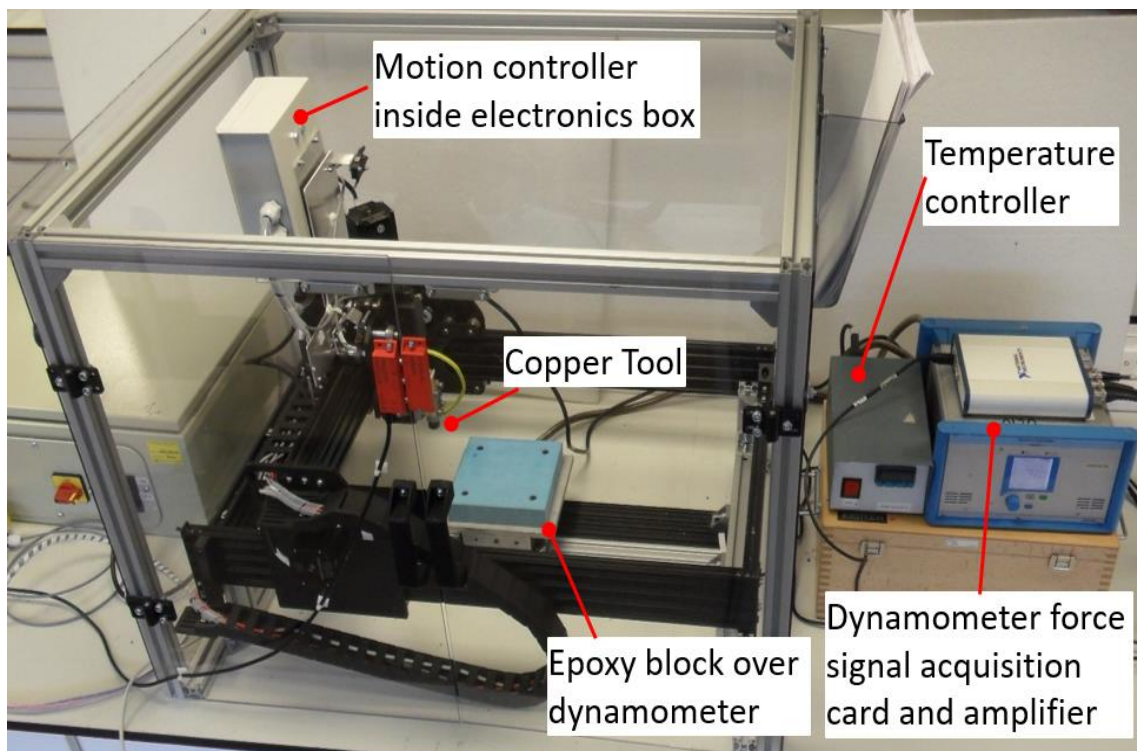


Figure 3-16. Automated in-situ consolidation set-up with its subsystems.

LabVIEW® is a software suite that facilitates the creation of applications that perform testing, measurement, and control functions that allows hardware integration through a “graphical approach to programming”. This graphical approach to programming is similar to a flow of data in a step-by-step process in which wires connect functions (shown as icons), as illustrated in Figure 3-17. First, the data acquisition function (DAQ system mentioned above)

collects the data. The analysis function then processes this data. Finally, the results are written into a file if it is required. Another benefit of LabVIEW® is that it allows parts of the code to execute tasks in parallel.

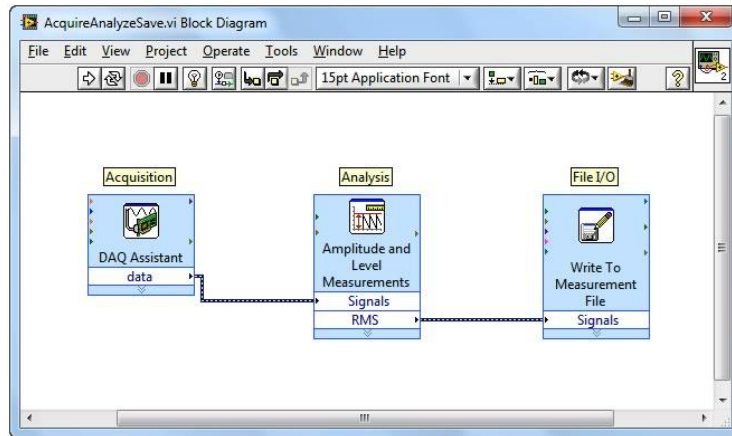


Figure 3-17 LabVIEW® Graphical Interface showing the graphical approach to programming

Figure 3-18 shows how one section of the code (Top square) oversees data generation while the other section (bottom square) processes the generated data. These capabilities make LabVIEW® suitable for closed-loop feedback systems since it can measure and process data from a sensor and provide a control signal according to the measured data.

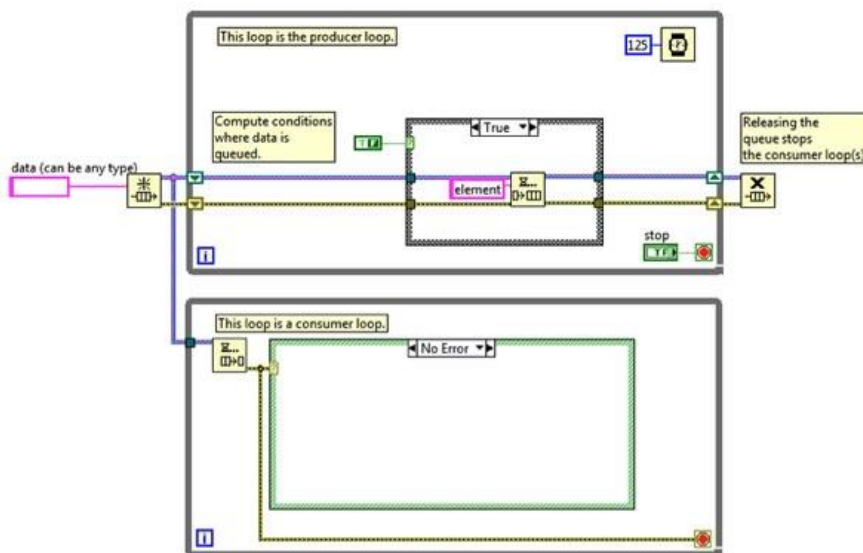


Figure 3-18 Parallel Tasks in LabVIEW®

It was described previously how LabVIEW® can be used to control the motion of the tool with serial communication. Moreover, due to its parallel tasks capabilities, it is possible to implement a closed-loop system. Several control challenges were presented during the development of the machine and will be described in the following sections. The goal is to

create an approach that can ensure a relatively constant compression of the material. The material is compressed by the vertical movement of the forming tool. In this way, the control will be exclusively adapted to the vertical displacements.

### **3.3.3.1 Software capabilities**

The control software is intended to operate on a dedicated computer running a standard operating system that supports LabVIEW®. As mentioned, communication between LabVIEW® and the motion controller is performed via USB with a serial communication protocol.

The control software provides a number of functions, including:

- Sending command signals to the hardware motion controller as g-code string lines to control motion and initiate/terminate the forming process.
- Providing a user interface for the operator to interact with the system, as shown in Figure 3-8.
- Reading and interpreting g-code commands within the toolpath file
- Monitoring and recording force signals from the sensor
- Processing incoming force signals for a force closed-loop actuation system

### **3.3.3.2 Forming stages and Open-Loop Control**

The forming cycle of the part is divided in several stages; being the last one, the proper forming operation as illustrated in Figure 3-19. The first stages (real measured force, online drift compensation, 1N force approaching, big jump, target force approach, and setting a new Z(0) position are dedicated to signal conditioning to achieve the desired level of compaction that the forming tool must exert over the material. The first stage (dark blue line) starts measuring and recording the force values without any movement of the tool or contact between the tool and the material. During this stage, the force increases linearly respect to the time with time. This change over time is common in piezoelectric force sensors and it is generally post process after testing or experimentation. However, in this project, this change is in-situ compensated as shown in the second stage (orange line) called online drift-compensation. This compensation corrects the drift (change over time) based on the previous

stage and it is used for the following stages. The next three stages (yellow, purple, and green line) are related to a force-approaching procedure in which the tool starts to move down to compress the material until it reaches the desired force target. First it moves down very slowly until it detects the material is being compressed (yellow line). This detection is set by reaching an arbitrary value of 1N. Second, to speed up the force approaching procedure, the tool is commanded to lower its position at a faster rate promoting a fast increase in the force (big jump) below the desired target force. Then, the tool moves down very slowly again to not exceed the desired force target. When it reaches this force value, the vertical position the of the forming tool is recorded. In this way, this position is associated to that level of force. This means that if the tool is raised and brought back to that position, the force should be the desired force target. Therefore, the fourth stage (light blue line) is a validation stage to corroborate that the vertical position previously recorded achieves the desired force target. To do this, the tool is raised 5 mm to separate it from the material (removing the force) and then put back down again. If the force is in range, this position is configured as the Z datum in the working coordinate system of the CNC program, and then the forming stage can start. In the forming stage, the tool follows a predetermined path. Like the previous stage, the tool is raised 5 mm to separate it from the material, moved to the beginning of the predetermined forming path, and then put back down again before starting the actual forming operation of the part. When the forming process finishes, the tool is raised and separated from the material. The software was initially designed to create an open-loop force system because it relies on a fixed vertical position-force relationship and no feedback was used for comparison and online corrections.

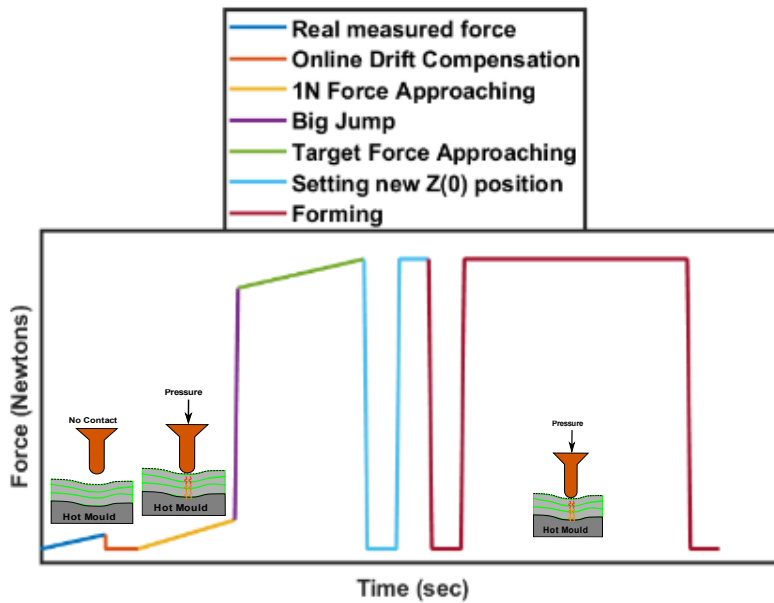


Figure 3-19 Force vs time profile representing the forming cycle stages of the automated process. Several stages are needed for signal conditioning before proceeding with the actual forming of the part

The following sections will explain in detail the development and signal conditioning of each of the stages of the forming cycle.

### 3.3.3.3 Online Force Compensation

As the program starts running, it acquires the real force measurements from the force transducer. By nature, the force generated by piezoelectric materials will present a drift in the signal with a constant slope (ideally) [163]. This means that the measured value increases with time even in the absence of forces, as shown in the first stage of Figure 3-19 or Figure 3-20. This happens for all force components (X, Y, and Z). Therefore, after a specific amount of time, previously selected by the user, a linear regression algorithm performs an online force drift compensation. This algorithm calculates the slope of the measured values in the first stage and subtracts it to the new measured values resulting in a force of zero if no force is applied, as shown in the orange line or the second stage of Figure 3-19 and Figure 3-20, respectively. Figure 3-20 shows a real example of the online drift compensation performance in which a 1 Kg load keeps a constant value around ~10 N without increasing, demonstrating the good performance of the compensation algorithm. Though the online-drift-compensation is entirely focus on the vertical force, it is also performed in the other two directions.

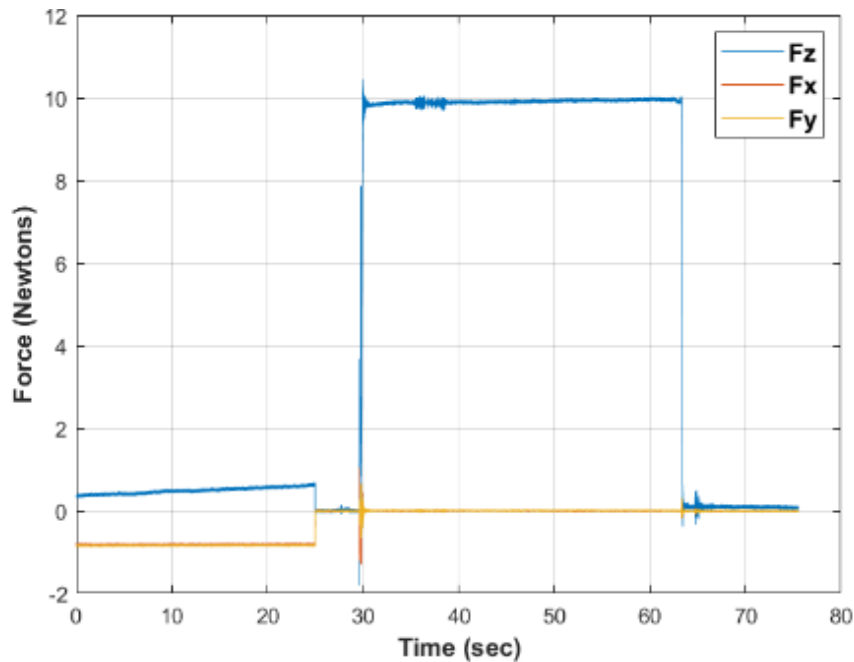


Figure 3-20 Online Drift Compensation. As the force data acquisition starts, the values of the force increase over time. These values are then used to perform an online drift compensation to the current values. It can be seen that a 1 kg load applied in the vertical direction (Z) does not increase over time due to the online compensation. The online compensation is equally performed in the X and Y axes, but as no load is applied in these directions, there is no change of force values for Fx and Fy.

### 3.3.3.4 Target force approaching method and Datum Setting

The next stage consists of approaching the target forming force, which is accomplished in three sub-stages as illustrated in Figure 3-19:

- a. **Third Stage:** Slowly approaching a force of 1N (yellow line).
- b. **Fourth Stage:** Increase the force close to the forming target force (purple line).
- c. **Fifth Stage:** Slowly approaching the forming target force (green line)

Figure 3-21 show the real force measurements after drift compensation when the machine performs the target forming force approach between seconds 15 to 50 (After second 50, the validation stage starts). Before the user starts the forming operation, the tool is not in contact with the material stack. The forming tool is lowered down by fixed small increments of 0.01 mm, as seen by the small vibrations between seconds 15 and 40. When the forming tool is in contact with the stack, then the force starts to increase up to an arbitrary value of 1N. When the measured force is higher than 1 N, the algorithm sends a new signal to lower down the forming tool according to (Equation 3-1). The displacement  $\Delta x$  depends on the difference between the target force and the current force reading and a proportional

constant selected by the user. The proportional constant was determined by experimentation, so the tool displacement results in a force increase below the target force. After the force increment was performed, the tool was again lowered down in small increments of 0.01 mm to reach the target force. The algorithm was designed to stop the vertical movement of the tool when the value of the sensed force is higher than the target force. When this happens, the datum setting stage starts by raising the tool 5 mm, to separate it from the material, and then moving back down, to perform the datum setting, as can be seen between seconds 48 to 70 of Figure 3-21. After setting up the vertical datum, the tool is raised before starting the forming operation.

$$\Delta x = \frac{F_{target} - F_{current}}{K} \quad \text{Equation 3-1}$$

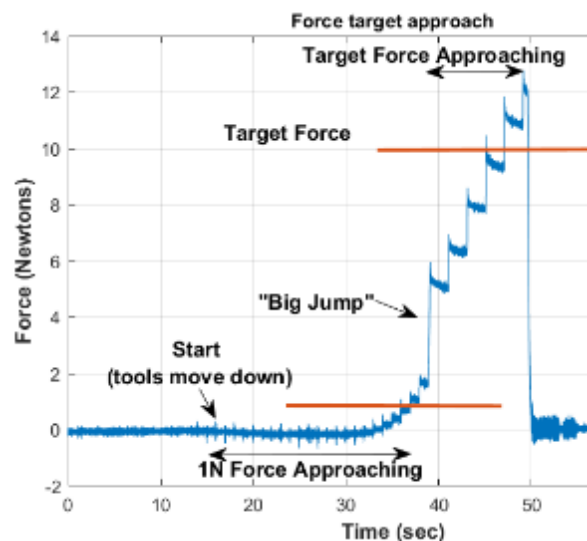


Figure 3-21 Stages of the force approaching procedure. First the tool moves down slowly to start compressing the material. Once the compression force achieves an arbitrary value of 1N, then the tool is move down faster to speed up the procedure before the target force. Then it again moves down slowly to not overshoot the target force. A  $K=40$  was used for polypropylene.

### 3.3.3.5 Forming stage

Once the program sets up the vertical datum, the forming operation starts by lowering the tool to compress the material and then moving it with a constant speed according to a predetermined path. An example of the predetermined path is shown in Figure 3-22 (left), in which the forming path cover the whole area to be formed with a fixed separation using parallel paths. The example shown is designed to form a flat laminate without touching the



clamping mechanism (dashed line). The path planning works in the X-Y plane while keeping the vertical position fixed as explained in the previous stages. The beginning and end of the forming path are selected by the user when creating the forming path, which can be done manually or using CAM tools such as FUSION 360. It is important to align the working coordinate system with the machine coordinate system when creating the path planning to avoid damage to equipment.

Figure 3-22 (right) shows the measured forces ( $F_z$ ,  $F_x$ , and  $F_y$ ) of the forming operation with a target force of 30N (compression). The forces have already past a filter to reduce the noise of the signal, however, noise was always present. The forming forces in the X and Z present big fluctuations during the whole forming period while the Y axes decreases slightly. In the case of the Forces in the X axis, this are due the movement of the forming tool in the positive and negative directions of this axis according to the path planning in Figure 3-22 (left). In the case of the vertical force, the fluctuation, and the drop in values during the whole process was unexpected. However, a close examination allowed to associate the fluctuation with an unlevelled or misaligned mould with the real working coordinate system of the machine. Therefore, even though the vertical position of the forming tool is fixed, the physical separation of the material and the forming tool changes. In this way, some regions have higher level of compression than others in a single path line. An analogue dial test indicator attached to the tool bracket, as shown in Figure 3-23, was used to validate the misalignment that causes changes in the forming forces, especially in the vertical force. Mechanical solutions were attempted to correct this misalignment; however, due to the modular nature of construction of the equipment and the involvement of several pieces of equipment attached, it was impossible to achieve low alignment tolerances.

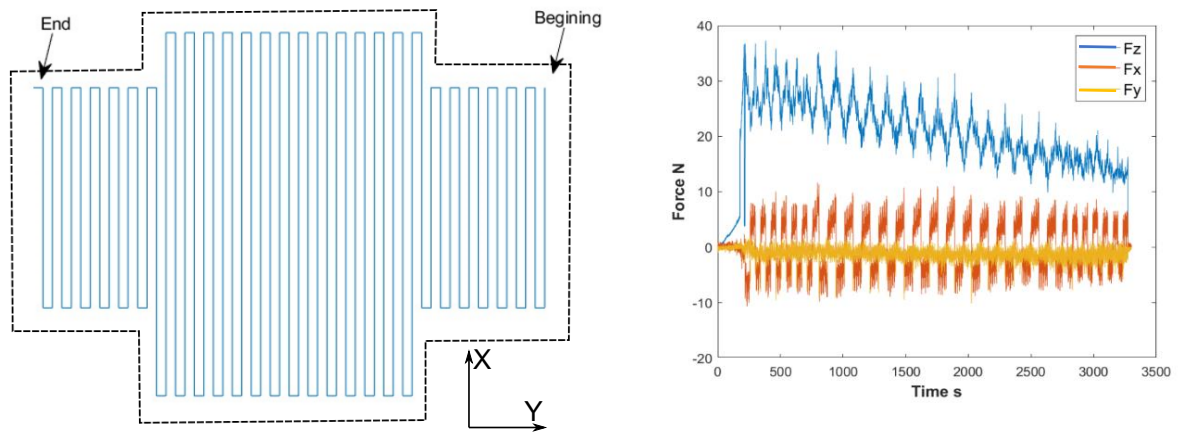


Figure 3-22. Path planning (left) and force measurements (right) during open-loop forming for a flat laminate.

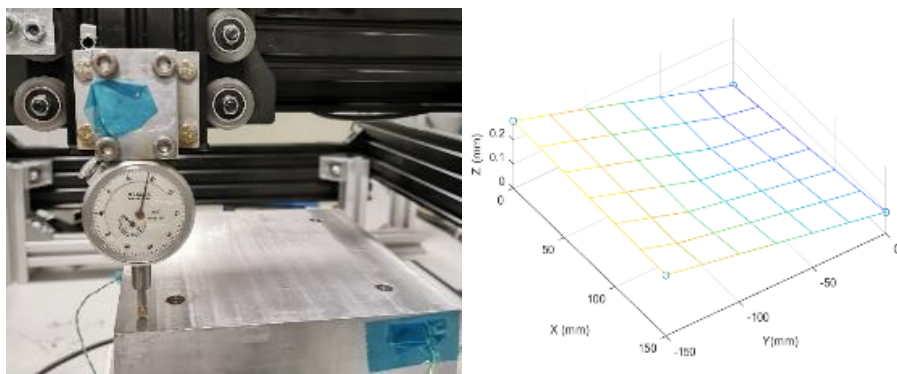


Figure 3-23. Left: measuring the alignment of the mould. Right: surface mapping of the mould.

### 3.3.3.6 Temperature influence

Piezoelectric force sensors are very sensitive to temperature and temperature changes leading to errors and long-term fluctuations [166, 167]. As mentioned before in this chapter, a 25-mm piece of an epoxy block with a low thermal conductivity was attached between the force sensor and the mould to prevent heat transfer from the mould to the dynamometer, as shown in Figure 3-16. However, temperature influence could not be overcome by this set-up alone. Figure 3-24 shows the force signal when the mould is at room temperature and subjected to a normal temperature cycle for automated in-situ consolidation. When the mould temperature is at room temperature, the force sensor keeps a stable value without any load. However, as soon as the mould changes its temperature, the force value varies without any load.

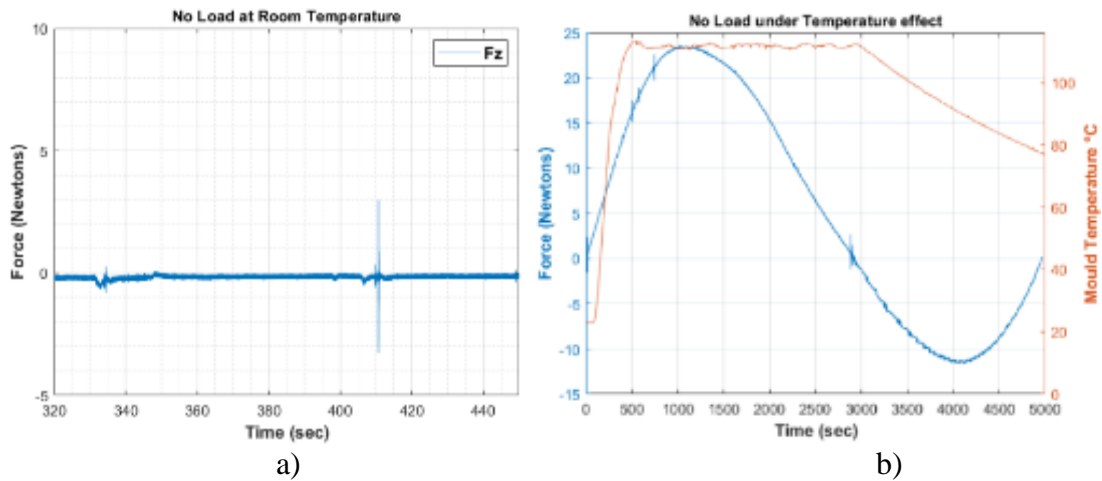


Figure 3-24. Force signals without (a) and with (b) temperature influence.

Different control measures were adopted to reduce as much as possible the temperature influence. Mechanical measures, as explained below, were not completely effective in reducing the effect of temperature. The most effective way to overcome this effect was to understand the problem and create a compensation algorithm explained in the forming force control section of this chapter.

The first measure was to eliminate or reduce the heat transfer path from the mould to the epoxy block insulator and then to the force sensor. Separators (washers) were located between the mould and the insulator; ventilation channels were machined in the bottom of the insulator, forced air convection was adapted in the bottom surface of the insulator, and metal bolts were replaced for nylon bolts to clamp the material to the insulator. All these measures are as illustrated in Figure 3-25.

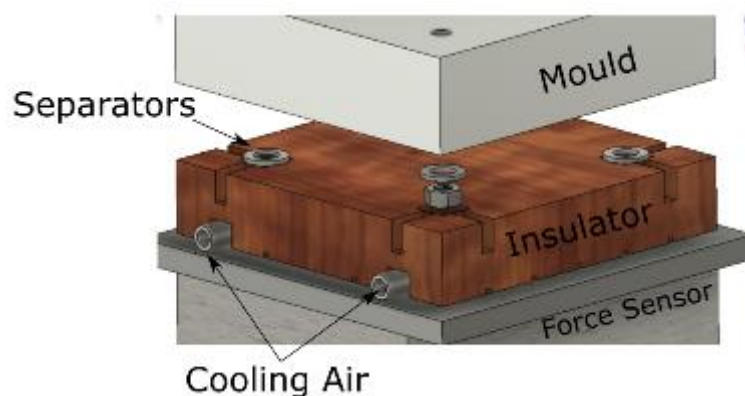


Figure 3-25. Measures to reduce heat transfer from the mould to the force sensor

### 3.3.3.7 Closed-loop Control

The unreliability of the open-loop force system, as described in previous sections, demands to improve the system to achieve the right forces. Furthermore, most multiple-axis load cells commercially available do not have a high temperature working range, and the budget did not allow to acquire a new load cell based on strain gauges. One possible could have been to design and built a new tool with integrated strain gauges, but due to the time constrains, it was not possible. Therefore, developing a closed-loop force system, was relatively faster and more economical.

A closed-loop system is defined as “a system that maintains a prescribed relationship between the output and the reference input by comparing them and using the difference as a means of control [153]”. They are particularly useful to control processes under the presence of external disturbances. Most industrial controllers may be classified according to their control action such as On-off, proportional (P), Integral (I), proportional-plus-integral (PI), proportional-plus-derivative (PD), or the most common, proportional-plus-integral-plus-derivative (PID). The following sections document the development and selection of suitable force closed-loop systems for the different forming stages involved in automated in-situ consolidation.

- **Target force approach**

As mentioned before (see Figure 3-21), approaching the target force takes 45 seconds approximately with this algorithm, though longer times were encountered while testing due to stack variability. The algorithm of the software was redesigned by implementing a proportional control. As shown in Figure 3-26, the target force is achieved in approximately 7 seconds. To perform the proportional control, the user must lower the tool with the commands in the graphical interface until it touches and compresses the stack achieving a positive force (e.g., ~2N as shown in Figure 3-26). Then, the user starts the approaching force set up by pressing the start button. When the force is achieved, then the tool is raised, which removes the compression force. The system moves back the tool to the last position to verify the compression force is in range, as seen in the last few seconds of Figure 3-26.

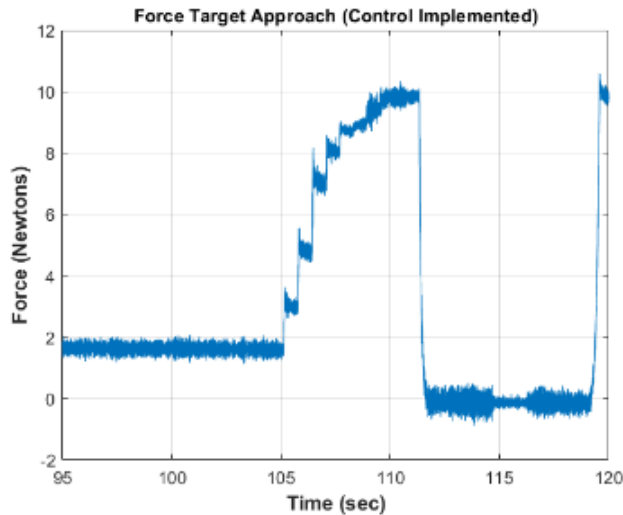


Figure 3-26 Force Target Approach with a proportional Control to target force of 10N

Figure 3-27 shows a comparison of the performance of different control algorithms such as Proportional + Integral (PI), Proportional + Integral + Derivative (PID) or fixed-small steps that were implemented to achieve a target force. A definition of each type of control can be found in reference [153]. The performance of a proportional control at different force targets is shown in Figure 3-27.a, indicating a very fast execution and stable control. The other algorithms created instability in the process (PI or PID), or the time reaching the target force was too long (Fixed-small steps), as shown in Figure 3-27.b, Figure 3-27.c, and Figure 3-27.d respectively. The LabView block diagram can be found in Appendix A

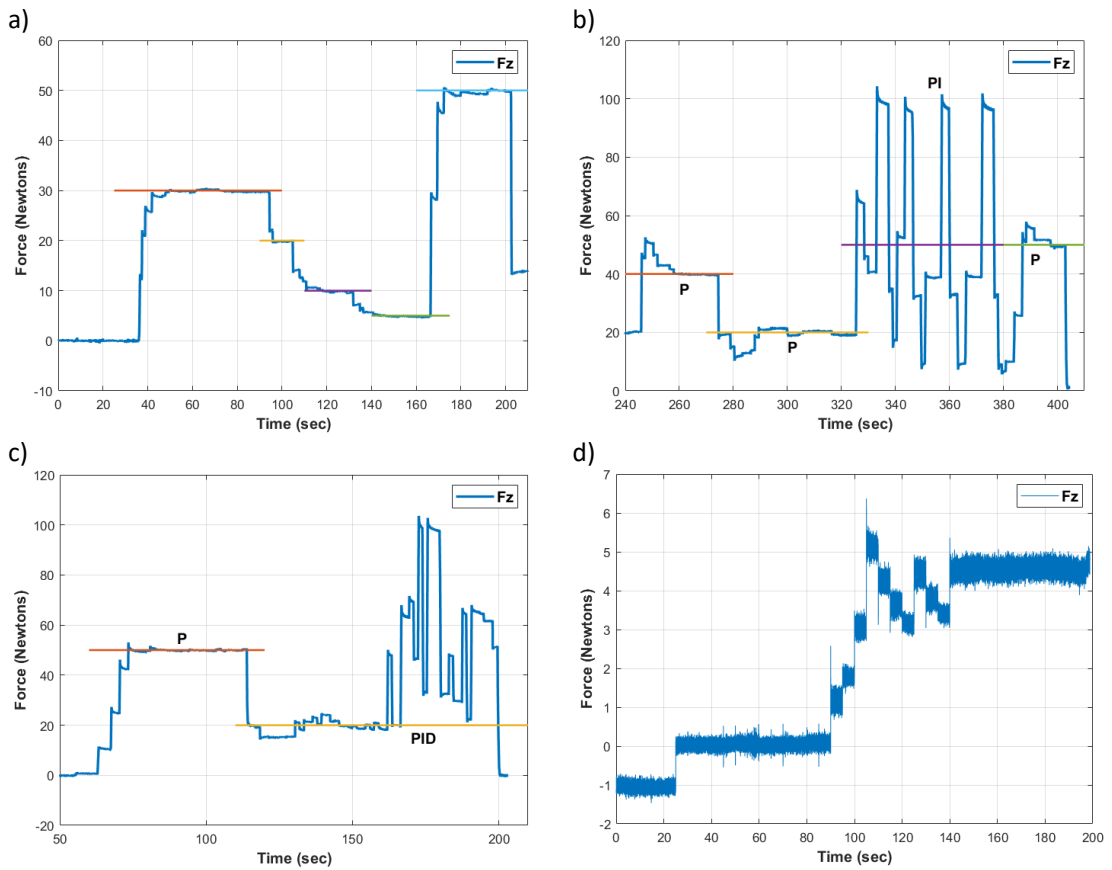


Figure 3-27. Force control approaches: a) Proportional Control, b) Proportional + Integral Control (PI), c) Proportional + Integral + Derivative (PID), d) fixed small steps. The colour lines are set point target forces to demonstrate the performance of the control algorithms.

- **Temperature Compensation**

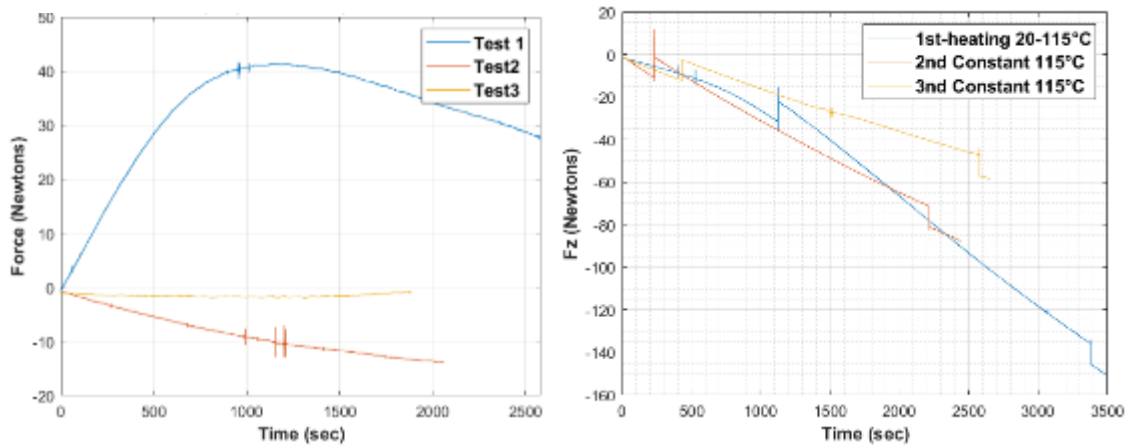


Figure 3-28. Force signals without (a) and with (b) loads under the temperature cycles of automated in-situ consolidation processing.

As explained previously (see section 3.3.3.6 *Temperature Influence*), the dynamometer force sensor is greatly influenced by temperature. Additional examples of the force readings under the influence of temperature without and with loads are shown in Figure 3-28. It can be seen that the data obtained from the force sensor is unpredictable in the sense of obtaining positive or negative values. As explained by the force sensor manufacturer [167], a dynamic error (signal change over time) is created when the surrounding temperature of the sensor changes because the sensor is not in thermal equilibrium with the environment. Keeping the sensor temperature constant is recommended, but any attempt to achieve it was unsuccessful in automated in-situ consolidation processing. This phenomenon also affects the reliability of the force close-loop system because it is based on the values it receives from the sensor to compare the sensed value with the target value. For example, using Figure 3-28 (left), where no load is applied to the sensor, the force control system will detect a value that will create an actuation of the forming tool. If the sensed force is higher than the target force, it will command the forming tool to raise its position; however, we know there is no load, and the tool should lower its position to start compressing the material. Therefore, a force control design must take into account this phenomenon.

Initially, the software was designed to move the forming tool while consolidating the material without lifting the tool, relying on the efficiency of the long-term accuracy of the sensor and the open-loop force system. However, as explained, the mould temperature affects the force sensor, so its output has a non-linear and unexpected long-term measurement behaviour. It was found that if the long-forming cycle is divided into short-forming cycles, it is possible to perform an online drift compensation before starting every cycle (See section 3.3.3.3 *Online Force Compensation*). This concept is better explained by looking at Figure 3-29. Instead of performing a continuous forming operation, the tool is raised after an interval selected by the user. When the forming tool is raised and separated from the material, the load value should be 0N. Because it is not 0, an online drift compensation is performed in this interval using a linear regression algorithm, compensating the temperature error for the next cycle. This action increases manufacturing time but facilitates the implementation and reliability of a force control system. The example shown in Figure 3-29 does not implement a force control system, which will be addressed in the subsequent sections.

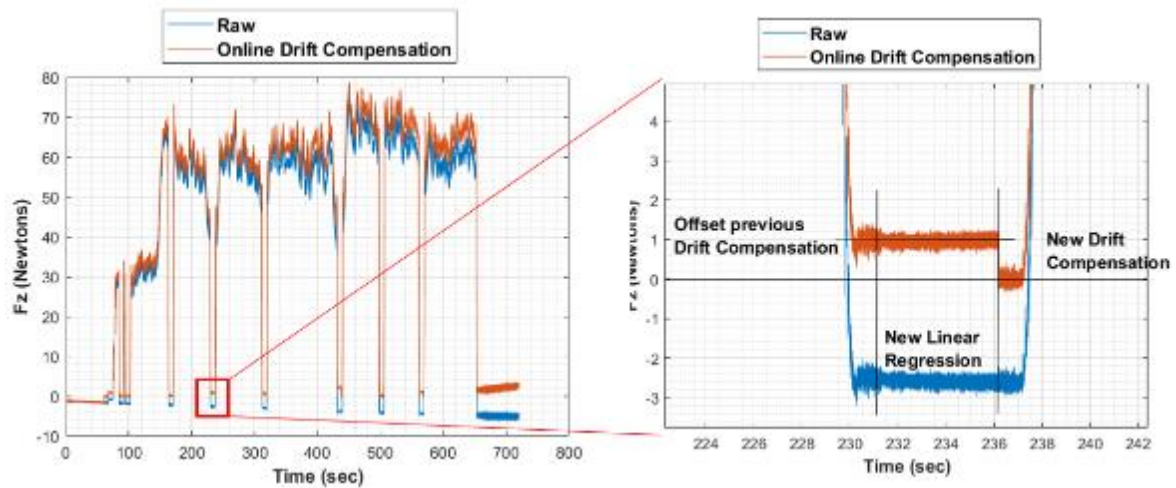


Figure 3-29. Temperature effect compensation using short forming cycles and an online-drift compensation. The forming process in this figure does not perform any force control system.

- **Forming Force Control**

Due to the success of a Proportional Control in finding the target force (See 1.4.3.3.1 *Target force approach*), initial attempts tried to implement a proportional control on a normal g-code file generated by the CAM software. For simplicity, the path planning was manually constructed by drawing lines between the coordinates (blue circles in Figure 3-31. a). An example of applying a proportional control system for the as-received g-code file is shown in Figure 3-30. The forming tool moves forwards and backwards, consolidating the material, and the values of the “Force-controlled” signal has been shifted for comparison purposes only. First, this control approach increases the forming time because the control system stops the movement in the X-plane and then adjusts the vertical position of the forming tool until the target force is found. After the force is found, the system acts as an open-loop system as no correction of the forming tool is performed.



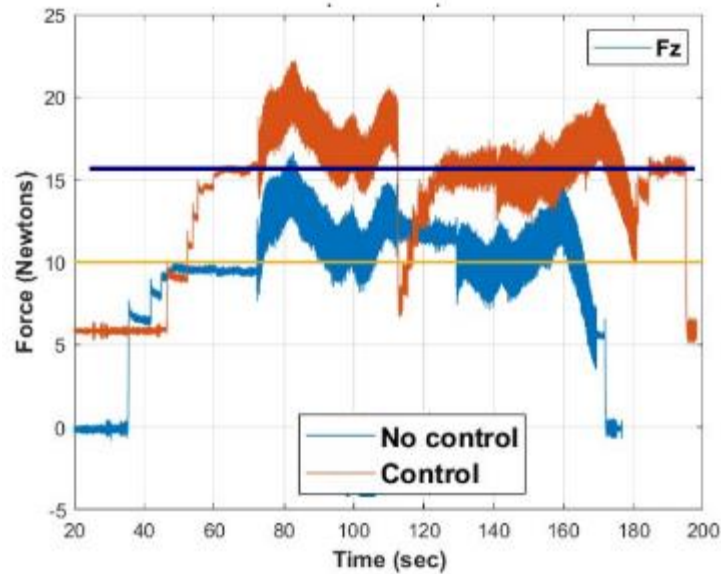


Figure 3-30. Proportional Control on

In order to increment the number of open-loop paths, the number of coordinates in a single tool path line. A program was written in MATLAB™ (see Appendix C) to modify the g-code file generated in CAM software to add more coordinates to the tool path, as shown in Figure 3-31. The results of this new approach can be observed in Figure 3-32 with a setpoint of 30N for the forming force. The force-controlled values are superimposed to the values received from the sensor to show the effectiveness of the temperature compensation strategy. A zoom of the forming forces demonstrates how the control is performed. “FC” stands for the force-controlled stage in which the proportional control modifies the vertical position of the tool to achieve the target force. “Path” refers to the forming operation in which the forming tool moves in the X/Y direction. Qualitatively speaking, there is good control of the force around the setpoint. However, this system still relies on combining a closed-loop system (FC) followed by an open-loop system (Path).

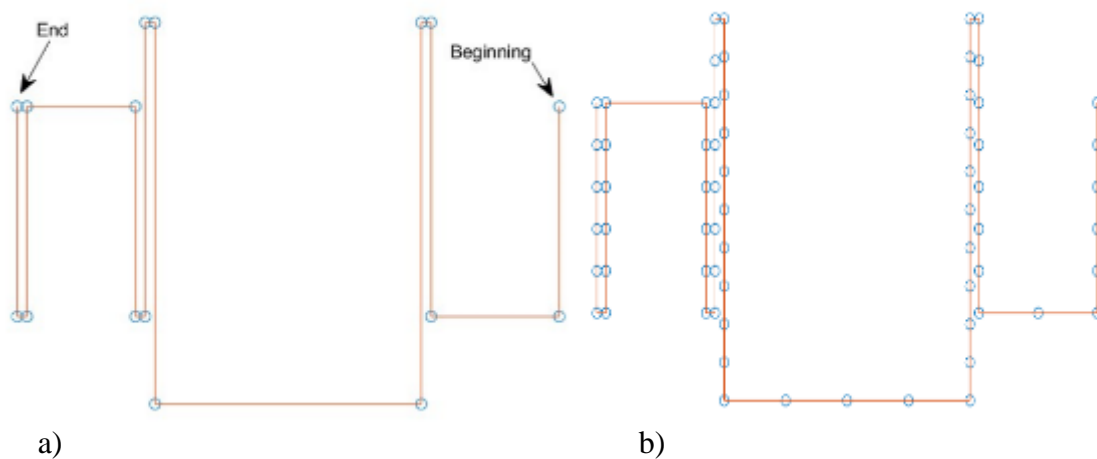


Figure 3-31. Tool Path transformation: a) original tool path and b) new tool path with additional coordinates

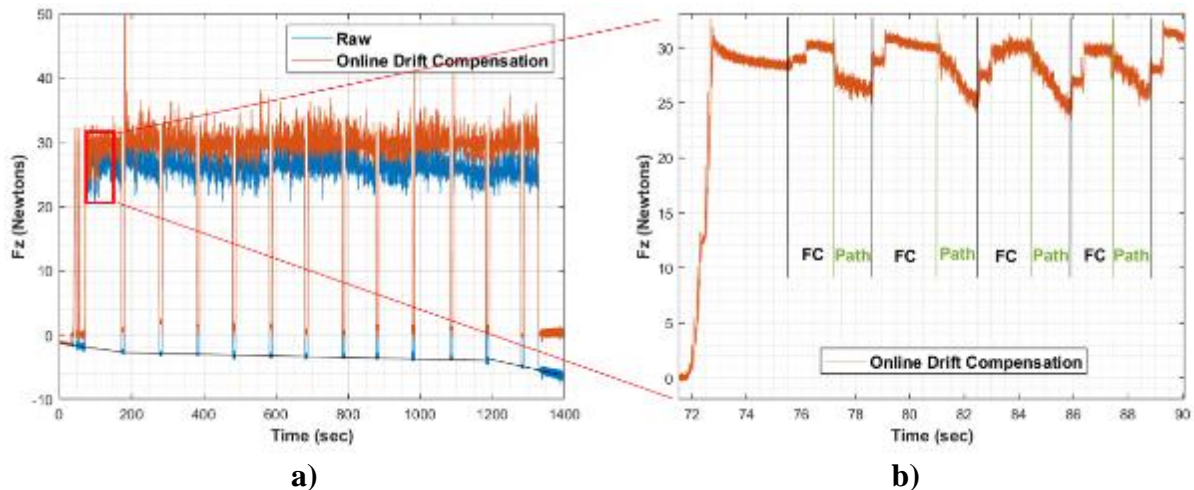


Figure 3-32. a) Forming forces with and without a Force closed-loop system (Proportional Control). b) zoom of the forming forces with a Force closed-loop system. FC=Force controlled

As mentioned, this control approach increases the forming time because the control system adjusts the forming tool position after every coordinate in the g-code file until the target force is found. Therefore, the forming time will depend on the number of coordinates of the toolpath and the time the force control system takes to find the force. While the first one can be predicted, the second one is unpredictable. Figure 3-33 shows examples of a force control system (closed-loop-plus-open-loop) in which the separation between coordinates varies. There is an increment in manufacturing time of 66% and 20% when the separation between coordinates is 2 mm and 5 mm, respectively, compared with a 10 mm separation.

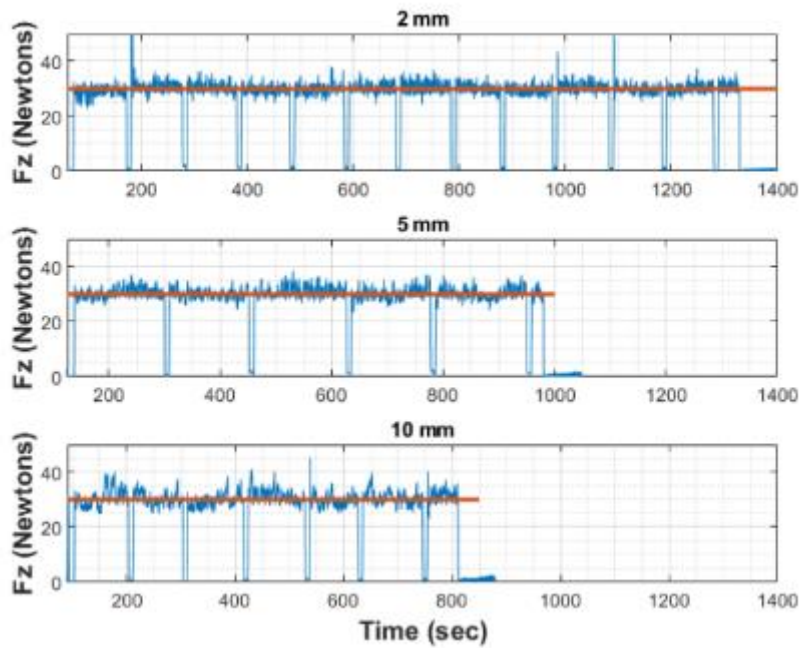


Figure 3-33. Forming forces with force closed-loop system with coordinates separated by a distance of 2 mm, 5 mm, and 10 mm.

- **PID Force Control**

Though the force control system previously described could be considered acceptable in terms of control, it had the limitation of increasing the manufacturing time. Furthermore, it relies on the combination of a closed-loop and an open-loop control system acting separately. The closed-loop is in charge of modifying the vertical position of the forming tool to achieve the desired force, and the open-loop is in charge of moving the forming tool in the X-Y plane. Knowing in advance the time it will take to perform these steps is unknown due to the closed-loop uncertainty, as shown in Figure 3-32. Table 3-1 shows the estimated manufacturing times for automated in-situ consolidation according to the length of the forming path. A tool path with a length of 648 mm corresponding to Figure 3-31, while a tool path with a length of 5000 mm corresponds to Figure 3-22 (see 1.4.3.2.3 *Forming stage*). The calculated times only consider the time the tool is moving, but not the heating and cooling times of the mould and forming tool. Unfortunately, due to the time scope of the project, a forming time of 174 min plus heating and cooling times was not acceptable.

*Table 3-1. Estimated manufacturing times for automated in-situ consolidation according to the length of the forming path*

Separation (mm)	Length of the path (mm)			
	648	5000	648	5000
	Time (seconds)		Time (min)	
2	1350	10417	22.50	173.61
5	975	7523	16.25	125.39
10	810	6250	13.50	104.17

The software was redesigned to make corrections on the vertical position of the forming tool while it is forming the material. The advantage of this process is that the forming tool does not need to stop the movement in the X-Y plane, reducing the forming times considerably, as shown in Figure 3-34, compared with Figure 3-33. Performing corrections while the forming tool moves in the X-Y plane was obtained by changing the proportional control to a PID control. A similar approach was performed to determine the influence of the distance between coordinate in the control system. It can be seen that a 0.5 mm separation distance presents a better control than the others. However, one disadvantage of a PID control is the stability of the system, as PID controls tend to create oscillations. The PID control parameters were set up empirically [168] to reduce oscillations as much as possible as shown in Table 3-2

*Table 3-2. PID Control Parameters found empirically*

Control Parameter	Force Approach Stage	Forming Stage
proportional gain (Kc)	-0.017	-0.005
integral time (Ti, min)	0	0.01
derivative time (Td, min)	0	0.005

For this project, the PID force control achieved acceptable levels of control (qualitative) using a 0.5 mm separation between coordinates. Therefore, it was used for the development of subsequent chapters.

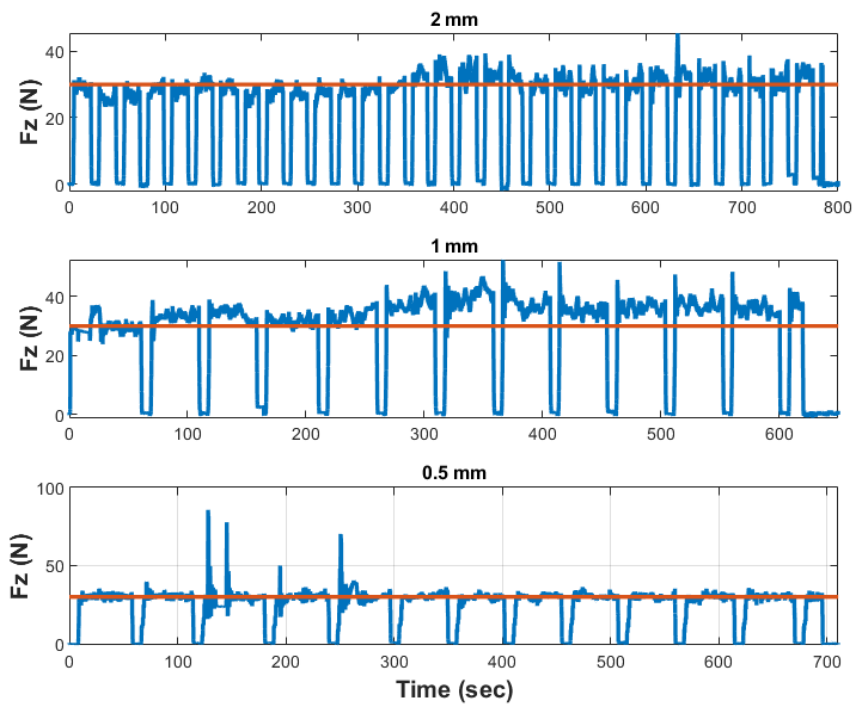


Figure 3-34. Forming forces with force PID closed-loop system with coordinates separated by a distance of 2 mm, 1 mm, and 0.5 mm.

### 3.3.4 Clamping

Most thermoplastic manufacturing systems ensure the stack of layers conforms to the mould in different ways. Autoclave and hot compression manufacturing processes use a double mould that completely restrains any degree of freedom of the stack. Automated methods such as AFP or ATP relying on the adhesion of the tapes or fibres when they are melted and deposited over the mould and subsequent layers. Other thermoforming processes such as vacuum forming clamp the edges of a pre-consolidated laminated.

In this project, clamping the stack of layers is used to ensure the forming process of the material does not create extreme distortions. It was seen in previous sections that the motion of the tool also creates transversal forces according to the direction of the forming path. If these forces are not compensated, the material is dragged by the forming tool as shown in Figure 3-35(a). Therefore, a degree of clamping is required over the material to compensate the force created by the forming tool. Figure 3-35(b) and Figure 3-36 shows the result of the manufacturing operation with clamping demonstrating the need for it, and the clamping mechanism used. The layers were cut from the fabric to create a laminate with a lay-up

configuration  $[0/90]_5$ . After cutting they were stacked on top of each other, and then a soldering tool with a temperature of  $250^\circ\text{C}$  was used to make the holes with a bigger diameter than the clamping bolts. The material is then clamped on to the mould by tightening the bolts of the clamping sheet. This clamping mechanism allows for extra room for further displacements if required, especially for double curvature laminates as described in Chapter 6 Three-dimensional laminates and characterisation.



Figure 3-35. in-situ consolidated laminate without (a) and with (b) clamping.

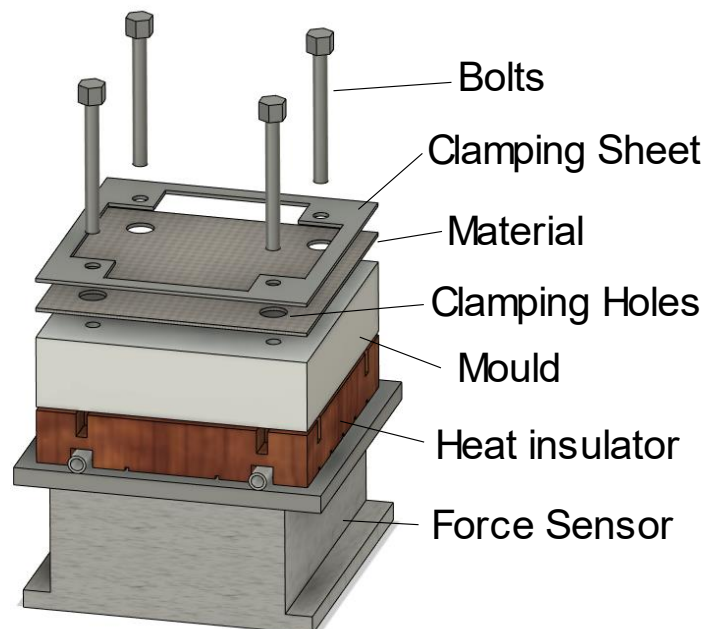


Figure 3-36 Clamping mechanism of the laminate over the hot mould. The layers are cut and stacked

### 3.4 Energy Consumption

“Life cycle assessment (LCA) is a technique to assess the environmental aspects associated with a product or process by identifying energy, materials, and emission over its life cycle [169]”. Several climate challenges are among the concern of scientists and politics, and new regulation forces industries to reduce the impact of their products and processes on the environment. Industries must improve their energy efficiency either by using renewable sources or implementing new low energy intensity procedures. Performing a full LCA is out of the scope of this project. Instead, this section focuses on measuring the energy intensity (MJ/kg) of the new low-cost automated in-situ consolidation machine and compares it with a 300w hot press. In this way, a relative comparison between the two methods can be made.

A household energy monitor (Intertek, UK) was used to measure the electricity consumed to produce a flat laminate for automated in-situ consolidation of self-reinforced composites. The monitor was reset every time before being used on each device that consumes electricity for both manufacturing techniques at a processing temperature of 160°C. Four measurements were taken to avoid variability.

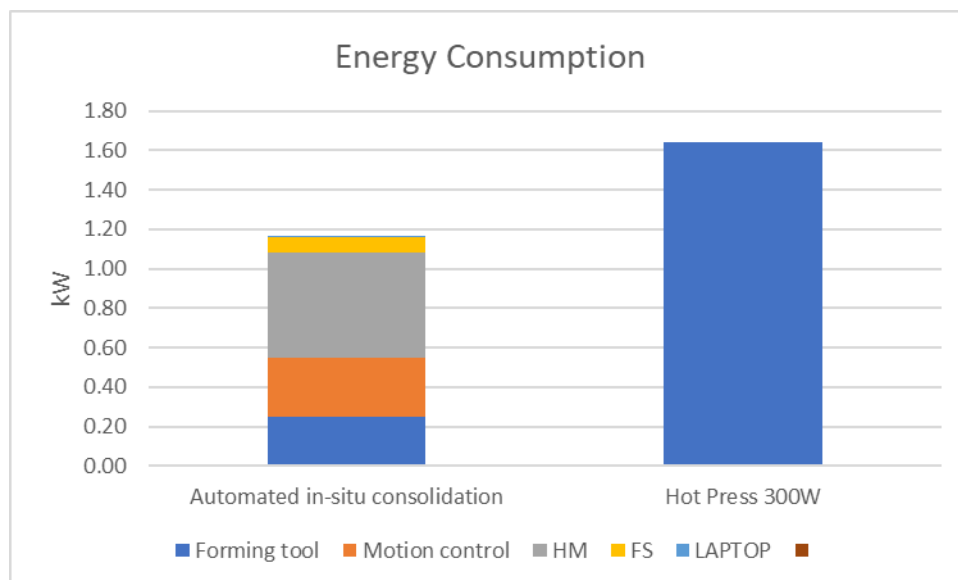


Figure 3-37. Energy consumption comparison between Hot Press and Automated in-situ consolidation of Self-reinforced polypropylene composites. HM=Hot mould, FS= Force Sensor. Error bars are small (~0.01) and have been omitted for clarity

Figure 3-37 shows the average energy consumption of each device for the automated in-situ consolidation machine and a 300W Hot Press with a total average energy consumption of  $1.17 \pm 0.03$  MJ and  $1.64 \pm 0.01$  MJ respectively, representing a 28.85% reduction in energy consumption compared with the hot press. This is expected since a hot press heats two moulds instead of one mould and a small forming tool for the automated in-situ machine. Interestingly, despite the small size of the copper forming tool and its lower heat capacity than aluminium ( $0.36 < 0.91 \text{ kJkg}^{-1}\text{C}^{-1}$  [170]), the energy consumed (0.25 MJ) is almost half the energy for the hot mould (0.53 MJ) in the automated in-situ consolidation machine. This is because in-situ consolidating the material is a transient and dynamic process, in which the tool needs to constantly transfer heat to the material so the copolymer can undergo a phase transition from solid to liquid: what is commonly named as melting. The latent heat of melting requires the temperature controller to increase the power to maintain or keep the temperature [171]. This is the opposite for the hot mould as its temperature is below the melting point of the copolymer. The job of the hot mould job is to help speed up the melting process by creating a smaller temperature gradient in the laminate thickness. If the temperature of the mould were lower, the forming tool should increase its temperature to compensate for the temperature gradient. However, this will promote melting of the reinforcement of the layers in contact with the forming tool. Of course, the mould must contribute to the heat transfer of the material during melting. However, because of the location of the temperature sensor on the hot mould (side of the mould as shown in Figure 3-23), fast local temperature changes will not raise the overall temperature of the mould, and therefore, the controller does not require to give more power to the heater of the hot mould. This also explains the difference in power required between the hot press and the automated in-situ consolidation machine. To melt the copolymer and/or homopolymer crystals, more heat must be given to the material. In this case, the temperature controller must provide more power to both the top and bottom mould.

Considering an energy cost of £0.16 per kWh, the average cost of electricity to produce a flat laminate with automated in-situ consolidation and a hot press is £0.05 and £0.07 respectively. A first sight, the price might not represent a difference for low volume manufacturing, mainly because better geometrical accuracies are achieved with hot processing. However, the price of the component increases in hot press processing due to the



need to produce two moulds instead of one. Similarly, the energy intensity of the processes, i.e., the energy required to produce one kilogram of a product [172], is 58.27 MJ/kg (1.17 MJ/0.020 kg) and 81.90 MJ/kg (1.64 MJ/0.020 kg) for the automated in-situ consolidation machine and hot press respectively. It is important to highlight that these values are specific for processing a flat panel of 20 grams of weight. There is a high variability of energy intensity values in the literature which prevent any comparison. For example, reported autoclave energy intensity values are 21.9 MJ/kg [169] or 600 MJ/kg [173]. For the purpose of this thesis, the proposed process for automated in-situ consolidation has a better energy intensity performance than Hot Press manufacturing of self-reinforced polypropylene composites.

A novel manufacturing process based on automated in-situ consolidation of self-reinforced composites has been 65% more energy efficient than a benchmark hot press processing. However, it is arguable whether automated in-situ consolidation of self-reinforced composites is cost-effective in the long term. Further research of automated in-situ consolidation, as shown in Chapter 7, will replace the hot mould with another small tool. This will increase design flexibility, reduce energy consumption, and, therefore, manufacturing costs.

### 3.5 Automated In-situ Consolidation Workflow

This section outlines the required procedures to use the proposed low-cost automated in-situ consolidation machine covering the initial design of the part to the manufacturing stage, as shown in Figure 3-38. A brief description of each step follows.

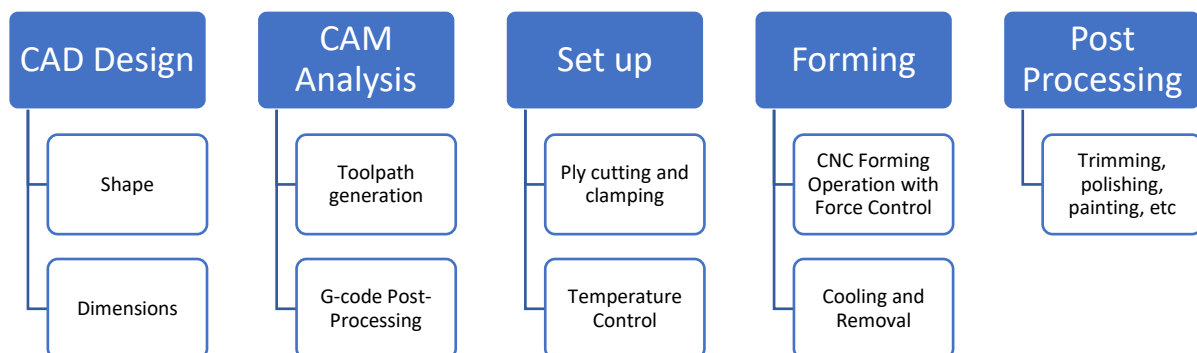


Figure 3-38. Automated In-situ Consolidation Workflow

1. Part/Mould design: A CAD Software (e.g., FUSION 360, SOLIDWORKS, etc.) should be used to design both the part and the mould according to the functional specifications.

The mould should be designed considering the size of the heating elements used, location of the thermocouples, earth connection, fixing connections to the insulator, and fixing connection to clamp the preform.

2. Automated Tool Path generation: A CAM software (e.g., FUSION 360, SOLIDWORKS, etc.) should be used to generate g-code files. The tool path should be designed for manufacturing, considering how the force control system works to promote the best achievable control. For example, there should not be high fluctuations in the vertical axes while forming, as explained in the chapter three-dimensional laminates and characterisation. Because an open-loop motion controller is used, the g-code file with the tool path must be modified using a Matlab program developed in this project. It is available in the Appendix C.
3. Material Preparation: the preform should be cut and stacked according to the design stage and clamped to the hot mould.
4. Machine preparation: Turn on the machine and set the temperature controllers to the required setpoints until the temperature reaches a constant value for the mould and forming tool.
5. Locate and clamp the stack on the mould: Use hands to conform the material to the mould if required.
6. Forming: Use the graphical interface of the software to operate the machine until the forming process starts. Once the forming process finishes, the forming tool is raised.
7. Cooling and part removal: Allow time to cool down so the material can crystallise. The part can be removed once the temperature mould has reached a temperature below the crystallisation temperature of the material.
8. Post-Processing: Trim edges and excess material accordingly.

### **3.6 Machine specifications**

Application of this technology is expected to be within low-volume, high-value manufacturing such as prototyping and development. The main features of the machine are described in Table 3-3.

Table 3-3 Automated in-situ consolidation machine specifications

<b>System Element</b>	<b>Description</b>	<b>Justification</b>
General system	Bench top size Powered using 220V AC single phase	Convenient to be used within most laboratory/research environments.
Motion platform	Three axis control Speed up to 2000 mm/mm*	Minimum for three-dimensional forming operations *Depends on the material being used. For self-reinforced polypropylene a speed of 90mm/min or lower should be used.
Build plate	100x100 * 300x300 if a load cell were used on top of the forming tool**	*Limited clamping options of the mould over the force sensor **Limited by machine construction limitations.
Force Load Cell	5KN piezo electric dynamometer	Existent piece of equipment in the research group
Heating element	240V cartridge heater	Easy to wire and operate. Easy to attach to a forming tool
Temperature control	PID temperature control for both mould and forming tool using thermocouples Temperature limit: 200°C*	Easy to wire and operate Temperature depends on the mater *Depends on the material being used
Software and Control	LabView Based * Control motion of the forming tool based on a closed-loop force system Provides feedback to the operator regarding machine status** Force software limits are set to 100N in the z axis for a flat tool, and 70 N for hemi-spherical tools**	*Easy to program with user friendly graphical interfaces **To achieve constant levels of consolidation through the area being formed without damaging the material ** software limits can be changed as they might depend on the material.
Toolpath generation	Production of parts using a single toolpath file Automated toolpath generation using MATLAB	To reduce at maximum operator tasks.

## 4 Forming Mechanisms of Automated In-situ Consolidation

Numerical modelling of the physical mechanisms can speed up optimisation procedures reducing the cost and time involved in developing a manufacturing process [46, 174]. Modelling is used to simulate the physics of the process to predict phenomena or performance outputs. In this section, the physics of the bonding mechanism is explained, however, its modelling was out of the scope of this project. On the other hand, a heat transfer model to predict the temperature distribution through the laminate thickness is developed and validated.

### 4.1 Theory of bonding polymer interfaces: Autohesion

The bonding process between two interfaces of the same polymer is called autohesion or self-diffusion and involves molecular mobility across two surfaces in contact. This mechanism governs the interfacial bonding strength of the thermoplastic composites, which is critical for the good performance of the part and depends on the processing temperature, contact pressure, and contact time. High temperature is necessary to ensure molecular mobility. Pressure is required to bring the surfaces in contact, and time allows the interdiffusion of the polymer chains. Finally, the ultimate interfacial bonding strength is achieved after a long contact time. A complete interpenetration is achieved due to the entanglement of the molecular chains between surfaces, making the interface no longer distinguished, as illustrated in Figure 4-1.

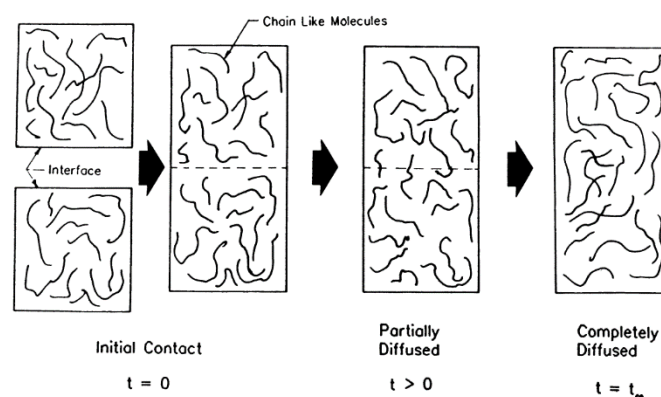


Figure 4-1. Schematic of autohesion or self-diffusion between two contact surfaces of the same polymer. Public use permitted [175].

The interdiffusion of polymer chains across an interface is based on the “reptation theory”, firstly proposed by Pierre-Gilles de Gennes [176, 177]. In the reptation theory, the motion of individual chains in the bulk of the polymer is restricted by imaginary tubes, created by the surrounding polymer chains. Each tube is surrounded and entangled to the other tubes of the other chains, as shown in Figure 4-2. a. Though the tubes are free to change their shape or move, they cannot penetrate other tubes. Moreover, a polymer chain (restricted by its tube) can move along the main axis of the tube but not in the radial direction, (hence “reptation”). As the polymer chain moves, the tube length changes accordingly, as shown in Figure 4-2. b. At  $t = 0$ , the chain is in its initial tube. At  $t = t_1$ , the chain moved from its position due to diffusion creating a new tube. The length that the chain moved from  $t=0$  to  $t=t_1$  is called the “minor chain”. As time passes, the “minor chain” increases with time as the polymer chain moves. Finally, after a time  $t_{\infty}$ , which is known as reptation time, the polymer chain has moved completely from its initial configuration. De Gennes demonstrated that the reptation time is proportional to the cube of the molecular weight of the polymer according to Equation 4-1.

$$t_{\infty} \cong M^3$$

Equation 4-1

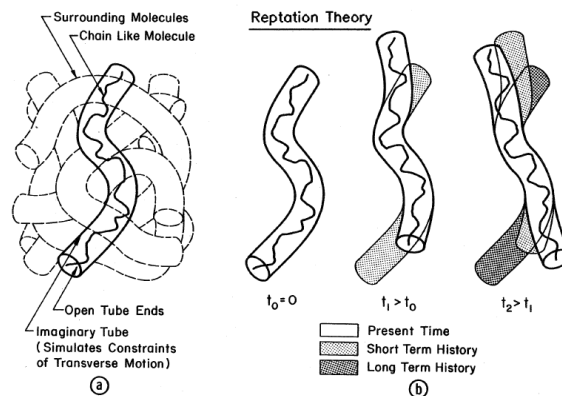


Figure 4-2. Reptation Model of polymer chains. Public use permitted [175].

The reptation theory was then expanded from the motion in the bulk polymer to the interface between two polymer surfaces, as shown in Figure 4-3. The reptation time refers to when a polymer chain has penetrated the interface of the polymer surfaces. The chain penetration then allows molecular entanglement in the interface between the surfaces, making the interface no longer distinguishable. Analytical relationships for the interfacial

bond strength were developed [178, 179] according to Equation 4-2. It is assumed that the interfacial strength is proportional to the fourth root of the contact time.

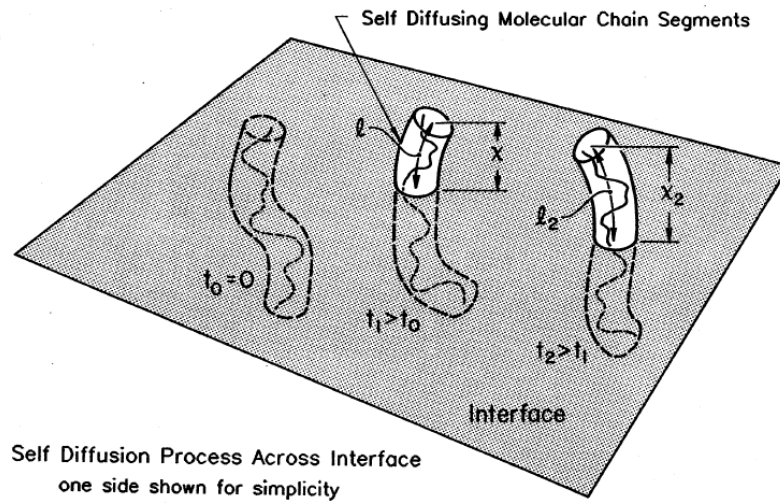


Figure 4-3. Reptation at an interface between two polymer surfaces. Public use permitted [175]

$$\sigma \sim t^{1/4} M^{-1/4} \quad \text{Equation 4-2}$$

Where  $\sigma$  is the interfacial bond strength,  $t$  is the contact time, and  $M$  is the molecular weight. Furthermore, as the bonding temperature increases, the interfacial bonding strength reaches its maximum at a higher rate, as illustrated in Figure 4-4. As can be seen, the slope of the curve ( $K = f(T)$ ) depends on the temperature and has been modelled assuming an Arrhenius temperature dependence, and can be written as:

$$K(T) = K_0 e^{\left(\frac{-E_a}{kT}\right)} \quad \text{Equation 4-3}$$

Where  $K_0$  and  $E_a$  are constants that can be determined empirically by plotting the natural log of  $K(T)$  versus the reciprocal temperature  $1/T$ .

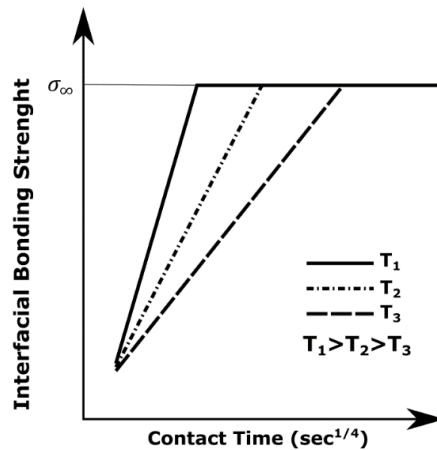


Figure 4-4 Interfacial bonding strength as a function of the fourth root of contact time for a given polymer at different temperatures ( $T$ ). The higher the temperature, the faster the contact time required to achieve maximum strength. Public use permitted [175]

## 4.2 Heat Transfer

As mentioned, as the forming tool in-situ consolidates a stack of layers, it compresses and transfers heat to the material to promote bonding between their interfaces, as shown in Figure 4-5. a. There are three parameters involved in this process: dwell time, temperature, and pressure. The dwell time is determined by the speed the tool moves and its diameter. The material undergoes deformation because of the pressure of the forming tool, which smooths the surface and reduces the thickness. However, high pressures can also lead to damage. Heat transfer in this in-situ consolidation process occurs in two different situations, as illustrated in Figure 4-5(b). Firstly, it is transferred from the mould to the laminate due to the contact between the bottom layers. As these layer heats, heat transfer is transmitted to the rest of the layers but not efficiently because they are not bonded. A minor secondary heat transfer also occurs due to convection because the hot mould heats the surface of the air surrounding it. Second, heat transfer occurs during compression in the nip of the tool because the forming tool is at a higher temperature than both the material and the mould, increasing the temperature of the stack. Finally, when the forming tool passes over the material, the material cools down and the molten polymer crystallises, giving out heat that is transferred to the surrounding air, and the mould.

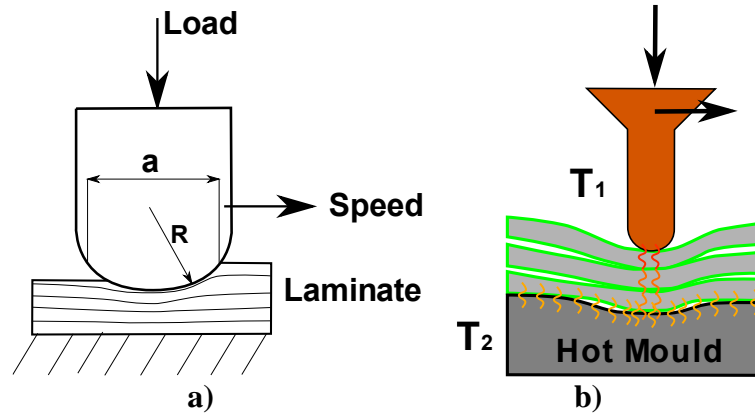


Figure 4-5. Schematic of single-point in-situ consolidation

Heat transfer modelling predicts the temperature distribution in the material when the forming tool passes over it. The heat transfer while bonding of polymer layers has been studied according to different manufacturing processes [180-183]. The transient state heat transfer model can be approximated with a one-dimensional model given by

$$\frac{\partial T}{\partial t} = \alpha \frac{\partial^2 T}{\partial x^2}; \text{ and } \alpha = \frac{\kappa}{\rho c_p} \quad \text{Equation 4-4}$$

Where  $T$  is the temperature,  $t$  is the time,  $\alpha$  is the thermal diffusivity in which  $k$  is the thermal conductivity,  $\rho$  is the density,  $c_p$  is the specific heat, and  $x$  is the direction of the heat propagation. In this case, the propagation direction is normal to the plane of the laminate (through-thickness). The solution of the above equation can be solved analytically with their corresponding initial and boundary conditions. Two cases are analysed: one in which the temperature of the tool and mould are the same, and another in which the temperatures are different, being the tool temperature higher than that of the mould.

**Case 1:** Both the forming tool and the mould have the same temperature,  $L$  is the thickness of the laminate,  $T_0$  is the initial temperature of the laminate, and  $T_r$  is the temperature of the forming tool and mould

$$T(x, 0) = T_0$$

$$T(0, t) = T_r$$

$$T(L, t) = T_r$$

**Case 2:** The forming tool temperature  $T_1$  is different from the temperature of the mould  $T_2$ .



$$T(x, 0) = T_0$$

$$T(0, t) = T_1$$

$$T(L, t) = T_2$$

The general solution of a differential equation as Equation 4-4 is given by

$$T(x, t) = C_1 e^{-\lambda^2 \alpha t} (C_2 \sin(\lambda x) + C_3 \cos(\lambda x))$$

Where  $C_1$ ,  $C_2$ ,  $C_3$ , And  $\lambda$  are constants that can be determined by using the boundary conditions. Therefore, applying the initial and boundary conditions for each case in the general solution and replacing them in Equation 4-4 results in:

case 1

$$T(x, t) = T_r + (T_o - T_r) * \frac{4}{\pi} \sum_{n=1,3,5}^{\infty} \frac{1}{n} \sin\left(n\pi \frac{x}{L}\right) * e^{-\frac{n^2 \pi^2 \alpha t}{L^2}} \quad \text{Equation 4-5}$$

case 2

$$T(x, t) = T_1 + \frac{(T_2 - T_1)x}{L} + \sum_{n=1}^{\infty} e^{-\frac{n^2 \pi^2 \alpha t}{L^2}} * \left[ \sin\left(\frac{n\pi x}{L}\right) * \left[ \frac{2}{n\pi} (T_2 (-1)^n - T_1) + \frac{2T_0}{n\pi} (1 - \cos * (n\pi)) \right] \right]$$

Or expanded for the  $n = 1, 2$

$$T(x, t) = T_1 + \frac{(T_2 - T_1)x}{L} + \left\{ e^{-\frac{\pi^2 \alpha t}{L^2}} * \left[ \sin\left(\frac{\pi x}{L}\right) \right] * \left[ \frac{2}{\pi} (-T_2 - T_1) + \frac{4T_0}{\pi} \right] + e^{-\frac{4\pi^2 \alpha t}{L^2}} * \left[ \sin\left(\frac{2\pi x}{L}\right) \right] * \left[ \frac{1}{\pi} (T_2 - T_1) \right] \right\} \quad \text{Equation 4-6}$$

Where  $t$  is the dwell time in the nip, and its calculation can be found in the Appendix "Heat transfer model."

Figure 4-6 and Figure 4-7 shows schematics of the through-thickness temperature distributions due to a transient heat transfer for both cases at different speeds, and the numerical program to calculate them is shown in Appendix B. When the forming tool and mould temperatures are the same, the temperature distribution has a shape like valleys in which its depth depends on the forming speed. The faster the speed, the higher the depth of the valley. On the opposite, the slower the speed, the lower the depth of the valley. When the forming tool temperature is higher than the mould temperature, the slowest possible speed will create a linear temperature gradient between the forming tool and the mould. When the speed increases, the temperature distribution has a shape like valleys similar to case 1 and a temperature gradient between the two hot surfaces. To validate the heat transfer model proposed, automated in-situ consolidation experiments at different speeds were performed.

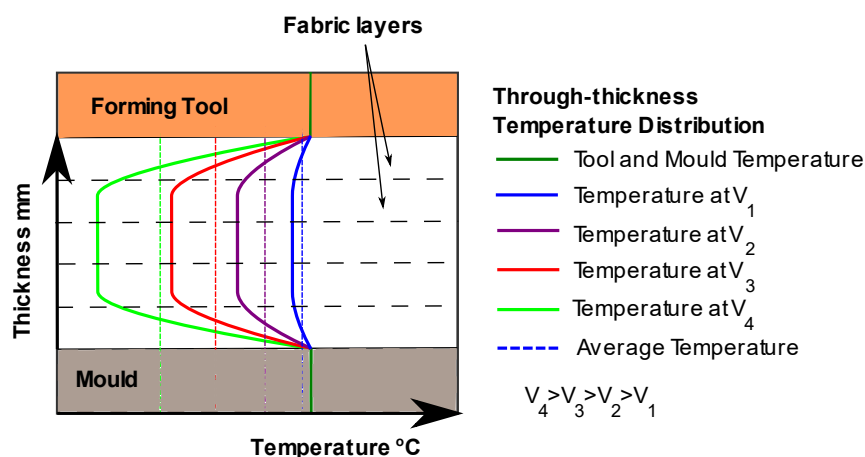


Figure 4-6. Through-thickness temperature distribution is caused by a transient heat transfer when the forming tool and the mould are at the same temperature at different forming tool speeds. The slower the speed, the smaller the gradient, and the highest the average temperature.

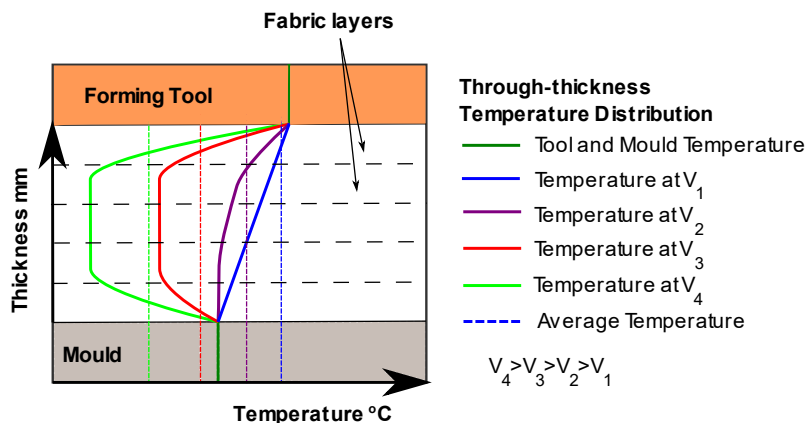


Figure 4-7. Through-thickness temperature distribution is caused by a transient heat transfer when forming tool has a higher temperature than the mould at different forming tool speeds. The slower the speed, the smaller the gradient.

#### 4.2.1 Experimental Set up

A thermocouple junction was created for by stripping and twisting together the wires of a Type-K thermocouple (RS Components, UK). The other end of the thermocouple wires was connected to a thermocouple connector (IEC Miniature plug, RS Components, UK), which was then connected to a temperature data logger (Picolog TC-08, PicoTechnologies, UK). The junctions were located and fixed with tape in the interfaces of a 6-ply laminate as illustrated in Figure 4-8. The forming path was design as to measure the temperature while the forming tool is consolidating the material in a normal forming operation as shown in Figure 3-22(left). In this way the forming tool is mean to get closer to the thermocouple as it forms the material. An additional thermocouple was located on the top surface in contact with the forming tool; however, it was dragged away when the forming tool passed over it. Because of this, the thermocouple, shown as a blue circle, was located far away from the forming tool path for monitoring the temperature of the top surface. The mould temperature was set at 115°C, the compression force was 50N, and the separation between forming paths was 2mm. several forming speeds were tested: 90 mm/min, 400 mm/min, 600 mm/min, 800 mm/min, 1000 mm/min, and 1200 mm/min.

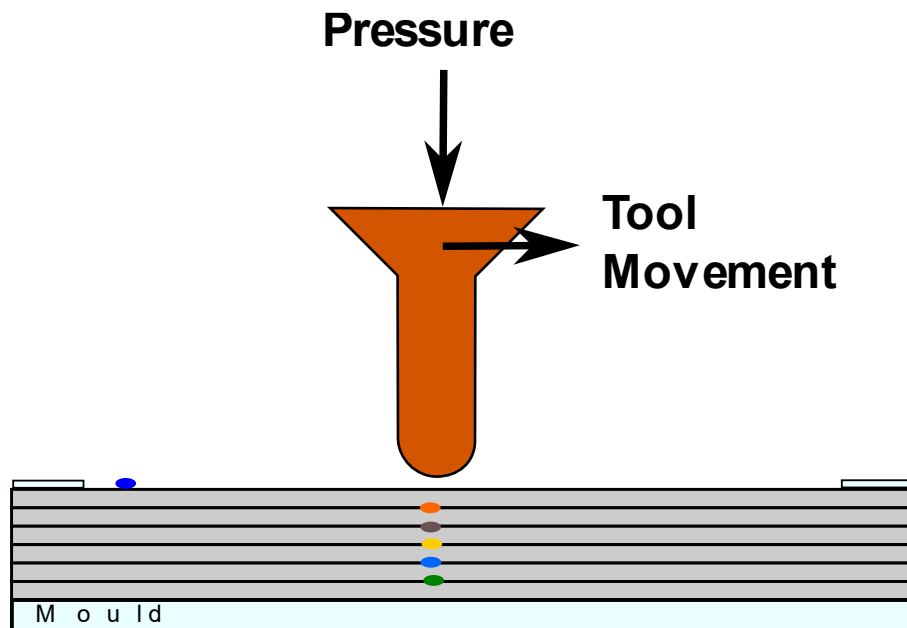


Figure 4-8. Thermocouples (represented by a colour dot) located in each interface through the thickness of a 6-ply laminate. The dark blue thermocouple represents the room temperature reading.

## 4.2.2 Results

Figure 4-9 shows typical temperature readings at the interfaces of a 6-ply laminate manufactured via automated in-situ consolidation. During the whole process, the dark blue thermocouple in Figure 4-8 is not in contact with the forming tool and shows a small amplitude sinusoidal variation at approximately 85°C. This variation is believed to occur due to the convection of the forming tool to the environment when the tool is close or far away from the position of the thermocouple. The reading value of the dark blue thermocouple (top surface of the laminate) is mainly caused by the heat transfer from the mould to the material, creating a temperature gradient as explained before. The initial temperature gradient through the thickness of the laminate can be observed in the first minute of the test, in which the temperature decreases from “layer 5” (the closest to the hot mould) to the top surface (in contact with the environment, or the forming tool respectively). When the forming tool starts to consolidate the material, and it then passes over the position of the thermocouples, their temperature starts to increase showing again a periodic variation. As just explained the variation is due to the distance of the forming tool from the exact position of the thermocouple. As the forming tool gets close, the temperature increases, but decreases when it moves away. Therefore, there is a considerable variation until the centre of the forming tool is just over the exact position of the thermocouple. In this case this happens when the temperature peaks for each thermocouple. As expected, the maximum peak temperature is achieved for the top 2 interfaces due to its proximity to the forming tool, while the subsequent interfaces have a lower temperature which is expected, as was explained in Figure 4-7.

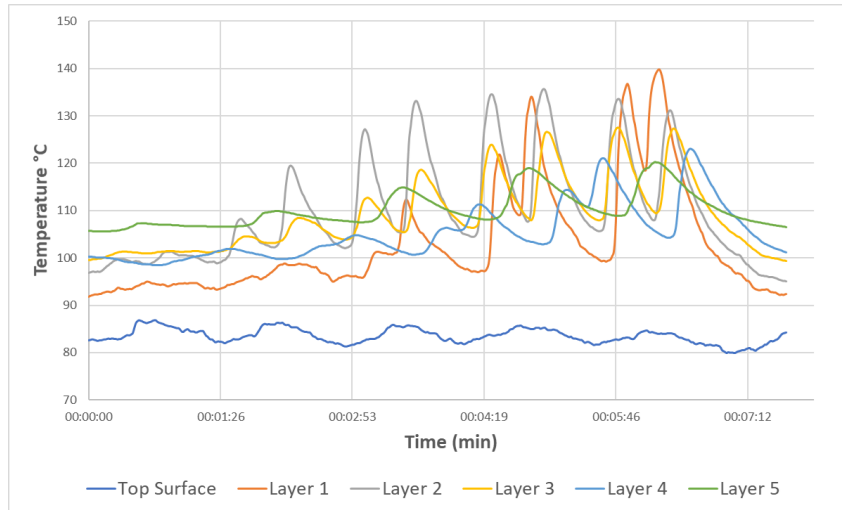


Figure 4-9. Typical Temperature readings a 6-ply laminate manufactured via automated in-situ consolidation at a forming speed of 90 mm/min, a forming temperature of 140°C and a compression force of 7 bars.

To validate the theoretical model from Equation 4-6, the maximum temperature achieved by each interface is recorded and presented in through thickness temperature distributions according to the forming speed as shown in Figure 4-10. In general, the experimental values have a good agreement with the theoretical models. However, at speeds above 400 mm/min, temperature readings are slightly below theoretical calculations. The assumptions of the theoretical model can cause discrepancies between the predicted values and the experimental ones. For example, it is assumed that the stack of material is composed of one single material, but the it is a stack composed of several layers with a wavy structure which can cause contact resistance to heat transfer [181]. Furthermore, each layer is made of a tape woven structure, and each tape is made of 3 layers with different behaviours under the action of temperature such as coefficient of thermal conductivity, viscosity and modulus, which were considered constant values in the theoretical model. Despite this, it can be seen that the minimum temperature is above the sealing temperature of the copolymer (106°C), which, even if it is not ideal, is the temperature at which interfacial adhesion starts. However, there is a good agreement between experimental and predicted values, which can help to speed up the selection of processing temperatures for the hot mould and forming tool, respectively.

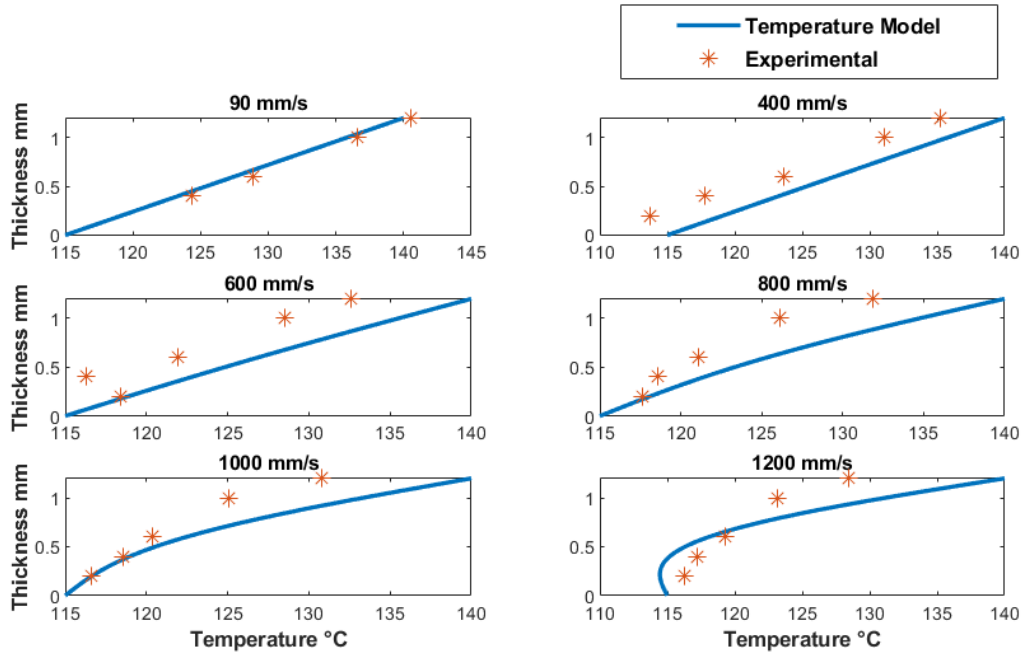


Figure 4-10 Temperature Distributions at different Speeds. Fix parameters for simulation are:  $\alpha = \frac{0.16W}{m^2K}$ ,  $Cp = \frac{70J}{kg^{\circ}K}$ ,  $\rho = \frac{904kg}{m^3}$ . Experimental values correspond to the maximum temperature reading recorded in each experiment.

### 4.2.3 Conclusions

This chapter explained the physics of the bonding mechanism of automated in-situ consolidation. It was shown that the consolidation process is based on the reptation theory that assumes the motion of polymer chains are constrained by an imaginary tube. This concept is expanded to the interdiffusion of polymer chains across the interface of two surfaces in contact and how the interface's strength depends on the temperature and molecular weight of the polymer. Finally, a heat transfer model was developed to simulate the through-thickness temperature distribution of the stack under the forming action of the process leading. Even though it is a relatively simple model, its prediction gives an indication of the processing speed at which good heat transfer occurs (90 mm/s), and as it could be seen in the following chapter, is in agreement with the speed that achieve the best consolidation for automatic in-situ consolidation.

## 5 Two-dimensional laminates and Characterisation

### 5.1 Introduction

Fibre-reinforced composites are commonly used as laminates because of the way they are manufactured as fibres are supplied as fabrics, tapes, or preforms. This chapter will validate the automated in-situ consolidation process by producing two-dimensional laminates of self-reinforced polypropylene composites based on bicomponent tapes. The manufacturing steps are described for this technique and a benchmark process: hot press. It is known that composite materials properties are linked to the manufacturing process. Therefore, the rationale behind selecting fixed and variable processing parameters are discussed. Processing parameters that can be adjusted easily will be selected to understand their influences over different mechanical properties.

### 5.2 Material

The material used in this thesis is Torodon™, which is a self-reinforced polypropylene *fabric* based on coextruded tapes (also known as bicomponent tapes) produced by Don & Low in the UK and shown in Figure 5-1 . It has a plain fabric structure which makes it drapable (ability to conform to the surface of moulds). As mentioned, the coextruded tape is made of three layers: the core (or reinforcement phase) layer is a PP homopolymer, and the skin layers are based on a random copolymer polypropylene. This preform has been commercially used in different industries such as aerospace, sports, automotive, and luggage because of its lightweight and impact resistant properties [17]. Some properties of the material used in this study and the rest of this thesis are described in Table 5-1. The density of the material is slightly lower than the known value of isotropic polypropylene ( $0.91 \text{ g/cm}^3$ ), which is due to defect regions (e.g., voids) in the core layer of the tape induced by the high draw ratio of the tape [184, 185]. The density of polypropylene extruded tapes has been associated with the draw ratio it is processed. The exact drawn ratio from the material used in this thesis cannot be determined since it is a proprietary processing parameter of the manufacturer. However, according to the literature, the reported density falls into draw ratios between 5 to 10. Lower

density values have been reported in the literature with drawn ratios higher than 11 [184, 186].

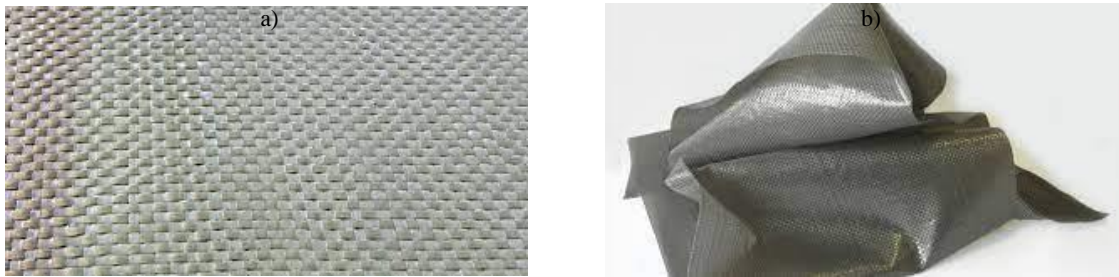


Figure 5-1. (a) Torodon™ Fabric Structure: Plain; (b) Torodon™ Fabric as received. [17]

**Table 5-1 Properties of Torodon™ as described by its manufacturer [187]**

Fabric Structure	Fabric weight (g/cm <sup>2</sup> )	Density (g/cm <sup>3</sup> )	Tensile Modulus (GPa)	Tensile Strength (MPa)	Elongation at break (%)
Plain	107	0.9	4.35	180	11

### 5.2.1 Temperature Processing Window

Thermoplastics are usually processed above their melting temperature, but this cannot be done for self-reinforced composites since the reinforcement layer, homopolymer PP, will lose its highly-aligned molecular orientation and its reinforcement effect. The benefit of using coextruded tapes is the relatively large processing temperature window in which the copolymer is completely melted so the layers can bond and diffuse, however, a very small fraction of the homopolymer, generally its interface with the copolymer, maybe is affected. This temperature window can be obtained using differential scanning calorimetry, which is a technique that determines phase changes and transition in materials. One tape from a piece of fabric was cut into 3-4 mm pieces and inserted into a 5-mm diameter aluminium pan before being sealed. The sealed pan was inserted into the furnace of a PerkinElmer DSC-8500, and the analysis was performed on Pyris DSC software. The temperature profile consisted of heating from 0°C to 200°C at a 10°C/min rate in a nitrogen environment purged at 19.8ml/min. Figure 5-2 shows the melting transitions for both the copolymer and the homopolymer obtained by differential scanning calorimetry. A magnification of the melting transition of the copolymer is shown in the same figure showing the characteristic peaks of a random copolymer with ethylene groups [133, 184]. The first peak is associated with the sealing



temperature at  $\sim 106^{\circ}\text{C}$ , and the second peak to the melting point of the copolymer at  $\sim 114^{\circ}\text{C}$ . The sealing temperature is the minimum temperature at which adhesion would be achieved between layers. The melting point is the temperature at which most of the copolymer is in a molten state.

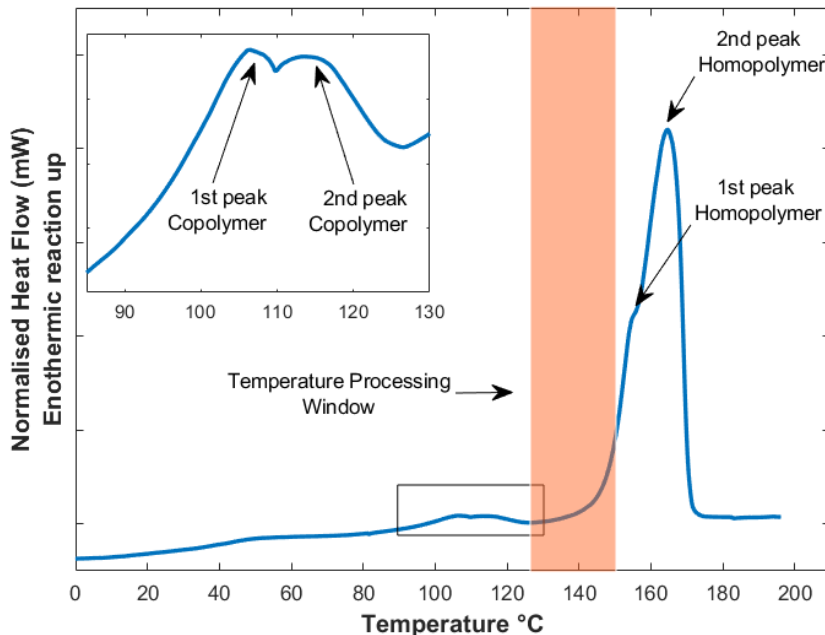


Figure 5-2 DSC trace of a co-extruded self-reinforced polypropylene tape showing a temperature processing window. Both copolymer and homopolymer show a double melting behaviour

The DSC trace also shows the melting behaviour of the reinforcement layer with two peaks. The second peak is  $\sim 167 \pm 1^{\circ}\text{C}$ , which is a few degrees higher than isotropic polypropylene ( $163^{\circ}\text{C}$ ) due to its higher orientation [35]. The difference between the melting point of the copolymer and the onset temperature of the melting trace of the homopolymer in the DSC trace is used to determine the temperature processing window  $\Delta T$ , which is around 25 degrees from  $125$  to  $145^{\circ}$  approximately (pink area in Figure 5-2).

Several factors promote the appearance of multiple peaks in homopolymer polypropylene, such as lamella crystals of different sizes (lamella thickness), different crystallographic forms, crystals with different degrees of perfection. Most of it can be influenced by cooling rates [188]. Different crystallographic forms were ruled out by a wide-

angle x-ray diffraction (WAXD<sup>1</sup> or XRD) pattern (Figure 5-3) performed on a piece of fabric. The fabric was scanned from 5° to 30°C in a 2 $\theta$  range with a step size of 5°/min [189] using an X-ray Powder Diffractometer with a Lynx Eye detector (D8 Advanced, Bruker AXS) using a Cu K $\alpha$  X-ray source with the following parameters:  $\lambda=1.54 \text{ \AA}$ , voltage = 40 kV, current = 40 mA. Three strong equatorial  $\alpha$ -form peaks of (110),(040),(130) at 2 $\theta$  = 14.09, 16.90, and 18.66°C, respectively, were present while neither a strong single  $\beta$ -form peak of (hkO) at 2 $\theta$  = 16.09° nor a strong  $\gamma$ -form peak of (120) at 2 $\theta$  = 20.10° was found [190].

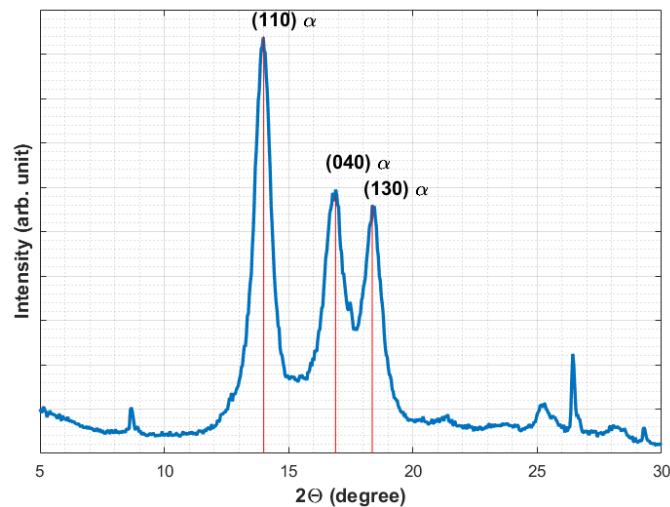


Figure 5-3 Crystalline structure of self-reinforced polypropylene measured by WAXD. Three strong equatorial  $\alpha$ -form peaks of (110), (040), (130) at 2 $\theta$  = 14.09, 16.90, and 18.66°C, are present

### 5.3 Specimen Manufacturing

This section describes two manufacturing processes: hot pressing and automated in-situ consolidation, being the last the focus of this research. In order to simplify the manufacturing process and to avoid warping effects due to lay-up configuration, a symmetrical and balanced laminate [0/90]<sub>5</sub> was selected as the basis for all laminates unless stated otherwise.

---

<sup>1</sup> The polymer community tends to refer to WAXD or WAXS but the materials science community prefers the term XRD. They are essentially the same technique.

### 5.3.1 Hot Press

#### 5.3.1.1 Short processing Cycle

The forming cycle in the automated in-situ consolidation process consists of applying pressure and transferring temperature to the material in a local region while the forming tool moves. As soon as the forming tool leaves that region, the material cools down following a non-isothermal crystallisation process. A similar processing cycle was simulated in a hydraulic hot press integrated with a temperature controller, which heats the top and bottom panels. The hot press platens were heated to the processing temperature with a small gap separation (~5mm). Then two layers of plain fabric were inserted into the gap, which was then closed, compressing the laminate to the required pressure. The laminates were compressed for 1 min before pressure was released, and the laminates were immediately removed from the hot press to cool down to room temperature. The Time-Temperature and Time-Pressure profile during consolidation for this route is illustrated in Figure 5-4.

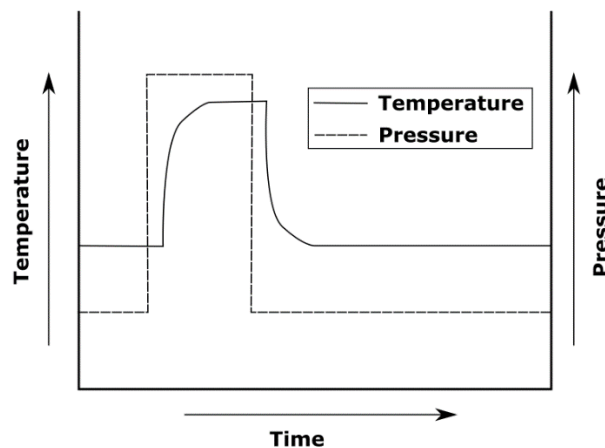


Figure 5-4. Time-Temperature and Time-Pressure fast-cycle manufacturing profile

Figure 5-5 shows the resulting laminates for each processing parameter. Wrinkles appear at all processing temperatures due to the in-plane forces created during shrinking and crystallisation. There is a considerable amount of shrinking, especially for temperatures above 140°C. This is due to the non-constrained state of the laminate during crystallisation which promotes shrinking and relaxation in the co-extruded tapes[16], which is accompanied by the subsequent loss of mechanical properties. Therefore, this Time-Temperature and Time-

Pressure profile for composites consolidation is not recommended and is not used throughout this work.

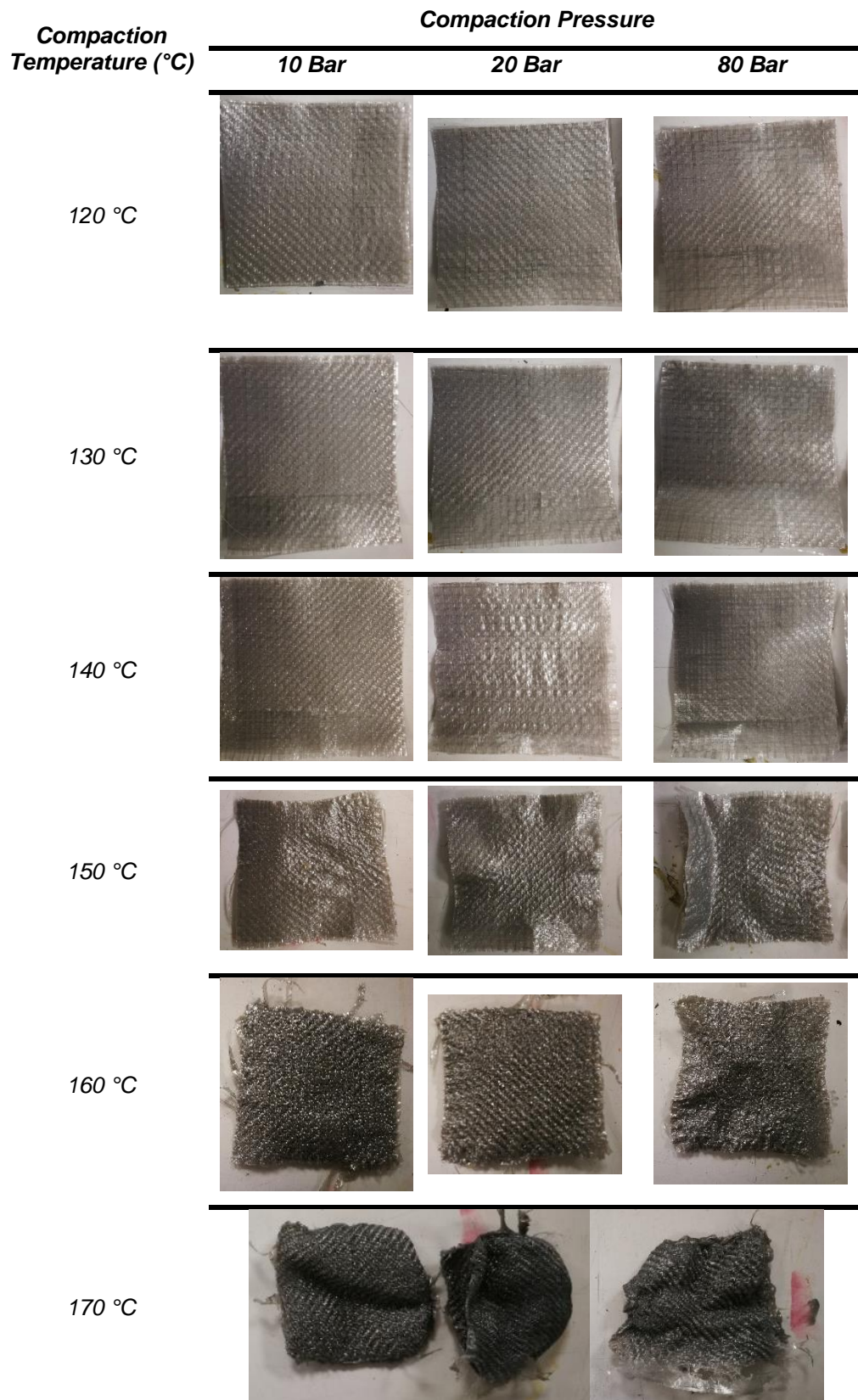


Figure 5-5 Hot Compaction manufacturing via Hot press and a Fast cycle like the Automated in-situ consolidation

### 5.3.1.2 Long processing Cycle

Following the results from the short processing cycle, a new processing cycle was selected. The hot press platens were heated to the processing temperature with a small gap separation (~5mm). Then 2 and 5 layers of plain fabric were stacked between aluminium plates, and this sandwich structure was inserted into the gap, which was then closed, compressing the laminate with a 10 bar pressure. The laminates were compressed for 15 min to allow enough thermal transfers from the platens to the aluminium plates and then to the fabric layers. Then the laminates were left to cool down without removing the pressure up to a temperature of 70°C (~1.5 hours). The Time-Temperature and Time-Pressure profile during consolidation for this route is illustrated in Figure 5-6. Figure 5-7 shows the resulting laminates with the new processing route in which no wrinkles appear, demonstrating the importance of the application of pressure during the crystallisation time of the material [16]. Throughout this thesis, this is the processing cycle selected for all laminates manufactured via Hot press.

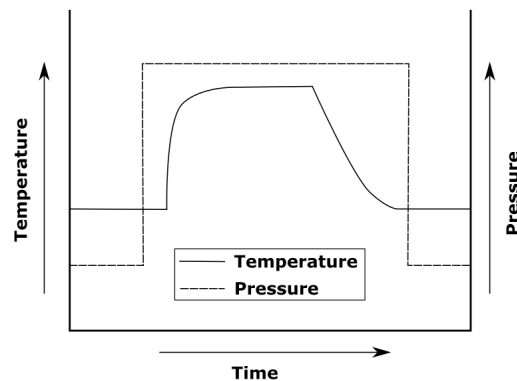
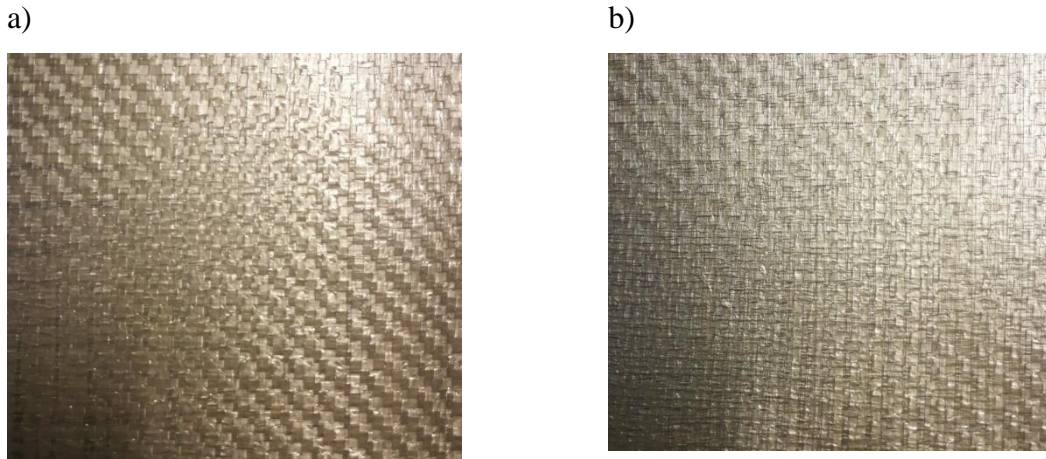


Figure 5-6 Time-Temperature and Time-Pressure profile of Hot-Pressing manufacturing



*Figure 5-7 Hot Compaction manufacturing via Hot pressing for a 5-layer composite produced at a) 130°C and 10 bars of pressure b) 150°C and 10 bars of pressure*

### **5.3.2 Automated In-Situ Consolidation**

When the forming tool passes over the material, it is subjected to a compression cycle that reduces its thickness while transferring heat to the stack. This thermomechanical process is essential to bond the interfaces of the fabric to each other. However, both the compression level (also known as consolidation level) and the amount of heat transfer are unknown because they depend on other processing parameters. While there are other processing variables, the most important parameters involved in automated in-situ consolidation of self-reinforced polypropylene composites are the temperature of the mould and forming tool, forming speed, path separation, and compression pressure. Some parameters and their influence on the quality of the product can be determined quickly through experimentation, including mould temperature, forming speed, and forming path separation. However, the consolidation pressure and forming tool temperature (at the contact point with the laminate) significantly influence the final properties of the part and are therefore considered processing variables.

#### **5.3.2.1 Hot Mould Temperature Selection**

Increasing the temperature of the mould, to be closer to the forming tool temperature, will reduce the temperature gradient through the thickness of the stack being consolidated.

A smaller temperature gradient can facilitate faster forming speeds, which will increase forming productivity. However, high temperatures will promote annealing and shrinkage in the tapes. An investigation of the influence of the temperature of the mould on the shrinkage of the stacks was performed via visual observation and measurement of the Areal texture.

A 3-ply flat laminate was formed with a forming tool at 140°C at a forming speed of 90 mm/min, and a compression force of 50N. The mould temperatures investigated were selected to avoid melting the homopolymer core of the tapes (~168°C) of the fabrics: 80°C, 110°C, 115°C, 120°C, 130°C, and 140°C. After forming, the surface of each sample was assessed for form and finish using an InfiniteFocus SL (Alicona imagin GmbH Austria) with a 5X optical magnification. A 16.83x3.79mm area was measured with a vertical resolution of 100 nm and a lateral resolution of 1µm. Exposure was set at 1ms and contrast at 0.7 ms. The obtained scan was analysed with Alicona IF software to obtain areal texture values in accordance with ISO 25178 [191].

The three-dimensional images of the surface in contact with the hot mould and their measured areal texture are shown in Figure 5-8. At a mould temperature of 80°C, the preform did not consolidate. A temperature of 80°C is well below the sealing temperature of the copolymer; therefore, adhesion or bonding between tapes did not occur as expected. The values of the areal texture indicate that as temperature increases, the surface roughness in contact with the mould also increases due to the expected shrinkage. Moreover, the images show that the tapes of the preform are bonded to each other except for the higher temperatures (130°C and 140°C). This confirms that a temperature above the sealing point is required, as expected. Higher temperatures promote molecular relaxation on the homopolymer, which is seen as the high level of shrinkage that leads to higher values of areal texture. The lowest areal texture value is achieved at a hot mould temperature of 110°C, close to the copolymer layers' melting point. Surface roughness measurements are important in metallic structures due to the link between surface-micro defects and failure due to crack propagation [192]. For composites, it is not clearly understood the relationship between final performance and surface roughness as it is assumed composites can arrest any crack growth [192]. However, small surface roughness implies better part conformity and, more importantly, reduced lateral shrinkage. Therefore, a hot mould temperature of 110°C will be used throughout the rest of this work.



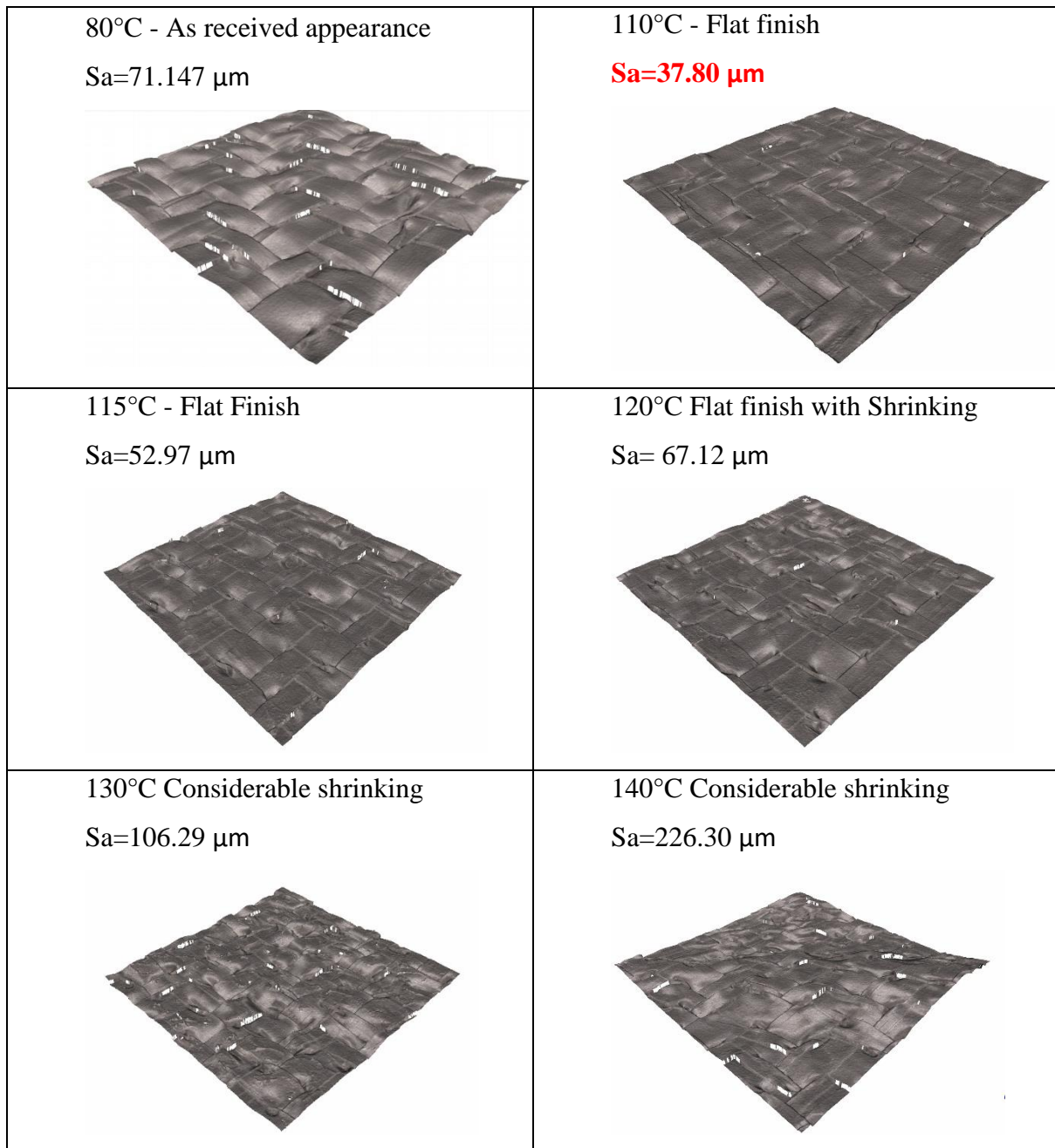


Figure 5-8 Three-dimensional surface finish of the layer in contact with the hot mould at different mould temperatures

### 5.3.2.2 Forming Speed Selection

An effective consolidation needs both pressure and sufficient heat transfer that increases the temperature of the tapes to above the melting point of the copolymer when the forming tool passes over the material. The melted copolymer layers of each tape will flow and mix with the adjacent ones. After the tool leaves the material, the copolymer cools down to crystallise, creating mechanical entanglement between adjacent polymeric chains.



Without experimentation, the amount of heat transferred to the material is unknown in an automated in-situ consolidation process, especially because of the very short heat transfer cycles. The material is always in a transient state wherein the temperature distribution through its thickness changes with time; therefore, it is a time-dependent process. A change in speed can introduce significant temperature changes. One consequence of a transient heat transfer is the creation of a temperature gradient through the thickness of the stack. Though chapter 4 developed a heat transfer model to predict the temperature distribution of the material, it does not give information about the strength of the bond between interfaces. This section attempts to discover a suitable speed that creates a temperature gradient that promotes an effective interlaminar bond strength.

The strength of the bond (also called interlaminar strength) between layers can be measured by performing peel tests [175, 178, 193] according to standard ASTM-D1876 [194]. Peeling test consists of pulling two unbonded ends to separate a bonded region (Figure 5-9.(a)) while measuring the force required to break the bond of the interface and recording the crack propagation. The non-bonded area was created by introducing PTFE films (Teflon) between the fabrics [16] before clamping the stack on top of the hot mould. The forming process was performed with the following fixed parameters: 5-layer laminate, a mould temperature of 110°C as previously determined, a 17-mm diameter forming tool with a flat end at a temperature of 150°C, and a forming force of 50N.

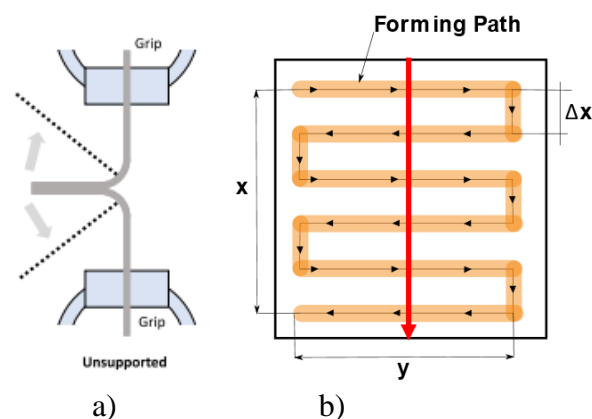


Figure 5-9. a) schematic of a peel test, b) schematic of forming paths without overlapping each other. The red arrow indicates the direction of the peel test c) forming a laminate via automated in-situ consolidation.

The forming path was designed with a separation between lines of 20 mm meaning there will be some material left without being consolidated as shown in Figure 5-9. b. In this

way, when performing a peel test in the perpendicular direction to the forming path, the load recorded will have peaks and valleys. The peaks relate to consolidated/bonded regions and vice-versa as shown in Figure 5-10. The forming speeds were set at four levels: 90 mm/s, 180 mm/s, 360 mm/s, and 720 mm/s. After forming, the specimens are cut into strips with a width of 15 mm. Each specimen has five unbonded ends (5 layers), so four interfaces are pulled apart starting from the top interface, which is closest to the forming tool. The top unbonded layer is clamped to the top grip, while the rest of the unbonded ends is clamped in the bottom grip. After the first interface is pulled apart, the procedure is repeated for the remaining interfaces. The pulling tests were performed using a universal testing machine adapted with a 5KN load cell (Tinius Olsen, USA) to peel apart the interface at a rate of 250 mm/min.

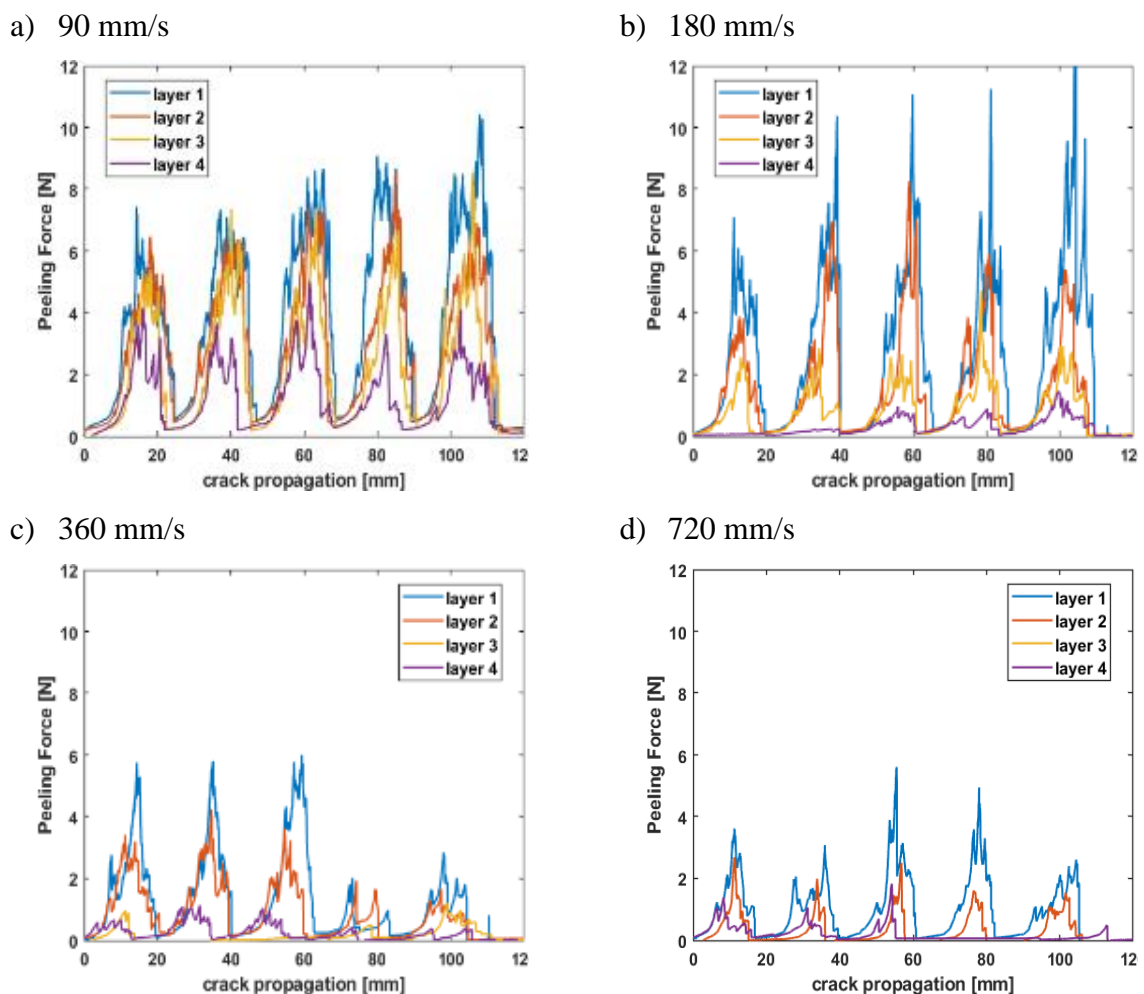


Figure 5-10 Through-thickness interlaminar strength as a function of the forming speed in automated in-situ consolidation with a flat tool. Forming speeds: a) 90 mm/s b) 180 mm/s c) 360mm/s, d) 720 mm/s.

Figure 5-10 shows the results of pulling apart each of the laminate interfaces, creating a through-thickness interlaminar strength representation of the laminate. “layer 1” refers to

the closest interface to the forming tool and so on. For all the forming speeds, the first layer has the strongest value interlaminar strength. Under the current boundary conditions, the transient heat transfer creates a temperature gradient in which the top layers will be subjected to a higher temperature. It was discussed in chapter 4 that higher bonding temperatures increase the interdiffusion rate improving the interlaminar strength. Because of this, it is expected that the last interface will have the lowest interlaminar strength because of the lower temperature it experiences.

Moreover, it was also demonstrated that as the forming speed increases, the through-thickness temperature distribution changes, and therefore, the temperature gradient that the material experiences also changes. This was proved both theoretically and experimentally for different speeds (see Chapter 4). However, as the forming speed increases, the total amount of heat transfer per millimetre is less, which does not give sufficient time for the polymer chains to diffuse under the exposed temperature and pressure conditions, decreasing the interlaminar strength of all interfaces, as shown in Figure 5-10(a), Figure 5-10(b), and Figure 5-10(c). From forming speeds of 180 mm/min, the interlaminar strength decreases or is barely achieved for the interfaces closest to the mould. A quantitative representation of Figure 5-10 where the interlaminar strength decreases as the speed increases can be obtained by using the average value of the maximum force recorded for each interface at each speed as shown in Figure 5-11. Faster speeds (180 to 720 mm/s) gave strength values close to zero which means the layers are not bonded to each other. On the other hand, the lowest speed is the only one in which all the layers bonded. Therefore, to achieve the best performance, a 90 mm/min speed was selected for the rest of this thesis as at least ensures bonding of all layers and the higher interlaminar strength.

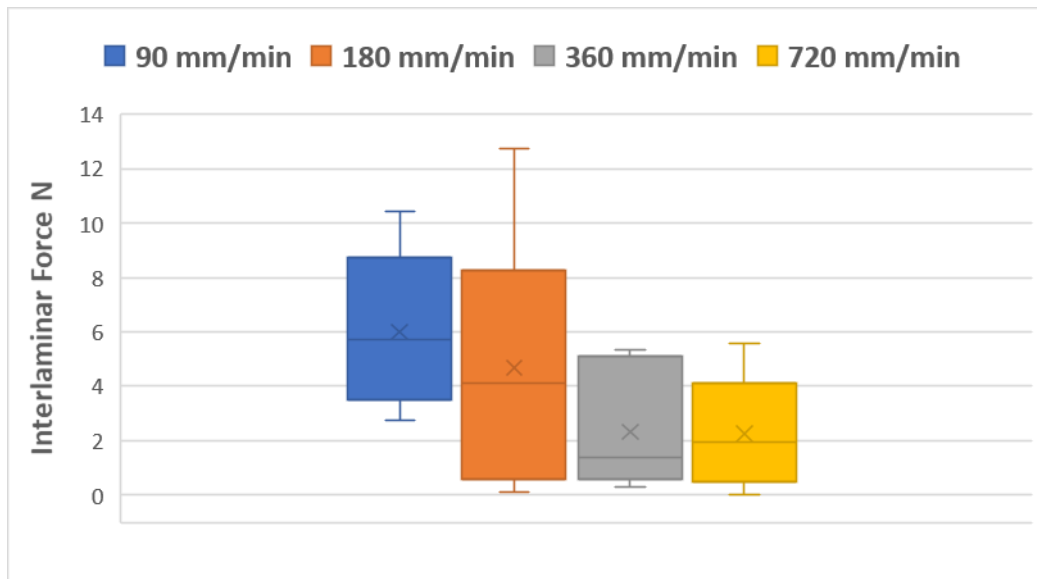


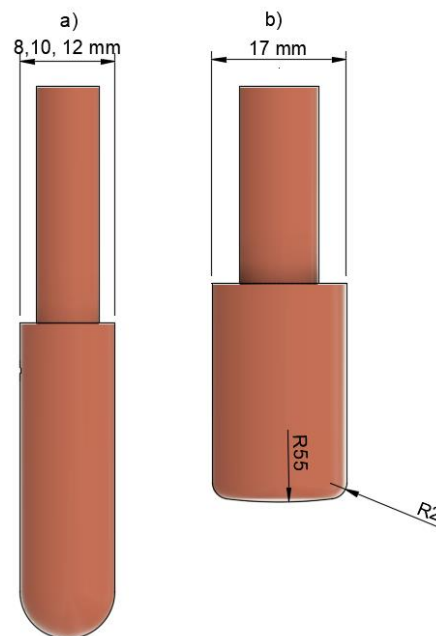
Figure 5-11. Average force through the thickness as a function of the speed

### 5.3.2.3 Forming Path Separation Selection

Figure 5-10 showed the through-thickness interlaminar strength as a function of the forming speed in automated in-situ consolidation with a flat tool with a forming path that does not overlap the previous one (Figure 5-9. A). Because of this, the interlaminar strength as a function of the crack propagation has peaks and valleys. Peaks represent a bonded region, while valleys represent an unbounded region. Unbonded regions in a final laminate are detrimental to the final properties of the material as they are a source of possible failure under stress. Therefore, for a given forming tool, there is forming path separation that should lead to a most effective consolidation rate without leaving unconsolidated regions.

Similarly, in the last experiment, the best way to test the level of consolidation is by finding out the interlaminar strength of the laminate in accordance with the standard ASTM-D1876 [194]. The interlaminar strength can be defined as the average load per unit width. The manufacturing procedure for the specimens is the same. Each specimen has five unbonded ends (5 layers), so four interfaces are pulled apart starting from the top interface, which is closest to the forming tool. The top unbonded layer is clamped to the top grip, while the rest of the unbonded ends is clamped in the bottom grip. After the first interface is pulled apart, the procedure is repeated for the remaining interfaces. The peel tests were performed using a universal testing machine adapted with a 5KN load cell (Tinius Olsen, USA) to peel apart the interface at a rate of 250 mm/min.

Four types of forming tools were used to find the right path separation: a 17-mm tool with a “flat” end and tools with a hemi-spherical end with the following diameters: 8 mm, 10 mm, and 12 mm as shown in Figure 5-12. The “flat tool” has a high curvature at the end to reduce the tangent forces on the structure while forming. Because the tool moves pressing the material, a force is created over a clamped beam (linear stage plus forming tool). This force will bend the structure, therefore, if the tool were completely flat, only a small region of the tool will make contact. The fixed processing parameters were a 5-layer laminate (4 interfaces), a mould temperature of 110°C, a forming tool temperature of 140°C, a forming speed of 90 mm/min, and a forming force of 50N. Finally, the path separation  $\Delta x$  (Figure 5-9. b) was 2 mm, 4 mm, and 8 mm. Four specimens per parameter were used to ensure repeatability.



*Figure 5-12 Forming tools for automated in-situ consolidation: a) 8, 10, 12-mm hemi-spherical tools, b) “Flat tool”. Though the term “flat” tool is used, it has a high diameter at the end to avoid deformation due to shearing forces.*

Figure 5-13 shows the calculated interlaminar strength of laminates for different forming path separations for the four forming tool geometries. Moreover, the interlaminar strength of a specimen manufactured via Hot Press provides a quality reference. It has been shown that the interlaminar strength increases with the temperature [133]; therefore, in order to produce comparable results, the temperature gradient generated by the forming tool should be taken into consideration. The hot press specimens were manufactured at a

temperature of 135°C, which is slightly higher than the average temperature between the hot mould and the forming tool in the automated in-situ consolidation process.

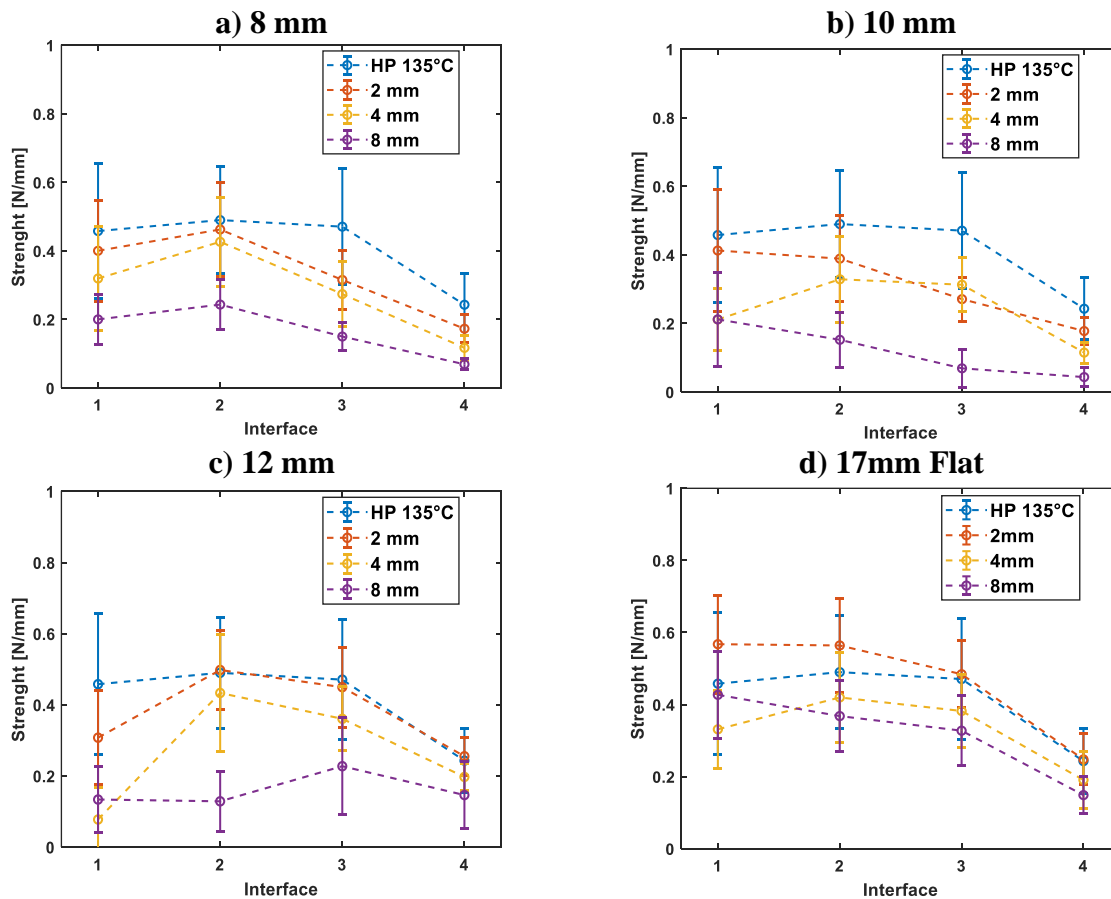


Figure 5-13 Interlaminar strength comparison for different forming path separations (legends) with different tool geometries: a) 8 mm hemi-spherical, b) 10 mm hemi-spherical, c) 12 mm hemi-spherical, d) 17 mm Flat. The interlaminar strength of a specimen manufactured via Hot Press at 135°C and 10 bar of pressure is also shown to have a quality reference.

A specimen manufactured via hot press is not expected to create a temperature gradient as in automated in-situ consolidation but a uniform temperature. Therefore, if the interlaminar strength depends on temperature[133] and the temperature is uniform, it would be expected to achieve a similar interlaminar strength value in every interface. However, it can be seen that there is variation in the strength values. Unfortunately, there is an inadequate standardisation of laminated composites and their characterisation techniques [195]. In the case of pulling or peeling tests, several testing parameters influence the calculated interlaminar strength, including specimen dimensions and symmetry, strain rate, molecular weight of the polymer, memory capability of the polymer and the failure mechanism at the interface, making it difficult to find a parameter independent of the testing

conditions [193, 196-198]. In this case, the testing order of each interface modifies the geometry for the specimen for the subsequent test. However, this chapter intention is to compare the results of laminates produce with both manufacturing techniques. The interlaminar strength patterns are similar for both hot press and automated in-situ consolidation. As long as both of them show similar behaviour or patterns, it ensures that the comparison is reliable.

Coming back to Figure 5-13, the interlaminar strength is the lowest when a forming path separation of 8 mm is used and then increases as the path separation decreases. This is observed for any forming tool geometry. The reason for these results is the number of times a forming path overlaps an area covered by the previous one. For example, an 8-mm separation with a 17-mm tool result in an overlap of 9 mm; therefore, an area of the laminate is subjected to a compression cycle at least twice. If the path separation is smaller, then the number of times that overlapping occurs increases, and therefore, the number of times an area of material is subjected to compression. The successive compressions cycles help to improve the interdiffusion of molecular chains across the interface. For small-size tools, an 8-mm path separation does not overlap previous forming paths, leading to the creation of unconsolidated zones for small-size tools (valleys in Figure 5-14. (b)). On the contrary, smaller forming path separations can successfully avoid the creation of unconsolidated zones (Figure 5-14(a)), increasing the calculated interlaminar strength (Figure 5-13). Moreover, when comparing the interlaminar strength values with the specimen manufactured via hot press, only the tool with a flat end presents similar and sometimes higher values when a forming path separation of 2 mm is used. In general, tools with a hemi-spherical end present lower interlaminar strength values except for a 12-mm tool using a forming path separation of 2 mm. In the last two cases just mentioned, a 2-mm forming path separation implies a superposition of the toolpaths over already consolidated areas, suggesting the interdiffusion of polymer chains can be improved if the operation is repeated. It was observed that the hemi-spherical tools sometimes drags the tapes that are penpendicular to the forming path, which is not observed in the flat tool. This could also alter the ability of the process to form strong interlaminar strenghts.

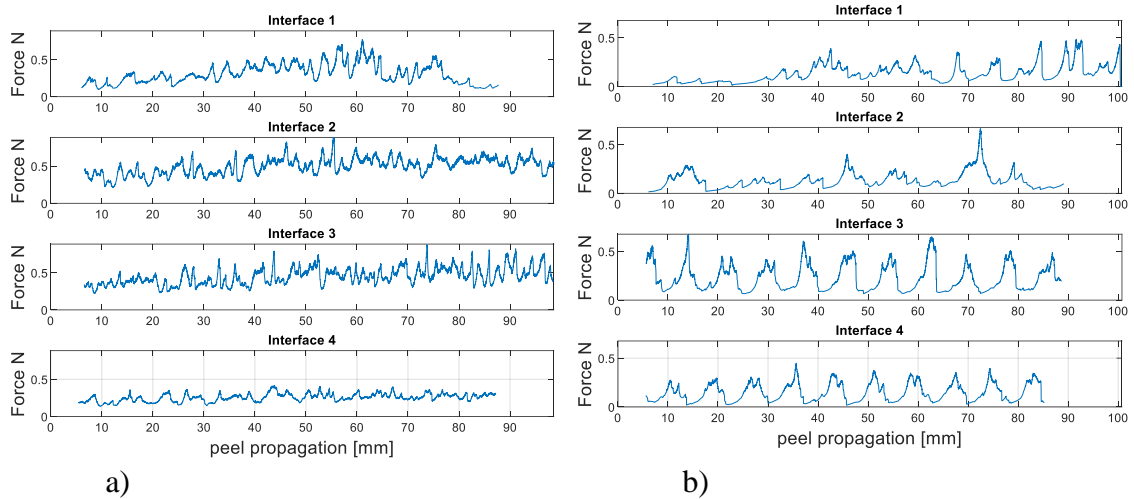


Figure 5-14. Force vs crack propagation for different layers in an automated in-situ consolidated laminate using a forming path separation of a) 2 mm and b) 8 mm when the interfaces are pulled apart. Because there is no overlap in the 8 mm path separation, the force presents peaks and valleys related to bonded and unbonded areas. \*Tool=12 mm.

Based on the interlaminar strength values, the best performance is achieved with a flat end 17mm-tool and a spherical end 12-mm tool with a forming path separation of 2 mm. Therefore, these parameters were selected for the rest of the experiments on this project.

#### 5.3.2.4 Main Processing parameters: Pressure and Temperature

As mentioned, when the forming tool passes over the material, it is subjected to a compression cycle that reduces its thickness while transferring heat to the stack for promoting bonding between interfaces. The compression is related to the pressure or force required to bring the surfaces of each layer into contact. This is not only true for the automated in-situ consolidation process proposed but for most composite manufacturing process. Having a uniform pressure distribution is required for optimal process performance [199]. For example, autoclave manufacturing can ensure a uniform pressure distribution over the surface of the part; however, misalignment in a mould set-up can promote a non-uniform pressure distribution leading to a variation of the properties across the part.

Pressure is a scalar value defined as the perpendicular force applied over a surface area according to Equation 5-1. Therefore, pressure can be increased by incrementing the force while keeping the area constant or by decreasing the area while keeping the force constant.



In this project, the force sensor gives the user a precise estimation of the force applied. However, the contact area depends on the geometry of the tool and is unknown.

$$\sigma = \frac{F}{A} \quad \text{Equation 5-1}$$

The contact area between two spheres or a sphere and a plane can be calculated using contact mechanics theories, particularly the Hertzian theory of Elastic deformation [200]. More information about contact mechanics and a Matlab program to calculate the contact area is shown in Appendix B. This theory is based on bodies with elastic properties. It has been expanded to cover other phenomena present in contact mechanics, such as adhesion in the contact zone and Van der Waals interactions. Most of the models depend on several parameters, such as geometry and force. However, polymers have viscoelastic properties, which depend on several parameters such as temperature and strain rate. To the author's knowledge, a model that attempts to predict the contact area for viscoelastic materials under temperature has not been proposed. To add more complexity, the material used in this thesis is made of bicomponent tapes. Both the matrix and reinforcement layers are expected to have different mechanical and rheological responses.

This section presents an empirical approach for determining an approximate contact area. Following the same methodology as previous experiments, a load peak pattern (Figure 5-15) can be created by pulling apart an interface where the forming paths do not overlap (Figure 5-9. a). The full width at half maximum (FWHM) of the load peaks can be considered a contact diameter that ensures adequate bonding in the interface and, therefore, can be transformed into an effective area.

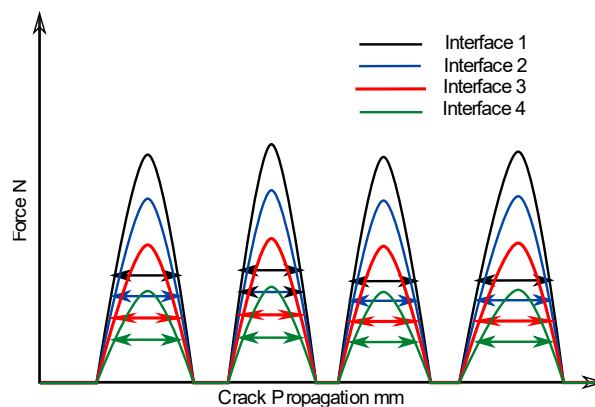


Figure 5-15. Load vs crack propagation of specimens with non-overlapping forming paths. The Full width at half maximum is calculated for each interface.

The manufacturing procedure for the specimens is the same as section 5.3.2.2 Forming Speed Selection. Each specimen has five unbonded ends (5 layers), so four interfaces are pulled apart starting from the top interface, which is closest to the forming tool. The top unbonded layer is clamped to the top grip, while the rest of the unbonded ends is clamped in the bottom grip. After the first interface is pulled apart, the procedure is repeated for the remaining interfaces. The pulling tests were performed using a universal testing machine adapted with a 5KN load cell (Tinius Olsen, USA) to peel apart the interface at a rate of 250 mm/min.

Four types of forming tools were used: a tool with a flat end and a 17 mm diameter and a spherical end with the following diameters: 8 mm, 10 mm, and 12 mm. The fixed processing parameters were a 5-layer laminate (4 interfaces), a mould temperature of 110°C, a forming tool temperature of 140°C, a forming speed of 90 mm/min, and two compression forces of 30 N and 50 N. Four specimens per parameter were used to ensure repeatability.

The apparent contact diameter is defined as the average width-at-half-height of the load peaks for all interfaces. Figure 5-16 shows the apparent contact diameter for a low level (30N) and high level (50N) compression force, and using these values, the area can be calculated with the equation of the area of a circle. Therefore, using Equation 5-1, the estimated pressure can be calculated as shown in Table 5-2. It is expected that the contact diameter will be smaller than the diameter of the forming tool in an automated in-situ consolidation process and that the contact diameter, and therefore, contact area will increase as the compression force increases.

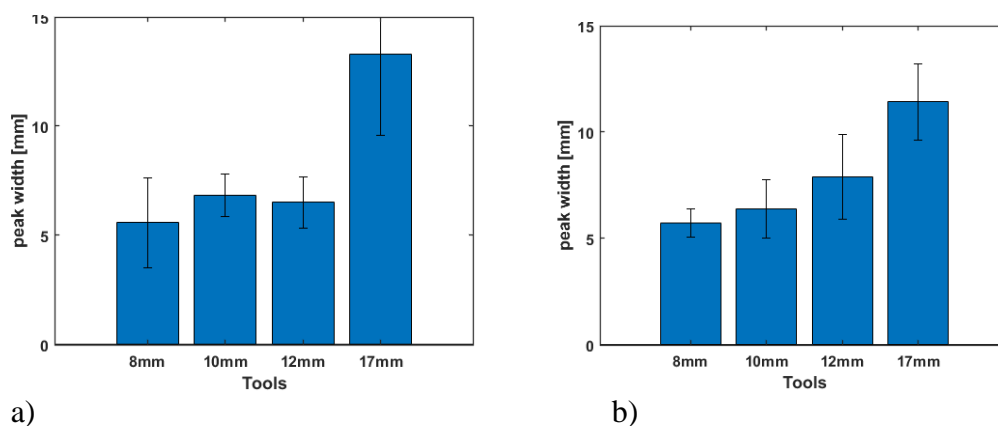


Figure 5-16 Influence of the compression force on the contact diameter of a forming tool with a processing temperature of 150°C, a forming force of 30N, and a forming speed of 1.5 mm/s.

Table 5-2 Estimated consolidation pressure with different tools and different compression forces.  
\*S=Hemi-spherical, \*F=Flat

Force (N)	S-8	S-10	S-12	F-17
	Pressure (bar)			
30	10.6	7.8	10.6	2.7
50	17.7	13.0	17.7	3.8

Hot press specimens were manufactured using consolidation pressure of 10 bar to compare the resultant properties of both processing technique; therefore, it would be beneficial to have similar consolidation pressures. In this way, preliminary experiments on the machine limited the compression force to a maximum of 100N for the 17-mm tool and 50N for the 12-mm tool before the motors stall. An emergency stop function was implemented in the software if the force goes above 100N to stop the operation. Missed steps occurred when a motor stall and because the system does not have a position feedback, the test is discarded. Therefore, Table 5-3 shows two levels of consolidation pressure used through the rest of the experiments in this thesis for the forming tools selected in the previous section: 12-mm spherical end and 17-mm flat end.

Table 5-3 Estimated consolidation pressure for the forming tools selected for the rest of this thesis.  
\*S=Hemi-spherical, \*F=Flat

S-12	F-17
7 bar (27 N)	2.7 bar(30N)
10.6 bar (30 N)	7 bar (80N)

Finally, the last processing parameter to be defined is the forming tool temperature. The first estimation to select the forming tool temperature is to use the temperature processing window of the material as a reference (Figure 5-2). However, this thesis intends to understand the influence of processing parameters on the final quality of the part. Therefore, it is necessary to know which temperature leads to optimal properties and which ones do not; and if they don't, to try to estimate why. For example, which parameters promote molecular relaxation in the reinforcement phase, reducing mechanical properties such as the Young Modulus.

Table 5-4 Processing Parameters

Tool or Process	Temperature °C				Pressure (bar)	
	135	155	170			
Hot Press					10	
12 mm (spherical)	140	150	160	170	7	10
17-mm (flat)	140	150	160	170	2.7	7

Moreover, using a benchmark manufacturing technique can help determine if the project has the potential for further development. In this way, two-dimensional laminates were manufactured under the variable processing conditions shown in Table 5-4. The fixed processing parameters are a mould temperature of 110°C, a forming speed of 90 mm/min, and a path planning with a forming path separation of 2 mm, as shown in Figure 5-17. Once the forming process finishes, the mould is left to cool to a temperature of 70°C, before removing the laminate from the mould.

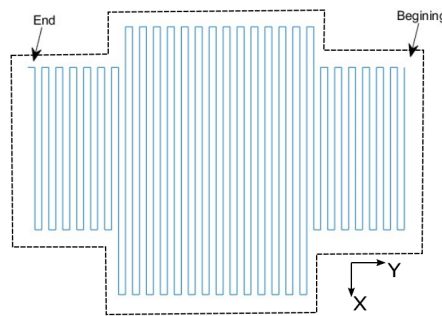


Figure 5-17. Path planning for automated in-situ consolidation of flat laminates

### 5.3.2.5 Force control vs No Control

It was explained in chapter 4 that the process of bonding two polymer surfaces depends on the interdiffusion of polymer chains through the interface and that the interdiffusion depends on both temperature and pressure. Chapter 3 described the development of a force closed-loop system that intends to keep constant compression levels in the forming process. This section intends to briefly show the benefits of the force control implementation by examining the cross-section of self-reinforced polypropylene laminates manufactured with an automated in-situ consolidation process with and without a force closed-loop system. The results are also compared with hot press specimens.

### 5.3.2.5.1 Methodology

Cross-section images can be obtained through microscopy. Sample preparation for microscopy analysis requires several steps: sample cutting, mounting, labelling, grinding, and polishing. Specimens were cut with standard scissors from panels manufactured under the in-situ automated consolidation and hot compaction. These were fixed in steel sample holders (Sample-Klip, Buehler) before being mounted in 32 mm-diameter mounting cups (1.25-in SamplKup, Buehler) with clear epoxy resin (glass cast 3 epoxy resin, Easy Composites Ltd). The resin was left to cure in an oven at 50°C for 12 hours to speed up the curing and removal process. The specimens were later labelled with a Dremel to create a permanent designation before grinding and polishing steps in an automatic grinder and polisher (Automet 250, Buehler), as shown in Figure 5-18 following the steps according to Table 5-5.

Table 5-5 Grinding and Polishing Procedure.

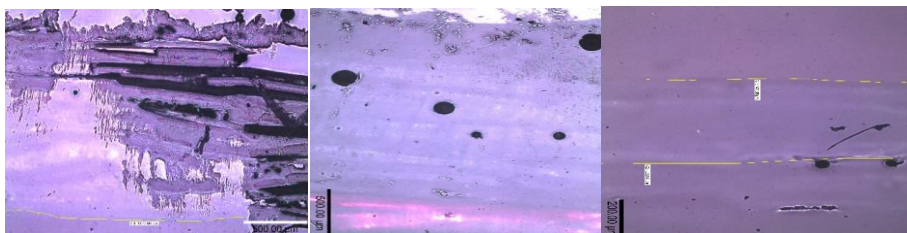
Step No.	Surface	Abrasive	Lubricant/ Extender	Single Force (/specimen)	Time (min:sec)	Platen Speed (rpm)	Head Speed (rpm)	Relative Rotation
1	CarbiMet SiC	P320	Water	20N	Until Plane (~1:00)	200rpm	60rpm	Comp
2	CarbiMet SiC	P600	Water	20N	00:40	200rpm	60rpm	Comp
3	CarbiMet SiC	P1200	Water	20N	00:40	200rpm	60rpm	Comp
4	CarbiMet SiC	P2500	Water	20N	00:40	200rpm	60rpm	Comp
5	VerduTex/TexMet C	3um Metadi Supreme	MetaDi	25N	04:00	150rpm	60rpm	Contra
6	ChemoMet	0.05um MasterPrep	Water**	20N	02:30	150rpm	60rpm	Contra
Notes	<p>&gt; ** last 10-15 seconds; only water            Total time approximately: 10 min per sample.</p>							



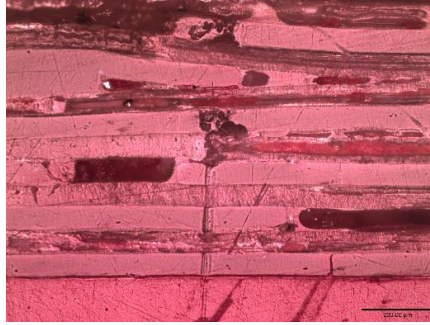
Figure 5-18 Automatic Grinder and polisher

Grinding disks are used from lower to higher grit accordingly. The lowest grit is used to remove unwanted, make the sample planar, and to expose the required section to the grinding and polishing media. This process is time consuming and requires expertise to avoid repeating the process. For example, Figure 5-19 shows attempts where the initial grinding process was not successful and therefore, the morphology could not be observed after the grinding and polishing process. It has been reported that the creation of polypropylene microscopy samples is notoriously difficult due to its low surface energy [201]. Essentially, epoxy resin does not stick to polypropylene. Therefore, it was found that higher grits and more polishing steps are necessary to remove the previous grinding and polishing marks to be able to obtain good quality pictures of the morphology as shown in

Figure 5-20. Finally, after the last polishing step, the samples were cleaned with an Ultrasonic Cleaner(Fisherbrand™ S-Series Heated Ultrasonic Cleaning Bath) for 15 min in acetone in a Fume Hood to avoid potential fire and explosion [202]. The cross-sections of the specimens were observed using a reflection microscope (Nikon Eclipse LV150) equipped with a digital camera and magnification lenses (5X, 10X, 20X, 50X, and 100X). Two or more images were connected to form a better image of the cross-section.



*Figure 5-19 Microscope images of three different mounted samples in which material removal was not achieved successfully.*



*Figure 5-20 Microscope images of (a) grinded and (b) polished specimens. The grinding marks have been greatly removed due to polishing. \*Red epoxy resin was used to mount the samples, and therefore, the red colour.*

### **5.3.2.5.2 Results and Discussion**

Figure 5-21 shows the cross-section of specimens manufactured via Hot Press at different temperatures (130, 150, and 170 °C). These specimens are well consolidated showing a relative flatness and/or waviness of the tapes which is in agreement with the literature [16]. The morphology of the laminate shows that the tapes have a different colour according to its direction. Tapes running in the horizontal direction have a dark colour while tapes in the perpendicular direction (pointing outside the page) are shown with a bright colour. However, It can be seen that at 130°C the percentage of dark areas is higher than at 150°C or 170°C. As the temperature increases, the molecular orientation is reduced causing a change in the morphology from a fibrillar structure to a uniform structure associated with a change of colour from dark to white as shown in Figure 5-22. Due to the dark colour of the tapes running in the horizontal direction it was difficult to determine a void percentage in the samples.

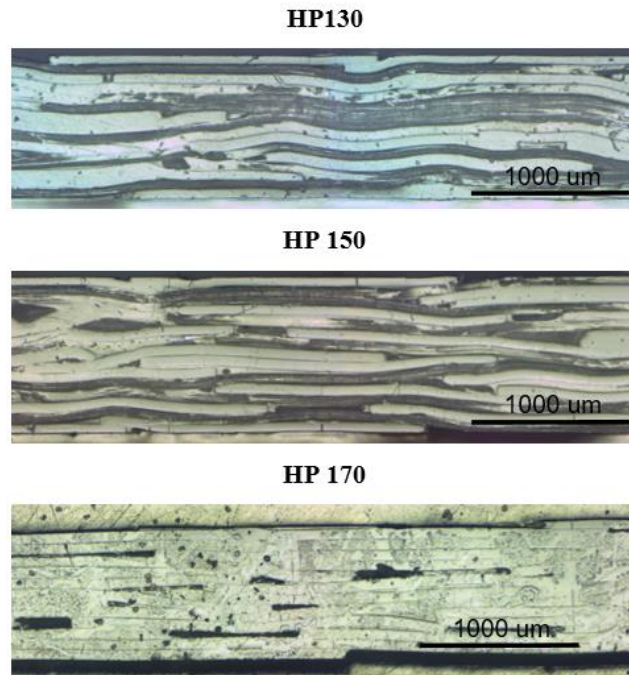


Figure 5-21 Microscope images of specimens manufactured via Hot compaction with a benchmark Hydraulic Hot Press with a 5X magnification at processing temperatures of 130°C, 150°, and 170°C. \*Clear epoxy resin was used to mount the samples.

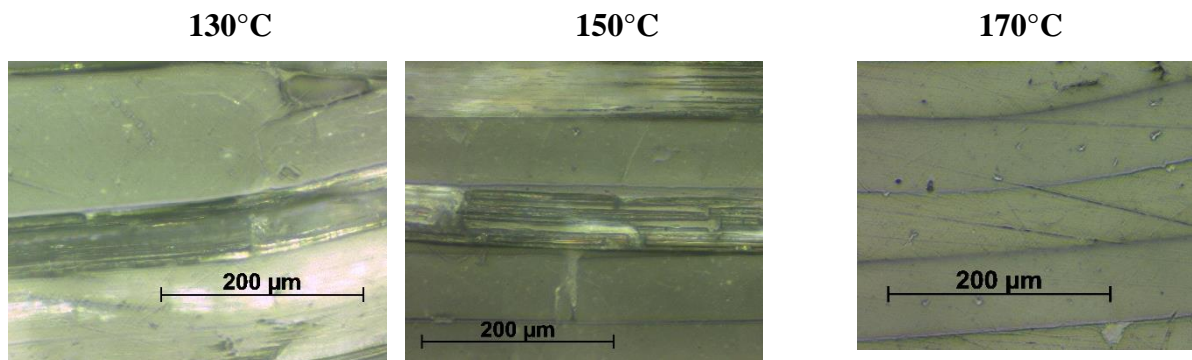

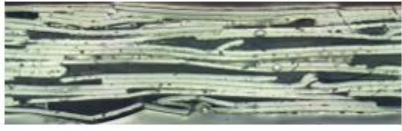


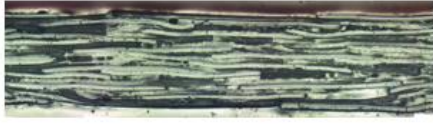



Figure 5-22 Microscope images of specimens manufactured via Hot compaction with a benchmark Hydraulic Hot Press with a 20X magnification at processing temperatures of 130°C, 150°, and 170°C

Figure 5-23 shows microscope images of the cross section of specimens manufactured via automated in-situ consolidation with a 5X magnification to assess the influence of pressure on the resultant morphology of self-reinforced composites. As explained, hot pressed specimens present a good level of consolidation. On the other hand, automated in-situ consolidated samples present a lower level of consolidation as the sections are thicker, the tapes of the fabric present a high level of waviness, and voids can be clearly recognised between layers. However, automated in-situ consolidated specimens using a force closed-loop system present smaller thicknesses and better consolidation that those without a force control system.



Control		No Control
<b>Spherical Tool 12 mm</b>		
<b>High Pressure</b> 	<b>Low Pressure</b> 	
<b>Flat Tool 17 mm</b>		
<b>High Pressure</b> 	<b>Low Pressure</b> 	

*Figure 5-23 Microscope images of specimens manufactured via Automated in-situ consolidation under the influence of pressure with a 5X magnification. High Pressure for a spherical tool is 10 bar. Low Pressure for a spherical tool is 7 bar. High Pressure for a flat tool is 7 bar. Low Pressure for a spherical tool is 2.7 bar.*

Furthermore, the effect of the temperature on the molecular relaxation and change of morphology is less noticeable than a hot press process as shown in Figure 5-24. Only at a temperature of 170°C degrees it can be seen a start point in which the morphology changes in a similar way than a hot-pressed specimen. This is because the specimens are subjected to a lower (average) temperature than in the hot press. It appears that one of the main challenges to overcome in the automated in-situ consolidation process is to achieve a good consolidation in the bottom layers (closer to the mould). However, this is not possible as a higher temperature of the mould will promote molecular relaxation and warpage of the material.

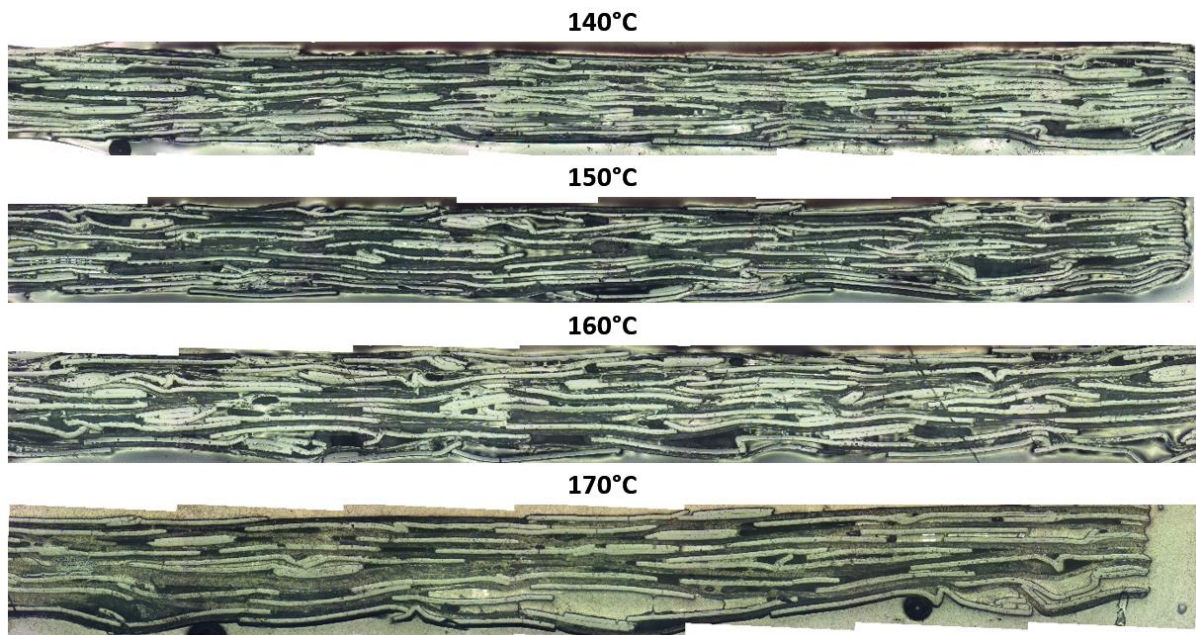


Figure 5-24 Microscope images of specimens manufactured via Automated in-situ consolidation using a flat tool at 140°C, a forming speed of 90 mm/min, and a consolidation pressure of 7 bar.

### 5.3.2.6 Geometric Accuracy

The main goal of a manufacturing process is to produce a product within specific tolerances to ensure interchangeability of parts and the desired properties. A part that does not fit the tolerances will be rejected. Therefore, it is important to evaluate the capability of the processes to ensure a repeatable geometry.

The two-dimensional laminates produced in this project are meant to be flat. However, both hot press and automated in-situ consolidated specimens presented some level of warpage (out-of-plane curvature) for all processing parameters. An example of warpage is shown in Figure 5-25 from 5mm\*60mm strips cut in the transverse direction to the forming path with a blade from manufactured panels. Warpage has been associated with steep thermal gradients [193], which is expected in the automated in-situ consolidation process. However, it was unexpected for Hot press specimens as it is expected to have a uniform temperature distribution. Warpage is common in composites manufacturing and can be caused by several factors such as volumetric shrinkage, residual stresses, mould expansion, etc. [203-205]. In this case, volumetric shrinkage can also be present in both manufacturing techniques. The temperature values ( $\geq 140^{\circ}\text{C}$ ) used as processing parameters can partially or entirely melt the crystals of the homopolymer as shown in Figure 5-25. Another reason for

the unexpected warpage is the odd number of plies used plus a predetermined “bend” from the roll of material. To overcome this, usually an even number of plies is used so the half the layers opposed the inherit “bend” from the material being rolled after manufacturing. In this case, only five layers were and the layers the predetermine “bend” was not considered during laying-up; therefore, leading to a warped composite.

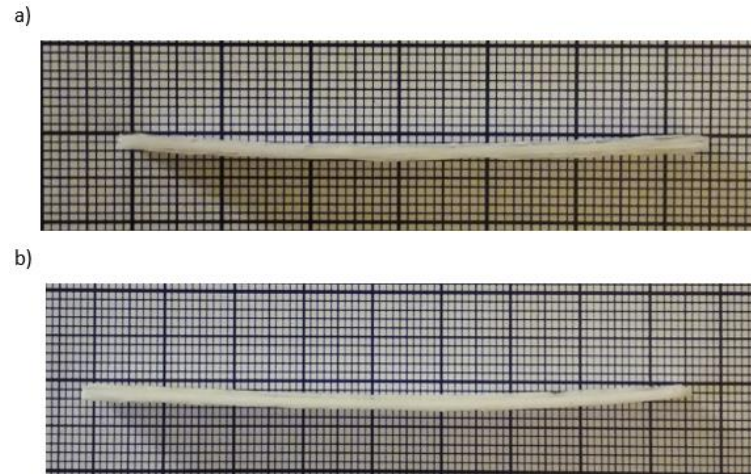


Figure 5-25 Cross-section from both manufacturing processes showing warpage: a) Automated in-situ consolidation, b) Hot Press Forming

### 5.3.2.7 Thickness

The cooling stage is different for hot press and automated in-situ consolidation processing. In the hot press process, the laminate cools down under the consolidation pressure. Section 0 In order to simplify the manufacturing process and to avoid warping effects due to lay-up configuration, a symmetrical and balanced laminate  $[0/90]_5$  was selected as the basis for all laminates unless stated otherwise.

Hot Press showed that removing the pressure from the laminate while it cools down is detrimental to the process. Pressure is needed to constrain the material while it solidifies from a molten state. This is more complex for automated in-situ consolidation processing. The forming tool locally melts and compresses a piece of material when it passes over it. Then, that piece of material cools down according to a new temperature gradient between the mould and the environment but without pressure. Because the mould temperature is kept at 110°C until the forming process ends, it is possible that some crystals of the copolymer in the bottom layers are being held in a molten stage until the manufacturing process finishes. (see

Figure 5-2). Then the mould temperature is left to cool to a temperature of 70°C (~ 40 min) before the laminate can be removed. Compared to hot press processing in which the material is fixed in all their degrees of freedom, automated in-situ consolidation processing the material is not under pressure when crystallises.

Figure 5-26 shows the laminate thickness as a function of the compaction temperature and pressure for both automated in-situ consolidation and hot press specimens. The thickness was measured using a micrometre in 3 different points of the laminate. It is clear that the thickness of hot press specimens is lower because the pressure keeps the material constrained during the crystallisation process. Therefore, it is expected that the thickness will be higher for the automated in-situ consolidation process because of the lack of constrain in the perpendicular axis.

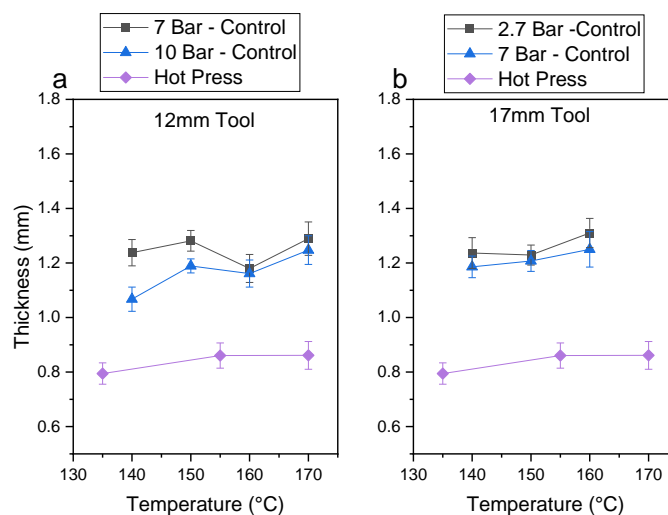


Figure 5-26 Laminate thickness as a function of the compaction temperature and pressure for both automated in-situ consolidation and Hot press specimens. a) Automated in-situ consolidation with a spherical 12 mm tool, b) Automated in-situ consolidation with a flat 17 mm tool.

## 5.4 Material Characterisation

This section summarises different material characterisation techniques to evaluate the influence of processing parameters on the final properties of self-reinforced composites. Specimen preparation methods are described in detail as they proved to be a challenging process and could help non-experienced users in the future.

### 5.4.1 Interlaminar Properties

The interlaminar properties of self-reinforced composites have been mainly tested via peel tests [32, 133, 189, 206, 207]. This section compares the interlaminar strength of laminates produced via Hot press and automated in-situ consolidation with different pressure and temperature processing parameters as described in Table 5-4. Specimen preparation for peel tests and fixed processing parameters (Mould temperature, path separation, and forming speed) have already been defined in previous sections (see 5.3.2 Automated In-Situ Consolidation), but in this case, a 6-layer laminate is used, and the unbonded region is created by introducing a single PTFE film in the middle interface. In this way, only the middle interface is used to measure the interfacial strength and ensuring symmetry of the specimen. The peel tests were performed using a universal testing machine adapted with a 5KN load cell (Tinius Olsen, USA) to peel apart the interface at a rate of 250 mm/min. The interlaminar strength is calculated by taking the average value of the peel strength (N/mm) in the range of 20 to 160 mm in accordance with [194]. Five specimens were evaluated in each processing parameter.

Furthermore, the peel test trace (form or shape) will also be used as a comparison performance parameter. This is done by defining the smoothness of the trace as the root-mean-square (RMS) error of the original data (strength vs crack propagation) compared with its own linear regression (first-order polynomial). The lower the RMS, the smoother the trace of the original data. The RMS is calculated according to Equation 5-2, in the same range as the interlaminar strength, where  $i$  is the variable,  $N$  is the number of data points,  $x_i$  is the actual observation, and  $\hat{x}_i$  is the estimated value.

$$RMS = \sqrt{\frac{\sum_{i=1}^N (x_i - \hat{x}_i)^2}{N}} \quad \text{Equation 5-2}$$

#### 5.4.1.1 Results and Discussion

Figure 5-27 shows the peeling strength of the intermediate interface for all tested configurations. For the hot press processing, as the temperature increases, the interlaminar strength also increases. This is in accordance with the literature for self-reinforced polypropylene composites composed of 2 layers, as seen in Figure 5-28. However, the opposite behaviour is observed for automated in-situ consolidation, in which as the

temperature increases, the interlaminar strength decreases. Moreover, the higher the pressure, the higher the interlaminar strength. Interestingly, at a processing temperature of 140°C, both automated in-situ configurations with a high-pressure level achieve a higher interlaminar strength value than hot press specimens. It is even higher than most values reported in the literature at this temperature. However, this result has to be treated with caution because the specimen geometry could cause it, or the material being not similar to the ones reported in the literature. For example, Bocz *et al.* [207] used extra layers of a polypropylene matrix in between the interfaces to improve the interlaminar strength.

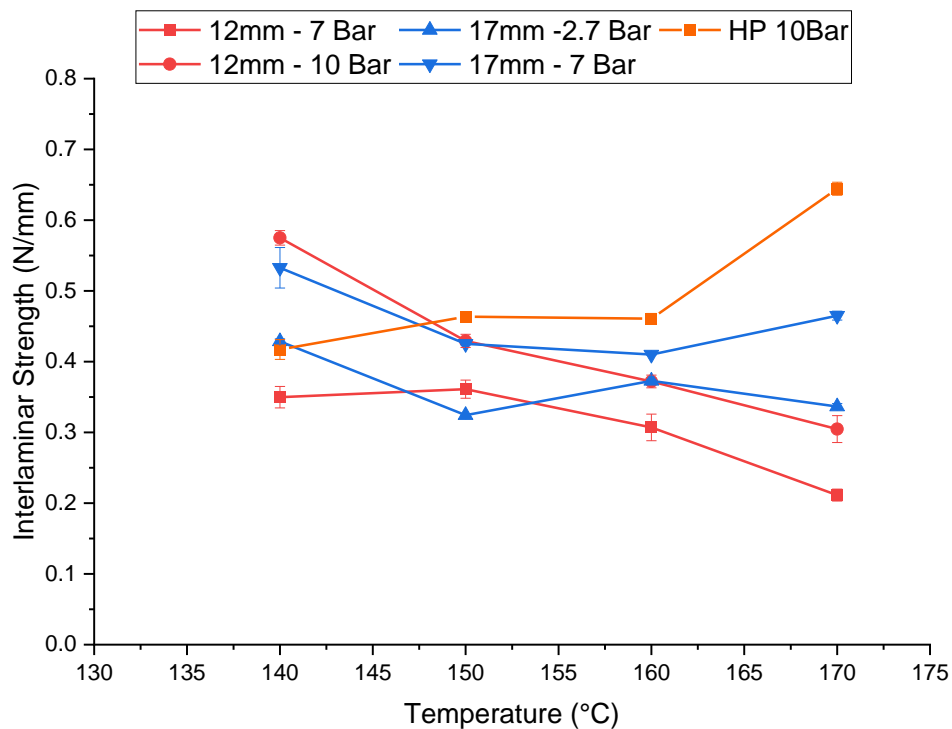


Figure 5-27 Interlaminar Strength vs Temperature for all tested configurations



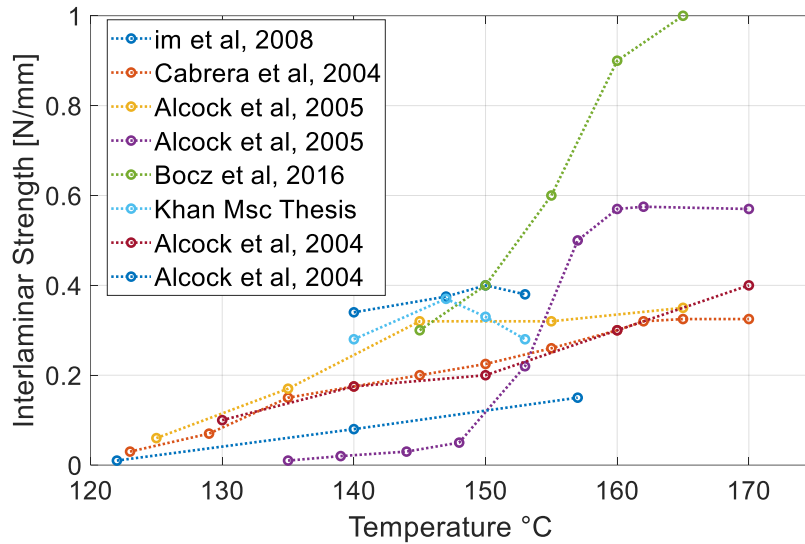


Figure 5-28. Summary of Interlaminar strengths reported in literature [32, 133, 189, 206, 207].

Figure 5-29 shows the peel test traces for both manufacturing routes. Hot pressing presents a relatively smoother peel trace than those manufactured via automated in-situ consolidation for all processing temperatures. This smoothness can be used as a parameter to measure the quality of self-reinforced polypropylene composites manufactured via automated in-situ consolidation. Figure 5-30 shows the root-mean-square error for each of the interlaminar-strength traces against its own linear fit. Hot pressed specimens present the smoother trend and therefore their low RMS value. Then it is followed by the 17 mm flat tool and then by 12-mm spherical tool. Hot press specimens have enough time for the interdiffusion of polymer chains through the interfaces and filling gaps. This is not the same for automated in-situ consolidation laminate due to its dynamic nature. The flat tool promotes a smoother trace because the forming path passes several times over the same area, improving the autohesion between polymer surfaces. The small contact area of the 12-mm does promote bonding, but not as efficiently as the flat tool because the number of times the tool passes over the same area is less than in the flat tool.

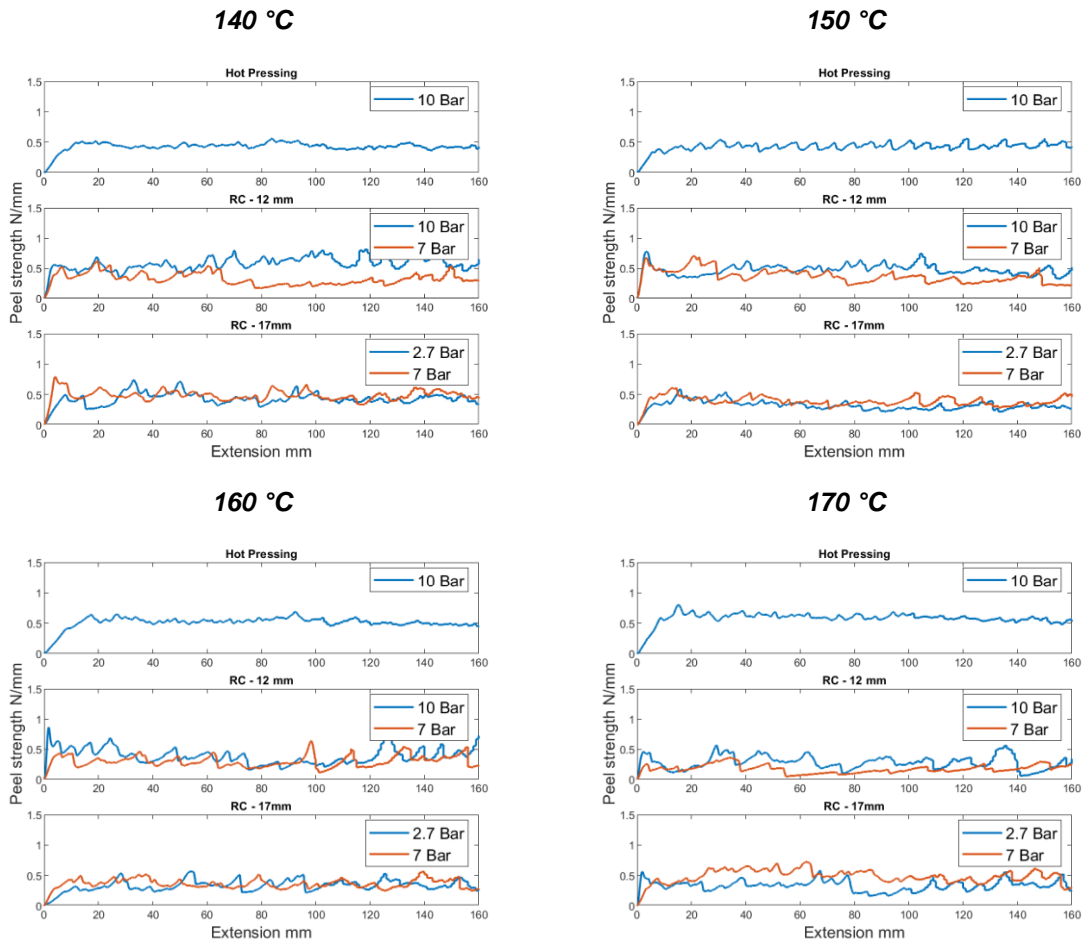


Figure 5-29 Peel test traces (Interlaminar strength vs crack propagation) at different temperatures and pressure for both manufacturing processes: Hot press and automated in-situ consolidation.

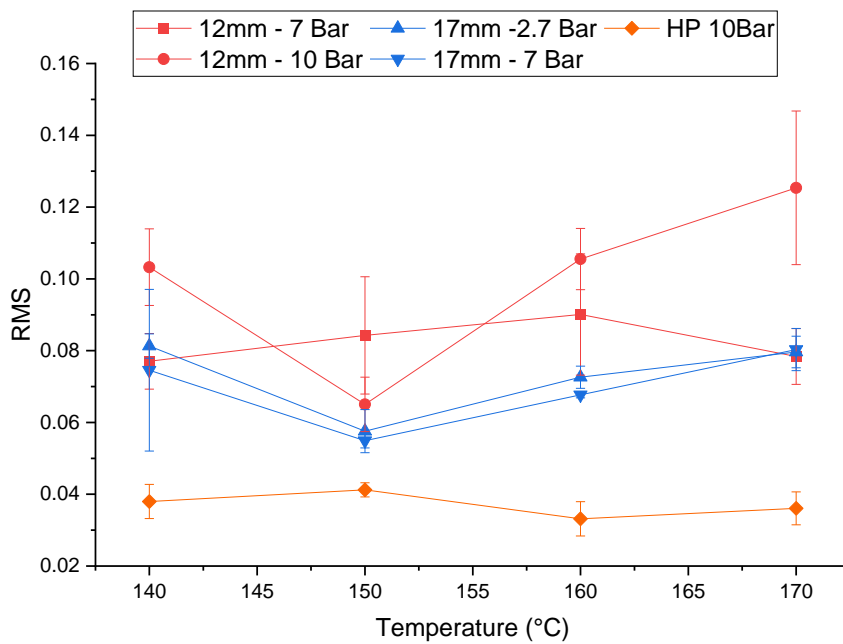


Figure 5-30 Root mean squared error of the interlaminar strength traces for both Hot press and automated in-situ consolidated specimens under different processing parameters.



## 5.4.2 Tensile Properties

Tensile testing is a characterisation technique that elongates a material up to its breaking point. After testing, a tensile profile is obtained, which is a force vs extension curve, or more commonly presented as a Stress vs Strain curve to give a comparable value with other materials. To calculate the stress from a force reading, Equation 5-3 is used where  $\sigma$  is the stress,  $F$  is the measure forced by the load cell, and  $A$  is the cross-sectional area. To calculate the strain from an extension reading, Equation 5-4 is used where  $\epsilon$  is the strain,  $l_i$  is the initial length of the specimen, and  $l_f$  is the final length of the specimen

$$\sigma = F/A \quad \text{Equation 5-3}$$

$$\epsilon = (l_f - l_i)/l_i \quad \text{Equation 5-4}$$

An example of typical tensile profiles for plastics is shown in Figure 5-31. The profile can determine different properties such as the elastic Modulus, Yield Point, Maximum Force, elongation, and other parameters. These parameters are useful for quality and design engineers as those properties explain how the material under study will behave for a specific application.

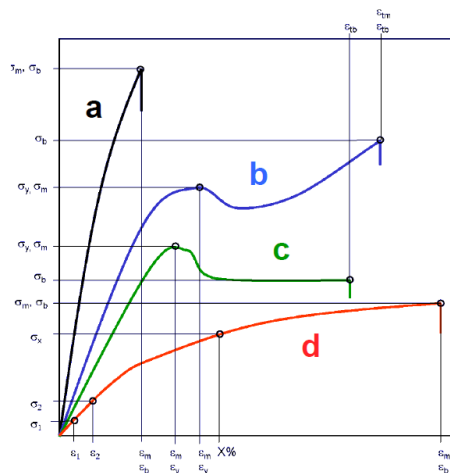


Figure 5-31 Stress vs Strain Curve Types for plastics. a) Brittle Materials, b) and c) tough materials with yield point, d) tough materials without yield point. Reproduced with permission from the authors [208].

While elongating the material, the deformation of the specimen must be measured to obtain the tensile profile. More advanced systems elongate a specimen by fixing one end while pulling the other. The machine can control different parameters such as the rate of deformation or keep a constant force. The force is measured using a load cell, a transducer

that transforms force into a measurable electrical output that can be then read in software. The deformation can be measured as the grip-to-grip distance as the specimen is elongated. However, this requires taking into account the deformations of the entire tensile system (machine, load cell, and grip deflections) [209]. These deformations are called machine compliance and lead to a higher deformation than the actual deformation of the actual specimen, as shown in Figure 5-32

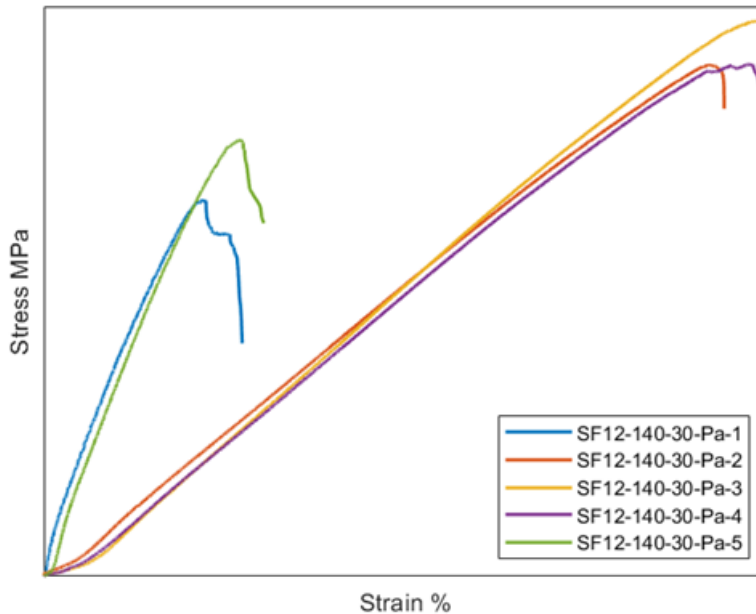
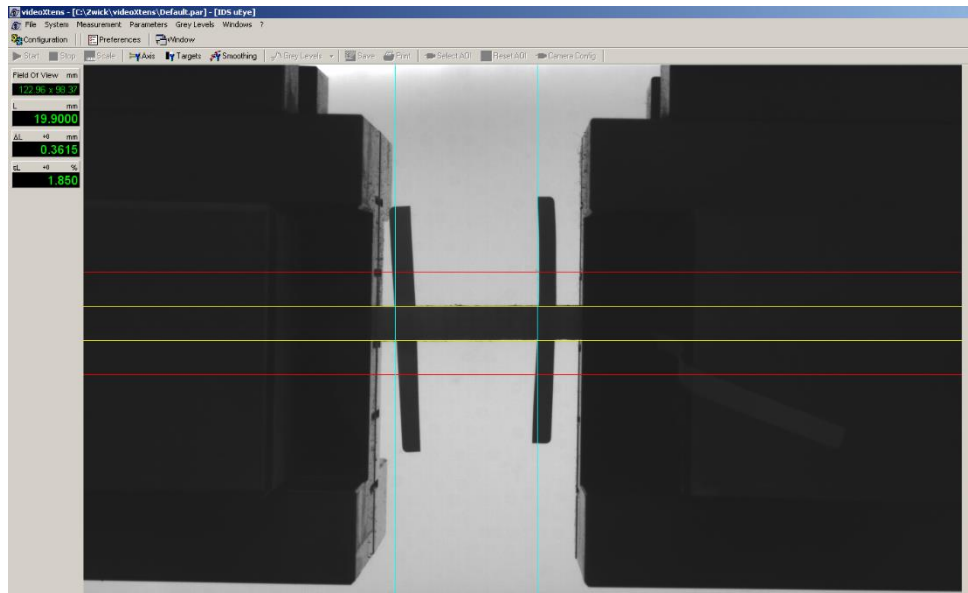


Figure 5-32 Tensile Profiles of Automated in-situ consolidated specimens with different strain measurement methods. Samples 1 and 5 use a video extensometer. Samples 2 to 4 use the grip-to-grip distance.

Currently, there are strain measurement devices to solve this problem [210]. These could be strain gauges, contacting extensometers, or non-contact extensometers. Strain gauges are electrical resistances that are attached or glued to the material. When the material is elongated, the strain gauges are also deformed, producing an electrical output, which is equivalent to the deformation of the material. Contacting extensometers are attached to specimens with clips or elastic bands with knife edges. When the material is elongated, the knife-edges separate from each other, and this distance is recorded. The last two types of extensometers have a short range of extension and are usually only used to obtain the tensile profile in the linear region. The device could be damaged or broken if the elongation is too high. Finally, non-contact extensometers could be of two types: laser extensometer or video extensometer. Their advantage is that they can be used up to the material breakpoint of the material. In both cases, the specimens have marks that are different from the surrounding

environment and can be detected by a sensor. In laser extensometers, reflective tapes attached to the specimen allows the laser to be reflected on the sensor. In video extensometers, straight marks are attached to the specimen so they can be detected by a video camera that uses an image recognition algorithm to measure the distance between the marks, as illustrated in Figure 5-33



*Figure 5-33 Video Extensometer Camera. The yellow lines help users to align the samples with the testing direction properly. The red lines narrow the target window of the video extensometer to avoid the surroundings and only focus on the specimens. The algorithm detects the marks and creates two blue lines at the centre of the marks. As the material is elongated, the marks, and therefore the blue lines move with it which allows the measurement of the deformation or strain of the material.*

#### **5.4.2.1 Methodology and Experimental Set up**

Self-reinforced polypropylene laminates were produced according to the processing parameters mentioned in sections 5.3.1.2 and 5.3.2.4. They were cut with their main axis parallel and perpendicular to the forming path, as shown in Figure 5-34. The dimensions of the specimens are in accordance with BS EN ISO 527-3:2018, Specimen type 1BA [211]. The cutting process was performed with a WaterJet Cutter (ProtoMAX, OMAX), as shown in Figure 5-35. Abrasive Water-Jet Cutter uses water and abrasive materials such as sand at extremely high pressures to cut different materials. It has the advantages of producing a better edge quality than other cutting method. Being a cold cutting technique, it prevents the formation of a heat affected zone that will change the properties of the material, and allows faster cutting rates than other methods.

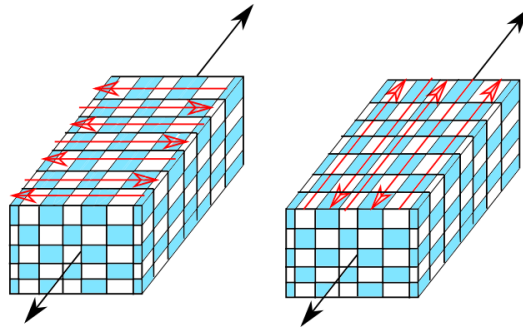


Figure 5-34. Direction of the force and forming paths (red arrows) in Tensile specimens. The blue and white squares represent tapes of the fabric



Figure 5-35 ProtoMax WaterJet Cutter used for cutting composite panels. Reproduced with permission from the authors [212].

A common problem when cutting flexible fibre composites is tearout or fibre-tearing, which leads to rough edges [213], as seen in Figure 5-36. Tearout occurs because the bottom surface is not supported, and therefore, the abrasive action of the water flexes the last layer rather than cutting it. To improve the edge quality, a medium that supports the fibres is needed. The composite panel was glued to an aluminium plate with a high strength double-sided tape, leading to clean and smooth edges, as seen in Figure 5-36.

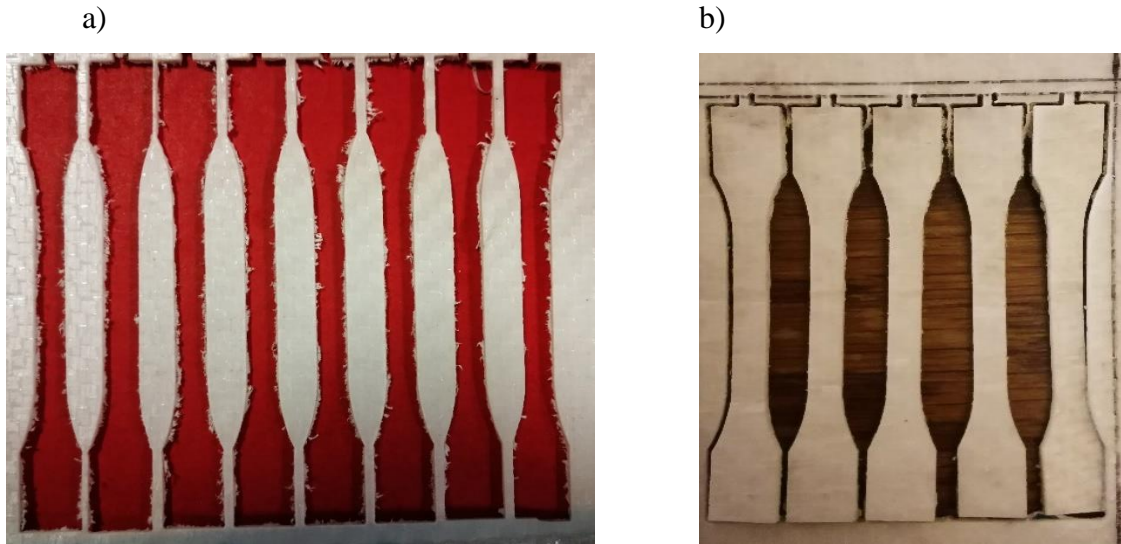


Figure 5-36 Water Jet Cuter of Self-Reinforced Polypropylene Composite Panels. Left images show rough edges after the process. The right image shows a better edge quality after using an aluminium plate as support.

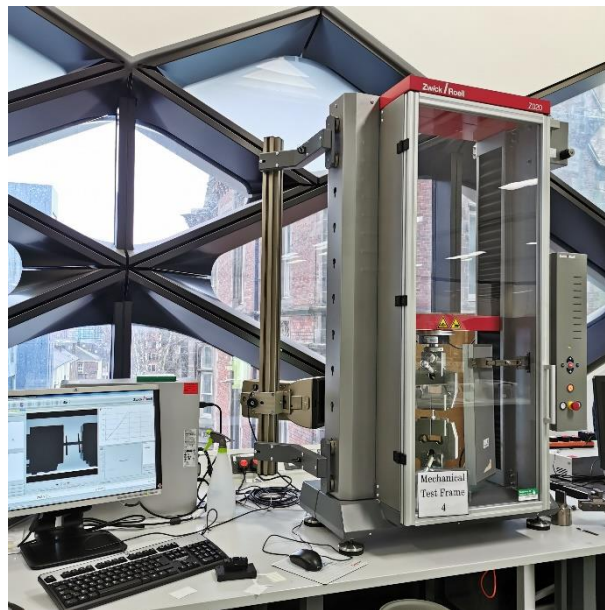


Figure 5-37 Universal Testing machine adapted for tensile testing with a Computer showing the video Extensometer software.

The tensile tests are performed on a Zwick tensometer model “2020 Proline MTM” equipped with a 20 KN load Cell, 20 KN Wedge grips and a video extensometer from the same manufacturer, as shown in Figure 5-37. Both the tensometer and the video extensometer are controlled by the manufacturer's software TextExpert II and VideoXtens, respectively. The tensile tests are performed under a strain rate of 2mm/min on dog-bone specimens. A preload of 15N was set up to avoid the toe region in the tensile profile. A Vernier Calliper was

used to measure the dimensions of both thickness and width. Three measurements were taken for each parameter, and the average was used to calculate the cross sectional area.

### 5.4.2.2 Results and Discussions

Figure 5-38 shows the Tensile Modulus of specimens with the central axis perpendicular and parallel to the forming path in an automated in-situ consolidation process. Hot press specimens are also presented for comparison purposes. The general trend is that the tensile Modulus decreases as the temperature increase. This is expected as the temperature promotes molecular relaxation leading to a reduction of mechanical properties [16]. The tensile modulus values of specimens produced with a Hot Press are at least 40% higher at a temperature of 140°C than those produced via automated in-situ consolidation regarding the direction of the forming path. This is also expected because of the better consolidation demonstrated in both interlaminar strength and microscopy cross-sections results. However, this difference decreases as the temperature increases because the average temperature in the temperature gradient of automated in-situ consolidation specimens is lower than the temperature in the hot press, leading to less molecular relaxation.

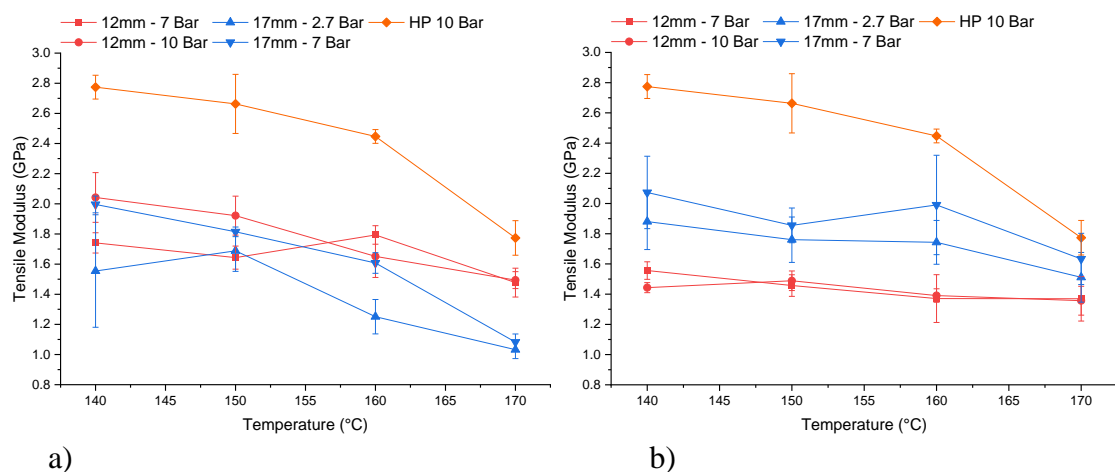


Figure 5-38. Tensile Modulus vs Temperature. Specimens main axis are a) perpendicular and b) parallel to the forming path in an automated in-situ consolidation process. Hot press specimens are also presented for comparison purposes.

Using a flat forming tool leads to higher tensile modulus values when the direction of the force is parallel to the forming path, and as expected, the tensile modulus increases with higher levels of consolidation pressure. On the opposite side, using a spherical tool leads

higher tensile modulus values at both low and high pressure levels when the specimen is stressed perpendicular to the forming path, and similarly, there is an improvement of the tensile modulus when increasing the level of consolidation pressure. However, this difference in tensile modulus in specimens formed with a spherical tool at different pressure decreases as the processing temperature increases. The reasons for the anisotropy according to the testing direction are not well understood. Evidence suggests that forming the material in the load direction is recommended for a flat tool to achieve higher stiffness values.

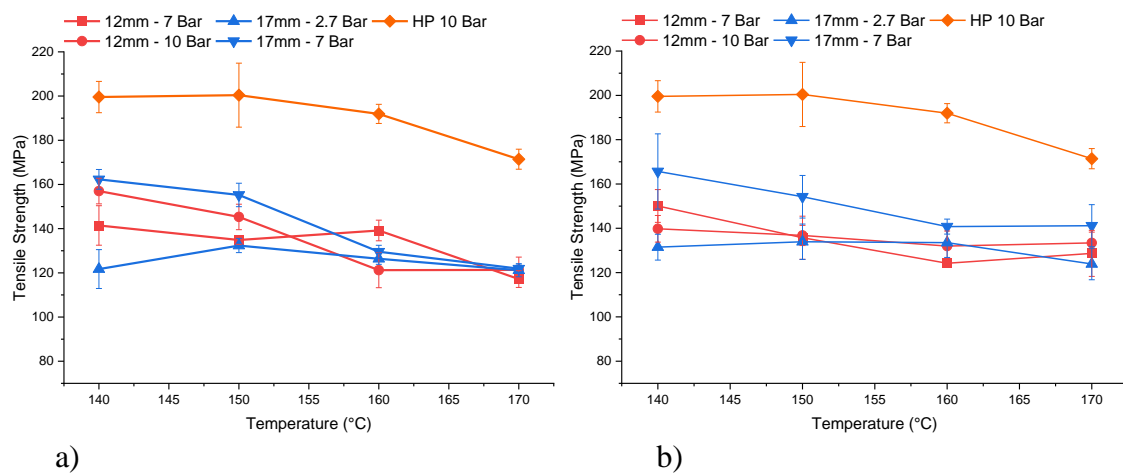


Figure 5-39 Tensile Strength vs Temperature. The main axis of the specimens are a) perpendicular and b) parallel to the forming path in an automated in-situ consolidation process. Hot press specimens are also presented for comparison purposes.

Figure 5-39 shows the Tensile strength of specimens with the central axis perpendicular and parallel to the forming path in an automated in-situ consolidation process. Hot press specimens are also presented for comparison purposes. The strength values for hot press specimens are at least 20% higher than automated in-situ consolidate specimens. However, and opposite to the tensile modulus, the difference with the automated in-situ consolidation technique appears to be kept constant regarding the increase of compaction temperature. Furthermore, and in accordance with the literature [189, 214], the tensile strength decreases as temperature increases due to molecular relaxation in the reinforcement phase for both manufacturing techniques.

The level of consolidation pressure has more influence over the tensile strength of the material at lower temperatures than at higher temperatures. It is known that the strength of a material depends on the flaws or defects it has; therefore, and as expected, a higher pressure improves the bonding strength, which reduces the quantity of flaws and, therefore,



increases the tensile strength. At lower temperatures, only the copolymer is melted, so the reduction of flaws depend on how fast the interlaminar gaps are filled when the forming tool compresses the material. However, at higher temperatures, both copolymer and homopolymer are melted and pressed, leading to a more “compacted” and similar material, and therefore, to a similar strength value or with less difference.

Figure 5-40 shows the strain to failure of specimens with the central axis perpendicular and parallel to the forming path in an automated in-situ consolidation process. Hot press specimens are also presented for comparison purposes. The effect of processing parameters is less clear, but specimens formed with a flat tool and tested perpendicularly to the forming path show the lower strain to failure values for all temperatures. However, they also present greater values at high temperatures when tested parallel to the forming path. On the other hand, 12 mm tool specimens tested in the perpendicular direction have the highest strain values and the lowest when tested in the parallel direction. The strain to failure values for hot press specimens falls in between the results of both tools and testing directions.

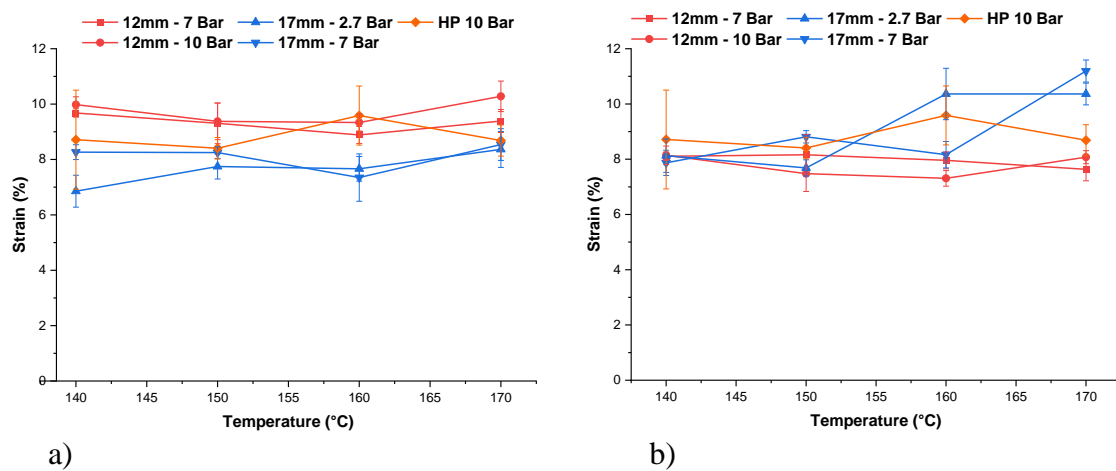


Figure 5-40. Strain to failure vs Temperature. Specimens main axis are a) perpendicular and b) parallel to the forming path in an automated in-situ consolidation process. Hot press specimens are also presented for comparison purposes.

### 5.4.3 Degree of Crystallinity

The Degree of Crystallinity (DOC) is related to the ordering of the molecular chains and is one of the most important structural characteristics. It determines many macroscopic properties in polymers, including storage modulus, density, and melting temperature. Crystallisation and the resulting morphology are strongly related to several processing



parameters such as temperature, applied shear rate or strain rate, and total strain achieved during flow. Complex thermomechanical conditions determine the supermolecular structure of polymeric materials and, as a consequence, their properties [5]. Polymers cannot fully crystallise. In reality, they are composed of crystalline and amorphous regions, so they are called semicrystalline polymers. In addition, crystallisation occurs in different types of forms. There are several methods to calculate the DOC, such as differential scanning calorimetry or X-Ray diffraction.

Differential scanning calorimeter is widely used for the determination of the degree of crystallinity of semicrystalline polymers. The crystallinity can be determined by quantifying the polymer's heat of fusion  $\Delta H_m$  and relating it with the heat of fusion of a 100% crystalline sample  $\Delta H_f$  of the same polymer according to Equation 5-5. The heat of fusion is determined by calculating the area under the melting peak of a DSC trace and using Equation 5-6 where  $m_{sample}$  is the mass of the sample. The heat of fusion of a 100% crystalline is obtained from the literature, and its value for polypropylene is 293 J/g [215].

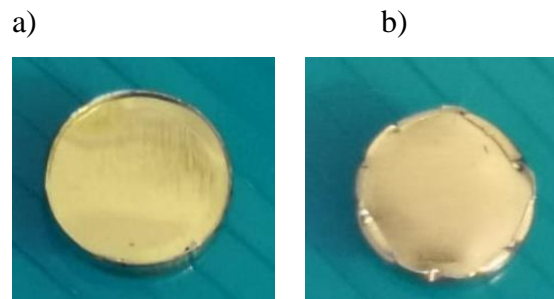
$$DOC = \frac{\Delta H_m}{\Delta H_f} * 100\% \quad \text{Equation 5-5}$$

$$\Delta H_m = \frac{Area}{Heating\ rate} * m_{sample} \quad \text{Equation 5-6}$$

#### 5.4.3.1 Methodology

A DSC 4000 from Perkin Elmer was used for differential scanning calorimetry. The samples were heated in a nitrogen environment purged at 19.8ml/min. A heating cycle from 50 to 200°C at a heating rate of 10°/min was applied to obtain the enthalpy of fusion of the samples. An empty sample was the first scan to create a baseline. 6-mm diameter Samples were punched from manufactured samples and weighted in a Mettler Toledo balance. Standard aluminium pans & covers (02190041, Perkin Elmer) were used to create sealed samples using a standard press crimper. However, due to the thickness of the samples, the press crimper could not bend the edges of the pan over the covers, as shown in Figure 5-41-a. This is detrimental to the calorimetry analysis of polymer films and sheets because the polymer is free to shrink and move, resulting in the lid being removed, resulting

in a non-smooth and wrong DSC trace [216]. Therefore, the pans were manually bent with tweezers over the covers to prevent them from bursting while the polymer reached the melting temperature, as shown in Figure 5-41. b. For each processing parameter (see 5.3.2.4 Processing Parameters), three samples were used to ensure repeatability.



*Figure 5-41 DSC aluminium pans and lids with self-reinforced polypropylene composite samples. (a) Pan without bent edges over the lid (b) Pan with bent edges over the lid to ensure a good thermal transfer between the material and the pan.*

#### **5.4.3.2 Results and Discussion**

The material as received was also examined resulting in a degree of crystallinity of  $\sim 3.6\%$  and  $\sim 49\%$  for the copolymer and homopolymer respectively. Figure 5-42 shows the degree of Crystallinity as a function of the temperature for the copolymer and homopolymer phase in each configuration and processing parameter. The copolymer refers to the matrix, while the homopolymer to the reinforcement phase. However, no trend can be associated with the influence of processing parameters (Pressure, temperature, tool, or manufacturing process) on the degree of crystallinity alone because the values increase and decrease. The only obvious reading is that the crystallinity of the copolymer is lower for Hot Press specimens than for automated in-situ consolidation with low and high pressures. This could be due to the annealing time at which the copolymer is exposed in an automated in-situ consolidation process that promotes lamellae growth [188]. An interesting result is that the degree of crystallinity increased for both copolymer and homopolymer when compared with the material as received for the automated in-situ consolidation process even at high temperatures. This could be attributed to the longer exposure to high temperatures below the melting temperature which could increase the size of the crystals, and therefore, increment the enthalpy of the melting curve in DSC scans. More research is needed to understand the relation between the degree of crystallinity and the final morphology of the samples after being processed.

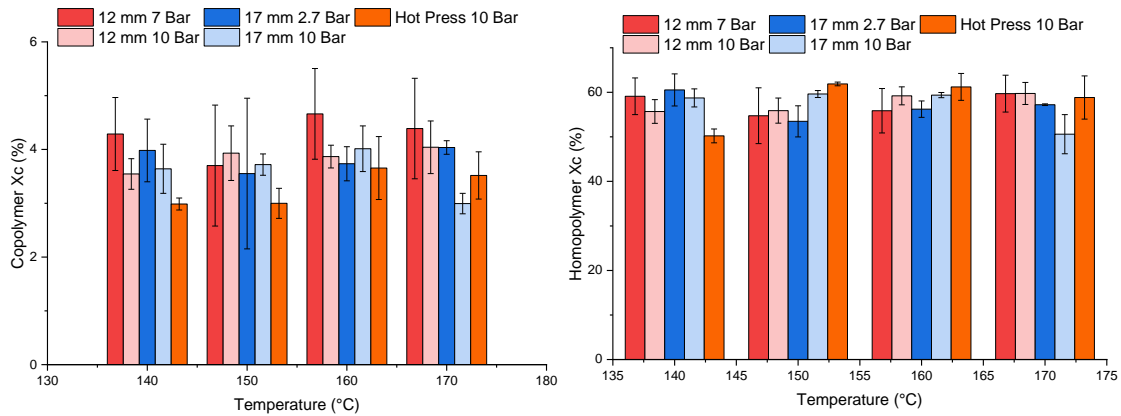


Figure 5-42 Degree of Crystallinity as a function of the temperature for the copolymer and homopolymer, respectively.

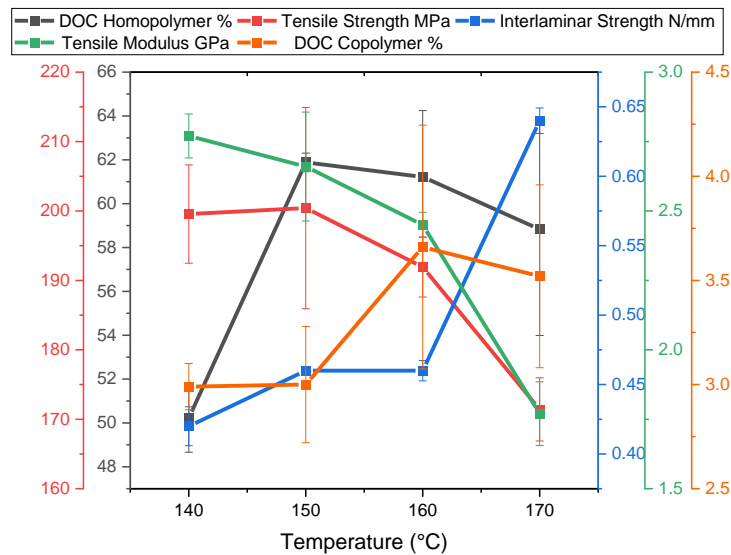


Figure 5-43 Material Properties as a function of the temperature for Hot Press specimens

It is known that the degree of crystallinity is linked to several properties of semicrystalline polymers, such as strength, because intermolecular bonding is more significant [5]. Therefore, Figure 5-43, Figure 5-44, and Figure 5-45 were created to show correlation patterns between different material properties as a function of the temperature for Hot Press and automated in-situ consolidated specimens at different consolidation pressures. From these, several relationships can be obtained. A clarification is made related to the term “pattern”, which is associated with the shape or behaviour but not its values. For example, in all cases, the tensile strength and tensile modulus have the same pattern as a

function of the processing temperature because both properties decrease as the temperature increases, which was explained previously. It also appears that the crystal growth during crystallisation is similar for both polypropylene phases (homopolymer and copolymer) in the fabric tapes as the degree of crystallinity has similar traces as a function of the temperature for all processing parameters and manufacturing process. This is expected as both copolymer and homopolymer are based on the same monomer. Furthermore, even though it is unclear, it appears to be a relationship between interlaminar strength and the degree of crystallinity for specimens manufactured via hot press and automated in-situ consolidation with a flat tool. However, the pattern is the opposite when using a 12 mm tool for automated in-situ consolidation.

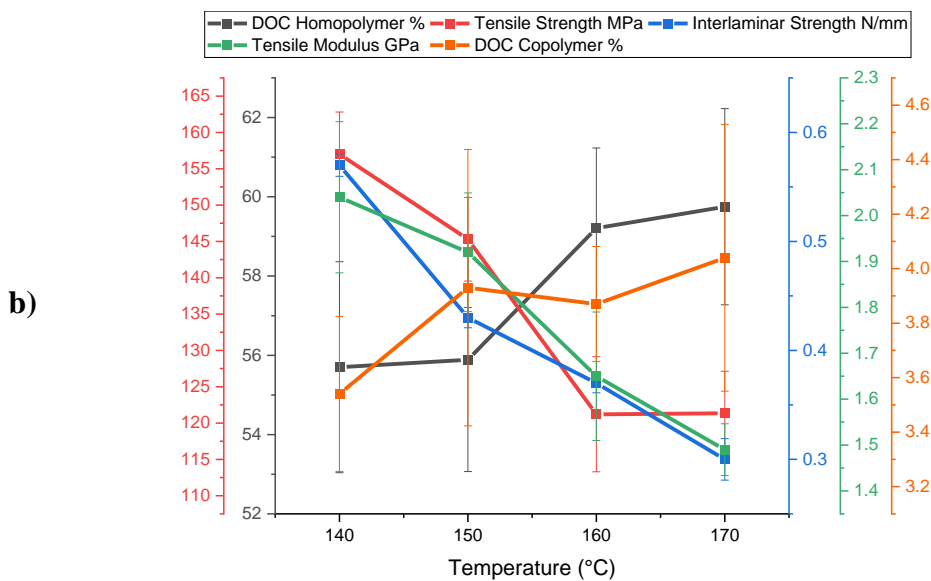
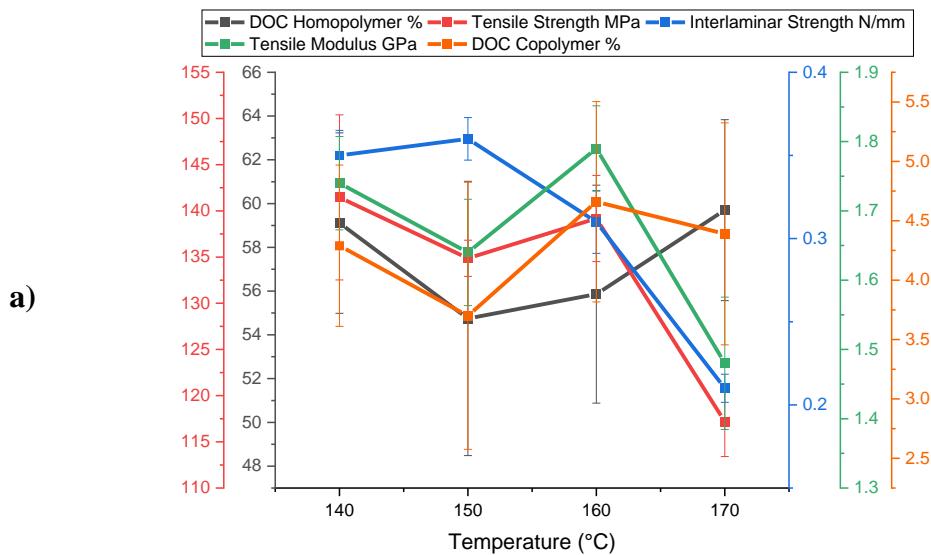


Figure 5-44 Material Properties as a function of the temperature for Automated in-situ consolidation specimens with a 12 mm to with processing pressures of a) 7 bar and b) 10 bar

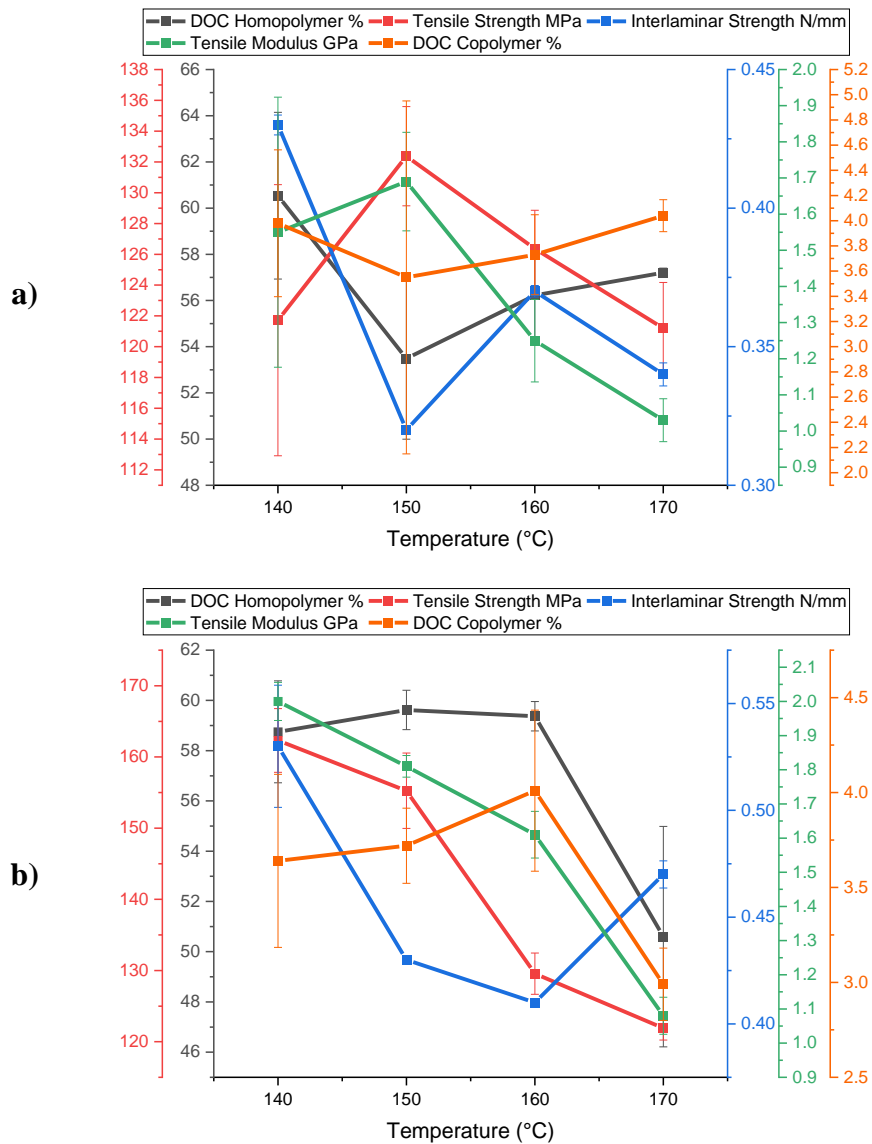


Figure 5-45 Material Properties as a function of the temperature for Automated in-situ consolidation specimens with a 17 mm to with processing pressures of a) 2.7 bar and b) 7 bar

## 5.5 Conclusions

Two-dimensional laminates of self-reinforced polypropylene composites based on bicomponent tapes were produce using a benchmark processing technique (hot press) and the proposed low-cost automated in-situ consolidation process. The rationale behind the selection of fixed processing parameters was explained through experimentation. This helped

to reduce the number of variables that were studied to understand their influence over the final properties of the laminates. The main findings can be summarised as follows:

- The manufacturing of two-dimensional laminates via hot press processing must be under pressure to prevent shrinkage in a flat laminate while it solidifies
- Peel tests have been proved to be an effective methodology to determine the effects of several processing parameters.
- Warpage will be expected when laminates are produced with the automated in-situ consolidation process. Surprisingly, hot press specimens also had some level of warpage.
- Implementing a force closed-loop system to in-situ consolidate self-reinforced polypropylene composites is essential to reduce the number of voids in the material.
- The effect of the processing temperature is more noticeable on Hot press specimens than in automated in-situ consolidation. However, this is because of the high number of processing variables that are involved in the process
- There is no clear influence of the main processing parameters (pressure and temperature) in the crystallisation process.
- Evidence suggests that the best forming parameters for two-dimensional laminates are to use, a “flat tool”, a forming tool at 140°C, a forming speed of 90 mm/min, and a consolidation pressure of 7 bar. This combination of parameters has resulted in the best mechanical properties such as interlaminar strength, and tensile strength

## **6 Three-dimensional laminates and characterisation**

### **6.1 Introduction**

This chapter introduces the reader to the development of three-dimensional laminates of self-reinforced polypropylene composites using the automated in-situ consolidation technique. Similarly, the manufactured specimens were characterised and compared with hot press specimens to understand the current state of the process and evaluate future areas that require more research and development.

### **6.2 Dome Geometry Manufacturing**

A dome is an architectural term for a hollow upper half of a sphere. However, a precise definition has not been achieved as different terms such as the hemispherical double curvature part could be used. Using a double-curvature geometry can help testing the current capability of the present development to perform forming operations with "difficult to process" geometries.

#### **6.2.1 Hot Press Processing**

The processing cycle to produce three-dimensional parts made of self-reinforced polypropylene composites is similar to the long processing cycle to produce two-dimensional laminates. The hot press platens were heated to the processing temperature with a small gap separation (~5mm). Then, five layers of plain fabric were stacked between two aluminium moulds with the dome shape, and this sandwich structure was inserted into the gap, which was then closed, compressing the laminate with a 10 bar pressure. Due to the heat transfer from the platens to the moulds once the gap is closed, the processing temperature was monitored until the target temperature was achieved. Then the laminates were compressed, maintaining the processing temperature for 15 min before cooling down without removing the pressure up to a temperature of 70°C. The Time-Temperature and Time-Pressure profile during consolidation for this route is illustrated in Figure 5-6

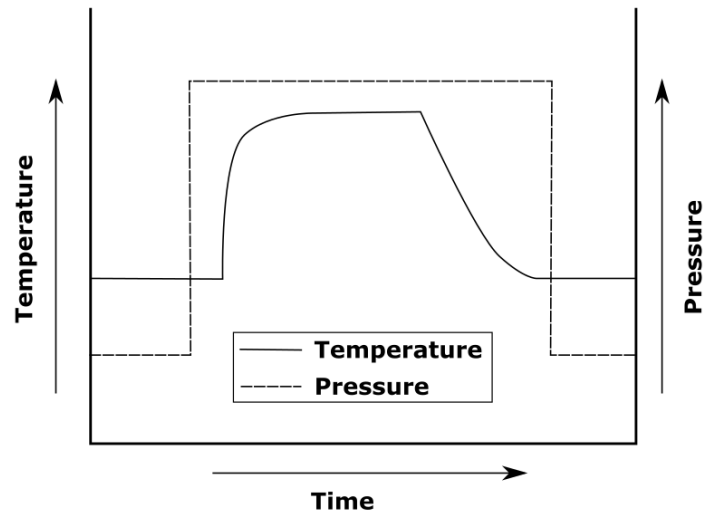


Figure 6-1 Time-Temperature and Time-Pressure profile of Hot-Pressing manufacturing

Figure 6-2 shows Hot press specimens in which no wrinkles appear, but a change of colour in the specimens from white at 125°C to transparent at 170°C. It has been shown that polypropylene fibres become opaque (white) when stretched, which is the case of the preform. When the temperature increases to a similar level to the melting point, molecular relaxation occurs, and the molecules pass from stretched and oriented to randomly oriented, making the bulk material transparent [35].

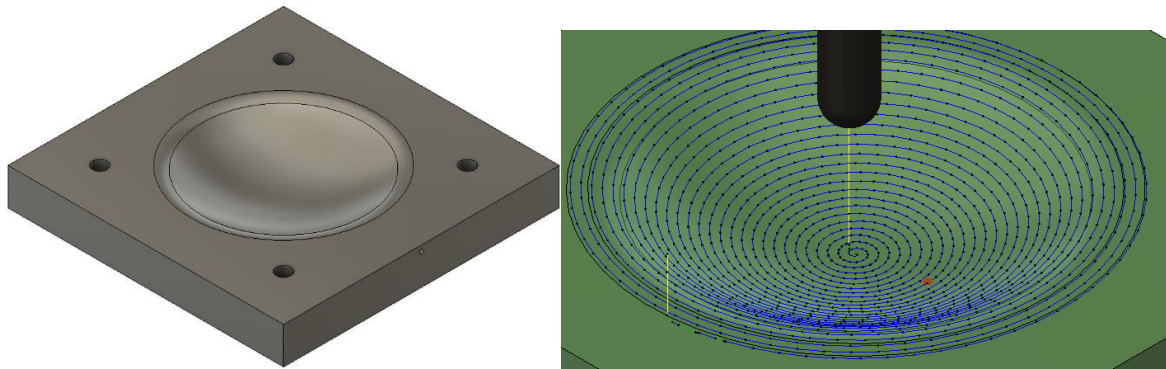


Figure 6-2 Hot Compaction manufacturing via Hot pressing for a 5-layer laminate

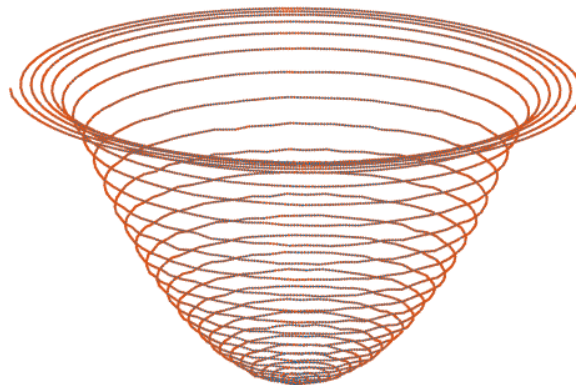


## 6.2.2 Automated In-Situ Consolidation

The first step is to design the part (Figure 6-3. Left). In this case, a mould of the intended geometry was created in a CAD software. Then a CAM software was used to obtain a spiral milling toolpath operation that will cover the surface of the expected forming operation (Figure 6-3. Right). By default, the separation between each G-code coordinates increases as the path reaches the final stages. To correct this, the G-code from FUSION 360, which is a text file of coordinates, was post-processed using a Matlab subroutine. This subroutine adds new coordinates to ensure the distance separation between each coordinate is 0.5mm (Figure 6-4) and creates a file in the right format to be read by the LabVIEW motion control program.



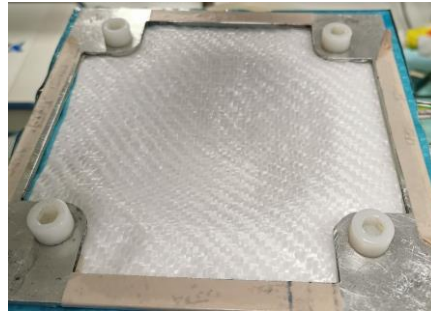
*Figure 6-3. Left: CAD part of the mould. Right: Toolpath simulation using a CAM milling operation. The start position of the toolpath is in the centre of the dome following concentric paths, and the finish position is in the outer boundaries*



*Figure 6-4. New Toolpath plan from Matlab Post-processing in which the separation between coordinates is reduced to 0.5 mm. The start of the path is at the apex of the dome and the end is the outer point in the mould plane.*

Once the tool path planning was reviewed and tested in Labview, the next step is to prepare the preform. 16x16cm plies were cut and stacked together before being perforated in their corners to allow enough space for clamping in the mould. The perforation consisted in creating four holes with a bigger diameter than the clamping bolts because, as explained in

3.3.4 Clamping, that allows the material to move so it can be conformed to the mould. The holes were made manually using a soldering tool at a temperature of 380°C. The preform dimensions are higher than the mould dimensions because the preform needs extra material to cover the whole surface of the mould and the clamping area. Once the stack was located in its position, it was manually pressed against the surface of the dome to re-accommodate the fibre alignment of the preform, as shown in Figure 6-5.



*Figure 6-5. The preform is manually pressed against the mould to aid the forming process*

The automated in-situ consolidation fixed processing parameters are a fixed tool path separation of 2 mm between path lines, a 90 mm/min forming speed, and a 12-mm copper forming tool with a spherical end. The processing temperature values were 125°C, 140°C, 170°C, and the forming pressure was set at 7 bar and 10 bar. The approximate forming time is 1 hour before cooling down. Once the temperature of the mould reaches 70°C (approximately 1.5 hours), the laminate is removed. Examples of specimens manufactured via automated in-situ consolidation is shown in Figure 6-6. While there is no apparent difference between the processing temperature of 125°C and 140°C, the specimen manufactured at 170°C presents a relatively flat plane on the top surface. Because this processing temperature is slightly above the melting temperature of the homopolymer, there is considerable molecular relaxation in the top layers that are in contact with the forming tool. This relaxation is enough to overcome any bonding force with the subsequent layers creating a cavity between the top and bottom surfaces.

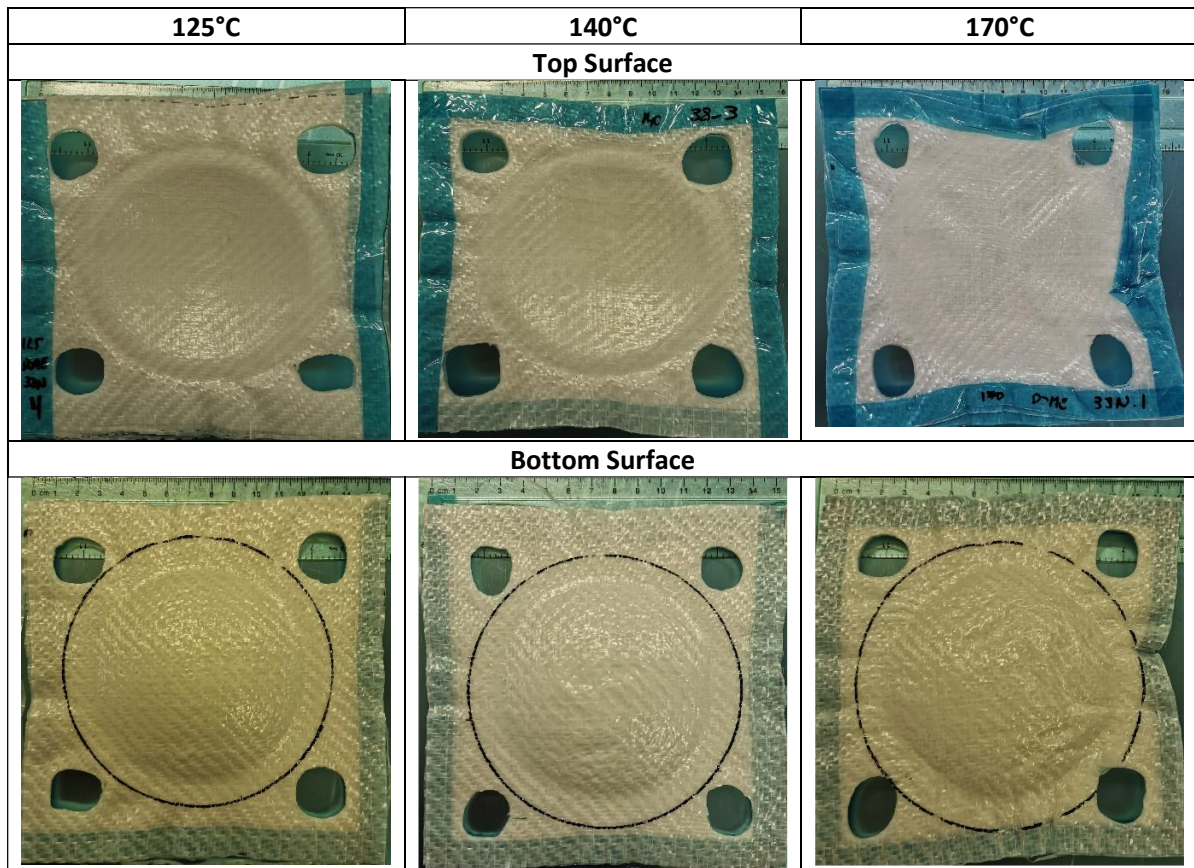


Figure 6-6. Dome laminates manufactured via automated in-situ consolidation at different temperatures

### 6.3 Curved Geometries

Two path planning strategies were attempted to create double curvature laminates: parallel and perpendicular to the curve profile, as shown in Figure 6-7. After the G-code path is generated in Fusion360, it is further post-processed in Matlab to create a fixed separation between coordinates of 0.5 mm and remove unwanted paths such as the yellow lines in Figure 6-7. b. It is important to mention that the machine is limited to three degrees of freedom (X-Y-Z), and therefore, the axis of the forming tool is always perpendicular to the z axis. The g-code path was created so the forming tool always contact the stack in their tangent surfaces. Unfortunately, due to the design of the PID force control algorithm and the data acquisition capabilities of the force control system, parallel forming was unsuccessful, and the operation had to stop to prevent damage to the equipment. As mentioned in a previous chapter, the force control system was designed to control only compression forces (z-axis). For curved laminates, it was found that the PID algorithm designed enters into an

uncontrollable state, as shown in Figure 6-8 (left), because there is a contribution forces in the Y-axis to the vertical axis. On the other side, the perpendicular strategy has a better force control performance in the Z axis (Figure 6-8. Right). PID control measures the error between the expected and the measured signal, and tuning its controlling parameters (proportional, integrative, derivative constants) was performed over flat panels. Attempts to find suitable PID parameters were performed without success. A figure of the automated in-situ consolidation machine forming a curved laminate, the finished part after forming and after post-processing is shown in Figure 6-9. It can be noticed that the stack is not completely clamped. As will be explained in future work, clamping is essential to improve the formability of automated in-situ consolidation parts.

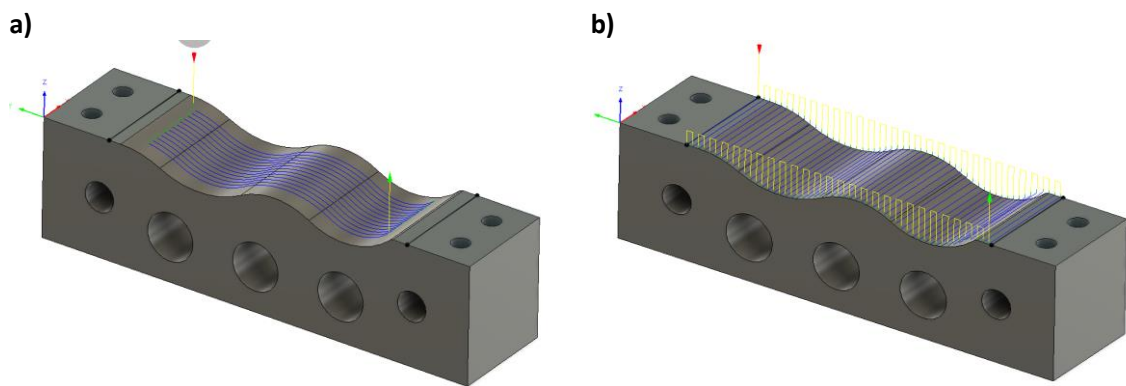


Figure 6-7. Path Planning for Curved laminates. a) Parallel to the curvature, b) Perpendicular to the curvature

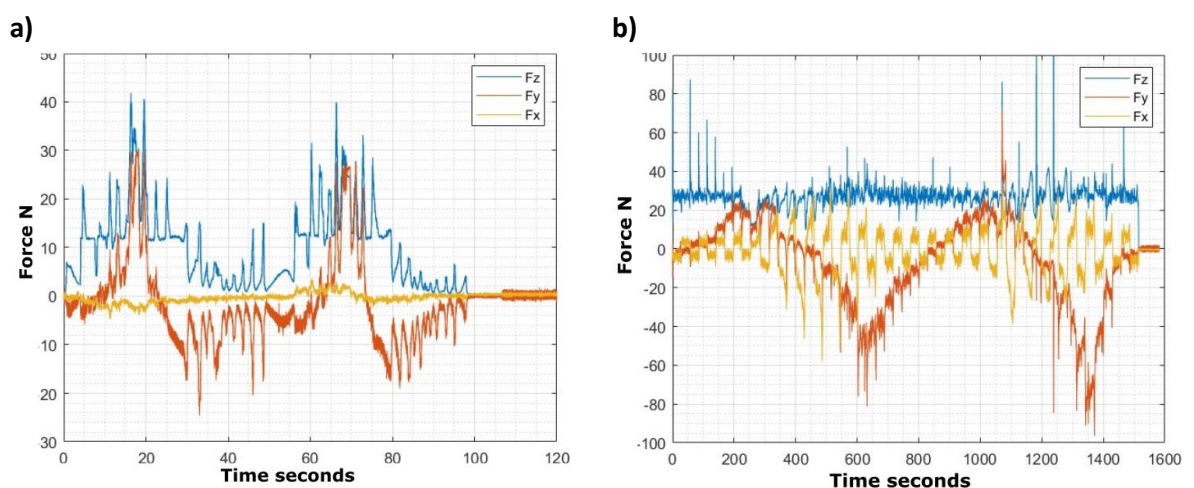


Figure 6-8. Forming Forces for curved laminates. a) Forming forces when the tool path is parallel to the curvature of the path. b) Forming Forces when the tool path is parallel to the curvature of the part



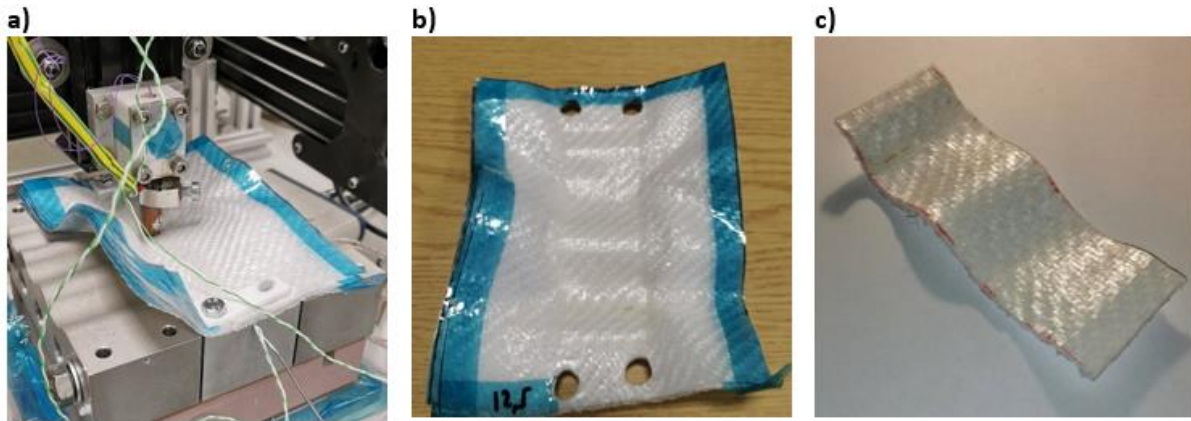


Figure 6-9. Automated in-situ consolidation of curvature laminates. a) experimental set-up in process\*, b) consolidated laminate\*, c) post-processed laminate. \*The blue boundary in the laminates is blue tape that was used to improve the cutting process of the preform and it is not related to any processing parameter.

## 6.4 Quality Control of Automated In-Situ Consolidated Parts

Metrology, the science and process of measurement, is of fundamental importance to manufacturing. Factory production efficiency relies on accurate quality control. The act of measuring a part can be taken for granted, but it is critical to manufacturing in all sectors, including automotive and aerospace. "Bad metrology will undermine business profitability and stifle its ability to improve. Good metrology is an added value activity increasing competitiveness and helping drive down production costs" [217]. Part design is continuously evolving using new materials and construction methods. This brings many benefits but can also add to the technical challenges faced throughout the manufacturing process. Measured data can be obtained from various measuring devices such as tactile articulated arms, non-contact scanning systems, coordinate measurement machines, and machining centres. Having measurement processes through the manufacturing process and being able to capture that data can help to evidence that the parts are fit for purpose and to control the processes.

To ensure that the parts fit for purpose, a comparison between a manufactured part and the desired part is required. In this chapter, a metrology system composed of a 3D scanner and software inspection tool to evaluate the deviations and tolerance performance of manufactured parts via Hot Press or Automated in-situ consolidation. This chapter first explains the science of 3D scanning and the methods used to measure the parts. Later, a detailed description and discussion of the results are presented. The results show that automated in-situ consolidated parts have poor accuracy in comparison with hot pressing.

### 6.4.1 3D Scanning

3D scanning or 3D imaging is a non-contact measurement technique that produces a three-dimensional model (e.g., a cloud of points) of an object based on the point observed on a computer. The most common 3D scanner techniques are based on lasers scanners (also known as LADARs or LIDARs), optical range cameras (also known as flash LIDARs), triangulation-based systems, or interferometry [218]. Laser scanners determine ranges (distances) using a laser beam targeted to the object and measuring the time of the reflected beam with a laser point sensor. Optical range cameras are similar to laser scanners but use a wide laser beam with a 1-D or 2-D sensor array. Each pixel in the array contains the 3D location and intensity, which are then used to build the model. A triangulation-based system uses structured light technology that projects light patterns (e.g., the array of straight lines) onto objects, as shown in Figure 6-10. A video camera records the distortion of the light patterns onto the shape, and a computer compares this distortion with the original light pattern. As the distance between the projector and camera is known, the depth of a specific point in the pattern is calculated via triangulation, and therefore, generating 3D information of the points [219].

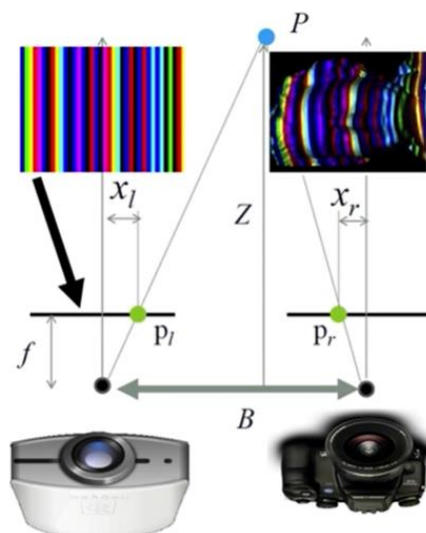


Figure 6-10 Triangulation base system using structured light. Reproduce with permission from the authors [220].

## 6.4.2 Materials, Specimens and Experimental Set up

Hot press and automated in-situ consolidated parts, as listed in Table 6-1, were cut to size (Figure 6-11) using a band saw (Startrite 430, UK). To improve edge quality, tape was fixed in the cutting line to prevent tearout or fibre tearing [213]. Then, the edge was ground using a deer-bench belt grinder (RJH AN150V3P, UK) to remove the remaining plastic fibrils. Three-dimensional scans were taken with a commercial triangulation-based system (Einscan 2X, CN) with a turntable base via its proprietary software Shining 3D (Figure 6-12). The software was also used to repair defects in the scans, such as holes. Whenever possible, three samples per processing parameter were used.

Table 6-1 Specimens and Process Parameters.

Process Parameters	Levels		
<b>Tool or Process</b>	Hot Press (HP)	No Force Controlled Automated consolidation with a 12 mm spherical tool	Forced Controlled Automated consolidation with a 12 mm spherical tool
<b>Pressure</b>	10 bar	7 bar	7 and 10 bar
<b>Temperature</b>	125 °C, 140 °C, 170 °C	125 °C and 140 °C	125 °C and 140 °C (Dome and Curved Shape)

\* A processing temperature of 170°C was discarded for automated in-situ consolidation because it fails to produce dome geometries as shown in Figure 6-6

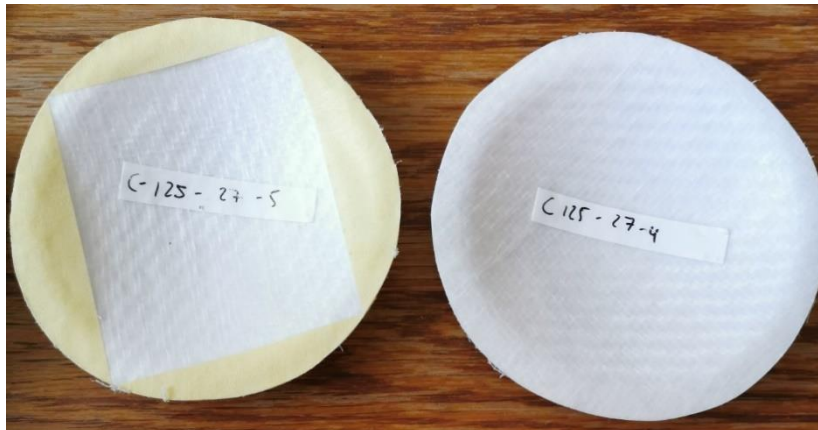


Figure 6-11 Automated in-situ consolidated domes after post processing

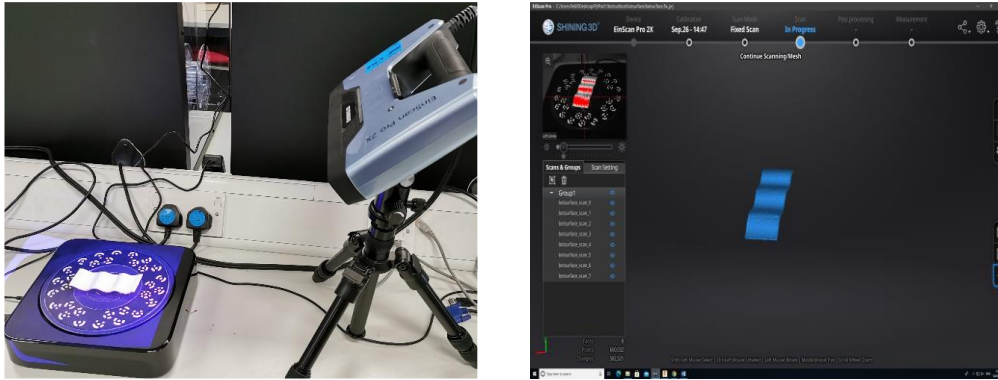


Figure 6-12 (Left) Triangulation-based scanner with turntable. (Right) Scanned sample of a curved shape self-reinforced polypropylene manufactured via automated in-situ consolidation in the software.

The 3D scanned parts were exported as stereolithography files (\*.stl) because they can be used in other software for reengineering or measure inspection purposes. In some cases, CAD software (Fusion 360, Autodesk) was used to repair scans that were not properly repaired by the 3D scanner software (Figure 6-13 a); however, some scans could not be repaired at all (Figure 6-13 b). In this case, the surface of some parts was highly reflective, which creates noise in the scanner's light patterns, making it impossible for the scanner to recognise the shape.



Figure 6-13. 3D scans: (a) repairable scan model. (b) Non-reparable scan model

Once the 3D scans were repaired, if needed, 3D measurement software [221-223] (PowerInspect 2021, Autodesk) was used to measure and compare the actual manufactured part with the true part. The true part is the CAD model, as shown in Figure 6-14 and Figure 6-15. The generic inspection procedure consists of [224]:



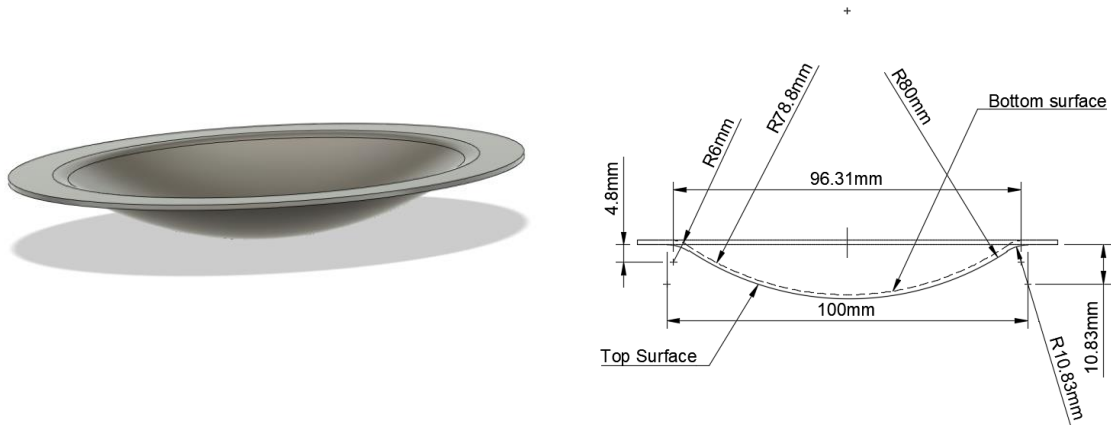


Figure 6-14 True CAD model of the dome: (Left) Isometric View; (Right) dimensional drawing showing the radius of the dome, radius of the fillet, and major diameter for both top and bottom surfaces.

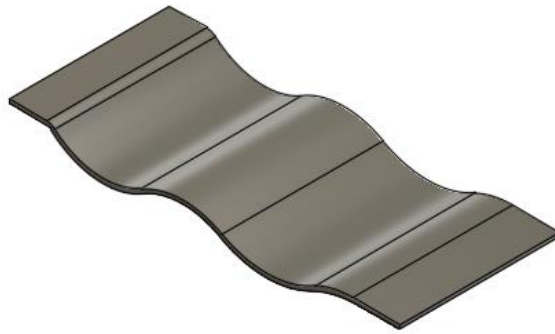


Figure 6-15 True CAD model of a curved shape laminate

1. To Upload the True CAD Part
2. To upload the scanned part based on a cloud of points from a \*.stl file.
3. To create geometry measurement features such as circles, planes, etc. For this project, the features selected were the dome's radius, the major diameter of the fillet tangent to the dome, and the radius of the fillet tangent to the dome. These geometric features are shown as a sphere and a toroid in Figure 6-16. Furthermore, a default tolerance of +/- 0.2mm was selected as the base measure for comparison between a true and a scanned measure.
4. To align the true CAD part with the scanned part using the tool alignment by points by selecting four points in the fillets at angles 0°, 90°, 180°, and 270° of the major diameter of the fillets. This is because the surfaces are concentric and therefore, the dimensions will not be the same.

5. To project the points of the scanned surface over the true surface (Gray Colour) to create colour-difference maps for qualitative visual assessment [221] as shown in Figure 6-17, Figure 6-20, and Figure 6-19. Green regions are an indication of an exact fit or in tolerance. Yellow or red points regions are out of tolerance with a positive discrepancy, while turquoise or blue regions are out of tolerance with a negative discrepancy. Purple regions indicate unprotected points because their tolerance is too far from the surface of the true CAD part. Furthermore, the general discrepancy is measured in absolute values resulting in mean and standard deviation (SD) values.

Regarding the use and requirements of the parts, out of tolerance indicates whether a part must be scrapped or used for its purposes. Defining pass tolerances is out of the scope of this project. The results intend to compare two manufacturing techniques, and therefore, only a comparison was required.

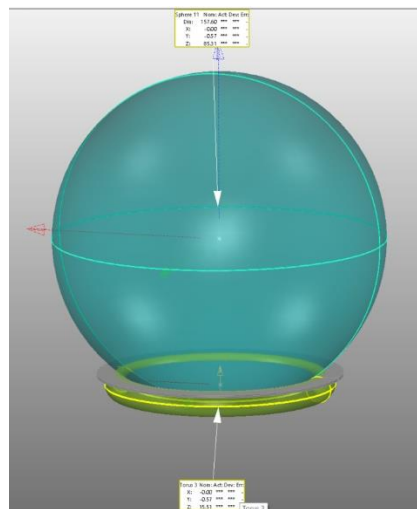


Figure 6-16 Geometrical features to be measured and compared in the true part. A sphere is the geometry that is used to measure either the diameter of the top and bottom surfaces (concentric diameters), while the toroid is the geometry that can be used to measure the radius of the fillet in the edge tangent to the dome.

## 6.4.3 Results and Discussions

### 6.4.3.1 Dome Geometry

Tolerance colour-difference maps are shown in Figure 6-17, Figure 6-19, and Figure 6-20 for hot pressed consolidate parts and automated in-situ consolidated parts. Figure 6-17 shows the results for hot press consolidated parts, which have the closest fit to the actual part as most of the cloud points are coloured in green which indicates an in-tolerance fit. This is expected because of the nature of the hot compaction method between two rigid moulds. Even though the hydraulic Hot Press does not possess a force control system, using two rigid moulds and a high force are enough to compress and conform the material to the shape while the matrix is melted. Similarly, because of the long cooling time under pressure, the shape keeps stable in the expected form until crystallisation occurs.

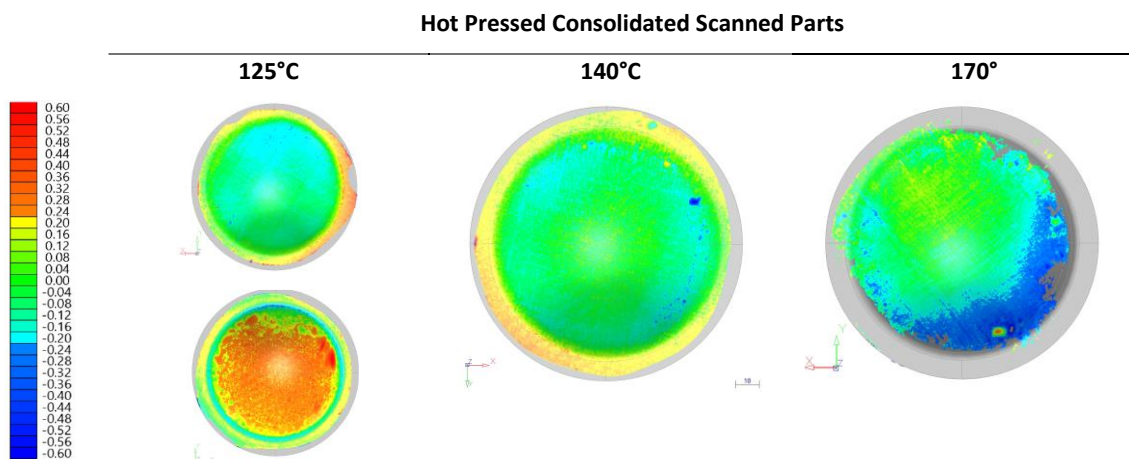


Figure 6-17 Tolerance colour-difference maps for hot pressed consolidated scanned parts against the true part. Yellow or red points regions are out of tolerance with a positive discrepancy, while turquoise or blue regions are out of tolerance with a negative discrepancy. Due to reflections, only the bottom surface of the sample processed at 125°C could be scanned. \*Tolerance units: mm.

For hot pressed consolidated parts, the only bottom surface that could be scanned was at 125°C due to its opaque surface. The scanner was not able to capture the bottom surface at 140°C and 170°C. This is because as the processing temperature increases, the proportion of melting of oriented molecules is higher. Polypropylene with elongated and aligned molecules are opaque, but when the elongation and alignment are lost, the colour is transparent, as shown in Figure 6-18. The edges of the dome for the samples manufactured at 125°C and 140°C are out of tolerance with a positive variation from the true part. The part manufactured at 170°C presents a high region within tolerance; however, a small fraction is

out of tolerance with a negative deviation. Instead of the sample having a geometry defect, this result is caused by the inability of the scanner in capturing the whole model. Therefore, the alignment and point projection over the true CAD part will present errors. The red regions in the bottom surface of the part manufactured at 125°C show they are out-of-tolerance with a positive deviation up to 0.6 mm. This indicates that either the part has a larger thickness or springback, which is very common for several manufacturing processes for fibre reinforced composites[225-227]. Table 4 in the appendix show the deviation measure for different geometric features for the Dome geometry. The sphere radius for the scanned part is higher than the nominal diameter of the true CAD part, which confirms there is springback after the manufacturing process.

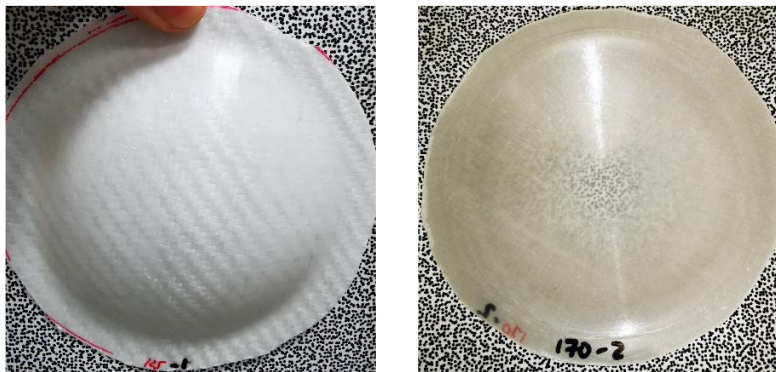


Figure 6-18. Manufactured parts via hot press consolidation at 125°C (Left) and 170°C (Right)

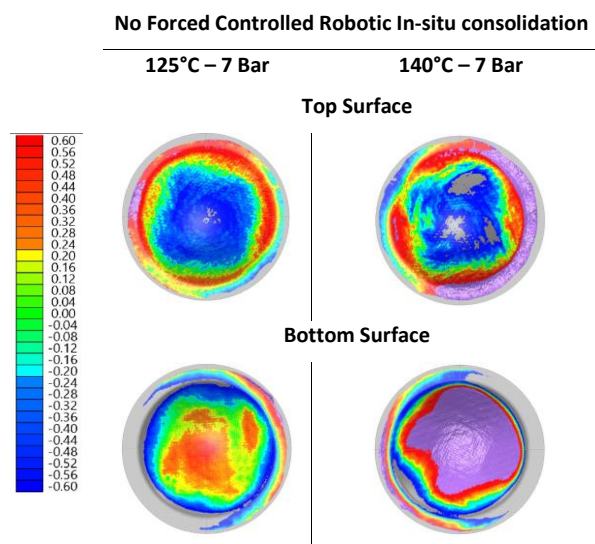


Figure 6-19 Tolerance colour-difference maps for Non-Force Controlled Automated in-situ consolidation scanned parts against the true part. Yellow or red points regions are out of tolerance with a positive discrepancy, while turquoise or blue regions are out of tolerance with a negative discrepancy. Purple regions indicate a discrepancy higher or lower than 0.6 or -0.6 mm respectively. Units: mm

Figure 6-19 and Figure 6-20 show the colour difference maps for parts manufactured via non-Force and Force Controlled Automated in-situ consolidation respectively. In these pictures both the scanned models and the true CAD parts are superposed to show the results of the alignment process when there are major discrepancies between them. For example, in Figure 6-19, the grey area corresponds to the true CAD part. If the scanned part were between the tolerance limits ( $\pm 0.6$  mm), the colour-difference map will be shown; however, as there are some regions out of the tolerance limits, these are shown as purple if those cloud points are above that surfaces (Top surface of the sample processed at  $140^{\circ}$ -7 bar in Figure 6-19) or grey if they are below of the surface being compared to (Bottom surface of the sample processed at  $140^{\circ}$ -7 bar in Figure 6-19).

The effect just mentioned before is greater in Figure 6-20, therefore, the last column indicates only the projected scanned model without superimposing the true CAD part for observation purposes of the colour-difference map. It is interesting to note that for both top and bottom surfaces at different processing temperatures, the colours create a rhomboid pattern. This pattern could be linked to the forming path of the tool as it is a spiral trajectory from the centre. The in-situ consolidation is a fast process based on pressure and shearing of a specific region of the material. While the vertical force that promotes pressure is constrained by the mould that supports the preform, the shearing force is only constrained by the surrounding material and the clamping force. We can assume the clamping force is constant and always acts as a reaction of the forming force. However, we cannot assume the same for the surrounding regions, which may experience a stretching process. In some cases, the patterns have a spiral pattern (Figure 6-20), confirming the shearing process promotes permanent stretching deformation.

Forced Controlled Robotic In-situ consolidation

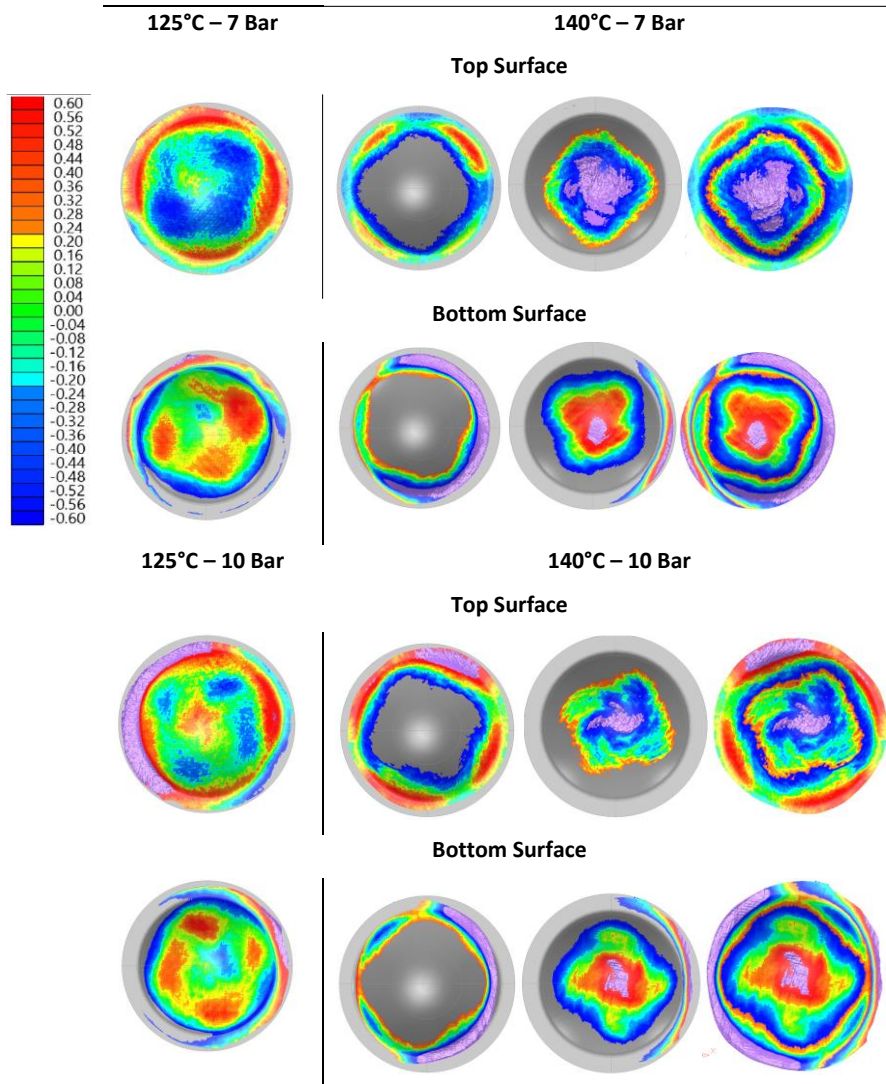


Figure 6-20 Tolerance colour-difference maps for Force Controlled Automated in-situ consolidation scanned parts against the true part. Yellow or red points regions are out of tolerance with a positive discrepancy, while turquoise or blue regions are out of tolerance with a negative discrepancy. Purple regions indicate a discrepancy higher or lower than 0.6 or -0.6 mm respectively. Scanned models at 140°C intersect the true model, and therefore, the whole colour-difference map cannot be observed. The last column indicates only the projected scanned model without superimposing the true CAD part. \*Tolerance units: mm

The colour-difference maps show that most of the surfaces are out-of-tolerance for both non-force and force-controlled systems present. From all the samples, the top surface always presents relatively better tolerances than the bottom surface. This could be explained by the fact that the top surface was always in contact with the hot mould that it conforms to the shape of the mould as much as possible while the bottom surface was in contact with the forming tool which by the shearing action promotes some dealignment from the true CAD part. For the bottom surfaces, there are purple regions indicating that the software could not

perform a projection and evaluation of the tolerance because their deviations are too high or low from the true part.

Table 6-2 shows the discrepancies in the measured deviation between scanned models and the true CAD part for a dome geometry, and Figure 6-21 and Figure 6-22 show a graphical representation of table 2 with the Tolerance performance and the Mean and Standard Deviation for Hot pressed and Automated in-situ Consolidated parts. Considering the average tolerance performance, the overall tolerance performance of hot-pressed manufactured parts is 30%-60% better than automated in-situ consolidated parts at different processing temperatures and pressures. However, the bottom surface of the Hot-Pressed sample at 125°C have a similar tolerance performance. It could be possible that the moulds from which the laminates were fabricated also have discrepancies from the true CAD part, but these were not measured after the mould was received. In addition, the moulds did not have proper location pins; therefore, a slight dealignment could have existed between the axis of moulds.

Similarly, considering the average tolerance performance for both top and bottom surfaces, automated in-situ consolidated parts manufactured at 125°C presents a better tolerance performance than 140°C for both samples with and without force control by 18% and 23% respectively. At 140°C, some crystals start to melt, promoting shrinkage in the external layer, leading to deviations in the geometrical accuracy. The difference of manufacturing samples with a force control system leads to an improvement of 4% and 9%. Finally, there is a slight improvement in the tolerance performance by increasing the forming pressure from 7 bar to 10 bar (2% at 125°C and 1% at 140°C)

It is important to highlight that all scanned parts for both manufacturing processes present maximum and minimum values of 0.8 and -0.8 mm respectively. It is possible that there are regions above these thresholds in the projection to the true CAD part, therefore it is not considered in the means, standard deviation, and tolerance performance. For the values that have been considered, both means and standard deviations for the top surface of Hot press manufactured parts are at least 50% lower than those of automated in-situ consolidated parts. Though the new proposed process can build a similar geometry, their current tolerances are not acceptable for industry standards.



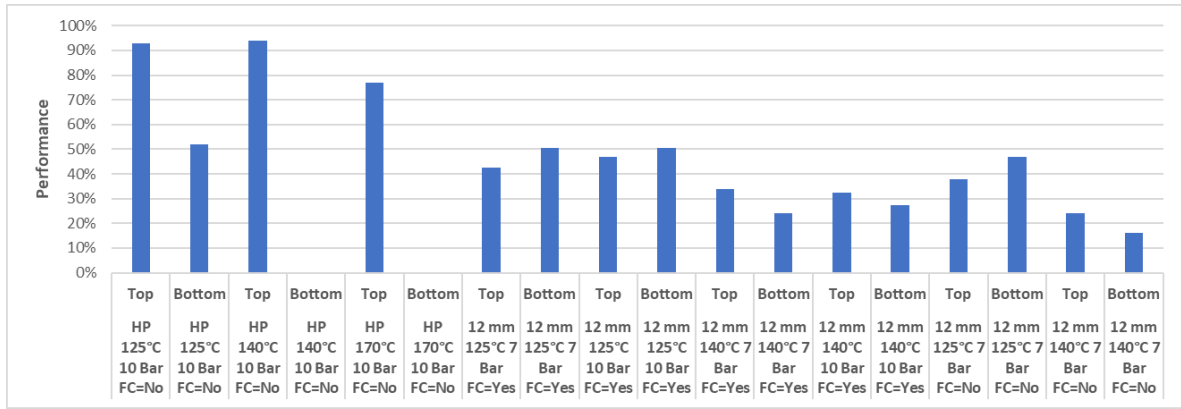


Figure 6-21 Tolerance performance of Scanned Models compared with the True Part for Dome Geometries.

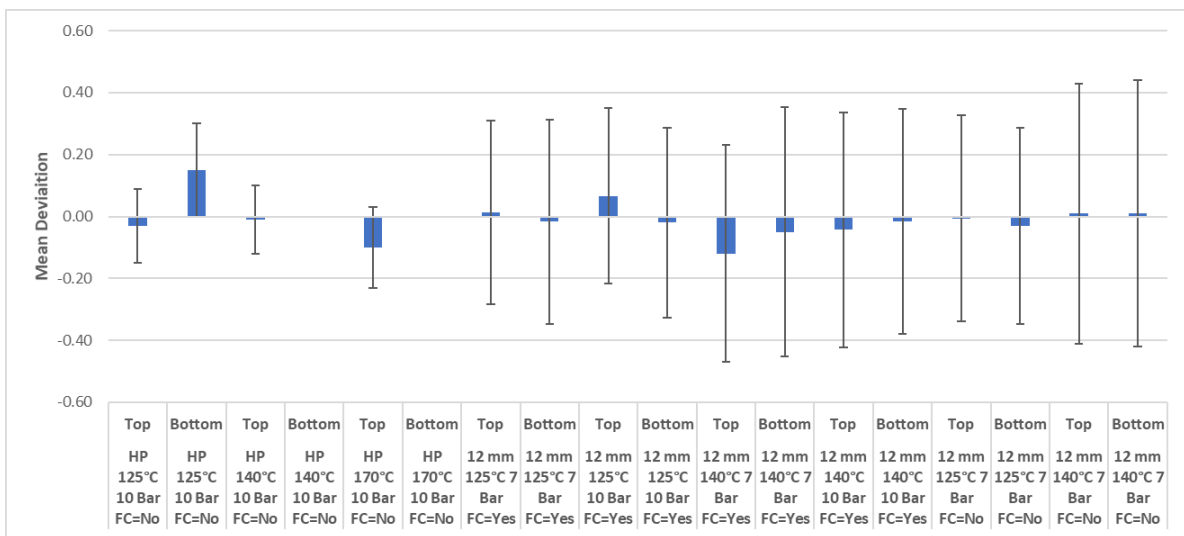


Figure 6-22 Mean and Standard deviation of Scanned Models compared with the True Part for Dome Geometries.



Table 6-2. Discrepancy of deviations between Scanned models from the True Part for Dome Geometries. (-) data could not be obtained due to parts being out of tolerance or difficult to scan.

Tool	°C	Pressure	Force Control	Scanned Surface	Mean	SD	Max Value	Min Value	Performance
HP	125	10 bar	No	Top	-0.03	0.12	0.8	-0.8	93%
HP	125	10 bar	No	Bottom	0.15	0.15	0.6	-0.8	52%
HP	140	10 bar	No	Top	-0.01	0.11	0.8	-0.8	94%
HP	140	10 bar	No	Bottom	-	-	-	-	-
HP	170	10 bar	No	Top	-0.1	0.13	0.8	-0.8	77%
HP	170	10 bar	No	Bottom	-	-	-	-	-
12 mm	125	7 bar	Yes	Top	0.01	0.30	0.8	-0.8	43%
12 mm	125	7 bar	Yes	Bottom	-0.02	0.33	0.8	-0.8	50%
12 mm	125	10 bar	Yes	Top	0.067	0.283	0.8	-0.8	47%
12 mm	125	10 bar	Yes	Bottom	-0.02	0.307	0.8	-0.8	50%
12 mm	140	7 bar	Yes	Top	-0.12	0.35	0.8	-0.8	34%
12 mm	140	7 bar	Yes	Bottom	-0.05	0.403	0.8	-0.8	24%
12 mm	140	10 bar	Yes	Top	-0.04	0.38	0.8	-0.8	32%
12 mm	140	10 bar	Yes	Bottom	-0.02	0.363	0.8	-0.8	27%
12 mm	125	7 bar	No	Top	-0.01	0.333	0.8	-0.8	38%
12 mm	125	7 bar	No	Bottom	-0.03	0.317	0.8	-0.8	47%
12 mm	140	7 bar	No	Top	0.01	0.42	0.8	-0.8	24%
12 mm	140	7 bar	No	Bottom	0.01	0.43	0.8	-0.8	16%

#### 6.4.3.2 Curved Sample

Figure 6-23 shows the colour-difference map for both the top and bottom surface of a curved laminate manufactured via Force Controlled Automated in-situ consolidation. Similarly, as in dome geometry, the surfaces fail to achieve a good tolerance. For the top surface, most regions are purple, indicating that the software was not able to project the cloud points over the surface, and therefore, no tolerance analysis can be performed. However, this could also be caused by the alignment of both the scanned and the true CAD model. The selected alignment in PowerInspect, *Point Cloud Picked-Points alignment* [228], requires that the scanned part cover at least three faces to align both models correctly. After selecting points in the surfaces, alignment usually failed by intersecting the models at 90 degrees or others. The alignment shown in Figure 6-23 is the best alignment that was achieved. Figure 6-24 shows the curved shape over a printed profile of the bottom surface. For the part to be in tolerance, the top or bottom surfaces should not be visible from the

angle the picture is taken. This confirms why the alignment is difficult to perform in the software. Similarly, voids in between the layers contribute to the high discrepancy between the true CAD part and the manufactured part.

*Table 6-3. The discrepancy of Scanned models with the True Part for a Curved Geometries*

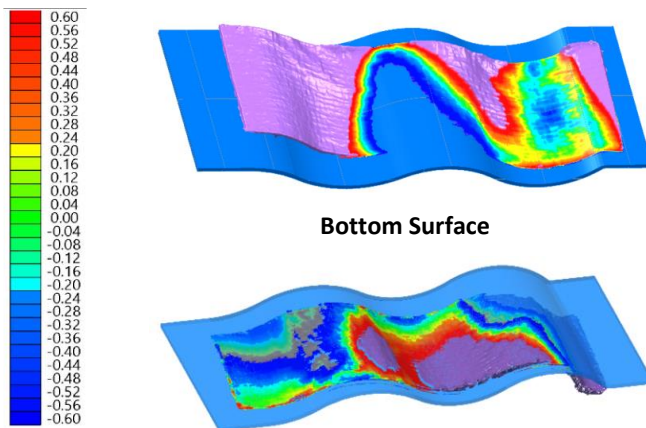
Tool	°C	Pressure	Force Control	Surface	Mean	SD	Max Value	Min Value	Performance
12-mm	140	7 bar	Yes	Top	0.014	0.364	0.8	-0.8	23%
12-mm	140	7 bar	Yes	Bottom	-0.01	0.416	0.8	-0.8	21%

Table 6-3 shows the means, standard deviation, maximum and minimum values, and the relative Tolerance performance of the scanned model from the true CAD part. Though very low mean values are achieved, the standard deviation is high, resulting in a poor tolerance performance of 23% for the top surface and 21% for the bottom surface. One of the main difficulties in manufacturing curved shape laminates was the forming strategy and suitable clamping. The forming path was perpendicular to the curved profile, but the laminate was only clamped parallel to the end lines of the profile. While forming the laminate, it was clear that material was being dragged in and out of position because of the lack of clamping. Future work should focus on redesigning a new mould that constrains the laminate in all directions considering drapability and excess material.

## Forced Controlled Robotic In-situ consolidation

140°C – 7 Bar

Top Surface



Bottom Surface

Figure 6-23 Tolerance inspection colour difference maps for Force Controlled Automated in-situ consolidation scanned parts. Yellow or red points regions are out of tolerance with a positive discrepancy, while turquoise or blue regions are out of tolerance with a negative discrepancy. Purple regions indicate a discrepancy higher or lower than 0.6 or -0.6 mm respectively. Scanned models at 140°C intersect the true model, and therefore, the whole colour-difference map cannot be observed. The last picture indicates only the projected scanned model without the true CAD part.



Figure 6-24 Right: Side view picture of the curved shape laminate with a printed profile as a reference for qualitative evaluation. Left: Visible void in between layers in the laminate.

There are several challenges in the scanning and measurement process that must be overcome. For parts with reflective or transparent surfaces, it is recommended to use a scan spray that deposits a fine layer of powder that triangulation-based scanners can easily detect [229-232]. It is important to mention that the calculation of mean and standard deviation only considers cloud points in a tolerance of +/- 0.8mm. This means all the purple regions in the figure are not considered for this calculation. For the points that are considered, there tolerance performance of the manufactured part is not acceptable in terms of accuracy. Since one of the reasons for this poor performance was the difficulty of alignment, different alignment strategies [233] should be studied to improve this result. Another difficulty found in the three-dimensional measuring processing was the post-processing cutting of the

laminate to eliminate excess materials. This process was entirely manual and therefore led to a great deal of error in the boundaries. That is the reason why none of the boundaries were considered in the analysis. It is recommended to design the parts, moulds, and preforms to be suitable for post-processing steps. Furthermore, it is possible that the moulds used in both the Hot press and in the Automated in-situ consolidation process may have discrepancies between the true CAD part. Therefore, a better estimate will be to scan the manufactured moulds to ensure they are in tolerance with the true CAD part or use this scan as the new true part in the inspection procedure. These results also validate the use of triangle-based scanner devices for quality control in parts for low volume applications [234]. Even though other scanners could have been used, such as laser scanners, white light scanners have demonstrated better performance, and faster scanner times [221, 235, 236].

#### **6.4.4 Conclusions**

3D scanning has been successfully used as a control quality methodology for the geometrical accuracy of both hot pressed and automated in-situ consolidated parts. Parts manufactured via Hot pressing present better tolerance performance from the true CAD part than automated in-situ consolidated parts with and without a force control system. However, they present spring back, which should be considered in the design stage of the part. For automated in-situ consolidated parts, a processing temperature of 125°C leads to better tolerance performance since it does not promote shrinkage in the material. Furthermore, using a force control system improves tolerance performance; however, there is little benefit in increasing the forming pressure. Different solutions to overcome scanning and manufacturing challenges have also been discussed.

### **6.5 Compressive Behaviour of Self-Reinforced Polypropylene Domes Between Two Platens**

This section aims to evaluate the deformation behaviour and energy absorption capabilities of a self-reinforced polypropylene composite dome manufactured with the new automated in-situ consolidation process and compare it with Hot Press specimens. To the

author's knowledge, there is no study of geodesical domes and their energy absorption capabilities under a controlled compression.

### 6.5.1 Introduction

The good low velocity impact resistance of self-reinforced polypropylene composites [28, 30, 32] makes them attractive for safety structures such as vehicle bumpers, armour equipment, etc. Understanding the physical responses of composite shell structures to compressive loads is important as it is related to the energy absorption capabilities, and therefore, to evaluate its crashworthiness. Crashworthiness is a safety definition referring to the ability of a structure to absorb an impact while keeping the occupants survivable. Penetration resistance refers to the ability to stop a projectile. Crashworthy structures must be designed to absorb energy in a controlled manner through known failure mechanisms that allow a gradual decay of the load profile during absorption.

Specific energy absorption is defined as the energy absorbed per unit mass of a material according to Equation 6-1, where  $\sigma$  is the mean crush stress, and  $\rho$  is the density of the material.

$$SEA = \frac{\sigma}{\rho} \quad \text{Equation 6-1}$$

Similarly, it can also be calculated from a load-displacement curved obtained from a compression test. The total energy is the area under the load-displacement profile:

$$W = \int_{S_i}^{S_b} P dS = \bar{P}(S_b - S_i) \quad \text{Equation 6-2}$$

Where  $W$  is the total energy absorbed,  $P$  is the load,  $\bar{P}$  is the average load between the compression distance  $S_b - S_i$  as indicated in Figure 6-25. Therefore, the specific energy absorption is defined as

$$E_s = \frac{W}{m} = \frac{\bar{P}(S_b - S_i)}{\rho V} = \frac{\bar{P}(S_b - S_i)}{\rho AL} = \frac{\bar{P}}{\rho A} = \frac{\bar{\sigma}}{\rho} \quad \text{Equation 6-3}$$

Where  $V$  is the volume of the material,  $A$  is the crosse sectional area,  $L = (S_b - S_i)$  is the length of the crushed portion,  $\rho$  is the density of the material, and  $\bar{\sigma}$  is the average crush stress.

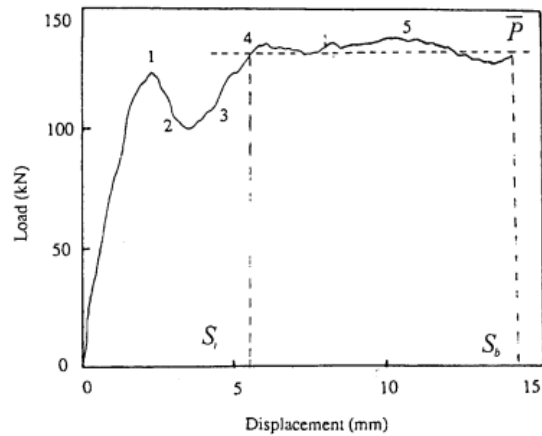


Figure 6-25 Typical load-displacement curve for a quasi-static compression test. Reproduce with permission from the authors [237].

### 6.5.2 Methodology

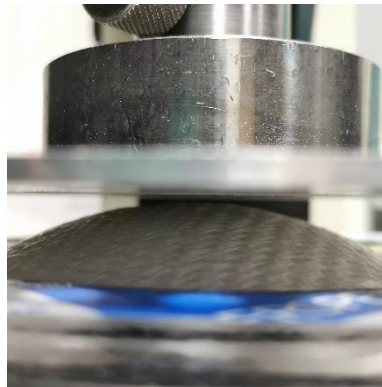


Figure 6-26. Experimental Set up for compression tests

Compression tests were performed in an adapted universal testing Machine (Tinius Olsen™) equipped with a 5KN load cell between two flat platens. The bottom platen had a fixture to fix in-plane translations of the dome as shown in Figure 6-26. For each test, the top platen moved at a constant speed of 2.5mm/min to simulate a quasi-static condition in the whole regime. The top platen stroke is 9 mm to avoid collisions with the bottom platen fixture. From these tests, a load displacement profile was obtained. Three tests were performed for each processing parameter as described in Table 6-4. The deformation pattern and possible damage were closely observed during testing.

Table 6-4 Manufacturing Processing Parameters

Manufacturing Technique	Force Control	Pressure	Temperature
AIC	No	7 bar	125 °C
AIC	No	7 bar	140 °C
AIC	Yes	7 bar	125 °C
AIC	Yes	10 bar	125 °C
AIC	Yes	7 bar	140 °C
AIC	Yes	10 bar	140 °C
HP	Yes	10 bar	125 °C
HP	Yes	10 bar	140 °C
HP	Yes	10 bar	170 °C

\* AIC stands for automated in-situ consolidation, HP stands for Hot Press

### 6.5.3 Results and Discussion

The load-displacement profiles for a dome compressed under two platens are shown in Figure 6-27 for several specimens. The profile presents different stages. As soon as the top platen touches and compresses the apex of the dome ( $r=0$ ), there is a relatively linear region in which the loading carrying capacity increases. After some point, the slope of the trend changes. This indicates the onset of initial buckling of the apex of the dome in which its shape inverts. This behaviour is similar to domes of isotropic and non-isotropic materials such as metals and other types of composites [238-240]. This buckling mechanism is called rolling-plastic hinge, which is moved at the contact of the plate outwards from the dome axis to the outer edge. Even after buckling, the dome can still sustain more loads in a stable process without a snap-through phenomenon. Finally, there is another change in the slope after which the load increases because as the material buckles, the apex of the dome touches the bottom platen promoting a reaction force that is added to the system. The deformation states of a typical dome are illustrated in Figure 6-28.

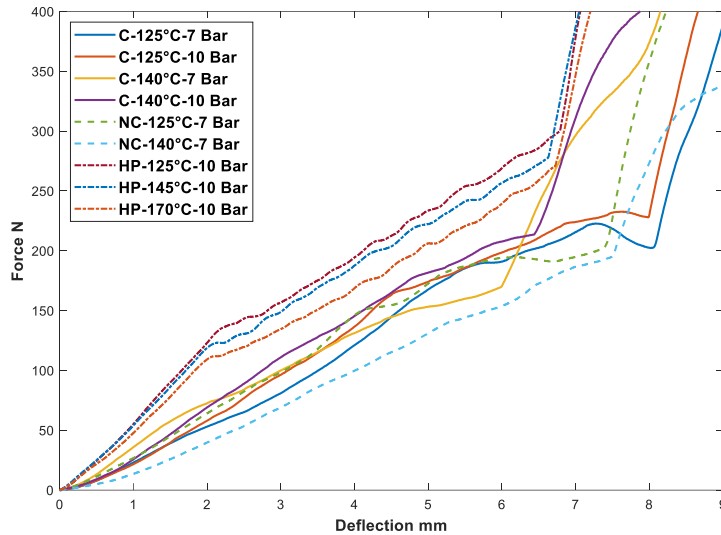


Figure 6-27 Load-Displacement compression profile of domes like structures. Legends: “C” stands for force controlled, “NC” stands for no-force controlled, “HP” stands for hot press.

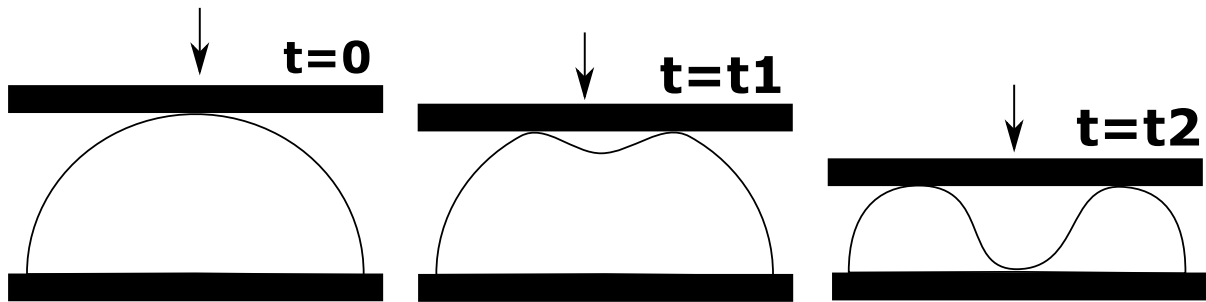


Figure 6-28 Dome deformation while being compressed.

The Hot Press specimens presents the higher load carrying capability and the higher stiffness represented as the linear region at the beginning of the test. The initial buckling for Hot Press specimens starts at a similar deformation level than automated in-situ consolidated parts. As the temperature increases, the stiffness of hot press specimens decreases due to the molecular relaxation of the molecules, which reduces the mechanical properties of the specimens. A visual effect of this molecular relaxation is the apparent loss of anisotropy related to the loss of colour in oriented tapes in Figure 6-31. The same behaviour is observed in specimens under no force control in automated in-situ consolidation; however, it is unclear for specimens under force control if the temperature has an effect. The only difference is when the apex of the dome touches the bottom platen. Automated in-situ consolidated specimens manufactured at a processing temperature of 125°C presents a higher carrying capability after buckling as the apex of the dome touches the bottom platen at a longer stroke than samples manufactured at 140°C.



Figure 6-29 show the energy absorbed in the quasi-static compression test for the different types of domes. As expected from the load-displacement profiles, hot pressed specimens present the higher energy absorbed (38% to 48% higher), and its value decreases with the temperature under which they are processed. There is an apparent increment in the energy absorption capability of automated in-situ consolidated laminates when the forming pressure increases. Similarly, there is also an improvement in the energy absorbed in automated in-situ consolidated laminates when a force control close-loop system is used. Finally, as the processing temperature increases, the energy absorbed increases. This combination of higher temperature and higher consolidation pressure help to improve adhesion and molecular diffusion to increase the mechanical properties of the laminate and close voids.

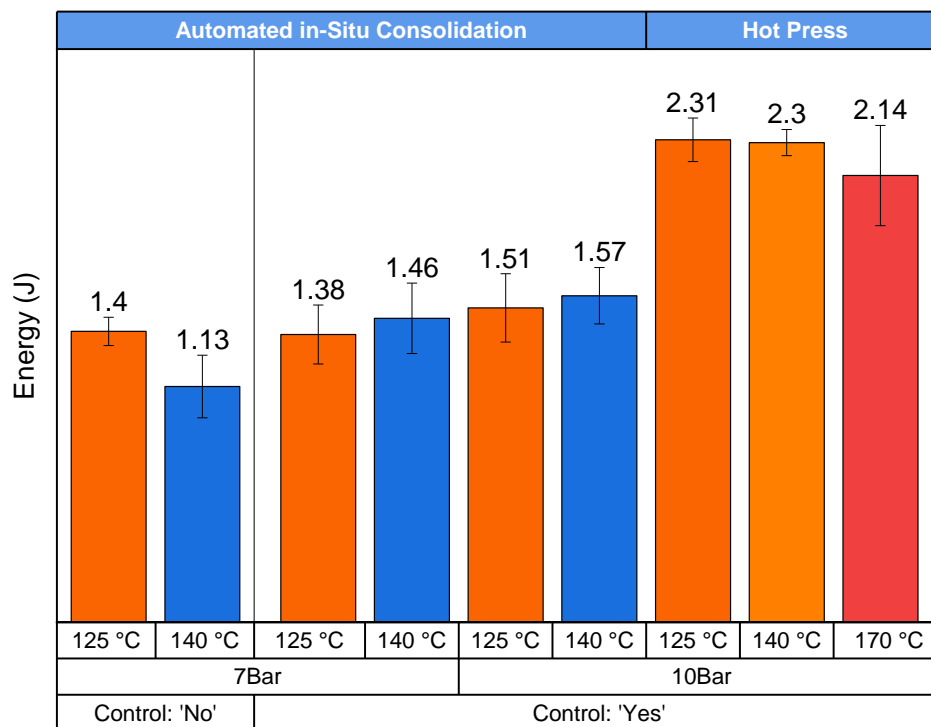


Figure 6-29 Energy Absorbed by the samples during a quasi-static crash test

Figure 6-30 shows the deformed specimens for the different samples tested in this study. The deformed pattern for the automated in-situ consolidated laminates with a target temperature of 125°C is a diagonal cross in the centre in the apex of the dome. Laminates consolidated at a temperature of 140°C presents a spiral pattern in the apex of the dome. On the other hand, Hot Press is snap-down, which means part of the structure inverts. This is

classical instability of geodesical domes under force-displacement controlled loading conditions and can be caused by several factors such as geometry, imperfections, boundary conditions, etc. [241].

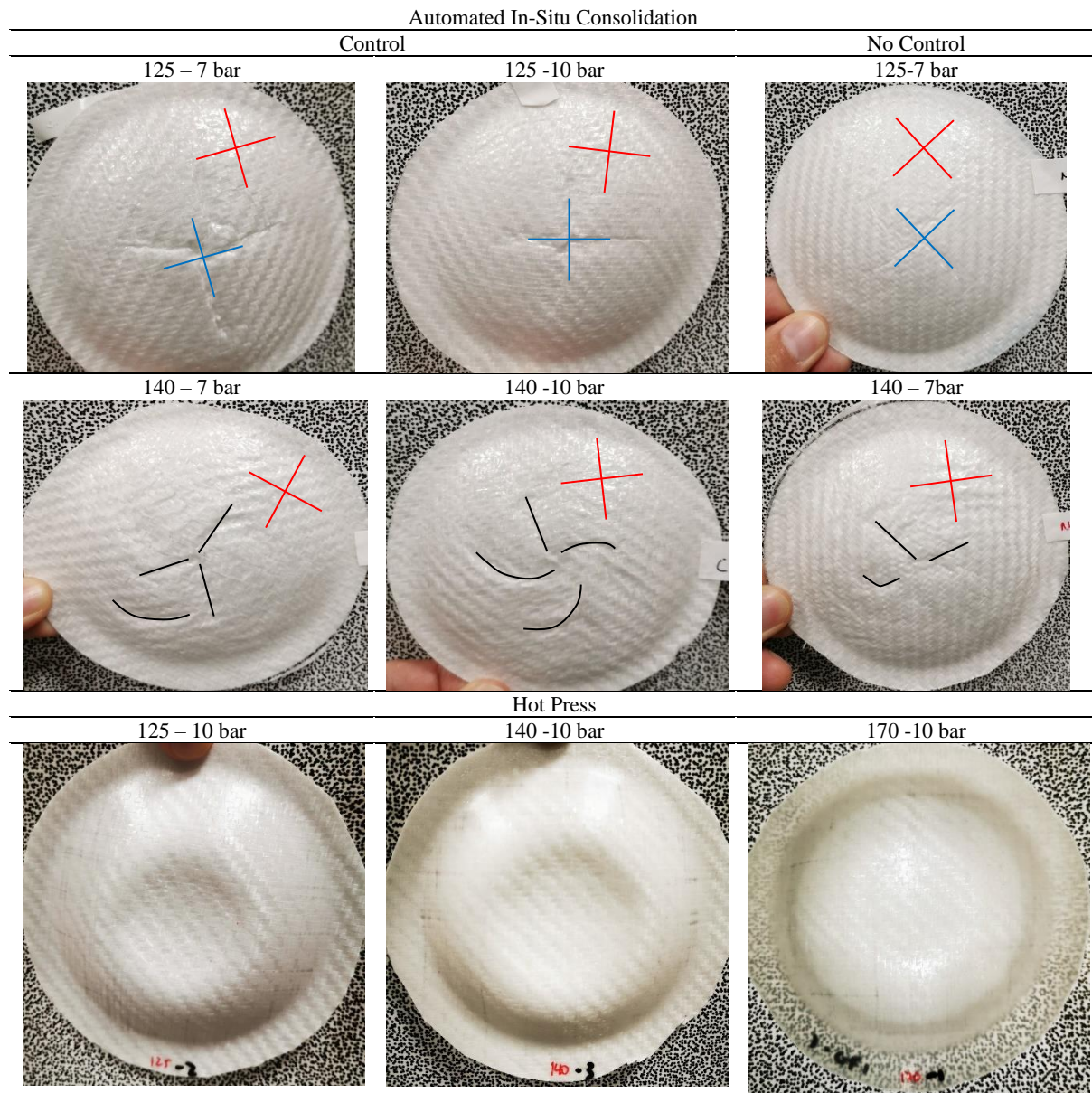


Figure 6-30 Deformed shapes for different dome structures made with different manufacturing techniques and/or processing parameters. Blue and black lines represent the direction of the buckling while the red lines represent the direction of the fabric structure.

The difference in failure modes between the hot press and automated in-situ consolidation samples can be explained by their internal morphologies, as shown in Figure 6-31. Micrographs of the cross section are used to evaluate the level of consolidation of the composite materials qualitatively and to recognize different constituents or phases in their morphology. For Automated in-situ consolidation specimens, their cross section indicates a

low level of consolidation because of its high-level voids, shown as bright regions, especially for the sample manufacture at 140°C at 7 bar. Also, the fibre alignment presents high levels of waviness, which is a source of instabilities such as buckling. In particular, both voids and waviness in the fibre alignment are responsible for the different failure modes in automated in-situ consolidation parts. On the opposite, hot press parts present less internal waviness and a high level of consolidation, which results in a smaller thickness. As mentioned before, the change of colour in the hot press specimen manufactured at 170°C is due to the loss of molecular orientation, making the whole structure more isotropic.

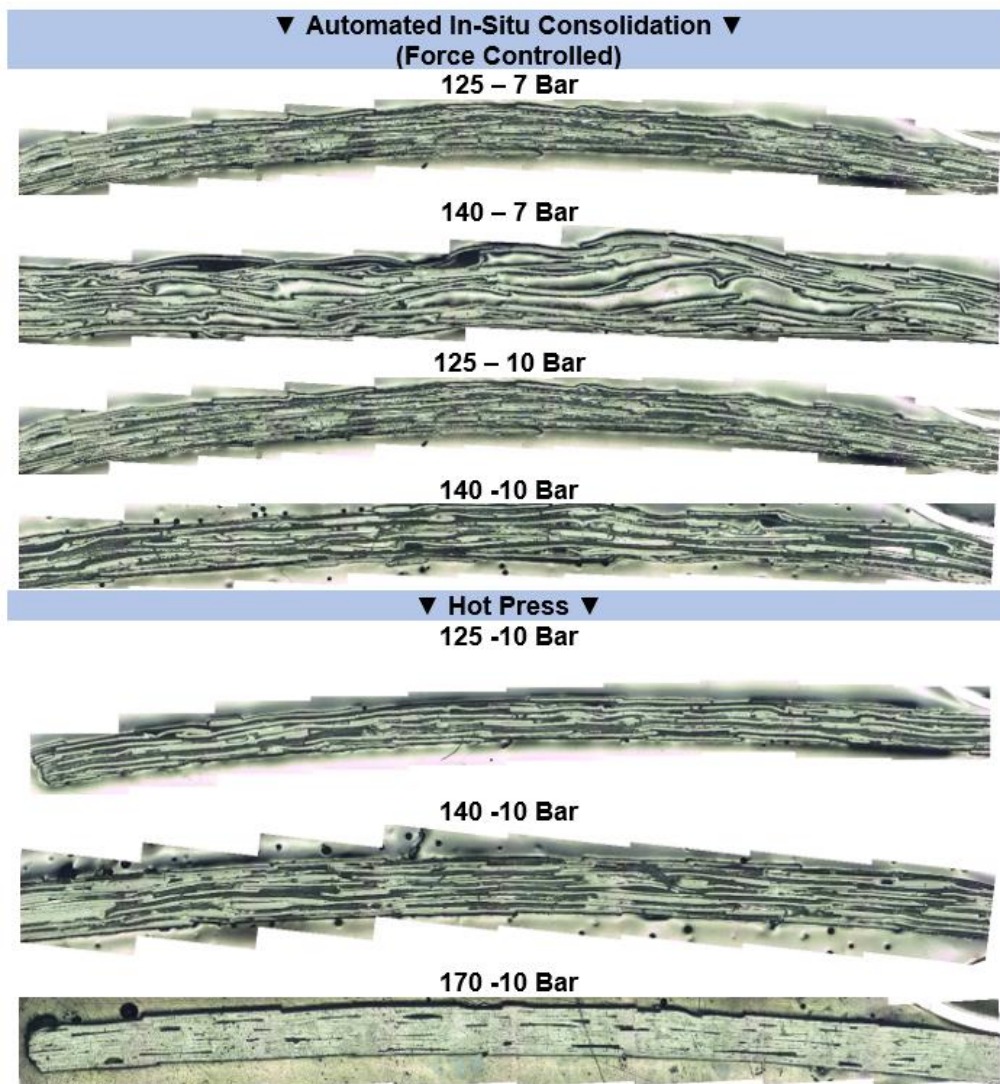


Figure 6-31. Microscope photographs of the cross section of the apex of a dome for both hot press and automated in-situ consolidation specimens at different processing temperatures and pressure.

#### **6.5.4 Conclusions**

The energy absorption capabilities of dome geometries manufactured via Hot Press and automated in-situ consolidation of self-reinforced polypropylene composites have been evaluated using a controlled quasi-static compression test. All samples have ductile behaviour with buckling mechanism called rolling-plastic hinge which moves at the contact of the plate outwards from the dome axis to the outer edge. Though the automated in-situ consolidation can produce three-dimensional geometries, its level of consolidation cannot compete with hot press specimens in terms of energy absorption ability. In addition, due to the lack of proper bonding between layers and the high level of voids, the alignment of the tapes presents a relative waviness which is the source of instabilities such as buckling. On the opposite hand, hot press specimens present good levels of consolidation and fibre alignment, which results in a better energy absorption capability. Nevertheless, more research is needed to quantitatively evaluate the damage tolerance of automated in-situ consolidated parts as the relative waviness can also represent a crack propagation stop mechanism.

## 7 Conclusions and future work

This thesis has documented the development of a new flexible and low-cost automated process for producing two-dimensional and three-dimensional self-reinforced polypropylene composites; inspired by advanced composite manufacturing techniques such as automated-tape-placement. While almost all methods to produce self-reinforced composites are based on closed moulds, this development is the first attempt to use a flexible approach in which the top mould is replaced by a small hot tool. The tool can in-situ consolidate a stack of self-reinforced composite fabrics using programmed forming paths and ensure a precise temperature control that prevents the molecular relaxation of the reinforcement phase. This means that the cost of the mould for low volume applications can be reduce by almost a half by replacing it with a relatively inexpensive forming tool.

The development stages of the new automated manufacturing process have been detailed in chapter 3. The machine consists of a gantry structure integrating open-source hardware, a piezoelectric force sensor, temperature sensors with PID temperature controllers, and control software. The control software provides several functions, including hardware communication, machine motion control with a g-code programming language, graphical user interface, monitoring, recording, online processing of force signals, and a software-PID force closed-loop actuation. The PID force closed-loop system proved to be a necessary development to achieve constant levels of compression during the forming operation without the need of an operator being involve. Furthermore, the system was demonstrated to be more energy-efficient than the benchmark process hot press with a 28% reduction in energy consumption. This offers the advantage of more cost reductions, and a more sustainable and flexible manufacturing processes, especially if the other part of the mould is replaced by another small hot tool as explained below in Future work.

The forming mechanism of the automated in-situ consolidation process is based on the autohesion (or bonding) of two polymer surfaces. Autohesion is based on the reptation model of molecular motion in which polymer chains interdiffusion across a polymer interface (two polymer surfaces in contact). Interdiffusion depends on pressure, temperature, and the contact time that the surfaces are in contact, and complete interdiffusion will occur when the interface is no longer distinguishable. Furthermore, a theoretical model that predicts the

temperature distribution through the thickness of the material was developed and validated with experimental data. The automated in-situ consolidation process falls into a conduction heat transfer model creating a temperature gradient through the thickness of the material with temperatures high enough to promote bonding in the fabric interfaces. The model was able to predict the required forming speed (90 mm/s) for the automated in-situ consolidation process which can save considerable experimentation time for further developments.

Two-dimensional laminates of self-reinforced polypropylene composites based on bicomponent tapes were produced using a benchmark processing technique (Hot Press) and the proposed low-cost automated in-situ consolidation process. The rationale behind the selection of fixed processing parameters was explained through experimentation. This helped to reduce the number of variables that were studied to understand their influence over the final properties of the laminates. The main findings can be summarised as follows:

- The manufacturing of two-dimensional laminates via Hot press processing must be under pressure to prevent shrinkage in a flat laminate while it solidifies
- Peel tests have been proved to be an effective methodology to determine the effects of several processing parameters.
- Warpage will be expected when laminates are produced with the automated in-situ consolidation process. Surprisingly, hot press specimens also had some level of warpage.
- Implementing a force closed-loop system to in-situ consolidate self-reinforced polypropylene composites is essential to reduce the number of voids in the material.
- The effect of the processing temperature is more noticeable on Hot press specimens than in automated in-situ consolidation. However, this is because of the high number of processing variables that are involved in the process except that as expected, a higher pressure leads to a better consolidation, and that higher temperatures promote excessive warpage on the top layers of the material.
- There is no clear influence of the main processing parameters (pressure and temperature) in the crystallisation process.
- Evidence suggests that the best forming parameters for two-dimensional laminates are to use, a “flat tool”, a forming tool at 140°C, a forming speed of 90 mm/min, and



a consolidation pressure of 7 bar. This combination of parameters has resulted in the best mechanical properties such as interlaminar strength, and tensile strength.

The construction of three-dimensional laminates via automated in-situ consolidation was achieved by combining digital fabrication techniques such as CAE and CAM. This allows a fast transition from design to manufacturing in which hand labour is reduced to a minimum. The operator task is reduced to cut and place the preform layers in position over the bottom mould and starting and disabling the machine, while the engineer work is to program the automated toolpath according to the design of the part. It was found that the closed-loop force system shows improved manufacturing results compared with a non-controlled force system and that the forming temperature window for three dimensional laminates of self-reinforced polypropylene is around 125°C and 140°C. Furthermore, the toolpath planning depends on the geometry of the material, however, the beginning of the toolpath should always start from the centre to the boundaries so the tool can conform the fabric against the bottom mould. Similarly, digital technologies are also used to validate and approve components as tolerances can be measured quickly and are reliable. The resultant laminates were compared against those of a benchmark process: hot press. It was found that the overall tolerance performance of hot-pressed manufactured parts is 30%-60% better than automated in-situ consolidated parts at different processing temperatures and pressures. Furthermore, automated in-situ consolidated specimens present poor consolidation quality levels, and lower energy absorption capability for dome geometries than Hot press specimens. However, this only represents the performance under a single measured property and more investigation is needed to quantify other properties.

It was demonstrated that the proposed low-cost automated in-situ consolidation process can produce two-dimensional and three-dimensional laminates using self-reinforced polypropylene composites. Under the right processing parameters, some properties can be compared with hot press specimens. However, tight industrial geometrical tolerances may limit the use of this process for immediate application. This is not necessarily a bad result as it is the first attempt to perform a three-dimensional automated in-situ consolidation process, and therefore, more research is needed to demonstrate its real potential as expansions of this process can offer increased flexibility and cost reductions.

## **7.1 Future Work**

### **7.1.1 Mould Alignment**

Designing and building a machine is not exempt from imperfections, especially if components are not designed with tight engineering tolerances. During the assembly of the machine, some components may have had clearance fits, while other had interference fits, leading to geometrical deviations. Moreover, the machine was supported by a flexible wood workbench which may have increased the deviations between the actual design and the real machine. The geometrical deviation implies a misalignment between the working coordinate system of the machine with the mould. The first approach to overcome this manufacturing error is to use an industrial build bed plate that supports the rest of the machine's structure.

Similarly, a finite element modelling should be used to ensure that machine deformations are negligible when the machine is working. Another approach to overcome machine dealignment is to use an inspection measuring software such as Power Inspect. This software can use data from a coordinate measuring probe or a 3D scanner to modify the original programming and, therefore, to adjust the mould imperfections.

### **7.1.2 Force Sensor**

One of the most difficult challenges in this project was to read reliable and accurate force values under temperature influence. Piezoelectric force sensors are highly influenced by temperature fluctuations leading to temperature errors and unpredictable fluctuations [162-164]. Though this was overcome using an online compensation algorithm in the control software, different approaches to reduce temperature influence over the force sensor should be adopted. For example, though strain-gauge force sensors are also affected by temperature, they could be manufactured with temperature compensated strain-gauges increasing the operating temperature range of the sensor. Similarly, better insulation and cooling devices should be investigated to avoid heat transfer from the mould or forming tool to the load cell.



### **7.1.3 Motion Controller**

As mentioned, this is the first time that a force closed-loop system was developed using a low-cost open-source motion controller and LabVIEW. One of the main difficulties found in the process was related to the communication protocol between the motion controller and the software. The buffer of the motion controller cannot support either very long files or have real-time communication. In theory, Grbl calculates in advance trajectories to avoid filling the buffer. However, if a long file is sent, there is a high probability that some commands are not processed. Furthermore, it was found by trial and error that the shortest time between commands is approximately 0.5 seconds. Below this time, the motion controller cannot process any command because the buffer is saturated, limiting the efficiency and setting it away from a real-time closed-loop system.

One way to overcome this limitation is by implementing different communication protocols via Ethernet [242]. Ethernet is the most common industrial communication platform for real-time protocols such as EtherCAT, Profinet, ModBus, etc. They are used in industrial applications such as robotics, high-performance PLC systems, motor control systems and inputs and Output systems. One advantage of ethernet communication is that there are large, mature, and well-proven hardware and software solutions, and their prices have been more accessible as the development progresses. For example, though relying on hardware for motion controllers is common, a computer and software can replace the hardware, simplifying development and reducing costs [243]. Adopting real-time communication will benefit both force and motion closed-loop systems leading to more reliable processing.

### **7.1.4 Ultrasonic Heating**

Ultrasonic heating is mostly used for welding processes in thermoplastic applications [46]. Heat is generated by the internal friction created by the vibration of a horn at high frequencies (10s of thousands of hertz), which can reduce the amount of energy used to in-situ consolidate thermoplastic composites [38] because no external elements such as tooling

are being heated. Using ultrasonic welding to consolidate the system may be possible by using a lower power system than that available to us on our limited budget. This could be a fruitful avenue for further research.

### **7.1.5 Machine Learning**

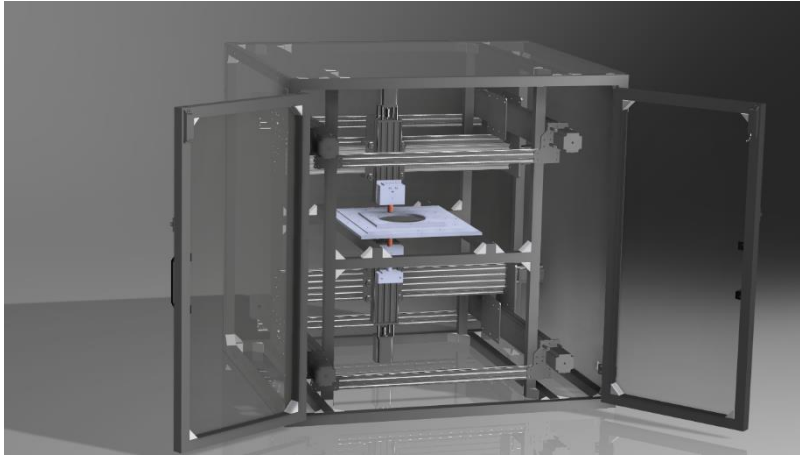
Machine learning is a promising tool for current and future manufacturing challenges[244] as it could transform data from sensors or other devices into valuable information for smart manufacturing [245]. The data acquisition systems developed during this project create vast quantities of force and temperature profiles. However, the implementation of advanced data analytics or advanced mathematical models was out of this project's scope. Investigation of the adoption of machine learning algorithms may facilitate and speed the learning stage of the influence of processing parameters over the final properties. Moreover, machine learning algorithms could complement the physical science of the forming mechanisms to improve the performance of the system by applying online decision-making tools which could modify path planning or predict springback.

### **7.1.6 Mould-Free Composites**

In this project, a double-point automated in-situ consolidation machine was designed and built (Figure 7-1) to produce structural composites without the need of tooling as the hot mould was replaced by a small tool. However, covid-19 imposed new time constraints to the project as access to the laboratories and facilities was restricted, resulting in to testing time for this prototype. A brief explanation of the future work is described below.

In the past few years, rapid prototyping techniques such as additive manufacturing or incremental sheet forming have attracted special attention due to the possibility to eliminate the production of moulds for different materials such as polymers and metals. However, the research field is still in its early stages, thus resulting in products with defects and poor properties such as high void content and poor interfacial strength between fibres and polymers. It is envisioned that this system can reduce time and costs, especially for low volume productions. Manufacturing time will be reduced as the time to cool down the matrix does not depend on the cooling down the mould. Costs will be reduced as there is no need to

manufacture two pieces of moulds, and there is no energy required to heat a mould. Similarly, it could lead to the exploration of new flexible routes for outside-factory production, and it can be built with low-cost materials and low-cost automation products. Furthermore, the system can be upgraded to add more degrees of freedom to increase design flexibility.



*Figure 7-1. Automated Double-Point forming of Fibre reinforced composites.*

## 8 References

- [1] P. C. Hiemenz, *Polymer chemistry*, Second edition. ed. Boca Raton, FL: Boca Raton, FL : CRC/Taylor & Francis, 2007, 2007.
- [2] H. Dodiuk and S. H. Goodman, *Handbook of thermoset plastics*, 3rd ed. ed. San Diego: San Diego : William Andrew, 2014, 2014.
- [3] M. C. Polymers. "Amorphous vs. Crystalline Polymers." Mallard Creek Polymers. <https://www.mcpolymers.com/library/amorphous-vs-crystalline-polymers> (accessed 2021).
- [4] C. C. Ibeh, *Thermoplastic materials : properties, manufacturing methods, and applications*. Boca Raton, Florida: Boca Raton, Florida : CRC Press, 2011, 2011.
- [5] C. De Rosa, *Crystals and crystallinity in polymers : diffraction analysis of ordered and disordered crystals*. Hoboken, New Jersey: Hoboken, New Jersey : Wiley, 2014, 2014.
- [6] U. W. Gedde, *Polymer Physics*. Springer, Dordrecht, 2020.
- [7] B. T. Astrom, "Thermoplastic Composites Manufacturing," in *Composites*, vol. 21: ASM International, 2001.
- [8] B. T. Åström, *Manufacturing of polymer composites*. London: London : Chapman & Hall, 2002, 2002.
- [9] B. T. Åström, "Introduction to Manufacturing of Polymer-Matrix Composites," in *Composites*, vol. 21: ASM International, 2001, pp. 421-422.
- [10] P. K. Mallick, *Fiber-reinforced composites : materials, manufacturing, and design*, 3rd ed., [expanded and rev. ed.]. ed. Boca Raton, FL: Taylor & Francis, 2008.
- [11] E. J. Barbero, *Introduction to composite materials design*, Second edition. ed. Boca Raton, Florida ; London, [England] ; New York: Boca Raton, Florida ; London, England ; New York : CRC Press, 2011, 2011.
- [12] S. L. Donalson and D. B. Miracle, "Introduction to Composites," in *Composites*, vol. 21: ASM International, 2001.
- [13] M. American Society for, "ASM handbooks online [electronic resource]. Vol. 21, Composites," in *Composites*, ed. Metals Park, Ohio: Metals Park, Ohio : American Society for Metals, 2001, 2001.
- [14] L. Mascia, *Thermoplastics, materials engineering*. Applied Science Publishers, 1982.
- [15] (2015). *QUADRENNIAL TECHNOLOGY REVIEW AN ASSESSMENT OF ENERGY TECHNOLOGIES AND RESEARCH OPPORTUNITIES*. [Online] Available: [https://www.energy.gov/sites/prod/files/2015/09/f26/Quadrennial-Technology-Review-2015\\_0.pdf](https://www.energy.gov/sites/prod/files/2015/09/f26/Quadrennial-Technology-Review-2015_0.pdf)
- [16] B. Alcock, N. O. Cabrera, N. M. Barkoula, J. Loos, and T. Peijs, "The mechanical properties of unidirectional all-polypropylene composites," *Composites.*, vol. 37, no. 5, pp. 716-726, 2006, doi: 10.1016/j.compositesa.2005.07.002.
- [17] D. L. Ltd. "Torodon®." Don & Low Ltd. <https://www.donlow.co.uk/gb/en/products/torodon/> (accessed 2018).
- [18] P. K. Mallick, *Fiber-reinforced composites [electronic resource] : materials, manufacturing, and design*, 3rd ed., [expanded and rev. ed.]. ed. Boca Raton, Fla. : London: Taylor & Francis, 2008.
- [19] C. E. Dictionary. "MOULD | meaning in the Cambridge English Dictionary." <https://dictionary.cambridge.org/dictionary/english/mould> (accessed 2018).

- [20] F. Campbell, "ASM Handbook Composites," in *Composites*, vol. 21, F. Campbell Ed.: ASM international, 2001, ch. Introduction to post-processing and assembly, p. 615.
- [21] C. Grant, "Automated processes for composite aircraft structure," *Industrial robot*, vol. 33, no. 2, pp. 117-121, 2006, doi: 10.1108/01439910610651428.
- [22] X. Wang, M. Jiang, Z. Zhou, J. Gou, and D. Hui, "3D printing of polymer matrix composites: A review and prospective," *Composites.*, vol. 110, pp. 442-458, 2017, doi: 10.1016/j.compositesb.2016.11.034.
- [23] J. Frketic, T. Dickens, and S. Ramakrishnan, "Automated manufacturing and processing of fiber- reinforced polymer ( FRP) composites: An additive review of contemporary and modern techniques for advanced materials manufacturing," *Additive Manufacturing*, vol. 14, pp. 69-86, 2017, doi: 10.1016/j.addma.2017.01.003.
- [24] G. A. Cooper and A. Kelly, "Role of the Interface in the Fracture of Fiber-Composite Materials." West Conshohocken, PA: ASTM International, 1969, pp. 90-106.
- [25] J. L. Thomason, "Glass fibre sizing: A review," *Composites. Part A, Applied science and manufacturing*, vol. 127, p. 105619, 2019, doi: 10.1016/j.compositesa.2019.105619.
- [26] N. Capiati and R. Porter, "The concept of one polymer composites modelled with high density polyethylene," *Journal of Materials Science*, vol. 10, no. 10, pp. 1671-1677, 1975, doi: 10.1007/BF00554928.
- [27] C. Gao, L. Yu, H. Liu, and L. Chen, "Development of self-reinforced polymer composites," *Progress in polymer science*, vol. 37, no. 6, pp. 767-780, 2012, doi: 10.1016/j.progpolymsci.2011.09.005.
- [28] B. Alcock, T. Peijs, A. Abe, H.-H. Kausch, M. Möller, and H. Pasch, "Technology and Development of Self-Reinforced Polymer Composites," *Advances in polymer science*, vol. 251, pp. 1-76, 2013, doi: 10.1007/12\_2011\_159.
- [29] I. M. Ward and P. J. Hine, "The science and technology of hot compaction," *Polymer (Guilford)*, vol. 45, no. 5, pp. 1413-1427, 2004, doi: 10.1016/j.polymer.2003.11.050.
- [30] B. Alcock, N. Cabrera, N. Barkoula, and T. Peijs, "Low velocity impact performance of recyclable all-polypropylene composites," *Composites science and technology*, vol. 66, no. 11-12, pp. 1724-1737, 2006, doi: 10.1016/j.compscitech.2005.11.010.
- [31] B. Alcock, N. O. Cabrera, N. M. Barkoula, J. Loos, and T. Peijs, "Interfacial properties of highly oriented coextruded polypropylene tapes for the creation of recyclable all-polypropylene composites," *Journal of Applied Polymer Science*, vol. 104, no. 1, pp. 118-129, 2007, doi: 10.1002/app.24588.
- [32] N. Cabrera, B. Alcock, J. Loos, and T. Peijs, "Processing of all-polypropylene composites for ultimate recyclability," *Zbornik radova Instituta za savremenu istoriju*, vol. 218, no. 2, pp. 145-155, 2004, doi: 10.1243/146442004323085563.
- [33] N. O. Cabrera, B. Alcock, E. T. J. Klompen, and T. Peijs, "Filament Winding of Co-Extruded Polypropylene Tapes for Fully Recyclable All-Polypropylene Composite Products," *Applied composite materials*, vol. 15, no. 1, pp. 27-45, 2008, doi: 10.1007/s10443-008-9055-5.
- [34] N. O. Cabrera, B. Alcock, and T. Peijs, "Design and manufacture of all-PP sandwich panels based on co-extruded polypropylene tapes," *Composites.*, vol. 39, no. 7-8, pp. 1183-1195, 2008, doi: 10.1016/j.compositesb.2008.03.010.
- [35] J. Loos, T. Schimanski, J. Hofman, T. Peijs, and P. J. Lemstra, "Morphological investigations of polypropylene single-fibre reinforced polypropylene model composites," *Polymer (Guilford)*, vol. 42, no. 8, pp. 3827-3834, 2001, doi: 10.1016/S0032-3861(00)00660-1.

- [36] P. F. G. C. KG. "Curv® - designed to make an impact." Propex Fabrics GmbH & Co. KG. <https://www.curvonline.com/> (accessed 2018).
- [37] Lankhorst. "Pure® is an important innovation from Lankhorst Yarns." Lankhorst. <https://www.lankhorstyarns.com/product-groups/pure/> (accessed 2018).
- [38] R. H. Rizzolo and D. F. Walczyk, "Ultrasonic consolidation of thermoplastic composite prepreg for automated fiber placement," *Journal of Thermoplastic Composite Materials*, vol. 29, no. 11, pp. 1480-1497, 2016, doi: 10.1177/0892705714565705.
- [39] A. K. Miller, M. Gur, A. Peled, A. Payne, and E. Menzel, "Die-Less Forming of Thermoplastic- Matrix, Continuous-Fiber Composites," *J. Compos Mater.*, vol. 24, no. 4, pp. 346-381, 1990, doi: 10.1177/002199839002400401.
- [40] L. C. Dorworth, "Composite Tooling | Composites | Handbooks | ASM International," in *Composites*, vol. 21: ASM International, 2001.
- [41] T. Altan, "Manufacturing of dies and molds," *CIRP annals ... manufacturing technology.*, vol. 50, no. 2, pp. 405-423, 2001.
- [42] M. G. Bader, "Selection of composite materials and manufacturing routes for cost-effective performance," *Composites.*, vol. 33, no. 7, pp. 913-934, 2002, doi: 10.1016/S1359-835X(02)00044-1.
- [43] A. B. Strong, *Fundamentals of Composites Manufacturing, Materials, Methods, and Applications*, Second Edi ed. 2008, pp. xi,528,435,437--450.
- [44] CompositesWorld. "Overview of AFP and ATL." CompositesWorld. <https://www.compositesworld.com/knowledgecenter/afp-atl-software/overview-of-afp-and-atl> (accessed 2020).
- [45] Z. Qureshi, T. Swait, R. Scaife, and H. M. El-Dessouky, "In situ consolidation of thermoplastic prepreg tape using automated tape placement technology: Potential and possibilities," *Composites.*, vol. 66, pp. 255-267, 2014, doi: 10.1016/j.compositesb.2014.05.025.
- [46] C. Ageorges, L. Ye, and M. Hou, "Advances in fusion bonding techniques for joining thermoplastic matrix composites: a review," *Composites.*, vol. 32, no. 6, pp. 839-857, 2001, doi: 10.1016/S1359-835X(00)00166-4.
- [47] *Standard Terminology for Additive Manufacturing Technologies*, ASTM, 2017. [Online]. Available: <https://compass-astm-org.sheffield.idm.oclc.org/Standards/WITHDRAWN/F2792.htm>
- [48] S. S. Crump and I. Stratasys, "Apparatus and method for creating three-dimensional objects," 1992. [Online]. Available: [https://www.google.com/patents/US5121329?dq=Apparatus+and+method+for+creating+three-dimensional+objects&hl=es-419&sa=X&ved=0ahUKEwix-5Syo7\\_UAhUGfxoKHUSHCZIQ6AEIJzAA](https://www.google.com/patents/US5121329?dq=Apparatus+and+method+for+creating+three-dimensional+objects&hl=es-419&sa=X&ved=0ahUKEwix-5Syo7_UAhUGfxoKHUSHCZIQ6AEIJzAA)
- [49] D. V. Isakov, Q. Lei, F. Castles, C. J. Stevens, C. R. M. Grovenor, and P. S. Grant, "3D printed anisotropic dielectric composite with meta- material features," *Materials & Design*, vol. 93, pp. 423-430, 2016, doi: 10.1016/j.matdes.2015.12.176.
- [50] A. R. Torrado Perez, D. A. Roberson, and R. B. Wicker, "Fracture Surface Analysis of 3D- Printed Tensile Specimens of Novel ABS- Based Materials," *Journal of Failure Analysis and Prevention*, vol. 14, no. 3, 2014, doi: 10.1007/s11668-014-9803-9.
- [51] C. Shemelya *et al.*, "Mechanical, Electromagnetic, and X- ray Shielding Characterization of a 3D Printable Tungsten–Polycarbonate Polymer Matrix Composite for Space- Based Applications," *Journal of Electronic Materials*, vol. 44, no. 8, pp. 2598-2607, 2015, doi: 10.1007/s11664-015-3687-7.

- [52] F. Castles *et al.*, "Microwave dielectric characterisation of 3D- printed BaTiO<sub>3</sub>/ ABS polymer composites," *Scientific Reports*, vol. 6, no. 1, 2016, doi: 10.1038/srep22714.
- [53] M. L. Shofner, K. Lozano, F. J. Rodríguez-Macías, and E. V. Barrera, "Nanofiber-reinforced polymers prepared by fused deposition modeling," *Journal of Applied Polymer Science*, vol. 89, no. 11, pp. 3081-3090, 2003, doi: 10.1002/app.12496.
- [54] Z. Weng, J. Wang, T. Senthil, and L. Wu, "Mechanical and thermal properties of ABS/montmorillonite nanocomposites for fused deposition modeling 3D printing," *Materials & Design*, vol. 102, pp. 276-283, 2016, doi: 10.1016/j.matdes.2016.04.045.
- [55] Z. Rymansaib *et al.*, "All - Polystyrene 3D - Printed Electrochemical Device with Embedded Carbon Nanofiber - Graphite - Polystyrene Composite Conductor," *Electroanalysis*, vol. 28, no. 7, pp. 1517-1523, 2016, doi: 10.1002/elan.201600017.
- [56] W. Xiaojun *et al.*, "3D Printable Graphene Composite," *Scientific Reports*, vol. 5, no. 1, 2015, doi: 10.1038/srep11181.
- [57] B. W. Grimsley *et al.*, "Additive Manufacturing of Multifunctional Components Using High Density Carbon Nanotube Yarn Filaments," ed, 2016.
- [58] W. Zhong, F. Li, Z. Zhang, L. Song, and Z. Li, "Short fiber reinforced composites for fused deposition modeling," *Materials Science & Engineering A*, vol. 301, no. 2, pp. 125-130, 2001, doi: 10.1016/S0921-5093(00)01810-4.
- [59] H. L. Tekinalp *et al.*, "Highly oriented carbon fiber-polymer composites via additive manufacturing," *Composites Science and Technology*, vol. 105, pp. 144-150, 2014, doi: 10.1016/j.compscitech.2014.10.009.
- [60] F. D. Ning, W. L. Cong, J. J. Qiu, J. H. Wei, and S. R. Wang, "Additive manufacturing of carbon fiber reinforced thermoplastic composites using fused deposition modeling," *Composites Part B*, 2015, doi: 10.1016/j.compositesb.2015.06.013.
- [61] F. Ning, W. Cong, Y. Hu, and H. Wang, "Additive manufacturing of carbon fiber-reinforced plastic composites using fused deposition modeling: Effects of process parameters on tensile properties," *J. Compos Mater.*, vol. 51, no. 4, pp. 451-462, 2017, doi: 10.1177/0021998316646169.
- [62] L. J. Love *et al.*, "The importance of carbon fiber to polymer additive manufacturing," *Journal of Materials Research*, vol. 29, no. 17, pp. 1893-1898, 2014, doi: 10.1557/jmr.2014.212.
- [63] S. Y. Fu, B. Lauke, E. Mäder, C. Y. Yue, and X. Hu, "Tensile properties of short- glass-fiber- and short- carbon- fiber- reinforced polypropylene composites," *Composites Part A*, vol. 31, no. 10, pp. 1117-1125, 2000, doi: 10.1016/S1359-835X(00)00068-3.
- [64] S. Kumar and J. P. Kruth, "Composites by rapid prototyping technology," *Materials and Design*, vol. 31, no. 2, pp. 850-856, 2010, doi: 10.1016/j.matdes.2009.07.045.
- [65] Z. Quan *et al.*, "Additive manufacturing of multi- directional preforms for composites: opportunities and challenges," *Materials Today*, vol. 18, no. 9, pp. 503-512, 2015, doi: 10.1016/j.mattod.2015.05.001.
- [66] Z. Quan *et al.*, "Microstructural design and additive manufacturing and characterization of 3D orthogonal short carbon fiber/ acrylonitrile- butadiene- styrene preform and composite," *Composites Science and Technology*, vol. 126, pp. 139-148, 2016, doi: 10.1016/j.compscitech.2016.02.021.
- [67] T. Hofstätter, D. B. Pedersen, G. Tosello, and H. N. Hansen, "Applications of Fiber-Reinforced Polymers in Additive Manufacturing," *Procedia CIRP*, vol. 66, pp. 312-316, 2017, doi: 10.1016/j.procir.2017.03.171.

- [68] A. Le Duigou, M. Castro, R. Bevan, and N. Martin, "3D printing of wood fibre biocomposites: From mechanical to actuation functionality," *Materials & Design*, vol. 96, pp. 106-114, 2016, doi: 10.1016/j.matdes.2016.02.018.
- [69] Y. Termonia, "Theoretical study of the stress transfer in single fibre composites," *Journal of materials science*, vol. 22, no. 2, pp. 504-508, 1987, doi: 10.1007/BF01160761.
- [70] T. H. J. Vaneker, "Material Extrusion of Continuous Fiber Reinforced Plastics Using Commingled Yarn," *Procedia CIRP*, vol. 66, pp. 317-322, 2017, doi: 10.1016/j.procir.2017.03.367.
- [71] D. Yang, H. Zhang, J. Wu, and E. D. McCarthy, "Fibre flow and void formation in 3D printing of short-fibre reinforced thermoplastic composites: An experimental benchmark exercise," *Additive manufacturing*, vol. 37, p. 101686, 2021, doi: 10.1016/j.addma.2020.101686.
- [72] N. Shadvar, E. Foroozmehr, M. Badrossamay, I. Amouhadi, and A. S. Dindarloo, "Computational analysis of the extrusion process of fused deposition modeling of acrylonitrile-butadiene-styrene," *International journal of material forming*, vol. 14, no. 1, pp. 121-131, 2021, doi: 10.1007/s12289-019-01523-1.
- [73] T. Nishimura and T. Kataoka, "Die swell of filled polymer melts," *An International Journal of Rheology*, vol. 23, no. 4, pp. 401-407, 1984, doi: 10.1007/BF01329192.
- [74] R. Matsuzaki *et al.*, "Three-dimensional printing of continuous-fiber composites by in-nozzle impregnation," (in English), *Scientific Reports*, Article vol. 6, p. 7, Mar 2016, Art no. 23058, doi: 10.1038/srep23058.
- [75] C. C. Yang, X. Y. Tian, T. F. Liu, Y. Cao, and D. C. Li, "3D printing for continuous fiber reinforced thermoplastic composites: mechanism and performance," (in English), *Rapid Prototyping Journal*, Article vol. 23, no. 1, pp. 209-215, 2017, doi: 10.1108/rpj-08-2015-0098.
- [76] Y. Nakagawa, K. I. Mori, and T. Maeno, "3D printing of carbon fibre- reinforced plastic parts," *International Journal of Advanced Manufacturing Technology*, vol. 91, no. 5-8, pp. 1-7, 2017, doi: 10.1007/s00170-016-9891-7.
- [77] J. S. Page and I. Autodesk, "Automated systems for composite part fabrication," 2015. [Online]. Available: <https://www.google.com/patents/US20150367576>
- [78] Y. Zhang, W. De Backer, R. Harik, and A. Bernard, "Build Orientation Determination for Multi- material Deposition Additive Manufacturing with Continuous Fibers," *Procedia CIRP*, vol. 50, pp. 414-419, 2016, doi: 10.1016/j.procir.2016.04.119.
- [79] X. Y. Tian, T. F. Liu, C. C. Yang, Q. R. Wang, and D. C. Li, "Interface and performance of 3D printed continuous carbon fiber reinforced PLA composites," (in English), *Compos. Pt. A-Appl. Sci. Manuf.*, Article vol. 88, pp. 198-205, Sep 2016, doi: 10.1016/j.compositesa.2016.05.032.
- [80] A. International, "Properties and Performance of Polymer-Matrix Composites," in *ASM Handbook*, vol. Composites, 21, A. International Ed.: ASM International, 2001, ch. Properties and Performance, pp. 803–837.
- [81] M. G. T. [US] and G. A. S. U. +, "THREE DIMENSIONAL PRINTING OF COMPOSITE REINFORCED STRUCTURES," United States Patent Appl. US201514942676 20151116, 2016. [Online]. Available: <https://worldwide.espacenet.com/publicationDetails/biblio?CC=US&NR=2016144566A1&KC=A1&FT=D&ND=3&date=20160526&DB=EPODOC&locale=en EP#>



- [82] A. N. Dickson, J. N. Barry, K. A. McDonnell, and D. P. Dowling, "Fabrication of continuous carbon, glass and Kevlar fibre reinforced polymer composites using additive manufacturing," *Additive Manufacturing*, vol. 16, pp. 146-152, 2017, doi: 10.1016/j.addma.2017.06.004.
- [83] A. International, "Properties of Wrought Aluminum and Aluminum Alloys, *Properties and Selection: Nonferrous Alloys and Special-Purpose Materials* ," in *ASM Handbook of Materials*, vol. 2, A. International Ed.: ASM International, 1990, pp. 62–122.
- [84] F. V. D. Klift, Y. Koga, A. Todoroki, M. Ueda, Y. Hirano, and R. Matsuzaki, "3D Printing of Continuous Carbon Fibre Reinforced Thermo-Plastic (CFRTP) Tensile Test Specimens," (in en), *Open Journal of Composite Materials*, Articles vol. 06, no. 01, p. 18, 2015-12-31 2015, doi: doi:10.4236/ojcm.2016.61003.
- [85] "Arevo Labs introduces robotic AM platform for 3d printing composite parts (Product Review)," vol. 60, ed, 2016, pp. 19-19.
- [86] Stratasys. "Stratasys Breaking Traditional Manufacturing Barriers at IMTS 2016 - Stratasys Blog." @3d\_printers. <http://blog.stratasys.com/2016/09/07/imts-2016/> (accessed).
- [87] A. Labs. "Arevo Labs Introduces First-of-its-Kind Robotic Additive Manufacturing Platform for 3D Printing Composite Parts - Arevo Labs." <http://arevolabs.com/arevo-labs-introduces-first-of-its-kind-robotic-additive-manufacturing-platform-for-3d-printing-composite-parts/> (accessed).
- [88] G. Mark, "Rapid prototyping options shrink development costs," *Modern Plastics*, vol. 70, no. 9, 1993.
- [89] P. C. Richard, "Composite tooling via laminated object manufacturing, a rapid and affordable method," *International SAMPE Technical Conference*, vol. 28, pp. 1048-1055, 1996.
- [90] D. Klosterman, R. Chartoff, G. Graves, N. Osborne, and B. Priore, "Interfacial characteristics of composites fabricated by laminated object manufacturing," *Composites Part A*, vol. 29, no. 9, pp. 1165-1174, 1998, doi: 10.1016/S1359-835X(98)00088-8.
- [91] P. Parandoush, L. Tucker, C. Zhou, and D. Lin, "Laser assisted additive manufacturing of continuous fiber reinforced thermoplastic composites," *Materials & Design*, vol. 131, pp. 186-195, 2017, doi: 10.1016/j.matdes.2017.06.013.
- [92] R. Swartz, B. CRIST, E. GORE, J. M. Jacobson, and I. O. LLC, "Methods and apparatus for three-dimensional printed composites," Patent Appl. PCT/US2014/018806, 2016. [Online]. Available: <https://www.google.com/patents/EP2961585A2?cl=en>
- [93] "Current achievements and future outlook for composites in 3D printing - ScienceDirect," *Reinforced Plastics*, Review vol. 60, no. 6, pp. 372-375, 2017, doi: <http://dx.doi.org/10.1016/j.repl.2016.10.002>.
- [94] I. Objects. "Technology - Impossible Objects." <http://impossible-objects.com/technology/> (accessed).
- [95] EnvisionTEC. "Large Format 3D Printer for Industrial Composites." @EnvisionTEC. <https://enviontec.com/3d-printers/slcom-1/> (accessed).
- [96] W. C. Emmens, G. Sebastiani, and A. H. van Den Boogaard, "The technology of Incremental Sheet Forming—A brief review of the history," *Journal of Materials Processing Tech.*, vol. 210, no. 8, pp. 981-997, 2010, doi: 10.1016/j.jmatprotec.2010.02.014.
- [97] B. Lu *et al.*, "A study of incremental sheet forming by using water jet," 2017.

- [98] S. Gatea, H. Ou, and G. McCartney, "Review on the influence of process parameters in incremental sheet forming," *The International Journal of Advanced Manufacturing Technology*, vol. 87, no. 1, pp. 479-499, 2016, doi: 10.1007/s00170-016-8426-6.
- [99] M. A. Davarpanah, S. Bansal, and R. Malhotra, "Influence of Single Point Incremental Forming on Mechanical Properties and Chain Orientation in Thermoplastic Polymers," *Journal of Manufacturing Science and Engineering-Transactions of the Asme*, vol. 139, no. 2, Feb 2017, Art no. 021012, doi: 10.1115/1.4034036.
- [100] V. Franzen, L. Kwiatkowski, P. A. F. Martins, and A. E. Tekkaya, "Single point incremental forming of PVC," *Journal of materials processing technology.*, vol. 209, no. 1, pp. 462-469, 2009, doi: 10.1016/j.jmatprotec.2008.02.013.
- [101] V. S. Le, A. Ghiotti, and G. Lucchetta, "Preliminary Studies on Single Point Incremental Forming for Thermoplastic Materials," (in English), *International Journal of Material Forming*, Article vol. 1, pp. 1179-1182, Apr 2008, doi: 10.1007/s12289-008-0191-0.
- [102] P. A. F. Martins, L. Kwiatkowski, V. Franzen, A. E. Tekkaya, and M. Kleiner, "Single point incremental forming of polymers," *Cirp Annals-Manufacturing Technology*, vol. 58, no. 1, pp. 229-232, 2009, doi: 10.1016/j.cirp.2009.03.095.
- [103] T. Marques, M. Silva, and P. Martins, "On the potential of single point incremental forming of sheet polymer parts," *International Journal of Advanced Manufacturing Technology*, vol. 60, no. 1-4, pp. 75-86, Apr 2012, doi: 10.1007/s00170-011-3585-y.
- [104] I. Bagudanch, G. Centeno, C. Vallellano, and M. L. Garcia-Romeu, "Revisiting formability and failure of polymeric sheets deformed by Single Point Incremental Forming," *Polymer Degradation and Stability*, vol. 144, pp. 366-377, 2017, doi: 10.1016/j.polymdegradstab.2017.08.021.
- [105] L. M. Lozano-Sanchez *et al.*, "Mechanical and structural studies on single point incremental forming of polypropylene-MWCNTs composite sheets," *Journal of Materials Processing Technology*, vol. 242, pp. 218-227, Apr 2017, doi: 10.1016/j.jmatprotec.2016.11.032.
- [106] M. B. Silva, L. M. Alves, and P. A. F. Martins, "Single point incremental forming of PVC: Experimental findings and theoretical interpretation," *European Journal of Mechanics / A Solids*, vol. 29, no. 4, pp. 557-566, 2010, doi: 10.1016/j.euromechsol.2010.03.008.
- [107] M. B. Silva, M. Skjoedt, P. A. F. Martins, and N. Bay, "Revisiting the fundamentals of single point incremental forming by means of membrane analysis," *International Journal of Machine Tools and Manufacture*, vol. 48, no. 1, pp. 73-83, 2008, doi: 10.1016/j.ijmachtools.2007.07.004.
- [108] M. B. Silva, T. M. Martinho, and P. A. F. Martins, "Incremental Forming of Hole-Flanges in Polymer Sheets," *Materials and Manufacturing Processes*, vol. 28, no. 3, pp. 330-335, Mar 2013, doi: 10.1080/10426914.2012.682488.
- [109] S. A. Yonan, M. B. Silva, P. A. F. Martins, and A. E. Tekkaya, "Plastic flow and failure in single point incremental forming of PVC sheets," *Express Polymer Letters*, vol. 8, no. 5, pp. 301-311, May 2014, doi: 10.3144/expresspolymlett.2014.34.
- [110] I. Bagudanch, M. L. Garcia-Romeu, G. Centeno, A. Elias-Zuniga, and J. Ciurana, "Forming force and temperature effects on single point incremental forming of polyvinylchloride," *Journal of Materials Processing Technology*, vol. 219, pp. 221-229, May 2015, doi: 10.1016/j.jmatprotec.2014.12.004.
- [111] I. Bagudanch, M. L. Garcia-Romeu, and M. Sabater, "Incremental forming of polymers: process parameters selection from the perspective of electric energy consumption

- and cost," *Journal of Cleaner Production*, vol. 112, pp. 1013-1024, Jan 2016, doi: 10.1016/j.jclepro.2015.08.087.
- [112] I. Bagudanch, M. Vives-Mestres, M. Sabater, and M. L. Garcia-Romeu, "Polymer incremental sheet forming process: Temperature analysis using response surface methodology," *Materials and Manufacturing Processes*, vol. 32, no. 1, pp. 44-53, 2017, doi: 10.1080/10426914.2016.1176191.
- [113] X. Xiao, J.-J. Kim, S.-H. Oh, and Y.-S. Kim, "Study on the incremental sheet forming of CFRP sheet," *Composites. Part A, Applied science and manufacturing*, vol. 141, 2021, doi: 10.1016/j.compositesa.2020.106209.
- [114] G. Ambrogio, R. Conte, F. Gagliardi, L. De Napoli, L. Filice, and P. Russo, "A new approach for forming polymeric composite structures," *Composite structures*, vol. 204, pp. 445-453, 2018, doi: 10.1016/j.compstruct.2018.07.106.
- [115] A. Al-Obaidi, A. Kunke, and V. Kräusel, "Hot single-point incremental forming of glass-fiber-reinforced polymer (PA6GF47) supported by hot air," *Journal of manufacturing processes.*, vol. 43, pp. 17-25, 2019, doi: 10.1016/j.jmapro.2019.04.036.
- [116] R. Conte, G. Ambrogio, D. Pulice, F. Gagliardi, and L. Filice, "Incremental Sheet Forming of a Composite Made of Thermoplastic Matrix and Glass-Fiber Reinforcement," *Procedia Engineering*, vol. 207, pp. 819-824, 2017, doi: 10.1016/j.proeng.2017.10.835.
- [117] S. Torres, R. Ortega, P. Acosta, and E. Calderón, "Hot incremental forming of biocomposites developed from linen fibres and a thermoplastic matrix," *Strojniski Vestnik/Journal of Mechanical Engineering*, vol. 67, no. 3, pp. 123-132, 2021, doi: 10.5545/sv-jme.2020.6936.
- [118] M. Fiorotto, M. Sorgente, and G. Lucchetta, "PRELIMINARY STUDIES ON SINGLE POINT INCREMENTAL FORMING FOR COMPOSITE MATERIALS," *International Journal of Material Forming*, vol. 3, pp. 951-954, Apr 2010, doi: 10.1007/s12289-010-0926-6.
- [119] M. Rimasauskas, K. Juzenas, R. Rimasauskiene, and E. Pupelis, "The research of single point incremental forming process for composite mould production," *Mechanika*, no. 4, pp. 414-419, 2014, doi: 10.5755/j01.mech.20.4.7045.
- [120] D. A. Kissounko, P. Taynton, and C. Kaffer, "New material: vitrimers promise to impact composites," *Reinforced Plastics*, 2017, doi: 10.1016/j.repl.2017.06.084.
- [121] K. Ramani, A. K. Miller, and M. R. Cutkosky, "A New Approach to the Forming of Thermoplastic-Matrix Continuous-Fiber Composites - Part 1: Process and Machine," *Journal of Thermoplastic Composite Materials*, vol. 5, no. 3, pp. 184-201, 1992, doi: 10.1177/089270579200500301.
- [122] K. Ramani, A. K. Miller, and M. R. Cutkosky, "A New Approach to the Forming of Thermoplastic-Matrix Continuous-Fiber Composites — Part 2: Experiments and Model," *Journal of Thermoplastic Composite Materials*, vol. 5, no. 3, pp. 202-227, 1992, doi: 10.1177/089270579200500302.
- [123] K. Ramani, A. Miller, and M. Cutkosky, "A new approach to the forming of thermoplastic-matrix continuous-fiber composites. I - Process and machine. II - Experiments and model," *Journal of Thermoplastic Composite Materials*, 1992.
- [124] A. B. Strong and P. Hauwiller, *INCREMENTAL FORMING OF LARGE FIBER-REINFORCED THERMOPLASTIC COMPOSITES* (Tomorrows Materials : Today, Book 1 and 2: 34th International Sampe Symposium and Exhibition). 1989, pp. 43-54.
- [125] H. P. B. [US] and S. A. B. [US], "Incremental forming of thermoplastic composites," United States Patent Appl. US19890348297 19890505, 1991. [Online]. Available:

<https://worldwide.espacenet.com/publicationDetails/biblio?FT=D&date=19910625&DB=&locale=&CC=US&NR=5026514A&KC=A&ND=1#>

- [126] D. F. Walczyk, J. F. Hosford, and J. M. Papazian, "Using Reconfigurable Tooling and Surface Heating for Incremental Forming of Composite Aircraft Parts," *Journal of Manufacturing Science and Engineering*, vol. 125, no. 2, p. 333, 2003, doi: 10.1115/1.1561456.
- [127] E. V. Sullivan, E. Has, R. C. Schwarz, M. Kesselman, A. N. Peck, and J. M. Papazian, "Individual motor pin module," United States Patent Appl. 08/903,476, 2000. [Online]. Available: <https://patents.google.com/patent/US6012314?q=patent:6012314>
- [128] C. B. Munro, D. Waiczyn, G. Dvorak, S. J. Slusarski, and E. Society Of Manufacturing, "Incremental double diaphragm forming of composite materials using reconfigurable tooling," *Transactions of the North American Manufacturing Research Institution of Sme, Vol 32, 2004*, pp. 495-502, 2004.
- [129] "Curve Works." Curve Works. <https://curveworks.nl/> (accessed 2021).
- [130] "Composites - Adapa - adaptive moulds." <https://adapa.dk/composites/> (accessed).
- [131] C. Munro and D. Walczyk, "Reconfigurable Pin-Type Tooling: A Survey of Prior Art and Reduction to Practice," *Journal of manufacturing science and engineering*, vol. 129, no. 3, pp. 551-565, 2007, doi: 10.1115/1.2714577.
- [132] C. Munro, D. Walczyk, G. Dvorak, and Asme, "Double diaphragm forming of a discontinuous advanced composite prepreg material: Process development and material modeling," Patent 1-2, 2005. [Online]. Available: <Go to ISI>://WOS:000242016100044
- [133] B. Alcock, N. O. Cabrera, N. M. Barkoula, J. Loos, and T. Peijs, "Interfacial properties of highly oriented coextruded polypropylene tapes for the creation of recyclable all-polypropylene composites," *Journal of applied polymer science*, vol. 104, no. 1, pp. 118-129, 2007, doi: 10.1002/app.24588.
- [134] T. Peijs, "Composites for recyclability," *Materials Today*, vol. 6, no. 4, pp. 30-35, 2003, doi: 10.1016/S1369-7021(03)00428-0.
- [135] D. Yao, R. Li, and P. Nagarajan, "Single-polymer composites based on slowly crystallizing polymers," *Polymer engineering and science*, vol. 46, no. 9, pp. 1223-1230, 2006, doi: 10.1002/pen.20583.
- [136] V. M. Cedeno-Campos, P. A. Jaramillo, C. M. Fernyhough, and J. P. A. Fairclough, "Online non-intrusive curing identification of CFRP assisted by pattern recognition with a novel in-situ curing apparatus," *2019 IEEE International Conference on Systems, Man and Cybernetics (SMC)*, vol. 2019-October, pp. 391-396, 2019, doi: 10.1109/SMC.2019.8914371.
- [137] V. M. Cedeno-Campos, P. A. Jaramillo, C. M. Fernyhough, and J. P. A. Fairclough, "Towards mold-free composites. A novel control method to cure carbon fiber through punctual force," *2019 24th IEEE International Conference on Emerging Technologies and Factory Automation (ETFA)*, vol. 2019-September, pp. 1461-1465, 2019, doi: 10.1109/ETFA.2019.8869454.
- [138] V. M. Cedeno-Campos, P. A. Jaramillo, C. M. Fernyhough, and J. P. A. Fairclough, "Towards mould free composites manufacturing of thermoset prepreps. Incremental curing with localised pressure-heat (ICULPH)," *Procedia CIRP*, vol. 85, pp. 237-242, 2019, doi: 10.1016/j.procir.2019.09.020.
- [139] "WorkBee Z1+ CNC Machine | Genuine UK Designed & Manufactured." ooznest. <https://ooznest.co.uk/product-category/machines/cnc-machines/> (accessed 2018).

- [140] "OPENBUILDS MACHINES | OpenBuilds." OpenBuilds. <https://openbuilds.com/?category=openbuilds-machines&id=314> (accessed).
- [141] H. Gürocak, *Industrial motion control : motor selection, drives, controller tuning, applications*. Chichester, England: Chichester, England : Wiley, 2016, 2016.
- [142] M. C. Tips. "What is a motion controller? Technical Summary for Motion Engineers." Motion Control Tips. <https://www.motioncontroltips.com/motion-controller/> (accessed 2019).
- [143] Spark-Concepts. "CNC xPro " Spark-Concepts. <https://github.com/Spark-Concepts/xPRO> (accessed 2018).
- [144] S. Skogsrud, Jeon, S.K. "Using grblShield." <https://github.com/grbl/grbl/wiki> (accessed 2020).
- [145] S. Skogsrud, Jeon, S.K. "GRBL." <https://github.com/gnea/grbl> (accessed).
- [146] A. Bohm, "AMi: a GUI-based, open-source system for imaging samples in multi-well plates," *Acta crystallographica. Section F, Structural biology communications*, vol. 75, no. 8, pp. 531-536, 2019, doi: 10.1107/S2053230X19009853.
- [147] S. Sarguroh, "Using GRBL-Arduino-based controller to run a two-axis computerized numerical control machine," *2018 International Conference on Smart City and Emerging Technology ;*, pp. 1-6, 2018, doi: 10.1109/ICSCET.2018.8537315.
- [148] M. T. Wayland and M. Landgraf, "A Cartesian Coordinate Robot for Dispensing Fruit Fly Food," *Journal of Open Hardware*, vol. 2, no. 1, p. 3, 2018, doi: 10.5334/joh.9.
- [149] *The NIST RS274NGC Interpreter - Version 3*, T. Kramer, Proctor, F. and Messina, E, Gaithersburg, 2000. [Online]. Available: [https://tsapps.nist.gov/publication/get\\_pdf.cfm?pub\\_id=823374](https://tsapps.nist.gov/publication/get_pdf.cfm?pub_id=823374)
- [150] W. a. B. Winder, Joacim. "Universal Gcode Sender." [http://winder.github.io/ugs\\_website/guide/common/](http://winder.github.io/ugs_website/guide/common/) (accessed 2020).
- [151] S. Skogsrud, Jeon, S.K. "Interfacing wit Grbl." <https://github.com/grbl/grbl/wiki/Interfacing-with-Grbl> (accessed 2020).
- [152] "VISA Configure Serial Port VI - LabVIEW 2018 Help - National Instruments." National Instruments. [https://zone.ni.com/reference/en-XX/help/371361R-01/lvinstio/visa\\_configure\\_serial\\_port/](https://zone.ni.com/reference/en-XX/help/371361R-01/lvinstio/visa_configure_serial_port/) (accessed 2020).
- [153] K. Ogata, *Modern control engineering*, 5th , International ed. Boston, [Mass.] ; London: Boston, Mass. ; London : Pearson, c2010, 2010.
- [154] N. Instruements. "Data Acquisition (DAQ)." National Instruments. [https://www.ni.com/en-gb/shop/data-acquisition.html?cid=Paid\\_Search-a240Z00000450srQAE-Consideration-Google\\_Daq\\_Daq&s\\_kwcid=AL!6304!3!449092046793!b!!g!!%2Bdaq&gclid=CjwKC\\_AiAriH\\_BRB2EiwALfbH1HEAG4tMvnX364HgX\\_epZgGpsiq\\_Tb0vvsuBeob5yjBG7rp2VPIulBoCYoiQAvD\\_BwE](https://www.ni.com/en-gb/shop/data-acquisition.html?cid=Paid_Search-a240Z00000450srQAE-Consideration-Google_Daq_Daq&s_kwcid=AL!6304!3!449092046793!b!!g!!%2Bdaq&gclid=CjwKC_AiAriH_BRB2EiwALfbH1HEAG4tMvnX364HgX_epZgGpsiq_Tb0vvsuBeob5yjBG7rp2VPIulBoCYoiQAvD_BwE) (accessed 2020).
- [155] "Thermocouple probes." Omega. <https://www.omega.com/en-us/resources/thermocouple-hub> (accessed 2017).
- [156] "3300 Single Loop Temperature Controller | West Control Solutions." West Control Solutions. <https://www.west-cs.co.uk/products-uk/models-uk/3300-single-loop-controller-uk/> (accessed 2017).
- [157] "TC-08 Thermocouple data logger | Pico Technology." PicoTechnology. <https://www.picotech.com/data-logger/tc-08/thermocouple-data-logger?gclid=Cj0KCQjw->

- [4SLBhCVARIsACrhWLUF3kgk4raix2L4Jtvc3m3fuVKfLQTtPm61DtaVFyZ6w49rFxcn3SoaAmfwEALw wcb](https://www.researchgate.net/publication/318118311) (accessed 2017).
- [158] D. Dore. "Cartridge Heater Applications & More." Cartridge Heater. <https://cartridgeheaters.co.uk/blog/cartridge-heater-applications/> (accessed).
- [159] N. Instruments. How to Measure a Load Cell. Available: <https://www.youtube.com/watch?v=2X6Ua1E4N04>.
- [160] N. Instruments. "Use NI DAQ Devices for Load, Pressure, and Torque Measurements - National Instruments." National Instruments. <https://knowledge.ni.com/KnowledgeArticleDetails?id=kA03q000000x1jjCAA&l=en-GB> (accessed 2020).
- [161] N. Instruments. "Measuring Load and Torque with Bridge-Based Sensors." National Instruments. <https://www.ni.com/en-gb/innovations/white-papers/12/measuring-load-and-torque-with-bridge-based-sensors.html> (accessed 2020).
- [162] KISTLER. "Multi-Component Dynamometer up to 10 kN." KISTLER. <https://www.kistler.com/en/product/type-9257b/> (accessed 2020).
- [163] HBK. "How Does a Piezoelectric Force Transducer Work." HBK. <https://www.hbm.com/en/7318/how-does-a-piezoelectric-force-transducer-work/> (accessed 2020).
- [164] KISTLER. "4-/8-Channel Laboratory Charge Amplifier with LCD (no longer available)." KISTLER. <https://www.kistler.com/en/product/type-5070a/> (accessed 2020).
- [165] N. Instruments. "USB-4431." National Instruments. <https://www.ni.com/en-gb/support/model.usb-4431.html> (accessed 2020).
- [166] X. Jiang, K. Kim, S. Zhang, J. Johnson, and G. Salazar, "High-temperature piezoelectric sensing," *Sensors (Basel)*, vol. 14, no. 1, pp. 144-169, 2013, doi: 10.3390/s140100144.
- [167] "Quartz 3-Component Dynamometer Type 9257B, Instruction Manual," ed. Winterthur, Switzerland: Kistler Group, 2017, pp. 37-38.
- [168] "How to tune a PID controller?" Omega. <https://www.omega.co.uk/technical-learning/tuning-a-pid-controller.html> (accessed).
- [169] Y. S. Song, J. R. Youn, and T. G. Gutowski, "Life cycle energy analysis of fiber-reinforced composites," *Composites. Part A, Applied science and manufacturing*, vol. 40, no. 8, pp. 1257-1265, 2009, doi: 10.1016/j.compositesa.2009.05.020.
- [170] S. Lupi and V. Rudnev, "Electromagnetic and Thermal Properties of Materials," in *Induction Heating and Heat Treatment*, vol. 4C, V. Rudnev and G. E. Totten Eds.: ASM International, 2014, p. 0.
- [171] G. S. H. Lock, *Latent heat transfer : an introduction to fundamentals*. Oxford: Oxford : Oxford University Press, 1994, 1994.
- [172] O. o. E. E. a. R. Energy. "Energy Efficiency vs. Energy Intensity." Office of Energy Efficiency and Renewable Energy. <https://www.energy.gov/eere/analysis/energy-efficiency-vs-energy-intensity> (accessed 2020).
- [173] T. J. Suzuki T, "Prediction of energy intensity of carbon fiber reinforced plastics for mass-produced passenger cars," presented at the Proceedings of 9th Japan International SAMPE Symposium, 2005 Nov 29, 2005.
- [174] I. Baran, K. Cinar, N. Ersoy, R. Akkerman, and J. H. Hattel, "A Review on the Mechanical Modeling of Composite Manufacturing Processes," *Archives of computational methods in engineering state of the art reviews.*, vol. 24, no. 2, pp. 365-395, 2017, doi: 10.1007/s11831-016-9167-2.



- [175] D. P. H. Loos A.C., "Processing of Thermoplastic Matrix Composites," presented at the Review of Progress in Quantitative Nondestructive Evaluation, Boston, MA, 1987. [Online]. Available: [https://link.springer.com/chapter/10.1007%2F978-1-4613-1893-4\\_143#citeas](https://link.springer.com/chapter/10.1007%2F978-1-4613-1893-4_143#citeas).
- [176] P. G. de Gennes, "Reptation of a Polymer Chain in the Presence of Fixed Obstacles," *The Journal of Chemical Physics*, vol. 55, no. 2, pp. 572-579, 1971, doi: 10.1063/1.1675789.
- [177] P. G. de Gennes, "Entangled polymers," *Physics Today*, vol. 36, no. 6, pp. 33-39, 1983, doi: 10.1063/1.2915700.
- [178] R. P. Wool and K. M. O'Connor, "A theory crack healing in polymers," *Journal of applied physics.*, vol. 52, no. 10, pp. 5953-5963, 1981, doi: 10.1063/1.328526.
- [179] R. P. Wool, "Molecular Aspects of Tack," *Rubber chemistry and technology*, vol. 57, no. 2, pp. 307-319, 1984, doi: 10.5254/1.3536010.
- [180] N. Kanth and A. K. Ray, "Analysis of heat conduction inside the nip of a machine calender for the same and different roll temperatures," *Heat transfer - Asian research.*, vol. 48, no. 8, pp. 3557-3573, 2019, doi: 10.1002/htj.21555.
- [181] J. K. Richard, "HEAT TRANSFER IN CALENDERING," *Trans Tech Sect Can Pulp Pap Assoc*, vol. 5, no. 3, pp. 66-71, 1979.
- [182] S. B. Warner, "Thermal Bonding of Polypropylene Fibers," *Textile research journal publication of Textile Research Institute, Inc. and the Textile Foundation.*, vol. 59, no. 3, pp. 151-159, 1989, doi: 10.1177/004051758905900304.
- [183] R. H. Hestmo, "Heat transfer during calendering of paper," *Journal of Pulp and Paper Science*, vol. 28, no. 4, pp. 128-135, 2002.
- [184] N. O. Cabrera, "**Recyclable all-polypropylene composites : concept, properties and manufacturing**," PhD Thesis, Technische Universiteit Eindhoven, 2004.
- [185] M. I. Abo El Maaty, D. C. Bassett, R. H. Olley, M. G. Dobb, J. G. Tomka, and I. C. Wang, "On the formation of defects in drawn polypropylene fibres," *Polymer (Guilford)*, vol. 37, no. 2, pp. 213-218, 1996, doi: 10.1016/0032-3861(96)81090-1.
- [186] T. Schimanski, "High-performance polypropylene structures for eco-friendly, fully recyclable composites," PhD Thesis, Technische Universiteit Eindhoven, Eindhoven, 2002.
- [187] "Torodon® | Don & Low Ltd." <https://www.donlow.co.uk/gb/en/products/torodon/> (accessed).
- [188] Y. Feng, X. Jin, and J. N. Hay, "Evaluation of Multiple Melting Peaks of Propylene-Ethylene Copolymers," *Polymer journal*, vol. 30, no. 3, pp. 215-221, 1998, doi: 10.1295/polymj.30.215.
- [189] K. J. Kim, W.-R. Yu, and P. Harrison, "Optimum consolidation of self-reinforced polypropylene composite and its time-dependent deformation behavior," *Composites. Part A, Applied science and manufacturing*, vol. 39, no. 10, pp. 1597-1605, 2008, doi: 10.1016/j.compositesa.2008.06.005.
- [190] Y. C. Kim, W. Ahn, and C. Y. Kim, "A study on multiple melting of isotactic polypropylene," *Polymer engineering and science*, vol. 37, no. 6, pp. 1003-1011, 1997, doi: 10.1002/pen.11745.
- [191] I. O. Aver'yanova, D. Y. Bogomolov, and V. V. Poroshin, "ISO 25178 standard for three-dimensional parametric assessment of surface texture," *Russian engineering research*, vol. 37, no. 6, pp. 513-516, 2017, doi: 10.3103/S1068798X17060053.

- [192] S. Ashworth *et al.*, "Effects of machine stiffness and cutting tool design on the surface quality and flexural strength of edge trimmed carbon fibre reinforced polymers," *Composites*, vol. 119, pp. 88-100, 2019, doi: 10.1016/j.compositesa.2019.01.019.
- [193] P. H. Dara, "Thermoplastic matrix composite processing model," 2019-06-24 2019. [Online]. Available: <https://ntrs.nasa.gov/search.jsp?R=19860012148>
- [194] *ASTM D1876-08(2015)e1, Standard Test Method for Peel Resistance of Adhesives (T-Peel Test)*, West Conshohocken, PA, 2015. [Online]. Available: [www.astm.org](http://www.astm.org)
- [195] A. J. Jefferson, V. Arumugam, and H. N. Dhakal, "1 - Introduction and context," in *Repair of Polymer Composites*, A. J. Jefferson, V. Arumugam, and H. N. Dhakal Eds.: Woodhead Publishing, 2018, pp. 1-43.
- [196] A. N. Gent and R. P. Petrich, "Adhesion of Viscoelastic Materials to Rigid Substrates," *Proceedings of the Royal Society of London. Series A, Mathematical and Physical Sciences*, vol. 310, no. 1502, pp. 433-448, 1969.
- [197] N. Padhye, D. M. Parks, A. H. Slocum, and B. L. Trout, "Enhancing the performance of the T-peel test for thin and flexible adhered laminates," *Review of Scientific Instruments*, vol. 87, no. 8, 2016, doi: 10.1063/1.4960172.
- [198] Z. Peng, C. Wang, L. Chen, and S. Chen, "Peeling behavior of a viscoelastic thin-film on a rigid substrate," *International Journal of Solids and Structures*, vol. 51, no. 25-26, pp. 4596-4603, 2014, doi: 10.1016/j.ijsolstr.2014.10.011.
- [199] "Composite Manufacturing Applications Of Pressure Indicating Film." Sensor Products Inc. <https://www.sensorprod.com/research-articles/2016/2016-02-Composite-Manufacturing-Applications/> (accessed 2021).
- [200] P. V.L, "Qualitative Treatment of Contact Problems – Normal Contact without Adhesion. In: Contact Mechanics and Friction," in *Contact Mechanics and Friction*. Berlin, Heidelberg: Springer, 2010.
- [201] "Categorizing Surface Energy | The Science of Adhesion | 3M United Kingdom." [https://www.3m.co.uk/3M/en\\_GB/bonding-and-assembly-uk/training-education/science-of-adhesion/categorizing-surface-energy/](https://www.3m.co.uk/3M/en_GB/bonding-and-assembly-uk/training-education/science-of-adhesion/categorizing-surface-energy/) (accessed).
- [202] B. Sandor. "How to Safely Use Acetone Cleaner in an Ultrasonic Bath | Tovatech Blog." Tovatech. <https://tovatech.com/blog/13537/explosion-proof-ultrasonic-cleaners/acetone-ultrasonic-cleaner> (accessed).
- [203] D. A. Darrow and L. V. Smith, "Isolating Components of Processing Induced Warpage in Laminated Composites," *Journal of composite materials*, vol. 36, no. 21, pp. 2407-2419, 2002, doi: 10.1177/0021998302036021784.
- [204] M. D. Azaman, S. M. Sapuan, S. Sulaiman, E. S. Zainudin, and A. Khalina, "Shrinkages and warpage in the processability of wood-filled polypropylene composite thin-walled parts formed by injection molding," *Materials in engineering*, vol. 52, pp. 1018-1026, 2013, doi: 10.1016/j.matdes.2013.06.047.
- [205] C. Albert, "Spring-in and warpage of angled composite laminates," *Composites science and technology*, vol. 62, no. 14, pp. 1895-1912, 2002, doi: 10.1016/S0266-3538(02)00105-7.
- [206] T. Bárány, A. Izer, and T. Czigány, "On consolidation of self- reinforced polypropylene composites," *Plastics, Rubber and Composites*, vol. 35, no. 9, pp. 375-379, 2006, doi: 10.1179/174328906X128234.
- [207] K. Bocz *et al.*, "Non-destructive characterisation of all- polypropylene composites using small angle X-ray scattering and polarized Raman spectroscopy," *Composites Part A*, vol. 114, pp. 250-257, 2018, doi: 10.1016/j.compositesa.2018.08.020.



- [208] *BS EN ISO 527-1:2012 Plastics — Determination of tensile properties Part 1: General principles*, T. B. S. Institution, 2012. [Online]. Available: <https://shop.bsigroup.com/products/plastics-determination-of-tensile-properties-general-principles>
- [209] Instron. "Advantages of Video Non-Contact Extensometers." Azo Materials. <https://www.azom.com/article.aspx?ArticleID=3684> (accessed 2020).
- [210] Z. G. C. KG. "Understanding Extensometry During Tensile Testing." AZoM Materials. <https://www.azom.com/article.aspx?ArticleID=6052> (accessed 2020).
- [211] *BS EN ISO 527-3:2018: Plastics – Determination of tensile properties, Part 3: Test conditions for films and sheet*, T. B. S. Institution, 2018.
- [212] O. Corporation. "Proto MAX - The First High Performance Personal Abrasive Waterjet." OMAXCorp. <https://www.protomax.com/> (accessed).
- [213] E. Sinkora. "New Tech Helps to Cut Tricky Aerospace Composites." <https://www.sme.org/technologies/articles/2018/february/new-tech-helps-cut-tricky-aerospace-composites/> (accessed 2020).
- [214] Y. Swolfs, Q. Zhang, J. Baets, and I. Verpoest, "The influence of process parameters on the properties of hot compacted self-reinforced polypropylene composites," *Composites Part A*, vol. 65, no. C, pp. 38-46, 2014, doi: 10.1016/j.compositesa.2014.05.022.
- [215] R. L. Blaine, "THERMAL APPLICATIONS NOTE - Polymer Heats of Fusion," New Castle, USA, 2017. [Online]. Available: <http://www.tainstruments.com/pdf/literature/TN048.pdf>
- [216] J. Schawe, R. Riesen, J. Widmann, M. Schubnell, and U. Jorimann, "Interpreting DSC Curves Part 1: Dynamic measurements," ed. Schwerzenbach, Schweiz: METTLER TOLEDO GmbH, 2000.
- [217] C. University. "Areas of expertise | Business | Engineering, Environment and Computing." Coventry University. <https://www.coventry.ac.uk/study-at-coventry/faculties-and-schools/engineering-environment-and-computing/business/work-with-us/areas-of-expertise/> (accessed 2021).
- [218] *ASTM E2544-11a(2019), Standard Terminology for Three-Dimensional (3D) Imaging Systems*, A. International, West Conshohocken, PA, 2019. [Online]. Available: [www.astm.org](http://www.astm.org)
- [219] G. Guidi, M. Russo, G. Magrassi, and M. Bordegoni, "Performance evaluation of triangulation based range sensors," *Sensors (Basel)*, vol. 10, no. 8, pp. 7192-7215, 2010, doi: 10.3390/s100807192.
- [220] @udacity. "Introduction to Computer Vision | Udacity Free Courses." @udacity. <https://www.udacity.com/course/introduction-to-computer-vision--ud810> (accessed).
- [221] J.-H. Jeon, K.-T. Lee, H.-Y. Kim, J.-H. Kim, and W.-C. Kim, "White light scanner-based repeatability of 3-dimensional digitizing of silicon rubber abutment teeth impressions," *The journal of advanced prosthodontics.*, vol. 5, no. 4, pp. 452-456, 2013, doi: 10.4047/jap.2013.5.4.452.
- [222] E. Ratajczyk, M. Rak, and T. Kowaluk, "The influence of method of point collection on results with the use of a measuring arm," *Metrology and Measurement Systems*, vol. 19, no. 3, pp. 541-552, 2012, doi: 10.2478/v10178-012-0047-2.
- [223] A. G. Koltsov, D. A. Blokhin, E. V. Krivonos, and A. N. Narezhnev, "Influence assessment of metal-cutting equipment geometrical accuracy on OMV-technologies accuracy,"

- 2016 *Dynamics of Systems, Mechanisms and Machines (Dynamics)*, pp. 1-7, 2016, doi: 10.1109/Dynamics.2016.7819029.
- [224] Autodesk. "PowerInspect | Autodesk Knowledge Network." <https://knowledge.autodesk.com/support/powerinspect?p=PWRI&sort=score&page=1&cg=Getting%20Started> (accessed).
- [225] L. Jerpdal, M. Åkermo, D. Ståhlberg, and A. Herzig, "Process induced shape distortions of self-reinforced poly(ethylene terephthalate) composites," *Composite structures*, vol. 193, pp. 29-34, 2018, doi: 10.1016/j.compstruct.2018.03.038.
- [226] W.-K. Jung, B. Kim, M.-S. Won, and S.-H. Ahn, "Fabrication of radar absorbing structure (RAS) using GFR-nano composite and spring-back compensation of hybrid composite RAS shells," *Composite structures*, vol. 75, no. 1-4, pp. 571-576, 2006, doi: 10.1016/j.compstruct.2006.04.077.
- [227] M. J. O'Dwyer, G. M. Maistros, S. W. James, R. P. Tatam, and I. K. Partridge, "Relating the state of cure to the real-time internal strain development in a curing composite using in-fibre Bragg gratings and dielectric sensors," *Measurement science and technology*, vol. 9, no. 8, pp. 1153-1158, 1998, doi: 10.1088/0957-0233/9/8/002.
- [228] PowerInspect. "To create a Point Cloud Picked-Points alignment using dynamic points | PowerInspect 2020 | Autodesk Knowledge Network." Autodesk. <https://knowledge.autodesk.com/support/powerinspect/learn-explore/caas/CloudHelp/cloudhelp/2020/ENU/PWRI-ReferenceHelp/files/GUID-0498B28D-030C-40D0-A9EE-64BC65910C6E-htm.html> (accessed 2021).
- [229] I. Willershausen, "Influence of three scan spray systems on human gingival fibroblasts," *Quintessence international.*, vol. 43, no. 6, pp. e67-e72, 2012.
- [230] H.-S. Oh, Y.-J. Lim, B. Kim, M.-J. Kim, H.-B. Kwon, and Y.-W. Baek, "Influence of Scanning-Aid Materials on the Accuracy and Time Efficiency of Intraoral Scanners for Full-Arch Digital Scanning: An In Vitro Study," *Materials.*, vol. 14, no. 9, p. 2340, 2021, doi: 10.3390/ma14092340.
- [231] A. V. Burde, "Three - Dimensional evaluations of the coating thickness of two optical conditioning scanning sprays," *Materiale Plastice*, vol. 53, no. 1, pp. 65-67, 2016.
- [232] M. Dehurtevent, L. Robberecht, and P. Béhin, "Influence of dentist experience with scan spray systems used in direct CAD/CAM impressions," *The journal of prosthetic dentistry.*, vol. 113, no. 1, pp. 17-21, 2015, doi: 10.1016/j.prosdent.2014.07.006.
- [233] G. Rodger, D. Flack, and M. McCarthy, "A review of industrial capabilities to measure free-form surfaces," 2007.
- [234] A. W. L. Yao, "Applications of 3D scanning and reverse engineering techniques for quality control of quick response products," *International journal of advanced manufacturing technology*, vol. 26, no. 11, pp. 1284-1288, 2005, doi: 10.1007/s00170-004-2116-5.
- [235] J. H. T. Daemen *et al.*, "Three-Dimensional Imaging of the Chest Wall: A Comparison Between Three Different Imaging Systems," *J Surg Res*, vol. 259, pp. 332-341, 2021, doi: 10.1016/j.jss.2020.09.027.
- [236] P. Amornvit and S. Sanohkan, "The Accuracy of Digital Face Scans Obtained from 3D Scanners: An In Vitro Study," *International journal of environmental research and public health.*, vol. 16, no. 24, p. 5061, 2019, doi: 10.3390/ijerph16245061.
- [237] G. C. Jacob, J. F. Fellers, S. Simunovic, and J. M. Starbuck, "Energy Absorption in Polymer Composites for Automotive Crashworthiness," *J. Compos Mater.*, vol. 36, no. 7, pp. 813-850, 2002, doi: 10.1177/0021998302036007164.

- [238] S. Wang, S. Li, J. He, and Y. Zhao, "Asymmetric Postbuckling Behavior of Hemispherical Shell Structure Under Axial Compression," *Journal of engineering materials and technology*, vol. 138, no. 1, 2016, doi: 10.1115/1.4031960.
- [239] P. K. Gupta and N. K. Gupta, "A study of different modes of collapse in metallic hemispherical shells resting on flat platen and compressed with hemispherical nosed indenter," *International journal of solids and structures*, vol. 51, no. 13, pp. 2518-2528, 2014, doi: 10.1016/j.ijsolstr.2014.03.023.
- [240] P. K. Gupta and N. K. Gupta, "Computational and experimental studies of crushing of metallic hemispherical shells," *Archive of applied mechanics (1991)*, vol. 76, no. 9, pp. 511-524, 2006, doi: 10.1007/s00419-006-0053-5.
- [241] Y. Guan, L. N. Virgin, and D. Helm, "Structural behavior of shallow geodesic lattice domes," *International journal of solids and structures*, vol. 155, pp. 225-239, 2018, doi: 10.1016/j.ijsolstr.2018.07.022.
- [242] I. S. C. Author, "A performance analysis of EtherCAT and PROFINET IRT," *2008 IEEE International Conference on Emerging Technologies and Factory Automation*, pp. 408-415, 2008, doi: 10.1109/ETFA.2008.4638425.
- [243] Intervalzero. "KINGSTAR Help - Introduction to KINGSTAR." Intervalzero. [https://help.kingstar.com/product\\_help/KS/Default.htm#ONLINETOPICS/Introduction.htm?TocPath=\\_\\_\\_\\_\\_2](https://help.kingstar.com/product_help/KS/Default.htm#ONLINETOPICS/Introduction.htm?TocPath=_____2) (accessed 2021).
- [244] T. Wuest, D. Weimer, C. Irgens, and K.-D. Thoben, "Machine learning in manufacturing: advantages, challenges, and applications," *Production & manufacturing research.*, vol. 4, no. 1, pp. 23-45, 2016, doi: 10.1080/21693277.2016.1192517.
- [245] J. Wang, Y. Ma, L. Zhang, R. X. Gao, and D. Wu, "Deep learning for smart manufacturing: Methods and applications," *Journal of manufacturing systems*, vol. 48, pp. 144-156, 2018, doi: 10.1016/j.jmsy.2018.01.003.
- [246] "Dataflow Programming Basics in NI LabVIEW - National Instruments." National Instruments. <https://www.ni.com/getting-started/labview-basics/dataflow> (accessed).
- [247] "PID Autotuning VI - LabVIEW 2018 Help - National Instruments." Natinoal Instruments. [https://zone.ni.com/reference/en-XX/help/371361R-01/lvpid/pid\\_with\\_autotuning/](https://zone.ni.com/reference/en-XX/help/371361R-01/lvpid/pid_with_autotuning/) (accessed 2018).

## 9 Appendix A

Figure 9-1 shows how the force closed-loop system was implemented in LabVIEW®. More information about the programming and the data flow can be found in [246]. The control system consists of a step sequence (inner boxes) that is repeated until a condition is met. First, the force is compared to the target force by the PID function, which returns a vertical output displacement for the forming tool to correct the force signal. The displacement is then transformed into a g-code line, which is then sent to the microcontroller. Since there are no encoders that can monitor the position of the forming tool, the system is designed to calculate the actuation time and wait before comparing the new force again with the target force. If the force is in range ( $\pm 0.3$  N), the loop finishes as the target force has been found. The PID parameters for the proportional, integral, and derivative terms are generally obtained through autotuning as it saves experimentation time [247], however, sometimes they were obtained empirically using the methodology stated in [168]. It was found that even the smallest integral or derivative parameters ( $\sim 0.0001$ ) promotes instability in the response.

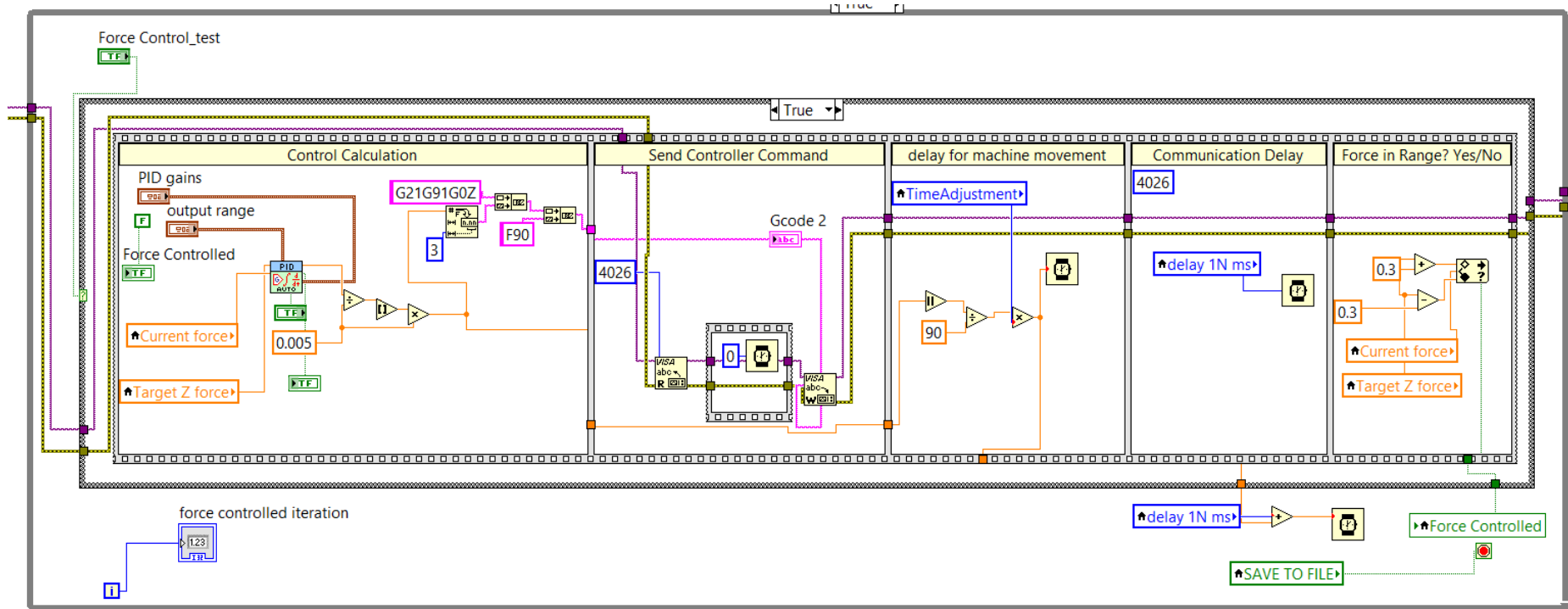


Figure 9-1 Force Control programming in LabVIEW®

## 10 Appendix B

### Heat transfer Model

#### Contact Area

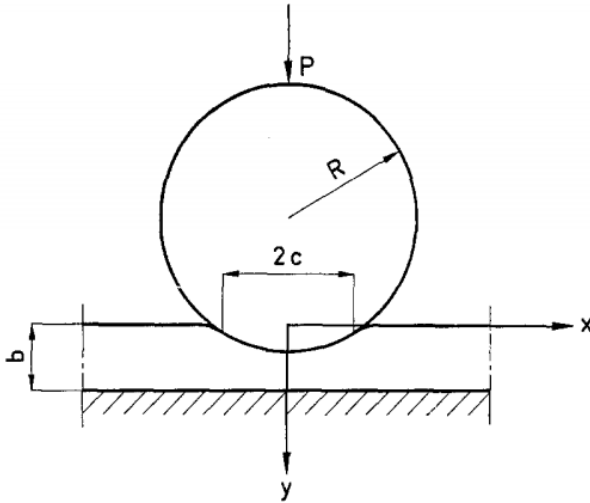


Figure 10-1. Schematic of a circle in contact with a plane

The radius of the circular contact area for a sphere with a plane has first calculated by hertz and is given by

$$a = \left( \frac{3LR_E}{4E^*} \right)^{\frac{1}{3}}$$

where  $a$  is the contact width,  $L$  is the applied load,  $R_E$  is the equivalent diameter, and  $E^*$  is the equivalent bulk modulus.

The equivalent diameter  $R_E$  is given by

$$\frac{1}{R_E} = \frac{1}{R_1} + \frac{1}{R_2}$$

Where  $R_1$  and  $R$  are the radius of the spheres.

In the same way, the equivalent bulk modulus  $E^*$  is given by

$$\frac{1}{E^*} = \frac{1 - \nu_1^2}{E_1} + \frac{1 - \nu_2^2}{E_2}$$

where  $E_1$ ,  $E_2$ ,  $\nu_1$ , and  $\nu_2$  are the bulk modulus and poisson ration of each of the spheres respectively.

Work of Adhesion

$\gamma_{PP} = 76 \frac{\text{mJ}}{\text{m}^2}$ ; %reference adhesion and surface forces in polymer tribology

$$a^3 = \frac{3}{4} \frac{R}{E^*} \left( F + 3\pi R\gamma + \sqrt{6\pi R F \gamma + (3\pi R\gamma)^2} \right)$$

The following values have been obtained from the literature

$$E_{\text{Copper}} = 128 \text{ GPa}$$

$$E_{\text{PP-125}^\circ\text{C}} = 1.5 \text{ GPa}$$

$$E_{\text{PP-140}^\circ\text{C}} = 1 \text{ GPa}$$

$$E_{\text{PP-155}^\circ\text{C}} = 0.5 \text{ GPa}$$

$$E_{\text{PP-170}^\circ\text{C}} \approx 0.1 \text{ GPa}$$

$$\nu_{\text{copper}} = 0.3$$

$$\nu_{\text{PP}} = 0.5$$

$$R_1 = 55 \text{ mm}$$

- $R_2 = \infty$

**Matlab Program**

```
Force=[30 40 50];
```

```
%E_pp=900;%Pa/mm2
```

```
R1=10; %mm
```

```
RE=R1;
```

```
E_pp=[1500 1000 500 50];
```

```
E_cu=128000; %Pa/mm2
```

```
Possion_pp=0.5;
```

```
Possion_cu=0.3;
```

```

Work_adhesion=(76*(1/1000000)); %J/mm2

E_equiv=zeros(4,1);

width_1=zeros(2,2);

width_2=zeros(2,2);

width_3=zeros(2,2);

for i=1:4

E_equiv(i)=1/((1-Possion_pp^2)/E_pp(i)+(1-Possion_cu^2)/E_cu);

width_1(1:length(Force),i)=2*sqrt((2*Force*RE)/(3.141516*E_equiv(i))); %meijers
model

width_2(1:length(Force),i)=2*((3*Force*RE)/(4*E_equiv(i))).^(1/3); % hertz model

width_3(1:length(Force),i)=2*((3*RE)/(4*E_equiv(i))*(Force+3*pi*RE*Work_adhesion
+sqrt(6*pi*RE*Force*Work_adhesion+(3*pi*RE*Work_adhesion)^2))).^(1/3);

plot(Force, width_2(:,i), '*', Force, width_3(:,i), 'o')

hold on

end

hold off

%plot(load, width, 'x', load, width_2, '*', load, width_3, 'o')

%legend('Meijer', 'Hertz', 'JKR')

legend('Hertz-125°C', 'JKR-125°C', 'Hertz-140°C', 'JKR-140°C', 'Hertz-155°C', 'JKR-
155°C', 'Hertz-170°C', 'JKR-170°C', 'location', 'northwest')

title('Contact radius R=55mm')

xlabel('Force N')

ylabel('Radius mm')

```



xlim([0 60])

### Dwell Time or Time In The Nip

The time in the nip for viscoelastic materials has been calculated assuming the distance between the initial point of contact until it stop being in contact with the round tool.

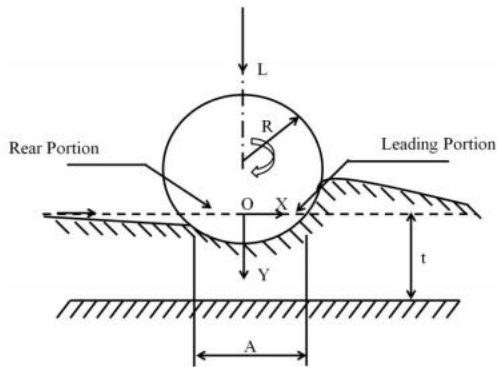


Figure 10-2. Geometry of a rolling sphere over a surface

This distance is calculated using the arc of the length of a circle and since the deformation are considered to be small,  $\sin\theta$  can be approximated as  $\theta$ .

$$\Delta S = R * (\theta_1 + \theta_2)$$

where  $\theta_1$  and  $\theta_2$  are the angles between the vertical axis and the initial and final point which depends on the initial and final thickness of the laminate. Therefore, the arc of the length results in:

$$y = \sqrt{R^2 - X^2} + R$$

$$\Delta S = \sqrt{R(C_R - C_N) - (C_R - C_N)^2} + \sqrt{2R(C_O - C_N) - (C_O - C_N)^2}$$

Where  $C_O$ ,  $C_N$ , and  $C_R$  are the initial thicknes, the thickness at the nip, and the final thickness of the laminate. Furthermore, the square terms can be discarded due to their small value resulting in:

$$\Delta S = \sqrt{R} (\sqrt{(C_O - C_R)})$$

The values of  $C_O$  and  $C_R$  depend on the pressure applied. From observations with a force of 50N, the diameter of contact area is around 7 mm.

Since the velocity is constant, then the dwell time is

$$t = \frac{\Delta S}{V} = \frac{\sqrt{R}(\sqrt{(C_O - C_R)})}{V} [\text{Secs}]$$

### Dwell Time Matlab Program

```
%%
Layer_number=[2 3 4 5 6 7 8 9 10 11];
Tool_speed=[1.5 2 4 6 8];
Force=[10 50];
Tool_radius=55;
X=-5:0.1:5;
Y=sqrt(Tool_radius^2-X.^2)+Tool_radius;

plot(X,Y)
hold off
xlim([-4 4]);
ylim([0 0.2]);

Layer_thickness_initial=0.3; %mm
Layer_thickness_end=0.2;
Layer_thickness_nip=0.193;
Thickness_initial=zeros(length(Layer_number),1);
Thickness_final=zeros(length(Layer_number),1);
Thickness_nip=zeros(length(Layer_number),1);
CO_CR=zeros(length(Layer_number),1);
for i=1:length(Layer_number)
Thickness_initial(i)=Layer_number(i)*Layer_thickness_initial;
Thickness_final(i)=Layer_number(i)*Layer_thickness_end;
Thickness_nip(i)=Layer_number(i)*Layer_thickness_nip;
CR_CN(i)=(Thickness_final(i)-Thickness_nip(i))/2;
CO_CN(i)=(Thickness_initial(i)-Thickness_nip(i))/2;
CR_CN_2(i)=(CR_CN(i))^2;
CO_CN_2(i)=(CO_CN(i))^2;
CO_CR(i)=Thickness_initial(i)-Thickness_final(i);
end

Displacement_nip=zeros(length(Layer_number),1);
for j=1:length(Layer_number)
Displacement_nip(j)=sqrt(Tool_radius*(CO_CR(j)));
for i=1:length(Tool_speed)
time_dwell(i,j)=Displacement_nip(j)/Tool_speed(i);
end
end

for i=1:length(Layer_number)
```

```

plot(Tool_speed,time_dwell(:,i))
hold on
end
hold off
title("dwell time in the nip")
legend("2","3","4","5","6","7","8","9","10","11")
xlabel('Speed (mm/s)')
ylabel ('time (s)')

```

### Heat Transfer Model Matlab Program

```

density=0.904*1000; %kg/m3
conductivity=0.16; %W/(m°K)
specific_heat=70; %(J/(Kg°K))
diffusivity=conductivity/(density*specific_heat); %(m^2/s)
T_0=100;
T_1=140;
T_2=115;
T_r=140;
%Thickness_final
%t=time_dwell(1,10);
Contact_width=2.5;
V=90;
V_vector=[90 400 600 800 1000 1200];
% V=(0:10:600);
t=Contact_width./(V/60);
t_vector=Contact_width./(V_vector/60);
%t=0.444;
%x(:,j)=0:0.1:Thickness_final(i);
thickness=1.2;
x=(0:0.01:thickness); %(mm)
C1=-(pi^2)*diffusivity*t/(thickness/1000)^2;
C1_vector=-(pi^2)*diffusivity*t_vector/(thickness/1000)^2;
C2=pi/thickness;
Sum=0;
Sum_1=0;
Sum2=0;
Sum_2=0;
series_number=13;
for n=1:2:series_number
    Sum=(1/n)*sin(n*C2.*x)*exp(n^2.*C1);
    Sum_1=Sum+Sum_1;
end

for n=1:series_number
    Sum2=exp(C1*n^2)*sin(n*pi*x/thickness)*((2/(n*pi))*((T_2*(-1)^n)-
T_1)+(2*T_0/(n*pi))*(1-cos(n*pi)));

```

```

    Sum_2=Sum2+Sum_2;
end

T_case1=T_r+(T_0-T_r)*(4/pi)*Sum_1;
T_case2=T_1+(T_2-T_1)*(x/thickness)+Sum_2;
T_case2_min=min(T_case2)

%min
Sum2_vector=0;
Sum_2_vector=0;
min_index=0;
T_case2_min_vector=0;
T_case2_minpos_vector=0;
for j=1:length(V_vector)
for n=1:series_number
    Sum2_vector=exp(C1_vector(j).*n^2)*sin(n*pi*x/thickness)*((2/(n*pi))*((T_2*(-
1)^n)-T_1)+(2*T_0/(n*pi))*(1-cos(n*pi))));
    Sum_2_vector=Sum2_vector+Sum_2_vector;
end
T_case2_vector(:,j)=T_1+(T_2-T_1)*(x/thickness)+Sum_2_vector;
[T_case2_min_vector(j),min_index(j)]=min(T_case2_vector(:,j));
T_case2_minpos_vector(j)=x(min_index(j));
end

figure
plot(V_vector,T_case2_min_vector)
hold off

figure
for j=1:length(V_vector)
plot(T_case2_vector(:,j),x)
hold on
end
legend('V=90 mm/min','V=400 mm/min','V=600 mm/min','V=800 mm/min','V=1000
mm/min','V=1200 mm/min')
hold off
xlabel('Temperature °C')
ylabel('thickness depth mm')

% load('T_experimental.mat')

figure
for j=1:length(V_vector)
subplot(3,2,j)
plot(x,T_case2_vector(:,j))
hold on
plot(T_experimental(:,1),T_experimental(:,j+1),'x')

```

```

    hold on
end
%legend('V=90 mm/min','V=400 mm/min','V=600 mm/min','V=800 mm/min','V=1000
mm/min','V=1200 mm/min')
hold off

%centre
Sum_2_centre=0;
Sum_2_centre_vector=0;
for n=1:series_number
    Sum2_centre=exp(C1*n^2)*sin(n*pi*1/2)*((2/(n*pi))*((T_2*(-1)^n)-
T_1)+(2*T_0/(n*pi))*(1-cos(n*pi)));
    Sum_2_centre=Sum2_centre+Sum_2_centre;
end

for n=1:series_number
    Sum2_centre_vector=exp(C1_vector*n^2)*sin(n*pi*1/2)*((2/(n*pi))*((T_2*(-1)^n)-
T_1)+(2*T_0/(n*pi))*(1-cos(n*pi)));
    Sum_2_centre_vector=Sum2_centre+Sum_2_centre_vector;
end

T_case2_center=T_1+(T_2-T_1)*(1/2)+Sum_2_centre
T_case2_center_vector=T_1+(T_2-T_1)*(1/2)+Sum_2_centre_vector
%plot(x,T_case1,x,T_case2)
figure
plot(x,T_case2)
%legend('case 1','case 2')
title('Temperature Distribution in a 2.4mm-thickness plate')
xlabel('depth (through thickness) [mm]')
ylabel('Temperature °C')
xlim([0 thickness])
ylim([0 T_1+10])
hold off
figure
plot(V_vector,T_case2_center)
Variation of temperature in the centre of the thickness with temperature
Fixed Parameters
Hot Mould= 115°C
Temperature records
%import and replace first colum for time in secs
load('temperature_records.mat')
X=F50N_S1200;
Time=(0:1:length(X(:,2))-1);
F50N_S1200(:,1)=Time;
clear X Time
save('temperature_records.mat','F50N_S1200','-append')
A=F10N_S90;

```

```

B=F10N_S400;
C=F10N_S600;
D=F10N_S800;
E=F10N_S1000;
F=F10N_S1200;
legends=[163'4','5','6'];
figure
plot(A(:,1),A(:,2),A(:,1),A(:,3),A(:,1),A(:,4),A(:,1),A(:,5),A(:,1),A(:,6),A(:,1),A(:,7),'LineWidth
th',2)
hold on
%
plot(B(:,1),B(:,2),B(:,1),B(:,3),B(:,1),B(:,4),B(:,1),B(:,5),B(:,1),B(:,6),B(:,1),B(:,7),'LineWidth',2)
% hold on
%
plot(C(:,1),C(:,2),C(:,1),C(:,3),C(:,1),C(:,4),C(:,1),C(:,5),C(:,1),C(:,6),C(:,1),C(:,7),'LineWidth',2)
% hold on
%
plot(D(:,1),D(:,2),D(:,1),D(:,3),D(:,1),D(:,4),D(:,1),D(:,5),D(:,1),D(:,6),D(:,1),D(:,7),'LineWidth',2)
% hold on
%
plot(E(:,1),E(:,2),E(:,1),E(:,3),E(:,1),E(:,4),E(:,1),E(:,5),E(:,1),E(:,6),E(:,1),E(:,7),'LineWidth',2)
% hold on
%
plot(F(:,1),F(:,2),F(:,1),F(:,3),F(:,1)+101-88,F(:,4),F(:,1)+101-96,F(:,5),F(:,1)-
3,F(:,6),F(:,1)-4,F(:,7),'LineWidth',2)
% hold on

grid on
xlim([0 inf])
% title('Tensile Tests Hot Press Vs SF 140-115 °C')
xlabel ('Time (s)')
% xticks([1 2 3 4 5 6]);
ylabel('Temperature °C')
ylim([-inf inf])
legend (legends,'location','best','FontSize',18)
ax=gca;
ax.FontSize = 18;
ax.FontWeight = 'Bold';
ax.LineWidth=2;

figure

[X,L]=xcorr(B(:,2),B(:,3));
[XX,I]=max(X);
lagdiff=L(I)
Filenameslayers=["F10N_layer1.fig","F10N_layer2.fig","F10N_layer3.fig","F10N_layer4
.fig","F10N_layer5.fig","F10N_layer6.fig"];

```

```

for i=6
n=i;
figure
% ('units','normalized','outerposition',[0 0 1 1])

Layer=[1,2,3,4,5,6];
legends2=('90','400','600','800','1000','1200');
% n=1
plot(A(:,1),A(:,Layer(n)+1),'LineWidth',2)
hold on
plot(B(:,1),B(:,Layer(n)+1),'LineWidth',2)
hold on
plot(C(:,1),C(:,Layer(n)+1),'LineWidth',2)
hold on
plot(D(:,1),D(:,Layer(n)+1),'LineWidth',2)
hold on
plot(E(:,1),E(:,Layer(n)+1),'LineWidth',2)
hold on
plot(F(:,1),F(:,Layer(n)+1),'LineWidth',2)
hold on
grid on
xlim([0 inf])
% title('Tensile Tests Hot Press Vs SF 140-115 °C')
xlabel('Time (s)')
% xticks([1 2 3 4 5 6]);
ylabel('Temperature °C')
ylim([-inf inf])
legend (legends2,'location','best','FontSize',18)
ax=gca;
ax.FontSize = 18;
ax.FontWeight = 'Bold';
ax.LineWidth=2;

end
% savefig(h,Filenamelayers(n))

```

## 11 Appendix C

### Matlab G-Code Generation Program

```
% define the name of the g-code file from a CAM software
mouldname="SphericalTool_20210321_post.txt";

%Use the readgcode function to read the file
Gcode_coor=readgcode(mouldname);

% new coordinate creation
Gcode_step=0.5; %step size
kf=0;
for i=1:height(Gcode_coor)-1
    Gcode_temp= Gcode_coor(i:i+1,1:3);
    step_separation(i,1)=pdist(Gcode_temp); %calculate de distance between both
coordinates
    step_separation(i,2)=round(step_separation(i,1)/Gcode_step); %divide the distance by
the expected separation
    step_separation(i,3)=pdist(Gcode_temp(:,1)); % distance between x coordinates
    step_separation(i,4)=pdist(Gcode_temp(:,2)); % distnace between y coordinates
    step_separation(i,5)=pdist(Gcode_temp(:,3)); % distnace between z coordinates
    xi=Gcode_temp(1,1);
    xf=Gcode_temp(2,1);
    yi=Gcode_temp(1,2);
    yf=Gcode_temp(2,2);
    zi=Gcode_temp(1,3);
    zf=Gcode_temp(2,3);
    %    m=(yf-yi)/(xf-xi);
    %    b=yf-m*xf;
    if step_separation(i,1)>Gcode_step
        distance=step_separation(i,1)/step_separation(i,2);
        xq=linspace(xi,xf,step_separation(i,2)); %create a vector between the x values
        yq=linspace(yi,yf,step_separation(i,2)); %create a vector between the y values
        zq=linspace(zi,zf,step_separation(i,2)); %create a vector between the y values
        ki=kf+1;
        kf=ki+step_separation(i,2)-1;
    else
        distance=step_separation(i,1);
        xq=linspace(xi,xf,step_separation(i,1));
        yq=linspace(yi,yf,step_separation(i,1));
        zq=linspace(zi,zf,step_separation(i,1));
        ki=kf+1;
        kf=ki+step_separation(i,1)-1;
    end
    Gcode_new(ki:kf,1)=round(xq',2);
    Gcode_new(ki:kf,2)=round(yq',2);
    Gcode_new(ki:kf,3)=round(zq',2);
end
end
```



```

clear Gcode_temp ki kf xq yq distance

step_separation;
% Gcode_new(:,3)=0;

%plot generation

[xq,yq] = meshgrid(min(Gcode_new(:,1))-10:10:max((Gcode_new(:,1))+10),...
    min(Gcode_new(:,2))-10:10:max(Gcode_new(:,2))+10);
vq = griddata(Gcode_new(:,1), Gcode_new(:,2),Gcode_new(:,3),xq,yq,'linear');
figure
% mesh(xq,yq,vq)
hold on
plot3(Gcode_new(:,1), Gcode_new(:,2),Gcode_new(:,3))
title(mouldname)
hold on
plot3(Gcode_new(:,1), Gcode_new(:,2),Gcode_new(:,3),'o','MarkerSize',1)

%save the new file, first open the right folder in forming paths
for i = 1:height(Gcode_new)
Gcode_str_post(i,1)="x"+string(Gcode_new(i,1))+ "y"...
    +string(Gcode_new(i,2))+ "z"+string(Gcode_new(i,3));
end
mouldpost=extractBefore(mouldname,".txt")+ "_" +num2str(Gcode_step)+"mm_expanded.txt"
fid = fopen(mouldpost,'w');
% for i= 1:length(Gcode_str)
fprintf(fid, "%s\n", Gcode_str_post);
% end
fclose(fid);

% Algorithm to read Gcode
% conditions, x, y, z in lower c
% 1) reads
% 2) obtain a file with coordinates
function Gcode_coor=readgcode(mouldname)
% mouldname="Curvemould2mm90deg.txt"; %fcode file name
%%
% Open and read the gcode to make it a string variable
fileID=fopen(mouldname);
Gcode=textscan(fileID, "%s");
fclose(fileID);
Gcode_str=string(Gcode(1));
%%
%analyze each line to extract the value of the coordinate

```

```

i = 1;
% if x,y,z are present
% if x,y,z are present, take the value in between the characters
% respectively
if isempty(strfind(Gcode_str(i),"x")) == 0 & isempty(strfind(Gcode_str(i),"y")) == 0 &
isempty(strfind(Gcode_str(i),"z"))==0
    Gcode_coor(i,1)=str2double(extractBetween(Gcode_str(i),"x","y"));
    Gcode_coor(i,2)=str2double(extractBetween(Gcode_str(i),"y","z"));
    Gcode_coor(i,3)=str2double(extractAfter(Gcode_str(i),"z"));
    %if only x present, y,z missing take the previous value
elseif isempty(strfind(Gcode_str(i),"x")) == 0 & isempty(strfind(Gcode_str(i),"y")) ==
1 & isempty(strfind(Gcode_str(i),"z")) == 1;
    Gcode_coor(i,1)=str2double(extractAfter(Gcode_str(i),"x"));
    Gcode_coor(i,2)=0;
    Gcode_coor(i,3)=0;
    %if only y present, x,z missing take the previous value
elseif isempty(strfind(Gcode_str(i),"x")) == 1 & isempty(strfind(Gcode_str(i),"y")) ==
0 & isempty(strfind(Gcode_str(i),"z")) == 1
    Gcode_coor(i,1)=0;
    Gcode_coor(i,2)=str2double(extractAfter(Gcode_str(i),"y"));
    Gcode_coor(i,3)=0;
    %if only z present, x,y missing take the previous value
elseif isempty(strfind(Gcode_str(i),"x")) == 1 & isempty(strfind(Gcode_str(i),"y")) ==
1 & isempty(strfind(Gcode_str(i),"z")) ==0
    Gcode_coor(i,1)=0;
    Gcode_coor(i,2)=0;
    Gcode_coor(i,3)=str2double(extractAfter(Gcode_str(i),"z"));
    %if only y,z present, x missing take the previous value
elseif isempty(strfind(Gcode_str(i),"x")) == 1 & isempty(strfind(Gcode_str(i),"y")) ==
0 & isempty(strfind(Gcode_str(i),"z"))==0
    Gcode_coor(i,1)=0;
    Gcode_coor(i,2)=str2double(extractBetween(Gcode_str(i),"y","z"));
    Gcode_coor(i,3)=str2double(extractAfter(Gcode_str(i),"z"));

    %if only x,z present, y missing take the previous value
elseif isempty(strfind(Gcode_str(i),"x")) == 0 & isempty(strfind(Gcode_str(i),"y")) ==
1 & isempty(strfind(Gcode_str(i),"z"))==0
    Gcode_coor(i,1)=str2double(extractBetween(Gcode_str(i),"x","z"));
    Gcode_coor(i,2)=0;
    Gcode_coor(i,3)=str2double(extractAfter(Gcode_str(i),"z"));

    %if only x,y present, z missing take the previous value or 0.
elseif isempty(strfind(Gcode_str(i),"x")) == 0 & isempty(strfind(Gcode_str(i),"y")) ==
0 & isempty(strfind(Gcode_str(i),"z"))==1
    Gcode_coor(i,1)=str2double(extractBetween(Gcode_str(i),"x","y"));
    Gcode_coor(i,2)=str2double(extractAfter(Gcode_str(i),"y"));

```

```

Gcode_coor(i,3)=0;

end
%%

for i = 2:length(Gcode_str)
    i;
    % if x,y,z are present, take the value in between the characters
    % respectively
    if isempty(strfind(Gcode_str(i),"x")) == 0 & isempty(strfind(Gcode_str(i),"y")) == 0 &
isempty(strfind(Gcode_str(i),"z"))==0
        Gcode_coor(i,1)=str2double(extractBetween(Gcode_str(i),"x","y"));
        Gcode_coor(i,2)=str2double(extractBetween(Gcode_str(i),"y","z"));
        Gcode_coor(i,3)=str2double(extractAfter(Gcode_str(i),"z"));
        %if only x present, y,z missing take the previous value
    elseif isempty(strfind(Gcode_str(i),"x")) == 0 & isempty(strfind(Gcode_str(i),"y")) ==
1 & isempty(strfind(Gcode_str(i),"z")) == 1;
        Gcode_coor(i,1)=str2double(extractAfter(Gcode_str(i),"x"));
        Gcode_coor(i,2)=Gcode_coor(i-1,2);
        Gcode_coor(i,3)=Gcode_coor(i-1,3);
        %if only y present, x,z missing take the previous value
    elseif isempty(strfind(Gcode_str(i),"x")) == 1 & isempty(strfind(Gcode_str(i),"y")) ==
0 & isempty(strfind(Gcode_str(i),"z")) == 1
        Gcode_coor(i,1)=Gcode_coor(i-1,1);
        Gcode_coor(i,2)=str2double(extractAfter(Gcode_str(i),"y"));
        Gcode_coor(i,3)=Gcode_coor(i-1,3);
        %if only z present, x,y missing take the previous value
    elseif isempty(strfind(Gcode_str(i),"x")) == 1 & isempty(strfind(Gcode_str(i),"y")) ==
1 & isempty(strfind(Gcode_str(i),"z")) ==0
        Gcode_coor(i,1)=Gcode_coor(i-1,1);
        Gcode_coor(i,2)=Gcode_coor(i-1,2);
        Gcode_coor(i,3)=str2double(extractAfter(Gcode_str(i),"z"));
        %if only y,z present, x missing take the previous value
    elseif isempty(strfind(Gcode_str(i),"x")) == 1 & isempty(strfind(Gcode_str(i),"y")) ==
0 & isempty(strfind(Gcode_str(i),"z"))==0
        Gcode_coor(i,1)=Gcode_coor(i-1,1);
        Gcode_coor(i,2)=str2double(extractBetween(Gcode_str(i),"y","z"));
        Gcode_coor(i,3)=str2double(extractAfter(Gcode_str(i),"z"));

        %if only x,z present, y missing take the previous value
    elseif isempty(strfind(Gcode_str(i),"x")) == 0 & isempty(strfind(Gcode_str(i),"y")) ==
1 & isempty(strfind(Gcode_str(i),"z"))==0
        Gcode_coor(i,1)=str2double(extractBetween(Gcode_str(i),"x","z"));
        Gcode_coor(i,2)=Gcode_coor(i-1,2);
        Gcode_coor(i,3)=str2double(extractAfter(Gcode_str(i),"z"));
        %if only x,y present, z missing take the previous value

```

```

elseif isempty(strfind(Gcode_str(i),"x")) == 0 & isempty(strfind(Gcode_str(i),"y")) ==
0 & isempty(strfind(Gcode_str(i),"z"))==1
    Gcode_coor(i,1)=str2double(extractBetween(Gcode_str(i),"x","y"));
    Gcode_coor(i,2)=str2double(extractAfter(Gcode_str(i),"y"));
    Gcode_coor(i,3)=Gcode_coor(i-1,3);

end
end
%delete repeated lines
for i = 1:length(Gcode_coor)-2;
    row(i,:)=Gcode_coor(i+1,:)==Gcode_coor(i,1:3);
end
Gcode_coor(mean(row,2)==1,:)=[];
end

```

## 12 Appendix D

### Quality Control

Table 12-1 Discrepancy of deviations between Scanned models from the True Part for Dome Geometries. (-) data could not be obtained.

Tool	°C	Pressure	Force Control	Surface	Sample ID	Mean	SD	Max Value	Min Value	Performance
HP	125	10 bar	N/A	Top	1	-0.03	0.12	0.8	-0.8	93%
HP	125	10 bar	N/A	Bottom	1	0.15	0.15	0.64	-0.8	52%
HP	140	10 bar	N/A	Top	2	-0.01	0.11	0.8	-0.78	94%
HP	140	10 bar	N/A	Bottom	2	-	-	-	-	-
HP	170	10 bar	N/A	Top	3	-0.1	0.13	0.76	-80	77%
HP	170	10 bar	N/A	Bottom	3	-	-	-	-	-
12 mm	125	7 bar	Yes	Top	1	-0.02	0.32	0.8	-0.8	41%
12 mm	125	7 bar	Yes	Bottom	1	0.01	0.31	0.8	-0.8	48%
12 mm	125	7 bar	Yes	Top	2	-0.05	0.31	0.8	-0.8	37%
12 mm	125	7 bar	Yes	Bottom	2	-0.02	0.38	0.8	-0.8	50%
12 mm	125	7 bar	Yes	Top	3	0.11	0.26	0.8	-0.8	50%
12 mm	125	7 bar	Yes	Bottom	3	-0.04	0.3	0.8	-0.8	53%
12 mm	125	10 bar	Yes	Top	1	0.08	0.28	0.8	-0.8	46%
12 mm	125	10 bar	Yes	Bottom	1	-0.01	0.31	0.8	-0.8	48%
12 mm	125	10 bar	Yes	Top	2	0.12	0.29	0.8	-0.8	47%
12 mm	125	10 bar	Yes	Bottom	2	-0.02	0.31	0.8	-0.8	50%
12 mm	125	10 bar	Yes	Top	3	0	0.28	0.8	-0.8	48%
12 mm	125	10 bar	Yes	Bottom	3	-0.03	0.3	0.8	-0.8	53%
12 mm	140	7 bar	Yes	Top	1	-0.17	0.33	0.75	-0.8	35%
12 mm	140	7 bar	Yes	Bottom	1	-0.08	0.4	0.8	-0.8	27%
12 mm	140	7 bar	Yes	Top	2	-0.02	0.39	0.8	-0.8	32%
12 mm	140	7 bar	Yes	Bottom	2	0.01	0.41	0.8	-0.8	18%
12 mm	140	7 bar	Yes	Top	3	-0.17	0.33	0.75	-0.8	35%
12 mm	140	7 bar	Yes	Bottom	3	-0.08	0.4	0.8	-0.8	27%
12 mm	140	10 bar	Yes	Top	1	-0.02	0.38	0.8	-0.8	36%
12 mm	140	10 bar	Yes	Bottom	1	-0.06	0.37	0.8	-0.8	37%
12 mm	140	10 bar	Yes	Top	2	-0.01	0.39	0.8	-0.8	28%
12 mm	140	10 bar	Yes	Bottom	2	-0.06	0.38	0.8	-0.8	27%
12 mm	140	10 bar	Yes	Top	3	-0.1	0.37	0.8	-0.8	33%
12 mm	140	10 bar	Yes	Bottom	3	0.07	0.34	0.8	-0.8	18%
12 mm	125	7 bar	No	Top	1	-0.04	0.38	0.8	-0.8	29%
12 mm	125	7 bar	No	Bottom	1	-0.02	0.33	0.8	-0.8	40%
12 mm	125	7 bar	No	Top	2	0.01	0.29	0.8	-0.8	47%
12 mm	125	7 bar	No	Bottom	2	-0.03	0.3	0.8	-0.8	53%
12 mm	125	7 bar	No	Top	3	0.01	0.33	0.8	-0.8	38%

12 mm	125	7 bar	No	Bottom	3	-0.04	0.32	0.8	-0.8	48%
12 mm	140	7 bar	No	Top	1	0.01	0.42	0.8	-0.8	24%
12 mm	140	7 bar	No	Bottom	1	0.01	0.43	0.8	-0.8	16%

Table 12-2 Deviation measure for geometric features for a Dome Geometry with different manufacturing processes such as Hot Pressing and Automated in-situ Consolidation. (-) data could not be obtained.

Tool	°C	Pressure	Force Control	Surface	Sample ID	Dome radius	Dome Deviation	Dome Error	Fillet Major diameter	Fillet Major diameter deviation	Fillet Major diameter Error	Fillet radius	Fillet radius deviation	Fillet radius Error
HP	125	10 bar	N/A	Top	1	92.66	12.66	12.61	103.82	7.51	7.41	26.15	15.32	15.27
HP	125	10 bar	N/A	Bottom	1	96.09	17.29	17.24	103.82	7.51	7.41	20.46	14.46	14.36
HP	140	10 bar	N/A	Top	2	94.56	14.56	14.51	107.43	7.43	7.33	27.01	16.18	16.13
HP	140	10 bar	N/A	Bottom	2	-	-	-	-	-	-	-	-	-
HP	170	10 bar	N/A	Top	3	-	-	-	-	-	-	-	-	-
HP	170	10 bar	N/A	Bottom	3	-	-	-	-	-	-	-	-	-
12 mm	125	7 bar	Yes	Top	1	98.62	18.62	18.57	110.8	10.8	10.7	31.91	21.08	21.03
12 mm	125	7 bar	Yes	Bottom	1	95.6	16.8	16.75	109.51	13.2	13.1	29.33	23.33	23.23
12 mm	125	7 bar	Yes	Top	2	95.88	15.88	15.83	112.46	12.46	12.36	33.95	23.12	23.07
12 mm	125	7 bar	Yes	Bottom	2	-	-	-	-	-	-	-	-	-
12 mm	125	7 bar	Yes	Top	3	-	-	-	-	-	-	-	-	-
12 mm	125	7 bar	Yes	Bottom	3	-	-	-	-	-	-	-	-	-
12 mm	125	10 bar	Yes	Top	1	95.79	15.79	15.74	110.59	10.59	10.49	32.12	21.29	21.24
12 mm	125	10 bar	Yes	Bottom	1	96.6	17.8	17.75	108.36	12.05	11.95	28.2	22.2	22.1
12 mm	125	10 bar	Yes	Top	2	94.62	14.62	14.57	112.19	12.19	12.09	34.42	23.59	23.54
12 mm	125	10 bar	Yes	Bottom	2	94.64	15.84	15.79	106.12	9.81	9.71	25.96	19.96	19.86
12 mm	125	10 bar	Yes	Top	3	96.08	16.08	16.03	108.95	8.95	8.85	30.75	19.92	19.87
12 mm	125	10 bar	Yes	Bottom	3	96.12	17.32	17.27	108.14	11.83	11.73	28.03	22.03	21.93
12 mm	140	7 bar	Yes	Top	1	-	-	-	-	-	-	-	-	-
12 mm	140	7 bar	Yes	Bottom	1	-	-	-	-	-	-	-	-	-
12 mm	140	7 bar	Yes	Top	2	-	-	-	-	-	-	-	-	-
12 mm	140	7 bar	Yes	Bottom	2	-	-	-	-	-	-	-	-	-
12 mm	140	7 bar	Yes	Top	3	106.47	26.47	26.42	109.65	109.65	9.55	32.45	21.62	21.57
12 mm	140	7 bar	Yes	Bottom	3	108.54	29.74	29.69	109.89	13.58	13.48	35.06	29.06	28.96

<b>Tool</b>	<b>°C</b>	<b>Pressure</b>	<b>Force Control</b>	<b>Surface</b>	<b>Sample ID</b>	<b>Dome radius</b>	<b>Dome Deviation</b>	<b>Dome Error</b>	<b>Fillet Major diameter</b>	<b>Fillet Major diameter deviation</b>	<b>Fillet Major diameter Error</b>	<b>Fillet radius</b>	<b>Fillet radius deviation</b>	<b>Fillet radius Error</b>
12 mm	140	10 bar	Yes	Top	1	-	-	-	-	-	-	-	-	-
12 mm	140	10 bar	Yes	Bottom	1	103.68	24.88	24.83	113.48	17.17	17.07	42	36	35.9
12 mm	140	10 bar	Yes	Top	2	102.81	22.81	22.76	108.98	8.98	8.88	31.58	20.74	20.69
12 mm	140	10 bar	Yes	Bottom	2	-	-	-	-	-	-	-	-	-
12 mm	140	10 bar	Yes	Top	3	-	-	-	-	-	-	-	-	-
12 mm	140	10 bar	Yes	Bottom	3	112.99	34.19	34.14	106.2	9.89	9.79	29.69	23.69	23.59
12 mm	125	7 bar	No	Top	1	99.27	19.27	19.22	112.69	12.69	12.59	34.08	23.24	23.19
12 mm	125	7 bar	No	Bottom	1	97.96	19.16	19.11	108.37	12.05	11.95	27.87	21.87	21.77
12 mm	125	7 bar	No	Top	2	94.56	14.56	14.51	114.77	14.77	14.67	36.78	25.95	25.9
12 mm	125	7 bar	No	Bottom	2	-	-	-	-	-	-	-	-	-
12 mm	125	7 bar	No	Top	3	94.82	14.82	14.77	112.39	12.39	12.29	35.09	24.25	24.2
12 mm	125	7 bar	No	Bottom	3	-	-	-	-	-	-	-	-	-
12 mm	140	7 bar	No	Top	1	101.22	21.22	21.17	109.62	9.62	9.52	32.67	21.83	21.78
12 mm	140	7 bar	No	Bottom	1	107.45	28.65	28.6	109.74	13.43	13.33	35.04	29.04	28.94



